



Universiteit  
Leiden

The Netherlands

## Highly accurate simulations and benchmarking of molecule-surface reactions

Tchakoua, T.

### Citation

Tchakoua, T. (2023, July 4). *Highly accurate simulations and benchmarking of molecule-surface reactions*. Retrieved from <https://hdl.handle.net/1887/3628451>

Version: Publisher's Version

License: [Licence agreement concerning inclusion of doctoral thesis in the Institutional Repository of the University of Leiden](#)

Downloaded from: <https://hdl.handle.net/1887/3628451>

**Note:** To cite this publication please use the final published version (if applicable).

# HIGHLY ACCURATE SIMULATIONS AND BENCHMARKING OF MOLECULE-SURFACE REACTIONS

Proefschrift

ter verkrijging van  
de graad van doctor aan de Universiteit Leiden,  
op gezag van rector magnificus prof.dr.ir. H. Bijl,  
volgens besluit van het college voor promoties  
te verdedigen op dinsdag 4 juli 2023  
klokke 10:00 uur

door

Théophile Tchakoua  
geboren te Foumban, Kameroen  
in 1988

**Promotor:** Prof. dr. G. J. Kroes  
**Co-promotor:** Dr. M. F. Somers

## Promotiecommissie

Prof. dr. M. Ubbink  
Prof. dr. A. Kros  
Prof. dr. P. Hyldgaard (Chalmers University of Technology, Sweden)  
Prof. dr. P. Larrégaray (University of Bordeaux, France)  
Dr. I. M. N. Groot

ISBN: 978-94-6473-148-4

The research reported in this thesis has been performed in the Theoretical Chemistry group at the Leiden Institute of Chemistry (Einsteinweg 55, 2333 CC, Leiden, the Netherlands). This work has been made possible by financial support by the Nederlandse Organisatie voor Wetenschappelijk Onderzoek (NWO) through an NWO/CW TOP Grant (No. 715.017.001) and by the European Research Council through an ERC-2013 advanced grant (Nr. 338580), and with computer time granted by the Physical Sciences division of NWO (NWO-EW).

Je voudrais dédier ce travail à ma grand-mère **Samou Marthe** qui est passée de vie à trépas le 7 février 2021. Tu as su durant les deux premières années de cette thèse, me motiver sans ménager un quelconque effort. Reposes en paix, car ton vœu le plus cher qui était de finir cette thèse s'est réalisé! Tu m'a offert un havre de paix pendant les moments épineux de ma vie depuis mon jeune âge.

*Celui qui sait et qui sait qu'il sait est un savant, il faut le suivre.*

*Celui qui sait et ne sait pas qu'il sait est un dormeur, il faut le réveiller.*

*Celui qui ne sait pas et sait qu'il ne sait pas est un chercheur, il faut le guider.*

*Celui qui ne sait pas et ne sait pas qu'il ne sait pas est un danger public, il faut l'éviter.*

Proverbe africain.

## Contents

<b>1</b>	<b>General Introduction</b>	<b>1</b>
1.1	Gas-surface reactions . . . . .	1
1.2	Molecule metal-surface reaction mechanisms . . . . .	3
1.3	Background to topics of this thesis . . . . .	4
1.3.1	H <sub>2</sub> reacting on metal surfaces . . . . .	4
1.3.2	Databases . . . . .	6
1.3.3	Mixed DFs for SRP-DF development . . . . .	7
1.4	Aims of this thesis . . . . .	8
1.5	Main results . . . . .	9
1.6	Outlook . . . . .	12
<b>2</b>	<b>Towards a Specific Reaction Parameter Density Functional for H<sub>2</sub> + Ni(111): Comparison of Theory with Molecular Beam Sticking Experiments</b>	<b>31</b>
2.1	Introduction . . . . .	32
2.2	Methods . . . . .	37
2.2.1	Dynamical model . . . . .	37
2.2.2	Construction of the PES . . . . .	37
2.2.3	Interpolation of PES . . . . .	40
2.2.4	Dynamics Methods . . . . .	41
2.2.4.A	Quasi-classical Dynamics . . . . .	41
2.2.4.B	Quantum Dynamics . . . . .	42
2.2.5	Computation of the Observables . . . . .	43
2.2.5.A	Degeneracy-Averaged reaction probabilities . . . . .	43
2.2.5.B	Molecular Beam sticking probabilities . . . . .	43
2.3	Results and Discussion . . . . .	45
2.3.1	Potential Energy Surfaces . . . . .	45
2.3.2	Comparison to experiment . . . . .	48
2.3.3	Causes for the discrepancies between theory and experiment . . . . .	53
2.4	Conclusions . . . . .	59

<b>3</b>	<b>SBH17: Benchmark Database of Barrier Heights for Dissociative Chemisorption on Transition Metal Surfaces</b>	<b>69</b>
3.1	Introduction . . . . .	70
3.2	Methods . . . . .	73
3.2.1	Density functionals tested . . . . .	73
3.2.2	Semi-empirical approaches to obtaining reference values of barrier heights . . . . .	76
3.2.2.A	The specific reaction parameter approach to density functional theory (SRP-DFT) . . . . .	78
3.2.2.B	Ad hoc semi-empirical approaches . . . . .	79
3.2.3	The SBH17 database . . . . .	80
3.2.3.A	Dissociative chemisorption of H <sub>2</sub> on transition metals . . . . .	81
3.2.3.B	N <sub>2</sub> dissociation on Ru surfaces . . . . .	84
3.2.3.C	CH <sub>4</sub> dissociation on transition metals . . . . .	85
3.2.4	Algorithms for computing minimum barrier heights . . . . .	88
3.2.4.A	Light Algorithm . . . . .	89
3.2.4.B	Medium Algorithm . . . . .	89
3.2.4.C	High Algorithm . . . . .	90
3.2.5	Computational details . . . . .	90
3.3	Results . . . . .	91
3.3.1	Structure of the metals . . . . .	91
3.3.2	Dissociative chemisorption barriers . . . . .	91
3.4	Discussion . . . . .	102
3.4.1	Description of the metal . . . . .	102
3.4.2	Description of barrier heights to DC . . . . .	103
3.4.2.A	Preferred algorithm . . . . .	103
3.4.2.B	Performance of DFs for SBH17 with medium algorithm . . . . .	104
3.4.2.C	Dependence on the type of system . . . . .	109
3.4.2.D	Comparison to present and previous results for SBH10 . . . . .	110
3.4.3	Comparison to results for adsorption and to gas phase results	113
3.4.4	Future improvements . . . . .	114
3.5	Conclusions and outlook . . . . .	117
<b>4</b>	<b>Simulating Highly Activated Sticking of H<sub>2</sub> on Al(110): Quantum versus quasi-classical dynamics</b>	<b>138</b>
4.1	Introduction . . . . .	139
4.2	Method . . . . .	141

4.2.1	Dynamical model . . . . .	141
4.2.2	DFT Method . . . . .	142
4.2.3	Interpolation of PES . . . . .	144
4.2.4	Calculations of observables . . . . .	146
4.2.5	Dynamics Methods . . . . .	150
	4.2.5.A Quantum Dynamics . . . . .	150
	4.2.5.B Quasi-classical dynamics . . . . .	152
4.3	Results and discussion . . . . .	153
4.3.1	The fitted potential energy surface . . . . .	153
4.3.2	Sticking probabilities computed with quantum and quasi-classical methods, and their comparison . . . . .	155
4.3.3	Analysis of the size of the quantum effects on the sticking: role of vibration and incidence energy . . . . .	159
4.4	Conclusions . . . . .	164
<b>5</b>	<b>Constructing Mixed Density Functionals for Describing Dissociative Chemisorption on Metal Surfaces: Basic Principles</b>	<b>174</b>
5.1	Introduction . . . . .	175
5.2	Methods . . . . .	176
	5.2.1 The SBH16 database . . . . .	176
	5.2.2 Mixed density functional expressions . . . . .	177
	5.2.3 Computational details . . . . .	180
5.3	Results and discussion. . . . .	181
	5.3.1 Equilibrium lattice constants computed with mixed density functionals . . . . .	181
	5.3.2 Performance of limiting forms of the mixed density functionals . . . . .	181
	5.3.3 Performance of mixed density functionals as tunable SRP DFs . . . . .	185
	5.3.4 Correlation of the mixing parameter with the charge transfer parameter . . . . .	190
5.4	Conclusions and outlook. . . . .	192
5.A	Appendix Tables and Figures . . . . .	195
	<b>Samenvatting</b>	<b>205</b>
	<b>Curriculum vitae</b>	<b>212</b>
	<b>List of publications</b>	<b>213</b>
	<b>Afterword</b>	<b>214</b>





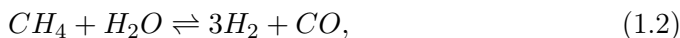
## General Introduction

### 1.1 Gas-surface reactions

We are surrounded by molecules. These molecules can interact with each other artificially (in the ways arranged by us) or naturally. These chemical interactions are then part of our everyday life. A well known example of a natural reaction of these molecules is the rusting of the metals left outside in a humid environment. An artificial example is the reduction of the toxic exhaust gases from cars by a catalytic converter<sup>1</sup>. Many of these reactions find their application in industry<sup>2</sup>. A well know example is the Haber-Bosch process,



used in the synthesis of ammonia which is an important chemical reaction in the production of artificial fertilizer<sup>3</sup> needed for food production. Another example is steam reforming<sup>4</sup>,



used to produce hydrogen ( $H_2$ ) and carbon monoxide ( $CO$ ) gas from methane ( $CH_4$ ) and steam. These chemical reactions proceed on a catalyst. For example, in the Haber-Bosch reaction, iron or ruthenium is used as a catalyst, whereas for steam reforming, nickel is commonly used as catalyst. Improving these reactions by designing new catalysts, either by allowing cheaper materials to be used as catalysts or by reducing the energy cost of a given reaction, have a potentially huge impact on the chemical industry<sup>5</sup>. Due to the considerable importance of these chemical reactions for industry, it is not surprising that they receive much attention from both theoretical and experimental studies. It is then the job of the chemist to understand why and how these reactions take place, at the experimental level, and also at the theoretical level in order to achieve improvements.

As a simple form of a chemical reaction let us consider two molecules (reactants) coming together with enough energy to overcome the energetic barrier to that reaction and then reacting to form the product(s). During this reaction, bonds are broken, and new bonds are formed. The chemical reaction that takes place in the presence of a catalyst is called a catalyzed reaction. A catalyst is a reaction partner that interacts with the reactants to provide an alternative reaction mechanism that is energetically more favorable. In general, a catalyst stabilizes the transition state of the reaction complex formed by the reactants coming together on a catalyst, thereby lowering the barrier (Fig.1.1) to reaction and facilitating the breaking of existing chemical bonds and the formation of new chemical bonds.

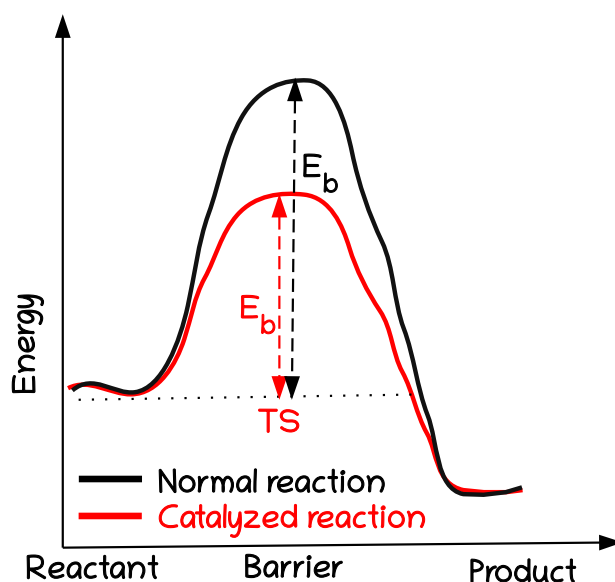


FIGURE 1.1: The schematic overview of the role of the catalyzed reaction.

The products that are formed after the reaction move away from the catalyst, allowing the catalyst to participate in a new catalytic cycle. The catalyst creates an alternative energetic pathway by lowering the energetic barrier to speed the reaction. It increases the reaction rate and may allow it to proceed under milder conditions (lower temperature and or pressure), reducing the cost. In many cases, it is also possible to increase the selectivity of the catalyst such that the formation of a desired reaction product is favored over an unwanted reaction product, reducing waste and pollution. If the reactants and the catalyst exist in distinct phases (plasma, gas, liquid, solid), we call it heterogeneous catalysis,

while in homogeneous catalysis both the catalyst and the reactants are in the same phase. Another important type of catalysis that cannot go unmentioned is biocatalysis, in which proteins act as highly specialized catalysts (enzymes) for nearly all biochemical reactions underpinning life as we know it<sup>6</sup>.

## 1.2 Molecule metal-surface reaction mechanisms

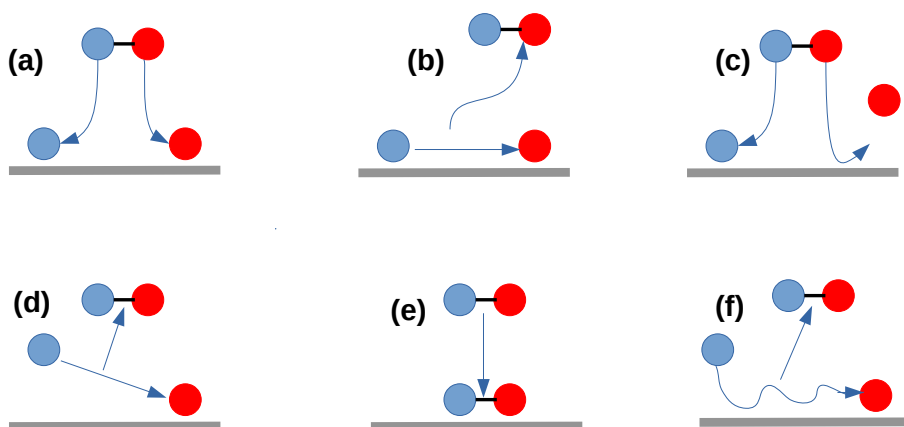


FIGURE 1.2: Schematic overview of different mechanisms for molecule metal-surface reactions. (a) dissociative chemisorption, (b) Langmuir-Hinshelwood reaction, (c) abstraction, (d) Eley-Rideal reaction, (e) molecular adsorption and (f) hot-atom reaction.

When a molecule interacts with a surface, reactions may proceed through several mechanisms, the most common mechanisms being shown in Fig.1.2. Three of these mechanisms involve the adsorption of the reactant molecule to the surface: dissociative chemisorption (DC), in which a bond in the incoming reactant is broken and both fragments are adsorbed to the surface (Fig.1.2.a); abstraction, in which after a bond in the reactant incoming molecule is broken, only one fragment is adsorbed to the surface while the other fragment returns to the gas phase (Fig.1.2.c); and molecular adsorption, in which the whole molecule is adsorbed to the surface, without bond breaking (Fig.1.2.e). This last mechanism can happen through chemisorption or physisorption. Other reaction mechanisms are: the Langmuir-Hinshelwood reaction, in which two atoms and/or molecules that are adsorbed to the surface can combine, form a new bond and the newly formed molecule desorbs (Fig.1.2.b); Eley-Rideal reaction, in which one atom/or molecule coming from the gas phase reacts directly with an adsorbed atom/or molecule on the surface and the newly formed molecule directly desorbs

from the surface (Fig.1.2.d); and Fig.1.2.f the hot-atom reaction, in which a molecule coming from the gas phase is temporarily trapped and bounces on the surface not achieving thermal equilibrium with it, and collides with another molecule adsorbed on the surface to form a bond, and the newly molecule formed desorbs. In 2007 Ertl was awarded the Nobel prize in chemistry for investigating elementary reaction steps in heterogeneous catalysis experimentally<sup>7</sup>.

In many cases DC is the rate-limiting step in a heterogeneously catalyzed process<sup>8,9</sup>. Creating a theoretical description of a complex reaction network ideally starts with the calculation of 'chemically accurate' barrier heights for such elementary reaction steps<sup>10</sup>. Calculating chemically accurate barrier heights for rate-controlling reactions to obtain accurate rates of the overall reaction network<sup>11</sup> is a complex task. This task not only needs to take into account the static electronic structures of both the reactant and the catalytic surface at the transition state, but often also dynamical effects such as the molecule's approach towards the transition state, the molecule's internal motion, as well as surface atom motion due to temperature<sup>12</sup>.

## 1.3 Background to topics of this thesis

### 1.3.1 H<sub>2</sub> reacting on metal surfaces

As mentioned in the previous section, DC is often a rate-limiting step in heterogeneously catalyzed process. From a fundamental point of view, understanding how a molecule reacts on a surface is helped by investigating how the simplest molecule (hydrogen) dissociates on a clean metal surface with a well-defined structure. Also, the dissociation of hydrogen is relevant to the industry. It is used in the synthesis of methanol from CO<sub>2</sub> over a Cu/ZnO/Al<sub>2</sub>O<sub>3</sub> catalyst, in which process the dissociation of hydrogen is considered to be an important step<sup>13-15</sup>. Another reaction that has an extensive use in the chemical industry<sup>16-21</sup> is the hydrogenation of unsaturated bonds in organic molecules through heterogeneous catalysis on solids.

The DC of hydrogen on metal surfaces has served as an ideal model system. It has been the subject of many theoretical and experimental studies. Experiments carried out in the ultra-high vacuum (UHV) have been used to study the dynamics of hydrogen dissociation, recombinative desorption, and scattering<sup>22-59</sup>. However, there is still a lot to do about the dynamics and kinetics of H<sub>2</sub> dissociation at industrially relevant temperatures and pressures<sup>60,61</sup>.

Experiments on the reaction scattering of H<sub>2</sub> from metal surfaces, have investigated a wealth of phenomena. Sticking probability versus collision energy curves can be obtained directly from molecular beam experiments<sup>23,24,29,36,39-41,48-52,62</sup>

or indirectly from associative desorption experiments<sup>23,25,29,38,63</sup> if detailed balance is assumed. From associative desorption experiments, we can derive information on the effect of the initial rovibrational state<sup>23,25,29,38,63</sup>, and also of the alignment of the molecule relative to the surface on the reverse DC reaction<sup>27</sup>. From state-resolved molecular beam experiments in which H<sub>2</sub> scatters from a surface, information on vibrational excitation<sup>31</sup>, rotationally elastic<sup>22</sup> and inelastic<sup>32</sup> scattering, and vibrationally and rotationally inelastic scattering<sup>33,54</sup> can be obtained. Elastic and inelastic diffractive scattering of H<sub>2</sub> from metal surfaces can be assessed as well<sup>55–59,64–68</sup>.

Using molecular beam techniques, the sticking probability can be measured directly using the King and Wells method<sup>69</sup>. In this technique, a gas (molecular beam) is collimated by skimmers, then supersonically expands into a UHV chamber toward the target surface. The initial pressure in the UHV chamber drops when the molecular beam entering the chamber interacts with the surface and molecules stick, and rises when the molecular beam entering the chamber does not react with the surface. The sticking probability can be obtained from the differences in the pressures measured.

Associative desorption<sup>25,29,38,42,43,63,70–72</sup> is another experimental technique where the potential energy surface of the molecule interacting with the surface can be explored. In this approach, resonance-enhanced multi-photon ionization<sup>23,25,29,38,63</sup> (REMPI) can be used to obtain information on state-specific reaction.

One of the biggest challenges to theorists is to help with understanding and improving the above experiments. Theoretically, to understand, control, and predict the rate of heterogeneously catalyzed processes, the DC of a molecule on a metal surface has been widely studied<sup>73–90</sup>. Typically density functional theory (DFT<sup>91,92</sup>) has been used. Some of the research focused on improving on existing exchange-correlation (XC) functionals. One example concerns the specific reaction parameter approach to density functional theory (SRP-DFT)<sup>79</sup> for dissociative chemisorption on metal surfaces, which has enabled achieving chemical accuracy for several systems<sup>63,79,80,87,93–95</sup>. In some cases, transferability of the SRP density functional (SRP-DF) among chemically similar systems has been found<sup>96–98</sup>.

To accurately simulate the experimental sticking coefficients ( $S_0$ ), many points have to be considered. In general, the product of the reaction between a molecule and a metal surface is influenced by the details of the interaction potential between the molecule and the surface. Many factors can play a role during the approach of a gas phase molecule to the surface. Firstly, due to their thermal motion, the surface atoms can be displaced from their equilibrium positions. As a consequence, the interaction potential between molecule and

surface might be modified. Secondly, due to the vibrational coupling with the phonons of the lattice, there can be energy exchange between the molecule and the surface. Finally, electron-hole pair excitation (a non-adiabatic effect) due to the transfer of a small amount of energy from molecular motion to electrons lying just below the Fermi level might also influence the reaction dynamics. The role played by surface temperature, surface atom motion, and non-adiabatic effects might differ from system to system.

In the literature, many studies have taken into account these processes. For example, electron-hole (e-h) pair excitation has been taken into account in the study of H<sub>2</sub> scattering from Pt(111). This study suggested that e-h pair excitation should not play a large role<sup>66</sup> in this system, as both reaction and diffraction could be well described with one and the same potential energy surface. Non-adiabatic effects have been taken into account directly in the study of H<sub>2</sub> dissociating on Cu(111)<sup>99,100</sup>, Cu(110)<sup>101</sup> and Ru(0001)<sup>102</sup> using electron friction models. From these studies, no large non-adiabatic effects have been found, suggesting that e-h pair excitation does not play a significant role for H<sub>2</sub> interacting with metals. In addition, because of the large mass mismatch between the H<sub>2</sub> molecule and a surface atom<sup>103,104</sup>, for activated systems, the amount of energy exchanged between H<sub>2</sub> and the surface atoms is not expected to be large<sup>12,105,106</sup>. For the thermal motion, a density functional molecular dynamics (DFMD) study of D<sub>2</sub> on Cu(111)<sup>80</sup> has revealed that for low surface temperatures (T<sub>s</sub>=120K) the Born-Oppenheimer static surface (BOSS) model works quite well.

In view of the above, it becomes computationally feasible to map out a potential energy surface in six dimensions (6D), for H<sub>2</sub> interacting with a metal surface, and use it to compute accurate molecular beam sticking probabilities (or DC probabilities) using the (quasi-)classical trajectory method or quantum dynamics.

### 1.3.2 Databases

In general, accurate barrier heights are key to understanding, controlling, and predicting chemical reactions. Our ability to understand and predict heterogeneous catalysis could be increased if there would exist accurate databases of barrier heights for molecule-metal surface reactions.

While databases exist for gas phase reactions<sup>107–110</sup> and for reaction energies on metal surfaces<sup>111–113</sup>, they are scarce for barriers to DC on metals. For adsorption bond energies to transition metal surface, for example, a database was recently built which contains data for 39 systems<sup>113</sup>. This database was

used to test several density functionals<sup>111–117</sup> and has been extended so that it now contains<sup>118</sup> data for 81 systems.

The first database (CatApp<sup>119,120</sup>) on barrier heights for DC was built using only one DF (RPBE<sup>121</sup>). A more recent database on DC is the SBH10<sup>122</sup> database containing results for 10 systems and benchmarked with the 2<sup>nd</sup> rung BEEF-vdW2<sup>111</sup>, 3<sup>rd</sup> rung MS2<sup>123</sup> and 4<sup>th</sup> rung HSE06<sup>124</sup> DF of Jacob's ladder<sup>125,126</sup>. Why are databases for barrier heights for DC scarce?

One of the main reasons has been that, until very recently, only DFT could be used to study DC on metals, which is less accurate. Therefore, until recently it was not well known how large the errors are in barrier heights when using semi-local XC functionals. Some indication in the literature can be found about the performance of semi-local functionals for gas phase reactions. A test on the BH206<sup>108</sup> database using the MN12-L<sup>127</sup> and N12<sup>128</sup> showed root-mean square deviations of 4.3 and 7.1 kcal/mol, respectively, which is still far from the chemical accuracy standard (1 kcal/mol). Very recently, the use of SRP-DFT (a semi-empirical method) has enabled a description of barrier heights for several DC systems (14) with chemical accuracy<sup>129</sup>. This suggests the construction of a new database for DC on metals, as discussed below.

### 1.3.3 Mixed DFs for SRP-DF development

As mentioned in the above subsection, the SRP-DFT approach has already allowed the construction of a small database (SRP14) containing 14 systems for molecule-metal surface reactions<sup>129</sup>. But there is still a conundrum at the heart of this approach, in particular about how to mix exchange and correlation DFs at the general gradient approximation (GGA) or meta-GGA level of theory to DFT to enable one to accurately reproduce barrier heights for DC. Several ways of mixing functionals can be found in literature: (i) using a weighted average of two exchange correlation (XC) functionals within the GGA<sup>63,79</sup>, (ii) using a weighted average of two exchange (X) functionals within the GGA and to combine the resulting X functional with a GGA correlation (C) functional<sup>80</sup>, (iii) as in (ii), but using a non-local C functional<sup>96,130–132</sup> also approximately describing the attractive van der Waals interaction<sup>133,134</sup>, (iv) by the use of a GGA exchange functional that was designed to be tunable<sup>135</sup> and by combining it with non-local van der Waals correlation<sup>95,136</sup>, and (v) by the use of meta-GGA functionals either with semi-local correlation<sup>137</sup> or in combination with non-local correlation<sup>87</sup>. An interesting question is whether a general expression of a mixed DF can be found that will allow one to reproduce the barrier for DC on metals for any system.



## 1.4 Aims of this thesis

The main goals of the thesis are to improve the theoretical description of reactive scattering of  $\text{H}_2$  from various transition metal surfaces, such as Ni(111) and Al(110), to build a database with barrier heights for DC to allow testing of electronic structure methods and to develop a more general expression of a mixed DF that can function as an SRP-DF for any DC-on-metal-surface system. For the two  $\text{H}_2$ -metal systems mentioned, we would like to reduce the bridge between theory and experiment regarding the description of reaction dynamics, through the design of accurate SRP-DFs. Furthermore, the explosion of computational studies in heterogeneous catalysis on metal surfaces has raised the question how reliable existing density functionals are. Therefore, there is a need for benchmark data sets. For this, we take a first step to build a database for barrier heights to DC. We also investigate several expressions of mixed DFs for their ability to function as SRP functionals, with the idea of deriving an SRP-DF that can work for all or most systems with a charge transfer energy greater than 7 eV. Here, the charge transfer energy is defined as the difference of the work function of the metal surface and the electron affinity of the molecule.

All the theories behind this thesis are discussed directly in the following **Chapters**. The **Chapters** in this thesis address the aims mentioned above as follows:

**In Chapter 2**, we aim to develop an entry to the database of chemically accurate barriers for DC on metal surfaces, i.e., the barrier height for DC of  $\text{H}_2$  on Ni(111), for which several molecular beam experiments exist. New potential energy surfaces for this system were computed at the GGA and the GGA + vdW level of theory using various density functionals. The PESs were used to evaluate sticking coefficients and reaction probabilities using the quasi-classical trajectory and the time-dependent wave packet method. The theoretical results obtained were then compared to experimental measurements, and an SRP DF and a chemically accurate barrier height were derived.

**In Chapter 3**, the aim is to present an extended database for the DC of molecules on metal surfaces, which can be used for benchmarking purposes. In our approach we avoid an important flaw from the previous SBH10 database<sup>122</sup>, in which transition states were modeled incorrectly by allowing the metal surface to relax in the molecule's presence. We introduce a new concept of algorithms (light, medium and higher). We tested these three algorithms and 14 density functionals on the database, which can now be used by other electronic structure

theorists to test their approaches to DC on metals.

In **Chapter 4** the focus lies on the highly activated DC of  $\text{H}_2$  on  $\text{Al}(110)$ . The goal is to establish whether the dynamics in this highly activated system can still be accurately described by the quasi-classical trajectory method. To answer this question, we performed dynamics calculations on a potential energy surface computed with a first principles based SRP density functional that has been fitted to recent diffusion Monte-Carlo calculations. Quantum dynamics (QD) and quasi-classical trajectory (QCT) calculations are used to compute sticking probabilities. A detailed comparison between QD and QCT calculations elucidates the importance of quantum effects on the DC in this highly activated system.

In **Chapter 5** the focus lies on a basic principle on how density functionals at the GGA and GGA +vdW levels can be mixed to construct an SRP DF that will reproduce with accuracy barrier heights for DC of molecules on metal surfaces. For this purpose, we tested 7 expressions of mixed DFs on a database with 16 entries we called SBH16 (the SBH17 database of **Chapter 3** with  $\text{H}_2+\text{Pt}(211)$  removed) using the medium algorithm method introduced in **Chapter 3**. We also investigated in this chapter how the amount of the RPBE exchange in an SRP DF correlates with the charge-transfer energy, which is defined as the difference of the work function of the metal surface and the electron affinity of the molecule.

## 1.5 Main results

The main results obtained in this thesis are summarized here.

In **Chapter 2**, we develop a SRP-DF for  $\text{H}_2$  on  $\text{Ni}(111)$ , also investigating if the SRP-DF derived previously for  $\text{H}_2+\text{Pt}(111)$ <sup>136</sup> is transferable to the system investigated. To address these questions, 6D PESs have been constructed for the dissociation of  $\text{H}_2+\text{Ni}(111)$  using nine different exchange-correlation functionals. The PESs calculated were then interpolated using the CRP method. To compare with experimentally measured sticking probabilities, quasi-classical trajectory and quantum dynamics calculations have been performed using the BOSS model.

The functionals investigated have shown that DFs with van der Waals correlation yield barriers closer to the surface and exhibit larger energetic corrugation than those with PBE correlation. The PBE-vdW-DF2 and RPBE:PBE(50:50)vdW-DF1 functionals describe the sticking experiments<sup>62</sup> performed by the Rendulic group quite well, with PBE-vdW-DF2 giving the best results. From the comparison with the most recent molecular beam experiments<sup>51</sup> performed by the

Rendulic group, we conclude that PBE-vdW-DF2 can be considered to be a candidate SRP-DF for  $\text{H}_2 + \text{Ni}(111)$ . However, the  $\text{PBE}_{\alpha=0.57}$ -vdW-DF2 functional, which is a SRP-DF for  $\text{H}_2$  on  $\text{Pt}(111)$  is not transferable to  $\text{H}_2 + \text{Ni}(111)$ , even though Ni and Pt belong to the same group.

Even if the PBE-vdW-DF2 is considered as a candidate SRP-DF for  $\text{H}_2 + \text{Ni}(111)$ , the sticking probabilities obtained for this DF are not yet in good agreement with the experiments of the Rendulic group<sup>51</sup> for incidence energies  $> 0.25$  eV. We found that for incidence energies  $> 0.25$  eV,  $S_0$  starts to exhibit a considerable dependence on the beam conditions, so that some of the discrepancies noted could be due to different beam parameters characterizing the experimental beams and the beams simulated in the calculations. Other possible causes of error in the experiments have also been discussed.

In **Chapter 3** we present a new database with barrier heights for DC on metal surfaces that can be used for benchmarking electronic structure methods. The new database is called SBH17 and contains barriers for 17 systems, including 8  $\text{H}_2$  metal systems, 2  $\text{N}_2$  metal systems, and 7  $\text{CH}_4$  metal systems. For 16 systems the work function of the metal surface minus the electron affinity of the molecule exceeds 7 eV. The barrier heights come from SRP-DFT (14 systems) and from estimates derived using more ad hoc semi-empirical methods (3 systems). The new database is meant to replace an older database (SBH10) that contained barriers for 10 of the 17 systems now treated.

We have tested 14 DFs on the new database, of which three were GGA DFs, 4 meta-GGA DFs and 7 DFs contained GGA exchange and vdW-DF1 or vdW-DF2 non-local correlation. Three different algorithms were tested, which were labeled "high", "medium" and "light" according to the investment of computer time that was required for the calculation.

Of the DFs tested, the meta-GGA DFs perform best at describing the metal, followed by PBE and optPBE-DF1. When the MAE is taken as the accuracy criterion, the workhorse PBE GGA DF performs best on the SBH17 database, with a MAE of 2.4 kcal/mol. Other top performers are the MS2 meta-GGA functional and two functionals consisting of GGA exchange and non-local correlation (SRP32-vdW-DF1 and  $\text{PBE}_{\alpha57}$ -vdW-DF2). None of the DFs tested systematically underestimates reaction barriers for DC on metals, in contrast to findings for gas phase reactions. We obtain different results regarding the relative accuracy of the MS2 and BEEF-vdW-DF2 functionals than obtained in an earlier study of the SBH10 database, which we attribute to an incorrect treatment of the surface atoms in the transition states in the earlier study.

For the sub-databases with  $\text{H}_2$ -metal systems,  $\text{N}_2$ -metal systems, and  $\text{CH}_4$ -metal systems, rankings are obtained that differ from the overall ranking for the

complete database. The SRP50-DF (the 50/50 mixture of the PBE and RPBE GGA DFs) performs best for H<sub>2</sub>-metal systems. BEEF-vdW-DF2 performs best for N<sub>2</sub>-metal systems, and SRP32-vdW-DF1 for CH<sub>4</sub>-metal systems.

The DFs performing best for DC barriers (i.e., kinetics) are not the ones that perform best for databases<sup>112,138</sup> (CE26, CE21b) of chemisorption energies on metals (i.e., thermochemistry). This trend is paralleled in the performance of DFs on databases for kinetics (BH76, BH206) and thermochemistry (AE6, TCE) in the gas phase. The meta-GGA MS2 DF is the functional with the best overall performance for DC barriers and chemisorption energies on metals. Of the five GGA and meta-GGA DFs considered for their performance on 6 databases for kinetics and thermochemistry on metal surfaces and in the gas phase (PBE, RPBE, revTPSS, MS2, and SCAN) again MS2 showed the best overall performance.

In **Chapter 4** we evaluate the accuracy of the QCT method, or, alternatively, the importance of quantum effects for the sticking of H<sub>2</sub> on Al(110), for conditions that should be close to the conditions under which molecular beam experiments have been done on this system<sup>139</sup>. For this purpose, QCT and QD calculations have been done with the BOSS model on a PES obtained with DFT, which exhibits a minimum barrier height close to that recently obtained with QMC calculations<sup>140</sup>. To keep the number of QD calculations to be performed small, a procedure was used in which Monte-Carlo averaging over the initial rovibrational states of H<sub>2</sub> was employed. This procedure allowed the quasi-classical calculation of sticking probabilities with a relative error < 7.5% for 5 of the six initial conditions investigated, and of 16% for one of these conditions, at approximately an order of magnitude less computation time.

The sticking probabilities computed with QD using the PMC procedure exceed the ones computed with the QCT method by 80 and 30% for the two beam conditions corresponding to the lowest average incidence energies (5.1 and 6.0 kcal/mol), decreasing to only 5% for the highest incidence energy of 9.4 kcal/mol. The sticking probability curve computed with QD is shifted to lower energies relative to the QCT curve by 0.21 to 0.05 kcal/mol, with the highest shift obtained for the lowest incidence energy.

These "quantum effects" may be viewed as being rather small for molecular beam sticking experiments in which the average incidence energies (5.1-8.5 kcal/mol) are much smaller than the minimum barrier height of the system investigated (24.8 kcal/mol). The smallness of the quantum effects is explained on the basis of the large vibrational efficacy of the system (> 1 for  $\nu=1$ ) and of the broadness of the translational energy distributions of the molecular beams used in the experiments we address.

Finally, in **Chapter 5** we have investigated the tunability of several expressions for mixed density functionals, in which a mixing parameter  $x$  can be tuned to enable the mixed DF to reproduce the reference value of the barrier height to DC of a molecule on a metal surface. The mixed functionals are tested on the barriers collected in the database we call SBH16, which is equal to the previously reported SBH17 database of **Chapter 3** with the  $\text{H}_2 + \text{Pt}(211)$  system removed from it.

Several findings are reported. Increasing the fraction of RPBE exchange incorporated in the mixed DFs leads to higher barriers. In addition, all mixed DFs tested are well tunable towards higher barriers, as their limiting forms (RPBE, RPBE-vdW1, and RPBE-vdW2) all systematically overestimate the barrier height for the systems in the SBH16 database. Furthermore, the mixed SRP $x$ sol-vdW2 DF could describe the minimum barrier height of 15 of the 16 systems using vdW-DF2 correlation, while the mixed SRP $x$ -vdW1 DF could do so for 14 of the 16 systems using vdW-DF1 correlation. The mixed SRP $x$ sol GGA DF could describe the minimum barrier height of all 16 systems tested.

Finally, we also tested whether and how the mixing coefficient of the mixed DFs is correlated with the charge transfer parameter describing the system, i.e., the difference between the work function of the metal surface and the electron affinity of the molecule. The answer depends on which mixed DF is used. For the SRP $x$  and SRP $x$ sol DFs, which both use PBE correlation, we found that the optimum fraction of RPBE exchange decreases with the charge transfer parameter, as could be expected on the basis of earlier results. However, the opposite relationship and weaker correlation was found for the mixed DFs using vdW-DF1 or vdW-DF2 correlation.

## 1.6 Outlook

All the questions that remain open with regard to the results that we have presented in this thesis are discussed in this Section, as well as the potential future investigations this research opens the door to.

The development of the SRP-DFs that can describe the reaction of a molecule with multiple transition metal surfaces to within chemical accuracy is still not yet clear. From the previous work of the DC of the  $\text{H}_2$  on  $\text{Pt}(111)$ <sup>136</sup>, it was suggested that the functional that allowed to achieve chemical accuracy for that system could also be transferable to  $\text{H}_2$  on  $\text{Ni}(111)$ . The results presented in **Chapter 2** show that the SRP-DF for  $\text{H}_2$  on  $\text{Pt}(111)$ <sup>136</sup> is not an SRP-DF for  $\text{H}_2$  on  $\text{Ni}(111)$  even though Ni and Pt belong to the same group in the periodic table. In contrast to this finding, the previous SRP-DF developed for  $\text{CH}_4$  on  $\text{Ni}(111)$ <sup>131</sup>

was found to be an SRP-DF for several other CH<sub>4</sub>-metal systems<sup>93,96,98,129,141</sup>. Why is the SRP-DF developed for CH<sub>4</sub>+Ni(111) transferable to CH<sub>4</sub>+Pt(111), while the SRP-DF for H<sub>2</sub> on Pt(111) is not transferable to H<sub>2</sub>+Ni(111)? This question is difficult to answer and remains open. Further studies are necessary to establish, for instance, whether the transferability depends on the nature of the mixed DF that is parameterized.

The ability to describe with accuracy the DC of a molecule on metal surfaces does not only depend on the performance of the parameterized mixed DF used, but also on the availability of highly accurate experimental data. The theoretical sticking probabilities obtained for H<sub>2</sub> on Ni(111) are not yet in good agreement with the experiment<sup>62</sup>. As discussed in **Chapter 2**, these discrepancies can perhaps be attributed to differences between the beam parameters that characterize the experiment and the beam parameters used for simulations. The comparison of different sets of experimental sticking coefficients also shows multiple discrepancies. To resolve this, the availability of highly accurate and well-defined experimental data is of great importance, and it would be good if new and accurate results would become available for H<sub>2</sub> on Ni(111).

The results for DC of H<sub>2</sub> on Cu(111)<sup>142</sup>, Cu(211)<sup>85</sup>, Ru(0001)<sup>130</sup> and also the results presented in **Chapter 2** suggest that quantum effects are not of large importance to DC of H<sub>2</sub> on metals. The sticking probability curve computed with quantum dynamics in **Chapter 4** for H<sub>2</sub> reacting on Al(110) is shifted to lower energies relative to the quasi-classical curve by 0.21 to 0.05 kcal/mol. This result shows that the quantum effects are also not very important for this highly activated system. This raises an important question. How important are quantum effects on the DC for highly activated H<sub>2</sub>-metal systems really since we know the H<sub>2</sub> on Al(110) system has a minimum barrier height > 1 eV? It will be worthwhile to also investigate whether the observation that quantum effects are not very important also holds for other systems with minimum barriers higher than 1 eV such as H<sub>2</sub> on Ag(111)<sup>87,142,143</sup> and Au(111)<sup>142-144</sup>.

On the basis of the results presented in **Chapter 3**, we see the following possible improvements of the present database for DC barriers on metals, and for testing DFs on the database.

First, we suggest that in future the entries in the database are as much as possible based on SRP-DFT, and not on more ad-hoc SE procedures. This would require dynamics calculations with trial DFs on CH<sub>4</sub> + Ru(0001) and CH<sub>4</sub> + Ni(100), for which molecular beam experiments are already available<sup>145,146</sup>, and new experiments and dynamics calculations on N<sub>2</sub> + Ru(10 $\bar{1}$ 0), for which molecular beam sticking experiments are, to our knowledge, not yet available. As noted above our comparison between MAEs computed with PBE for SBH17 and SBH14-SRP suggests that replacing the reference values with SRP-DFT values

for the three systems mentioned is likely to lead to smaller MAEs for a thus improved version of the SBH17 database. Second, we suggest that the database be extended with additional N<sub>2</sub>-metal systems. It may be possible to do this by semi-empirically fitting SRP-DFs to supersonic molecular beam sticking data on N<sub>2</sub> + Fe(111)<sup>147,148</sup>, W(110)<sup>149,150</sup>, and W(100)<sup>150–153</sup>. Adding these data is desirable to make the database more balanced, as it is now dominated by data for DC of H<sub>2</sub> and CH<sub>4</sub> on metal surfaces. Also, it would show whether our results for the MS2 DF are robust to addition of more N<sub>2</sub>-metal systems to the database, for which this DF did not perform so well, and the same holds for the optPBE-vdW-DF1 and PBE DFs.

On the longer term, it should be necessary to extend the database with systems for which the charge transfer energy, which equals (WF-EA), where WF is the work function of the metal surface and EA the electron affinity of the molecule, is less than 7 eV. As noted in Ref.<sup>154</sup>, DFs with semi-local exchange would appear to systematically overestimate the reactivity of such systems, suggesting that DFs with screened exact exchange are required for a good description. Examples of systems for which molecular beam sticking data are available include e.g. H<sub>2</sub>O + Ni(111)<sup>155</sup>, HCl + Au(111)<sup>156</sup>, and O<sub>2</sub> + Al(111)<sup>157,158</sup>, Ag(110)<sup>159,160</sup>, Cu(100)<sup>161</sup>, and Cu(111)<sup>162</sup>. Inclusion of such systems in the database would certainly alter the view of the performance of DFs for DC on metal surfaces, where the view offered in the present work is specific to systems with (WF-EA) > 7 eV, the only exception being N<sub>2</sub> + Ru(1010).

Finally, a far larger number of DFs exists than we tested. While we could mention specific DFs here that would be nice to test, this might not do justice to others, as several DFs exist (see e.g. the DFs tested in Refs.<sup>107,108,110</sup>). However, a particular DF we would like to mention is the new machine learned DF DM21<sup>163</sup>. Even though this DF has not been trained on interactions involving transition metals, it would be good to see how it performs on SBH17. It would also be good to test recently developed functionals combining screened exact exchange with vdW-DF1 and vdW-DF2 correlation<sup>164,165</sup>, which may work especially well for the representative database we envisage. We advocate that such future benchmark tests would also incorporate calculations employing the CE26 database for chemisorption on metals<sup>112</sup>.

Finally, for **Chapter 5**, the results presented have opened the door to several new lines of research. First of all the results underscore the need to obtain better reference values for the H<sub>2</sub> + Ag(111), CH<sub>4</sub> + Ru(0001), and CH<sub>4</sub> + Ni(100) systems. For all mixed DFs the optimized mixing coefficients for these systems appear as outliers when plotted as a function of the charge transfer parameter, and removing these systems from the database leads to correlation coefficients with an increased absolute value for the mixed SRP $\boldsymbol{x}$  and SRP $\boldsymbol{x}$ sol DFs for the

H<sub>2</sub>-metal surface and the CH<sub>4</sub>-metal surface systems.

A small improvement over using the SRP $\boldsymbol{x}$ sol mixed DF could be to use a DF that simply mixes the RPBE and the PBEsol exchange-correlation functionals. This would avoid the use of an exchange correlation functional with unbalanced exchange and correlation at the lower  $\boldsymbol{x}=0$  end of the spectrum, i.e., PBEsol.

When it comes to designing mixed functionals incorporating vdW-DF1 or vdW-DF2 correlation, another idea worth testing might be to investigate mixtures of weakly repulsive GGA exchange DFs that are appropriate matches for the vdW1 and vdW2 correlation functionals with the rather repulsive<sup>165</sup> exchange functionals combined with these C functionals in the original vdW-DF1<sup>133</sup> and vdW-DF2<sup>134</sup> DFs. Examples of such exchange functionals have been incorporated in the C09<sup>166</sup> and CX<sup>167</sup> vdW functionals, and other exchange functionals mentioned in Ref.<sup>165</sup>. Another idea would be to explore mixtures of repulsive meta-GGA DFs (such as MS-B86b1<sup>137</sup>) and attractive meta-GGA DFs (such as SCAN<sup>168</sup>) that tend to overestimate respectively underestimate barriers to DC of molecules on metals<sup>169</sup>. It would also be of interest to investigate the performance of mixtures of, or parameterized forms of screened hybrid functionals such as HSE06<sup>124</sup> and screened functionals incorporating van der Waals correlation<sup>164,165</sup>. However, it might be most productive to test such hybrid functionals once a database becomes available that also incorporates good reference values of barrier heights for systems characterized by charge transfer parameters  $< 7$  eV, such as O<sub>2</sub> + Ag(111)<sup>154</sup> and HCl + Au(111)<sup>156</sup>. Such systems presently defy an accurate description based on DFs incorporating GGA exchange<sup>154,156,170</sup>.



## References

- (1) Bagot, P. A. J. Fundamental surface science studies of automobile exhaust catalysis. *J. Mater. Sci. Technol.* **2004**, *20*, 679–694.
- (2) Somorjai, G. A.; Li, Y. Impact of surface chemistry. *Proc. Natl. Acad. Sci.* **2011**, *108*, 917–924.
- (3) Ertl, G. Primary steps in catalytic synthesis of ammonia. *J. Vac. Sci. Technol.* **1983**, *1*, 1247–1253.
- (4) Chorkendorff, I.; Niemantsverdriet, J. W., *Concepts of modern catalysis and kinetics*; John Wiley & Sons, Weinheim: 2017.
- (5) Park, G. B.; Kitsopoulos, T. N.; Borodin, D.; Golibrzuch, K.; Neugeboren, J.; Auerbach, D. J.; Campbell, C. T.; Wodtke, A. M. The kinetics of elementary thermal reactions in heterogeneous catalysis. *Nature Rev. Chem.* **2019**, *3*, 723–732.
- (6) Voet, D.; Voet, J. G., *Biochemistry, 4th Edition*; New York: John Wiley & Sons Inc: 2011.
- (7) Ertl, G. Reactions at surfaces: from atoms to complexity (Nobel lecture). *Angew. Chem. Int. Ed.* **2008**, *47*, 3524–3535.
- (8) Wolcott, C. A.; Medford, A. J.; Studt, F.; Campbell, C. T. Degree of rate control approach to computational catalyst screening. *J. Catal.* **2015**, *330*, 197–207.
- (9) Sabbe, M. K.; Reyniers, M.-F.; Reuter, K. First-principles kinetic modeling in heterogeneous catalysis: an industrial perspective on best-practice, gaps and needs. *Catal. Sci. Technol.* **2012**, *2*, 2010–2024.
- (10) Kroes, G. J. Toward a database of chemically accurate barrier heights for reactions of molecules with metal surfaces. *J. Phys. Chem Lett.* **2015**, *6*, 4106–4114.
- (11) Stegelmann, C.; Andreasen, A.; Campbell, C. T. Degree of rate control: how much the energies of intermediates and transition states control rates. *J. Am. Chem. Soc.* **2009**, *131*, 8077–8082.
- (12) Kroes, G. J.; Díaz, C. Quantum and classical dynamics of reactive scattering of H<sub>2</sub> from metal surfaces. *Chem. Soc. Rev.* **2016**, *45*, 3658–3700.
- (13) Waugh, K. Methanol synthesis. *Catal. Today* **1992**, *15*, 51–75.
- (14) Grabow, L.; Mavrikakis, M. Mechanism of methanol synthesis on Cu through CO<sub>2</sub> and CO hydrogenation. *Acs Catalysis* **2011**, *1*, 365–384.

- (15) Behrens, M.; Studt, F.; Kasatkin, I.; Kühl, S.; Hävecker, M.; Abild-Pedersen, F.; Zander, S.; Girgsdies, F.; Kurr, P.; Knief, B.-L., et al. The active site of methanol synthesis over Cu/ZnO/Al<sub>2</sub>O<sub>3</sub> industrial catalysts. *Science* **2012**, *336*, 893–897.
- (16) Rylander, P. N., *Hydrogenation methods*; Academic Press: London: 1990.
- (17) Veldsink, J. W.; Bouma, M. J.; Schöön, N. H.; Beenackers, A. A. Heterogeneous hydrogenation of vegetable oils: a literature review. *Catal. Rev.: Sci. Eng.* **1997**, *39*, 253–318.
- (18) Blaser, H.-U.; Malan, C.; Pugin, B.; Spindler, F.; Steiner, H.; Studer, M. Selective hydrogenation for fine chemicals: Recent trends and new developments. *Adv. Synth. Catal.* **2003**, *345*, 103–151.
- (19) Chen, B.; Dingerdissen, U.; Krauter, J. G. E.; Rotgerink, H. G. J. L.; Möbus, K.; Ostgard, D. J.; Panster, P.; Riermeier, T.; Seebald, S.; Tacke, T., et al. New developments in hydrogenation catalysis particularly in synthesis of fine and intermediate chemicals. *Appl. Catal. A* **2005**, *280*, 17–46.
- (20) Mäki-Arvela, P.; Hájek, J.; Salmi, T.; Murzin, D. Y. Chemoselective hydrogenation of carbonyl compounds over heterogeneous catalysts. *Appl. Catal. A* **2005**, *292*, 1–49.
- (21) Hu, C.; Creaser, D.; Siahrostami, S.; Grönbeck, H.; Ojagh, H.; Skoglundh, M. Catalytic hydrogenation of C=C and C=O in unsaturated fatty acid methyl esters. *Catal. Sci. Technol.* **2014**, *4*, 2427–2444.
- (22) Gostein, M.; Parhikhteh, H.; Sitz, G. Survival probability of H<sub>2</sub> ( $\nu=1$ ,  $J=1$ ) scattered from Cu(110). *Phys. Rev. Lett.* **1995**, *75*, 342.
- (23) Michelsen, H.; Rettner, C.; Auerbach, D.; Zare, R. Effect of rotation on the translational and vibrational energy dependence of the dissociative adsorption of D<sub>2</sub> on Cu(111). *J. Chem. Phys.* **1993**, *98*, 8294–8307.
- (24) Berger, H.; Leisch, M.; Winkler, A.; Rendulic, K. A search for vibrational contributions to the activated adsorption of H<sub>2</sub> on copper. *Chem. Phys. Lett.* **1990**, *175*, 425–428.
- (25) Kaufmann, S.; Shuai, Q.; Auerbach, D. J.; Schwarzer, D.; Wodtke, A. M. Associative desorption of hydrogen isotopologues from copper surfaces: characterization of two reaction mechanisms. *J. Chem. Phys.* **2018**, *148*, 194703.
- (26) Anger, G.; Winkler, A.; Rendulic, K. Adsorption and desorption kinetics in the systems H<sub>2</sub>/Cu(111), H<sub>2</sub>/Cu(110) and H<sub>2</sub>/Cu(100). *Surf. Sci.* **1989**, *220*, 1–17.

- 1 Chapter
- (27) Hou, H.; Gulding, S.; Rettner, C.; Wodtke, A.; Auerbach, D. The stereo-dynamics of a gas-surface reaction. *Science* **1997**, *277*, 80–82.
  - (28) Comsa, G.; David, R. The purely “fast” distribution of H<sub>2</sub> and D<sub>2</sub> molecules desorbing from Cu(100) and Cu(111) surfaces. *Surf. Sci.* **1982**, *117*, 77–84.
  - (29) Rettner, C.; Michelsen, H.; Auerbach, D. Quantum-state-specific dynam-ics of the dissociative adsorption and associative desorption of H<sub>2</sub> at a Cu(111) surface. *J. Chem. Phys.* **1995**, *102*, 4625–4641.
  - (30) Rettner, C.; Auerbach, D.; Michelsen, H. Dynamical studies of the inter-action of D<sub>2</sub> with a Cu(111) surface. *J. Vac. Sci. Technol. A* **1992**, *10*, 2282–2286.
  - (31) Rettner, C.; Michelsen, H.; Auerbach, D. Determination of quantum-state-specific gas—surface energy transfer and adsorption probabilities as a function of kinetic energy. *Chem. Phys.* **1993**, *175*, 157–169.
  - (32) Hodgson, A.; Samson, P.; Wight, A.; Cottrell, C. Rotational excitation and vibrational relaxation of H<sub>2</sub> ( $\nu=1, J=0$ ) Scattered from Cu(111). *Phys. Rev. Lett.* **1997**, *78*, 963–966.
  - (33) Watts, E.; Sitz, G. O. State-to-state scattering in a reactive system: H<sub>2</sub> ( $\nu=1, j=1$ ) from Cu(100). *J. Chem. Phys.* **2001**, *114*, 4171–4179.
  - (34) Michelsen, H.; Rettner, C.; Auerbach, D. On the influence of surface temperature on adsorption and desorption in the D<sub>2</sub>/Cu(111) system. *Surf. Sci.* **1992**, *272*, 65–72.
  - (35) Andersson, S.; Persson, M. Sticking in the physisorption well: influence of surface structure. *Phys. Rev. Lett.* **1993**, *70*, 202.
  - (36) Cao, K.; Füchsel, G.; Kleyn, A. W.; Juurlink, L. B. Hydrogen adsorption and desorption from Cu(111) and Cu(211). *Phys. Chem. Chem. Phys.* **2018**, *20*, 22477–22488.
  - (37) Harten, U.; Toennies, J. P.; Wöll, C. Molecular beam translational spectroscopy of physisorption bound states of molecules on metal surfaces. I. HD on Cu(111) and Au(111) single crystal surfaces. *J. Chem. Phys.* **1986**, *85*, 2249–2258.
  - (38) Shuai, Q.; Kaufmann, S.; Auerbach, D. J.; Schwarzer, D.; Wodtke, A. M. Evidence for electron–hole pair excitation in the associative desorption of H<sub>2</sub> and D<sub>2</sub> from Au(111). *J. Phys. Chem. Lett.* **2017**, *8*, 1657–1663.
  - (39) Luntz, A.; Brown, J.; Williams, M. Molecular beam studies of H<sub>2</sub> and D<sub>2</sub> dissociative chemisorption on Pt(111). *J. Chem. Phys.* **1990**, *93*, 5240–5246.

- (40) Groot, I.; Ueta, H.; Van der Niet, M.; Kleyn, A.; Juurlink, L. Supersonic molecular beam studies of dissociative adsorption of H<sub>2</sub> on Ru(0001). *J. Chem. Phys.* **2007**, *127*, 244701.
- (41) Cottrell, C.; Carter, R.; Nesbitt, A.; Samson, P.; Hodgson, A. Vibrational state dependence of D<sub>2</sub> dissociation on Ag(111). *J. Chem. Phys.* **1997**, *106*, 4714–4722.
- (42) Murphy, M.; Hodgson, A. Translational energy release in the recombinative desorption of H<sub>2</sub> from Ag(111). *Surf. Sci.* **1997**, *390*, 29–34.
- (43) Murphy, M.; Hodgson, A. Role of surface thermal motion in the dissociative chemisorption and recombinative desorption of D<sub>2</sub> on Ag(111). *Phys. Rev. Lett.* **1997**, *78*, 4458–4461.
- (44) Resch, C.; Berger, H.; Rendulic, K.; Bertel, E. Adsorption dynamics for the system hydrogen/palladium and its relation to the surface electronic structure. *Surf. Sci.* **1994**, *316*, L1105–L1109.
- (45) Beutl, M.; Riedler, M.; Rendulic, K. D. Strong rotational effects in the adsorption dynamics of H<sub>2</sub>/Pd(111): evidence for dynamical steering. *Chem. Phys. Lett.* **1995**, *247*, 249–252.
- (46) Beutl, M.; Lesnik, J.; Rendulic, K.; Hirschl, R.; Eichler, A.; Kresse, G.; Hafner, J. There is a true precursor for hydrogen adsorption after all: the system H<sub>2</sub>/Pd (1 1 1)+ subsurface V. *Chem. Phys. Lett.* **2001**, *342*, 473–478.
- (47) Gostein, M.; Sitz, G. O. Rotational state-resolved sticking coefficients for H<sub>2</sub> on Pd(111): testing dynamical steering in dissociative adsorption. *J. Chem. Phys.* **1997**, *106*, 7378–7390.
- (48) Steinrück, H.-P.; Rendulic, K.; Winkler, A. The sticking coefficient of H<sub>2</sub> on Ni(111) as a function of particle energy and angle of incidence: A test of detailed balancing. *Surf. Sci.* **1985**, *154*, 99–108.
- (49) Robota, H. J.; Vielhaber, W.; Lin, M.-C.; Segner, J.; Ertl, G. Dynamics of interaction of H<sub>2</sub> and D<sub>2</sub> with Ni(110) and Ni(111) surfaces. *Surf. Sci.* **1985**, *155*, 101–120.
- (50) Hayward, D.; Taylor, A. The variation of the sticking probability of hydrogen and deuterium on Ni(111) with energy and angle of incidence. *Chem. Phys. Lett.* **1986**, *124*, 264–267.
- (51) Resch, C.; Zhukov, V.; Lugstein, A.; Berger, H.; Winkler, A.; Rendulic, K. Dynamics of hydrogen adsorption on promoter- and inhibitor-modified nickel surfaces. *Chem. Phys.* **1993**, *177*, 421–431.

- (52) Salmeron, M.; Gale, R. J.; Somorjai, G. A. Molecular beam study of the H<sub>2</sub>-D<sub>2</sub> exchange reaction on stepped platinum crystal surfaces: Dependence on reactant angle of incidence. *J. Chem. Phys.* **1977**, *67*, 5324–5334.
- (53) Gee, A. T.; Hayden, B. E.; Mormiche, C.; Nunney, T. S. The role of steps in the dynamics of hydrogen dissociation on Pt(533). *J. Chem. Phys.* **2000**, *112*, 7660–7668.
- (54) Gostein, M.; Watts, E.; Sitz, G. O. Vibrational relaxation of H<sub>2</sub> ( $\nu = 1$ ,  $J = 1$ ) on Pd(111). *Phys. Rev. Lett.* **1997**, *79*, 2891–2894.
- (55) Goncharova, L. V.; Braun, J.; Ermakov, A. V.; Bishop, G. G.; Smilgies, D.-M.; Hinch, B. J. Cu(001) to HD energy transfer and translational to rotational energy conversion on surface scattering. *J. Chem. Phys.* **2001**, *115*, 7713–7724.
- (56) Nieto, P.; Farías, D.; Miranda, R.; Luppi, M.; Baerends, E. J.; Somers, M. F.; van der Niet, M. J. T. C.; Olsen, R. A.; Kroes, G. J. Diffractive and reactive scattering of H<sub>2</sub> from Ru(0001): experimental and theoretical study. *Phys. Chem. Chem. Phys.* **2011**, *13*, 8583–8597.
- (57) Whaley, K. B.; Yu, C.-f.; Hogg, C. S.; Light, J. C.; Sibener, S. J. Investigation of the spatially anisotropic component of the laterally averaged molecular hydrogen/Ag(111) physisorption potential. *J. Chem. Phys.* **1985**, *83*, 4235–4255.
- (58) Berndt, R.; Toennies, J. P.; Wöll, C. Evidence for coupled rotational and phonon quantum excitation in the scattering of a nearly monoenergetic HD beam from the Ni(001) surface. *J. Chem. Phys.* **1990**, *92*, 1468–1477.
- (59) Laurent, G.; Barredo, D.; Farías, D.; Miranda, R.; Díaz, C.; Riviere, P.; Somers, M. F.; Martín, F. Experimental and theoretical study of rotationally inelastic diffraction of D<sub>2</sub> from NiAl(110). *Phys. Chem. Chem. Phys.* **2010**, *12*, 14501–14507.
- (60) Johansson, M.; Skulason, E.; Nielsen, G.; Murphy, S.; Nielsen, R. M.; Chorkendorff, I. Hydrogen adsorption on palladium and palladium hydride at 1 bar. *Surf. Sci.* **2010**, *604*, 718–729.
- (61) Fiordaliso, E. M.; Murphy, S.; Nielsen, R.; Dahl, S.; Chorkendorff, I. H<sub>2</sub> splitting on Pt, Ru and Rh nanoparticles supported on sputtered HOPG. *Surf. Sci.* **2012**, *606*, 263–272.
- (62) Rendulic, K.; Anger, G.; Winkler, A. Wide range nozzle beam adsorption data for the systems H<sub>2</sub>/nickel and H<sub>2</sub>/Pd(100). *Surf. Sci.* **1989**, *208*, 404–424.

- (63) Sementa, L.; Wijzenbroek, M.; Van Kolck, B. J.; Somers, M. F.; Al-Halabi, A.; Busnengo, H. F.; Olsen, R. A.; Kroes, G. J.; Rutkowski, M.; Thewes, C., et al. Reactive scattering of H<sub>2</sub> from Cu(100): comparison of dynamics calculations based on the specific reaction parameter approach to density functional theory with experiment. *J. Chem. Phys.* **2013**, *138*, 044708.
- (64) Cowin, J. P.; Yu, C.-F.; Sibener, S. J.; Wharton, L. HD scattering from Pt(111): rotational excitation probabilities. *J. Chem. Phys.* **1983**, *79*, 3537–3549.
- (65) Yu, C.-f.; Whaley, K. B.; Hogg, C. S.; Sibener, S. J. Investigation of the spatially isotropic component of the laterally averaged molecular hydrogen/Ag(111) physisorption potential. *J. Chem. Phys.* **1985**, *83*, 4217–4234.
- (66) Nieto, P.; Pijper, E.; Barredo, D.; Laurent, G.; Olsen, R. A.; Baerends, E.-J.; Kroes, G. J.; Farías, D. Reactive and nonreactive scattering of H<sub>2</sub> from a metal surface is electronically adiabatic. *Science* **2006**, *312*, 86–89.
- (67) Bertino, M. F.; Hofmann, F.; Toennies, J. P. The effect of dissociative chemisorption on the diffraction of D<sub>2</sub> from Ni(110). *J. Chem. Phys.* **1997**, *106*, 4327–4338.
- (68) Farías, D.; Díaz, C.; Rivière, P.; Busnengo, H. F.; Nieto, P.; Somers, M. F.; Kroes, G. J.; Salin, A.; Martín, F. In-plane and out-of-plane diffraction of H<sub>2</sub> from metal surfaces. *Phys. Rev. Lett.* **2004**, *93*, 246104.
- (69) King, D. A.; Wells, M. G. Molecular beam investigation of adsorption kinetics on bulk metal targets: Nitrogen on tungsten. *Surf. Sci.* **1972**, *29*, 454–482.
- (70) Michelsen, H. A.; Auerbach, D. J. A critical examination of data on the dissociative adsorption and associative desorption of hydrogen at copper surfaces. *J. Chem. Phys.* **1991**, *94*, 7502–7520.
- (71) Wetzig, D.; Dopheide, R.; Rutkowski, M.; David, R.; Zacharias, H. Rotational Alignment in Associative Desorption of D<sub>2</sub> ( $\nu'' = 0$  and 1) from Pd(100). *Phys. Rev. Lett.* **1996**, *76*, 463–466.
- (72) Darling, G. R.; Holloway, S. Vibrational effects in the associative desorption of H<sub>2</sub>. *Surf. Sci.* **1992**, *268*, L305–L310.
- (73) Gross, A.; Hammer, B.; Scheffler, M.; Brenig, W. High-dimensional quantum dynamics of adsorption and desorption of H<sub>2</sub> at Cu(111). *Phys. Rev. Lett.* **1994**, *73*, 3121.

- 1 Chapter
- (74) Darling, G. R.; Holloway, S. The dissociation of diatomic molecules at surfaces. *Rep. Prog. Phys.* **1995**, *58*, 1595–1672.
  - (75) Dai, J.; Light, J. C. Six dimensional quantum dynamics study for dissociative adsorption of H<sub>2</sub> on Cu(111) surface. *J. Chem. Phys.* **1997**, *107*, 1676–1679.
  - (76) Kroes, G. J.; Baerends, E. J.; Mowrey, R. C. Six-dimensional quantum dynamics of dissociative chemisorption of ( $v=0, j=0$ ) H<sub>2</sub> on Cu(100). *Phys. Rev. Lett.* **1997**, *78*, 3309–3323.
  - (77) Dai, J.; Light, J. C. The steric effect in a full dimensional quantum dynamics simulation for the dissociative adsorption of H<sub>2</sub> on Cu(111). *J. Chem. Phys.* **1998**, *108*, 7816–7820.
  - (78) Wang, Z. S.; Darling, G. R.; Holloway, S. Surface temperature dependence of the inelastic scattering of hydrogen molecules from metal surfaces. *Phys. Rev. Lett.* **2001**, *87*, 226102.
  - (79) Díaz, C.; Pijper, E.; Olsen, R.; Busnengo, H.; Auerbach, D.; Kroes, G. Chemically accurate simulation of a prototypical surface reaction: H<sub>2</sub> dissociation on Cu(111). *Science* **2009**, *326*, 832–834.
  - (80) Nattino, F.; Díaz, C.; Jackson, B.; Kroes, G. J. Effect of surface motion on the rotational quadrupole alignment parameter of D<sub>2</sub> reacting on Cu(111). *Phys. Rev. Lett.* **2012**, *108*, 236104.
  - (81) Kroes, G. J.; Díaz, C.; Pijper, E.; Olsen, R. A.; Auerbach, D. J. Apparent failure of the Born–Oppenheimer static surface model for vibrational excitation of molecular hydrogen on copper. *Proc. Natl. Acad. Sci.* **2010**, *107*, 20881–20886.
  - (82) Wijzenbroek, M.; Somers, M. Static surface temperature effects on the dissociation of H<sub>2</sub> and D<sub>2</sub> on Cu(111). *J. Chem. Phys.* **2012**, *137*, 054703.
  - (83) Marashdeh, A.; Casolo, S.; Sementa, L.; Zacharias, H.; Kroes, G. J. Surface temperature effects on dissociative chemisorption of H<sub>2</sub> on Cu(100). *J. Phys. Chem. C* **2013**, *117*, 8851–8863.
  - (84) Nattino, F.; Genova, A.; Guijt, M.; Muzas, A. S.; Díaz, C.; Auerbach, D. J.; Kroes, G. J. Dissociation and recombination of D<sub>2</sub> on Cu(111): Ab initio molecular dynamics calculations and improved analysis of desorption experiments. *J. Chem. Phys.* **2014**, *141*, 124705.
  - (85) Smeets, E. W. F.; Fücksel, G.; Kroes, G. J. Quantum dynamics of dissociative chemisorption of H<sub>2</sub> on the Stepped Cu(211) Surface. *J. Phys. Chem. C* **2019**, *123*, 23049–23063.

- (86) Zhu, L.; Zhang, Y.; Zhang, L.; Zhou, X.; Jiang, B. Unified and transferable description of dynamics of H<sub>2</sub> dissociative adsorption on multiple copper surfaces via machine learning. *Phys. Chem. Chem. Phys.* **2020**, *22*, 13958–13964.
- (87) Smeets, E. W. F.; Kroes, G. J. Performance of Made Simple Meta-GGA Functionals with rVV10 Nonlocal Correlation for H<sub>2</sub>+ Cu(111), D<sub>2</sub>+Ag(111), H<sub>2</sub>+Au(111), and D<sub>2</sub>+Pt(111). *J. Phys. Chem. C* **2021**, *125*, 8993–9010.
- (88) Smits, B.; Somers, M. F. Beyond the static corrugation model: dynamic surfaces with the embedded atom method. *J. Chem. Phys.* **2021**, *154*, 074710.
- (89) Godsí, O.; Corem, G.; Alkoby, Y.; Cantin, J. T.; Krems, R. V.; Somers, M. F.; Meyer, J.; Kroes, G. J.; Maniv, T.; Alexandrowicz, G. A general method for controlling and resolving rotational orientation of molecules in molecule-surface collisions. *Nat. Commun.* **2017**, *8*, 15357.
- (90) Chadwick, H.; Somers, M. F.; Stewart, A. C.; Alkoby, Y.; Carter, T. J. D.; Butkovicova, D.; Alexandrowicz, G. Stopping molecular rotation using coherent ultra-low-energy magnetic manipulations. *Nat. Commun.* **2022**, *13*.
- (91) Hohenberg, P.; Kohn, W. Inhomogeneous electron gas. *Phys. Rev.* **1964**, *136*, B864–B871.
- (92) Kohn, W.; Sham, L. J. Self-consistent equations including exchange and correlation effects. *Phys. Rev.* **1965**, *140*, A1133–A1138.
- (93) Migliorini, D.; Chadwick, H.; Kroes, G. J. Methane on a stepped surface: Dynamical insights on the dissociation of CHD<sub>3</sub> on Pt(111) and Pt(211). *J. Chem. Phys.* **2018**, *149*, 094701.
- (94) Nour Ghassemi, E.; Somers, M.; Kroes, G. J. Test of the transferability of the specific reaction parameter functional for H<sub>2</sub>+ Cu(111) to D<sub>2</sub>+ Ag(111). *J. Phys. Chem. C* **2018**, *122*, 22939–22952.
- (95) Ghassemi, E. N.; Smeets, E. W. F.; Somers, M. F.; Kroes, G. J.; Groot, I. M.; Juurlink, L. B.; Füchsel, G. Transferability of the specific reaction parameter density functional for H<sub>2</sub>+ Pt(111) to H<sub>2</sub>+ Pt(211). *J. Phys. Chem. C* **2019**, *123*, 2973–2986.



- (96) Migliorini, D.; Chadwick, H.; Nattino, F.; Gutiérrez-González, A.; Dombrowski, E.; High, E. A.; Guo, H.; Utz, A. L.; Jackson, B.; Beck, R. D., et al. Surface reaction barriometry: methane dissociation on flat and stepped transition-metal surfaces. *J. Phys. Chem. Lett.* **2017**, *8*, 4177–4182.
- (97) Chadwick, H.; Gutiérrez-González, A.; Beck, R. D.; Kroes, G. J. Transferability of the SRP32-vdW specific reaction parameter functional to CHD<sub>3</sub> dissociation on Pt(110)-(2×1). *J. Chem. Phys.* **2019**, *150*, 124702.
- (98) Jackson, B. Direct and trapping-mediated pathways to dissociative chemisorption: CH<sub>4</sub> dissociation on Ir (111) with step defects. *J. Chem. Phys.* **2020**, *153*, 034704.
- (99) Luntz, A. C.; Persson, M. How adiabatic is activated adsorption/associative desorption? *The Journal of chemical physics* **2005**, *123*, 074704.
- (100) Muzas, A. S.; Juaristi, J. I.; Alducin, M.; Díez Muiño, R.; Kroes, G. J.; Díaz, C. Vibrational deexcitation and rotational excitation of H<sub>2</sub> and D<sub>2</sub> scattered from Cu(111): adiabatic versus non-adiabatic dynamics. *J. Chem. Phys.* **2012**, *137*, 064707.
- (101) Juaristi, J.; Alducin, M.; Muiño, R. D.; Busnengo, H. F.; Salin, A. Role of electron-hole pair excitations in the dissociative adsorption of diatomic molecules on metal surfaces. *Phys. Rev. Lett.* **2008**, *100*, 116102.
- (102) Füchsel, G.; Schimka, S.; Saalfrank, P. On the role of electronic friction for dissociative adsorption and scattering of hydrogen molecules at a Ru(0001) surface. *J. Phys. Chem. A* **2013**, *117*, 8761–8769.
- (103) Sexl, T. Ergänzung zu B. Baule "Theoretische Behandlung der Erscheinungen in verdünnten Gasen". *Annalen der Physik* **1926**, *385*, 515–523.
- (104) Gross, A. Theoretical surface science. *A Microscopic Perspective. Originally published in the series: Advanced Texts in Physics*, **2003**, 132.
- (105) Busnengo, H.; Dong, W.; Sautet, P.; Salin, A. Surface temperature dependence of rotational excitation of H<sub>2</sub> scattered from Pd (111). *Phys. Rev. Lett.* **2001**, *87*, 127601.
- (106) Busnengo, H.; Di Césare, M.; Dong, W.; Salin, A. Surface temperature effects in dynamic trapping mediated adsorption of light molecules on metal surfaces: H<sub>2</sub> on Pd (111) and Pd (110). *Phys. Rev. B* **2005**, *72*, 125411.

- (107) Goerigk, L.; Hansen, A.; Bauer, C.; Ehrlich, S.; Najibi, A.; Grimme, S. A look at the density functional theory zoo with the advanced GMTKN55 database for general main group thermochemistry, kinetics and noncovalent interactions. *Phys. Chem. Chem. Phys.* **2017**, *19*, 32184–32215.
- (108) Mardirossian, N.; Head-Gordon, M. Thirty years of density functional theory in computational chemistry: an overview and extensive assessment of 200 density functionals. *Mol. Phys.* **2017**, *115*, 2315–2372.
- (109) Morgante, P.; Peverati, R. ACCDB: A collection of chemistry databases for broad computational purposes. *J. Comput. Chem.* **2019**, *40*, 839–848.
- (110) Peverati, R.; Truhlar, D. G. Quest for a universal density functional: the accuracy of density functionals across a broad spectrum of databases in chemistry and physics. *Philos. Trans. R. Soc., A* **2014**, *372*, 20120476.
- (111) Wellendorff, J.; Lundgaard, K. T.; Møgelhøj, A.; Petzold, V.; Landis, D. D.; Nørskov, J. K.; Bligaard, T.; Jacobsen, K. W. Density functionals for surface science: Exchange-correlation model development with Bayesian error estimation. *Phys. Rev. B* **2012**, *85*, 235149.
- (112) Mallikarjun Sharada, S.; Karlsson, R. K. B.; Maimaiti, Y.; Voss, J.; Bligaard, T. Adsorption on transition metal surfaces: Transferability and accuracy of DFT using the ADS41 dataset. *Phys. Rev. B* **2019**, *100*, 035439.
- (113) Wellendorff, J.; Silbaugh, T. L.; Garcia-Pintos, D.; Nørskov, J. K.; Bligaard, T.; Studt, F.; Campbell, C. T. A benchmark database for adsorption bond energies to transition metal surfaces and comparison to selected DFT functionals. *Surf. Sci.* **2015**, *640*, 36–44.
- (114) Schmidt, P. S.; Thygesen, K. S. Benchmark database of transition metal surface and adsorption energies from many-body perturbation theory. *J. Phys. Chem. C* **2018**, *122*, 4381–4390.
- (115) Duanmu, K.; Truhlar, D. G. Validation of density functionals for adsorption energies on transition metal surfaces. *J. Chem. Theory. Comp.* **2017**, *13*, 835–842.
- (116) Hensley, A. J.; Ghale, K.; Rieg, C.; Dang, T.; Anderst, E.; Studt, F.; Campbell, C. T.; McEwen, J.-S.; Xu, Y. DFT-based method for more accurate adsorption energies: an adaptive sum of energies from RPBE and vdW density functionals. *J. Phys. Chem. C* **2017**, *121*, 4937–4945.
- (117) Mahlberg, D.; Sakong, S.; Forster-Tonigold, K.; Groß, A. Improved DFT adsorption energies with semiempirical dispersion corrections. *J. Chem. Theory. Comp.* **2019**, *15*, 3250–3259.

- 1 Chapter
- (118) Silbaugh, T. L.; Campbell, C. T. Energies of formation reactions measured for adsorbates on late transition metal surfaces. *J. Phys. Chem. C* **2016**, *120*, 25161–25172.
- (119) <http://suncat.slac.stanford.edu/catapp/>.
- (120) Hummelshøj, J. S.; Abild-Pedersen, F.; Studt, F.; Bligaard, T.; Nørskov, J. K. CatApp: a web application for surface chemistry and heterogeneous catalysis. *Angew. Chem., Int. Ed.* **2012**, *51*, 272–274.
- (121) Hammer, B.; Hansen, L. B.; Nørskov, J. K. Improved adsorption energetics within density-functional theory using revised Perdew-Burke-Ernzerhof functionals. *Phys. Rev. B* **1999**, *59*, 7413–7421.
- (122) Mallikarjun Sharada, S.; Bligaard, T.; Luntz, A. C.; Kroes, G. J.; Nørskov, J. K. SBH10: A benchmark database of barrier heights on transition metal surfaces. *J. Phys. Chem. C* **2017**, *121*, 19807–19815.
- (123) Sun, J.; Haunschild, R.; Xiao, B.; Bulik, I. W.; Scuseria, G. E.; Perdew, J. P. Semilocal and hybrid meta-generalized gradient approximations based on the understanding of the kinetic-energy-density dependence. *J. Chem. Phys.* **2013**, *138*, 044113.
- (124) Krukau, A. V.; Vydrov, O. A.; Izmaylov, A. F.; Scuseria, G. E. Influence of the exchange screening parameter on the performance of screened hybrid functionals. *J. Chem. Phys.* **2006**, *125*, 224106.
- (125) Perdew, J. P.; Schmidt, K. Jacob’s ladder of density functional approximations for the exchange–correlation energy, in *Density Functional Theory and its Application to Materials*, edited by V. van Doren, C. van Alsenoy, and P. Geerlings. *AIP Conf. Proc.* **2001**, *577*, 1–20.
- (126) Perdew, J. P. Climbing the ladder of density functional approximations. *MRS bull.* **2013**, *38*, 743–750.
- (127) Peverati, R.; Truhlar, D. G. An improved and broadly accurate local approximation to the exchange–correlation density functional: The MN12-L functional for electronic structure calculations in chemistry and physics. *Phys. Chem. Chem. Phys.* **2012**, *14*, 13171–13174.
- (128) Peverati, R.; Truhlar, D. G. Exchange–correlation functional with good accuracy for both structural and energetic properties while depending only on the density and its gradient. *J. Chem. Theory Comput.* **2012**, *8*, 2310–2319.
- (129) Kroes, G. J. Computational approaches to dissociative chemisorption on metals: towards chemical accuracy. *Phys. Chem. Chem. Phys.* **2021**, *23*, 8962–9048.

- (130) Wijzenbroek, M.; Kroes, G. J. The effect of the exchange-correlation functional on H<sub>2</sub> dissociation on Ru(0001). *J. Chem. Phys.* **2014**, *140*, 084702.
- (131) Nattino, F.; Migliorini, D.; Kroes, G. J.; Dombrowski, E.; High, E. A.; Killelea, D. R.; Utz, A. L. Chemically accurate simulation of a polyatomic molecule-metal surface reaction. *J. Phys. Chem. Lett.* **2016**, *7*, 2402–2406.
- (132) **Tchakoua, T**; Smeets, E. W.; Somers, M.; Kroes, G. J. Toward a Specific Reaction Parameter Density Functional for H<sub>2</sub>+ Ni(111): Comparison of Theory with Molecular Beam Sticking Experiments. *J. Phys. Chem. C* **2019**, *123*, 20420–20433.
- (133) Dion, M.; Rydberg, H.; Schröder, E.; Langreth, D. C.; Lundqvist, B. I. Van der Waals Density Functional for General Geometries. *Phys. Rev. Lett.* **2004**, *92*, 246401.
- (134) Lee, K.; Murray, É. D.; Kong, L.; Lundqvist, B. I.; Langreth, D. C. Higher-accuracy van der Waals density functional. *Phys. Rev. B* **2010**, *82*, 081101.
- (135) Madsen, G. K. H. Functional form of the generalized gradient approximation for exchange: The PBE $\alpha$  functional. *Phys. Rev. B* **2007**, *75*, 195108.
- (136) Ghassemi, E. N.; Wijzenbroek, M.; Somers, M. F.; Kroes, G. J. Chemically accurate simulation of dissociative chemisorption of D<sub>2</sub> on Pt(111). *Chem. Phys. Lett.* **2017**, *683*, 329–335.
- (137) Smeets, E. W. F.; Voss, J.; Kroes, G. J. Specific Reaction Parameter Density Functional Based on the Meta-Generalized Gradient Approximation: Application to H<sub>2</sub>+Cu(111) and H<sub>2</sub>+Ag(111). *J. Phys. Chem. A* **2019**, *123*, 5395–5406.
- (138) Garza, A. J.; Bell, A. T.; Head-Gordon, M. Nonempirical meta-generalized gradient approximations for modeling chemisorption at metal surfaces. *J. Chem. Theory Comput.* **2018**, *14*, 3083–3090.
- (139) Berger, H. F.; Rendulic, K. D. An investigation of vibrationally assisted adsorption: the cases H<sub>2</sub>/Cu(110) and H<sub>2</sub>/Al(110). *Surf. Sci.* **1991**, *253*, 325–333.
- (140) Powell, A. D.; Kroes, G. J.; Doblhoff-Dier, K. Quantum Monte Carlo calculations on dissociative chemisorption of H<sub>2</sub>+ Al (110): minimum barrier heights and their comparison to DFT values. *J. Chem. Phys.* **2020**, *153*, 224701.

- 1 Chapter
- (141) Guo, H.; Menzel, J. P.; Jackson, B. Quantum dynamics studies of the dissociative chemisorption of CH<sub>4</sub> on the steps and terraces of Ni(211). *J. Chem. Phys.* **2018**, *149*, 244704.
- (142) Smeets, E. W. F.; Kroes, G. J. Designing new SRP density functionals including non-local vdW-DF2 correlation for H<sub>2</sub> + Cu(111) and their transferability to H<sub>2</sub> + Ag(111), Au(111) and Pt(111). *Phys. Chem. Chem. Phys.* **2021**, *23*, 7875–7901.
- (143) Jiang, B.; Guo, H. Six-dimensional quantum dynamics for dissociative chemisorption of H<sub>2</sub> and D<sub>2</sub> on Ag (111) on a permutation invariant potential energy surface. *Physical Chemistry Chemical Physics* **2014**, *16*, 24704–24715.
- (144) Wijzenbroek, M.; Helstone, D.; Meyer, J.; Kroes, G. J. Dynamics of H<sub>2</sub> dissociation on the close-packed (111) surface of the noblest metal: H<sub>2</sub>+ Au(111). *J. Chem. Phys.* **2016**, *145*, 144701.
- (145) Larsen, J. H.; Holmblad, P. M.; Chorkendorff, I. Dissociative sticking of CH<sub>4</sub> on Ru(0001). *J. Chem. Phys.* **1999**, *110*, 2637–2642.
- (146) Luntz, A. CH<sub>4</sub> dissociation on Ni(100): Comparison of a direct dynamical model to molecular beam experiments. *J. Chem. Phys.* **1995**, *102*, 8264–8269.
- (147) Rettner, C. T.; Stein, H. Effect of vibrational energy on the dissociative chemisorption of N<sub>2</sub> on Fe(111). *J. Chem. Phys.* **1987**, *87*, 770–771.
- (148) Rettner, C. T.; Stein, H. Effect of translational energy on the chemisorption of N<sub>2</sub> on Fe(111): Activated dissociation via a precursor state. *Phys. Rev. Lett.* **1987**, *59*, 2768–2771.
- (149) Pfnür, H. E.; Rettner, C. T.; Lee, J.; Madix, R. J.; Auerbach, D. J. Dynamics of the activated dissociative chemisorption of N<sub>2</sub> on W(110): A molecular beam study. *J. Chem. Phys.* **1986**, *85*, 7452–7466.
- (150) Rettner, C. T.; Schweizer, E. K.; Stein, H. Dynamics of the chemisorption of N<sub>2</sub> on W(100): Precursor-mediated and activated dissociation. *J. Chem. Phys.* **1990**, *93*, 1442–1454.
- (151) Rettner, C. T.; Schweizer, E. K.; Stein, H.; Auerbach, D. J. Role of surface temperature in the precursor-mediated dissociative chemisorption of N<sub>2</sub> on W(100). *Phys. Rev. Lett.* **1988**, *61*, 986–989.
- (152) Rettner, C. T.; Stein, H.; Schweizer, E. K. Effect of collision energy and incidence angle on the precursor-mediated dissociative chemisorption of N<sub>2</sub> on W (100). *J. Chem. Phys.* **1988**, *89*, 3337–3341.

- (153) Beutl, M.; Rendulic, K. D.; Castro, G. R. Does the rotational state of a molecule influence trapping in a precursor? An investigation of N<sub>2</sub>/W(100), CO/FeSi(100) and O<sub>2</sub>/Ni(111). *Surf. Sci.* **1997**, *385*, 97–106.
- (154) Gerrits, N.; Smeets, E. W. F.; Vuckovic, S.; Powell, A. D.; Doblhoff-Dier, K.; Kroes, G. J. Density functional theory for molecule–metal surface reactions: When does the generalized gradient approximation get it right, and what to do if it does not. *J. Phys. Chem. Lett.* **2020**, *11*, 10552–10560.
- (155) Hundt, P. M.; Jiang, B.; van Reijzen, M. E.; Guo, H.; Beck, R. D. Vibrationally promoted dissociation of water on Ni(111). *Science* **2014**, *344*, 504–507.
- (156) Gerrits, N.; Geweke, J.; Smeets, E. W. F.; Voss, J.; Wodtke, A. M.; Kroes, G. J. Closing the Gap Between Experiment and Theory: Reactive Scattering of HCl from Au(111). *J. Phys. Chem. C* **2020**, *124*, 15944–15960.
- (157) Österlund, L.; Zoric-Acute, I.; Kasemo, B. Dissociative sticking of O<sub>2</sub> on Al(111). *Phys. Rev. B* **1997**, *55*, 15452–15455.
- (158) Kurahashi, M.; Yamauchi, Y. Steric effect in O<sub>2</sub> sticking on Al(111): Preference for parallel geometry. *Phys. Rev. Lett.* **2013**, *110*, 246102.
- (159) Raukema, A.; Butler, D. A.; Kleyn, A. W. The interaction of oxygen with the Ag(110) surface. *J. Phys.: Condens. Matter* **1996**, *8*, 2247–2263.
- (160) Kurahashi, M. Chemisorption of aligned O<sub>2</sub> on Ag(110). *J. Chem. Phys.* **2019**, *151*, 084702.
- (161) Hall, J.; Saksager, O.; Chorkendorff, I. Dissociative chemisorption of O<sub>2</sub> on Cu(100). Effects of mechanical energy transfer and recoil. *Chem. Phys. Lett.* **1993**, *216*, 413–417.
- (162) Minniti, M.; Fariás, D.; Perna, P.; Miranda, R. Enhanced selectivity towards O<sub>2</sub> and H<sub>2</sub> dissociation on ultrathin Cu films on Ru(0001). *J. Chem. Phys.* **2012**, *137*, 074706.
- (163) Kirkpatrick, J.; McMorro, B.; Turban, D. H.; Gaunt, A. L.; Spencer, J. S.; Matthews, A. G. D. G.; Obika, A.; Thiry, L.; Fortunato, M.; Pfau, D., et al. Pushing the frontiers of density functionals by solving the fractional electron problem. *Science* **2021**, *374*, 1385–1389.
- (164) Shukla, V.; Jiao, Y.; Frostenson, C. M.; Hyldgaard, P. vdW-DF-ahcx: a range-separated van der Waals density functional hybrid. *J. Phys.: Condens. Matter* **2021**, *34*, 025902.

- (165) Shukla, V.; Jiao, Y.; Lee, J.-H.; Schröder, E.; Neaton, J. B.; Hyldgaard, P. Accurate Nonempirical Range-Separated Hybrid van der Waals Density Functional for Complex Molecular Problems, Solids, and Surfaces. *Phys. Rev. X* **2022**, *12*, 041003.
- (166) Cooper, V. R. Van der Waals density functional: An appropriate exchange functional. *Phys. Rev. B* **2010**, *81*, 161104.
- (167) Berland, K.; Hyldgaard, P. Exchange functional that tests the robustness of the plasmon description of the van der Waals density functional. *Phys. Rev. B* **2014**, *89*, 035412.
- (168) Sun, J.; Ruzsinszky, A.; Perdew, J. P. Strongly constrained and appropriately normed semilocal density functional. *Phys. Rev. Lett.* **2015**, *115*, 036402.
- (169) **Tchakoua, T.**; Gerrits, N.; Smeets, E. W. F.; Kroes, G. J. SBH17: Benchmark Database of Barrier Heights for Dissociative Chemisorption on Transition Metal Surfaces. *J. Chem. Theory Comput.* **2023**, *19*, 245–270.
- (170) Behler, J.; Delley, B.; Lorenz, S.; Reuter, K.; Scheffler, M. Dissociation of O<sub>2</sub> at Al(111): The role of spin selection rules. *Phys. Rev. Lett.* **2005**, *94*, 036104.

## Towards a Specific Reaction Parameter Density Functional for $\text{H}_2 + \text{Ni}(111)$ : Comparison of Theory with Molecular Beam Sticking Experiments

This Chapter is based on:

**Tchakoua, T**; Smeets, E. W.; Somers, M.; Kroes, G. J. Toward a Specific Reaction Parameter Density Functional for  $\text{H}_2 + \text{Ni}(111)$ : Comparison of Theory with Molecular Beam Sticking Experiments. *J. Phys. Chem. C* **2019**, *123*, 20420–20433

### Abstract

Accurate barriers for rate controlling elementary surface reactions are key to understanding, controlling and predicting the rate of overall heterogeneously catalyzed processes. The specific reaction parameter approach to density functional theory (SRP-DFT) in principle allows chemically accurate barrier heights to be obtained for molecules dissociating on metal surfaces, and such accurate barriers are now available for four  $\text{H}_2$ -metal and three  $\text{CH}_4$ -metal systems. Also, there is some evidence that SRP density functionals (SRP-DFs) may be transferable among systems in which the same molecule interacts with a low index face of metals belonging to the same group. To extend the SRP database, here we take a first step to obtain an SRP-DF for  $\text{H}_2 + \text{Ni}(111)$ , by comparing sticking probabilities ( $S_0$ ) computed with the quasi-classical trajectory method with  $S_0$  measured in several molecular beam experiments, using potential energy surfaces computed with several density functionals. We find that the SRP-DF for  $\text{H}_2 + \text{Pt}(111)$  is not transferable to  $\text{H}_2 + \text{Ni}(111)$ . On the other hand, the PBE-vdW2 functional describes the molecular beam experiments on  $\text{H}_2 + \text{Ni}(111)$  we deem to be most accurate with chemical accuracy, and may therefore be considered a candidate SRP-DF for this system, of which the quality still



needs to be confirmed through comparison with an experiment it was not fitted to. However, the different molecular beam sticking measurements we considered showed discrepancies with one another and with the theory for incidence energies  $> 0.2$  eV, and it would be good if better defined and more accurate experiments would be done for these energies to resolve these differences.

## 2.1 Introduction

The dissociative chemisorption (DC) of a molecule on a metal surface is often the rate-controlling step of a heterogeneously catalyzed process, famous examples of such processes being steam reforming<sup>1</sup> and ammonia production<sup>2</sup>. These processes are important to industrial companies<sup>3</sup>(e.g., the steam reforming reaction is used for the commercial production of the hydrogen<sup>1</sup>) and improving the efficiency of heterogeneously catalyzed processes is of huge importance.

To understand how heterogeneous catalysis works from a quantitative point of view, being able to accurately model DC is important. For this, it is relevant to have an accurate potential energy surface (PES) with accurate barrier heights available. Experimentally, it is not possible to measure the barrier height for DC. The observable usually measured experimentally is the sticking probability  $S_0$ . Therefore, the only way to assess a computed barrier height and PES is through a theoretical approach in which a PES is used in dynamics calculations to calculate  $S_0$  as a function of average incidence energy and comparison with experiment for this and other observables<sup>4,5</sup>. Only when experimental data are reproduced to a sufficiently large extent can a claim be made that the computed barrier is of high accuracy, with chemical accuracy defined as accurate to within 1 kcal/mol<sup>4-6</sup>.

Unfortunately, *ab initio* or non-empirical electronic structure methods that can compute molecule-metal surface interaction energies to within chemical accuracy are not yet available (see also Refs.<sup>6</sup> and<sup>7</sup>, and **Chapter 3**). Presently, the most efficient electronic structure method that can be used to map out the PES of the interaction of the molecule with metal surface is density functional theory (DFT) using an approximate exchange-correlation (XC) functional, which is usually taken at the generalized gradient approximation (GGA) level<sup>8-10</sup>. With the best GGA functional for barrier heights (MOHLYP) the mean unsigned error (MUE) for a database of gas phase barrier heights is 3.8 kcal/mol<sup>11</sup>. Even with the highest level semi-local functionals chemical accuracy has not been achieved yet for such reactions, the best result (MUE=1.8 kcal/mol) having been obtained with a functional at the meta non-separable gradient approximation level<sup>12</sup>. From the benchmark study we will present in **Chapter 3**, the PBE

GGA functional performs best on the SBH17 database for DC on metal surfaces, with a MAE of 2.4 kcal/mol.

To overcome this problem of DFT accuracy, Díaz et al.<sup>4</sup> proposed an implementation of specific reaction parameter (SRP) DFT (SRP-DFT). In this approach the exchange-correlation functional is fitted with one adjustable parameter to a set of experimental data for a molecule reacting on the surface that is particular sensitive to the reaction barrier height. Ideally, the quality of the SRP functional is tested by checking that it can also be used to reproduce other experiments on the same system, to which it was not fitted<sup>4,5</sup>. With this SRP approach, one might say we have now obtained a small database of chemically accurate barriers for molecules reacting on metal surfaces, as discussed in **Chapter 3**.

In some cases, transferability of an SRP density functional (SRP-DF) among similar systems has been established. In the study of Migliorini et al.<sup>13</sup>, it has been shown that the SRP-DF for CH<sub>4</sub>+Ni(111) could also be used to obtain chemical accuracy for CH<sub>4</sub>+Pt(111). This suggests that an SRP-DF for a specific molecule interacting with a low index face of a specific metal might also be an SRP-DF for the same molecule reacting on a low index face of a metal belonging to the same group. However, this type of transferability was found not to hold when the SRP-DF for H<sub>2</sub>+Cu(111) was tested for D<sub>2</sub>+Ag(111)<sup>14</sup>, for which chemical accuracy was not obtained. Clearly more tests are needed on to what extent SRP-DFs might be transferable among similar systems, and how the SRP-DFs should be designed to achieve maximum transferability.

Given the number of the above systems for which the SRP functional could be fitted to reproduce the experimental results, there is no a doubt that the approach can be effective. However, this effort is still at an early stage, and more efforts are needed to extend the database. Being semi-empirical and in need of validation, the SRP-DFT approach is not without problems. One important problem for some systems concerns the availability of accurate and well-defined experiments (see H<sub>2</sub>+Pd(111)<sup>15</sup> and H<sub>2</sub>+Pt(111)<sup>16</sup>). Obviously, the semi-empirical SRP-DFT approach is no more accurate than the underlying experimental data. This problem can become severe if different sets of measurements of the sticking probability for a specific system show widely differing results<sup>15</sup>.

H<sub>2</sub> DC on a metal surface may be considered as a benchmark system for electronic structure and surface science reaction dynamics methods<sup>17-20</sup>, for several reasons. First of all, hydrogen is a small and simple molecule just containing two electrons. If the surface degrees of freedom are neglected, the PES of the H<sub>2</sub> reacting on this surface depends on only six degrees of freedom (six-dimensional, 6D), and can be mapped out easily. In principle, also the degrees of freedom of the surface atoms should be taken in to account (the

surface phonons) and electron-hole (e-h) pair excitation<sup>6,18,21,22</sup>. However, for H<sub>2</sub> dissociation on metal surfaces, the approximation of keeping the surface static with the metal atoms in their ideal lattice position (neglecting surface phonons) has been proven to work well for activated sticking on cold surfaces (surface temperature not larger than room temperature)<sup>20</sup>. Likewise, it is usually a good approximation to neglect electron-hole (e-h) pair excitation<sup>20</sup>, as also shown in very recent work<sup>23,24</sup>. Finally, a large amount of experimental data is available for reaction of H<sub>2</sub> on metal surfaces<sup>20</sup>.

H<sub>2</sub>+Ni(111) has been the subject of many investigations, theoretically as well as experimentally. Steinrück et al.<sup>25</sup> performed molecular beam experiments on the sticking using Maxwellian beams of hydrogen, predicting a linear dependence of the sticking probability upon mean incidence energy in the range 1.7-15 kJ.mol<sup>-1</sup> (see Fig. 2.1). In contrast, Robota et al.<sup>26</sup> in the same year (1985) predicted a parabolic dependence of the sticking probability upon mean energy in the range of 1.0-11.6 kJ.mol<sup>-1</sup> using nozzle beams (i.e supersonic) of H<sub>2</sub> and D<sub>2</sub> (see Fig. 2.1). Hayward and Taylor<sup>27</sup> also used nozzle beams, of H<sub>2</sub> and D<sub>2</sub> with collision energies in the range of 1.0-9.2 kJ.mol<sup>-1</sup>, and found a linear dependence of the sticking coefficient of H<sub>2</sub> on Ni(111) upon energy, as Steinrück et al. did (Fig. 2.1). They concluded that there was probably a problem with the experiments of Robota et al., which did not yield a linear dependence.

In 1989, Rendulic et al.<sup>28</sup> reported new experimental data on H<sub>2</sub> + Ni(111), extending the incidence energy range to higher energies, i.e., to almost 0.4 eV. They also used supersonic beams and found a linear dependence of the sticking coefficient upon mean energy in the conflicting region of Robota et al. and Hayward and Taylor (Fig. 2.1). At lower incidence energies, the S<sub>0</sub> of Rendulic et al. were in good agreement with those of Hayward and Taylor. Somewhat later, Resch et al. (from the group of Winkler and Rendulic) revisited the H<sub>2</sub>/Ni(111) system with supersonic molecular beam experiments<sup>29</sup>, focusing on the effect of co-adsorbed inhibitors and promoters (potassium and oxygen). They found that potassium on Ni(111) acts as an inhibitor to the dissociation of hydrogen (Fig. 2.1). The clean surface S<sub>0</sub> of Resch et al. agree well with those of Rendulic et al. for E<sub>i</sub> up to 0.2 eV, but exceed the values of Rendulic et al. for larger E<sub>i</sub> (Fig. 2.1). This discrepancy, which was not addressed by Resch et al., may indicate some uncertainty in the supersonic molecular beam data for E<sub>i</sub> > 0.2 eV. Most recently, new experimental data for H<sub>2</sub>+Ni(111) were reported by Christine Hahn of the Juurlink/Kleyn group, in her Ph.D thesis<sup>30</sup>. Their observed S<sub>0</sub> are somewhat larger than those of Rendulic et al. and Resch et al., which may be related to the data having been taken for a circular crystal so that more reactive stepped surfaces are also sampled and to the data not having been presented as a function of the average beam energy.

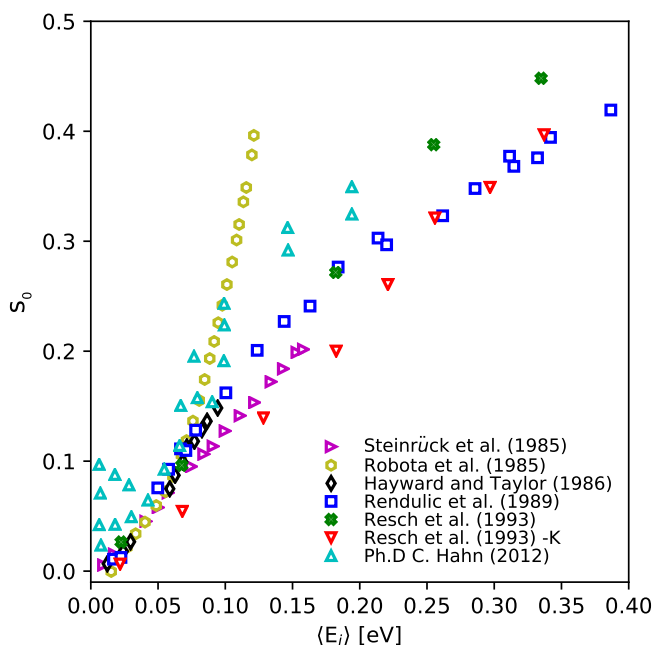


FIGURE 2.1: Comparison of the energy dependence of the sticking probability of  $\text{H}_2$  on Ni(111) for seven different sets of experimental data: Steinrück et al.<sup>25</sup> (magenta left triangle), Robota et al.<sup>26</sup> (olive hexagon), Hayward and Taylor<sup>27</sup> (black rhombus), Rendulic et al.<sup>28</sup> (blue square), Resch et al.<sup>29</sup> (green cross) using a clean surface of Ni(111) (Zero-coverage), Resch et al.<sup>29</sup> (red down triangle) using an inhibitor (Ni(111) surface coverage by potassium) and C. Hahn Ph.D thesis<sup>30</sup> (cyan upper triangle).

A common point of the experimental data is that extrapolation to lower incidence energies yields a negative intercept, which indicates that the dissociation is slightly activated, with a positive minimum barrier height. Three experiments show similar results for the low energy range, i.e., those of Rendulic et al.<sup>28</sup>, Resch et al.<sup>29</sup> and Hayward and Taylor<sup>27</sup>. For this study, we will focus on the Rendulic et al.<sup>28</sup> experiments, which also give results for high energies, but we will also compare our computational results to those of Resch et al..

To understand the experiments discussed, several theoretical studies have been carried out. Unfortunately, most of these studies suffer from the use of a somewhat inaccurate PES. This may have been due to the use of an approximate fit expression (e.g., a London -Eyring -Polanyi -Sato form)<sup>31</sup> or to the use of

a standard GGA functional<sup>32</sup>. Kresse<sup>32</sup> used a non-empirical GGA functional to obtain a PES for  $\text{H}_2+\text{Ni}(111)$ , employing the PW91 functional<sup>33,34</sup>. The classical trajectory method was used to compute the sticking coefficient, with the vibrations and rotations of  $\text{H}_2$  described by an ideal gas at the temperature of the nozzle used in the experiments. His theoretical data for the DC of  $\text{H}_2$  at specific incidence energy was compared to the molecular beam data of Rendulic et al.. Kresse obtained qualitative agreement, but quantitative agreement was not yet obtained. Specifically, Kresse found that the reaction was activated, but the reaction probability was overestimated. He concluded that at least part of the difference might have been due to the use of the classical trajectory method he used not taking into account zero-point energy effects appropriately. He suggested that improved agreement with experiment might be obtainable with a quantum dynamical method.

In the present work, we attempt to derive a SRP-DF for  $\text{H}_2+\text{Ni}(111)$ . We first test the transferability of the previously fitted SRP functional for  $\text{H}_2+\text{Pt}(111)$ <sup>35</sup> to  $\text{H}_2+\text{Ni}(111)$ . However, we also use other functionals to generate the PES, where DFs are tested that are semi-local (GGA) and that are non-local (GGA for exchange and vdW-DF1<sup>36</sup> or vdW-DF2<sup>37</sup> for correlation). We also evaluate the sensitivity of the computed sticking probabilities to the molecular beam parameters that are employed to simulate the experiment. Additionally, we investigate the accuracy of the dynamics method we use for the simulation of molecular beam sticking probabilities (i.e., the quasi-classical trajectory (QCT) method) by comparing with quantum dynamics (QD) results for a few selected initial rovibrational states.

Our **Chapter** is organized as follows: First, we describe the theoretical methods used in this work in Section 2.2. Section 2.2.1 describes the dynamical model and Section 2.2.2 describes the construction of the PES. The CRP interpolation method is described in Section 2.2.3. The dynamics methods that are used here to study  $\text{H}_2+\text{Ni}(111)$  are explained in Section 2.2.4. Section 2.2.5 describes how we calculate the observables. In Section 2.3, the results of the calculations are shown and discussed. Section 2.3.1 describes the computed PESs, and Sections 2.3.2 and 2.3.3 provide discussion on the comparison of our computed sticking probabilities to the molecular beam experiments and the causes for discrepancies between theory and experiment. Conclusions are provided in Section 2.4.

TABLE 2.1: The exchange-correlation functionals used in this work.

Name	Type	Exchange	Correlation
$\text{PBE}_\alpha = 0.57\text{-vdW-DF2}$	vdW-DF	$\text{PBE}_\alpha^{38}$	$\text{vdW-DF2}^{37}$
$\text{PBE}_\alpha = 1.25\text{-vdW-DF2}$	vdW-DF	$\text{PBE}_\alpha^{38}$	$\text{vdW-DF2}^{37}$
$\text{PBE-vdW-DF2}$	vdW-DF	$\text{PBE}^{10}$	$\text{vdW-DF2}^{37}$
$\text{SRPB86R-vdW-DF2}$	vdW-DF	$0.68\text{B86R}^{39} + 0.32\text{RPBE}^{40}$	$\text{vdW-DF2}^{37}$
$\text{SRP0.5-vdW-DF2}$	vdW-DF	$0.5\text{RPBE}^{40} + 0.5\text{PBE}^{10}$	$\text{vdW-DF2}^{37}$
$\text{SRP0.32-vdW-DF2}$	vdW-DF	$0.32\text{RPBE}^{40} + 0.68\text{PBE}^{10}$	$\text{vdW-DF2}^{37}$
$\text{SRP0.5-vdW-DF1}$	vdW-DF	$0.5\text{RPBE}^{40} + 0.5\text{PBE}^{10}$	$\text{vdW-DF1}^{36}$
$\text{SRP48}$	GGA	$0.48\text{RPBE}^{40} + 0.52\text{PBE}^{10}$	$\text{PBE}^{10}$
$\text{PBE}$	GGA	$\text{PBE}^{10}$	$\text{PBE}^{10}$

## 2.2 Methods

### 2.2.1 Dynamical model

In all calculations, we used the Born-Oppenheimer static surface (BOSS) model<sup>4</sup>. For reasons that we mentioned earlier in our introduction, this approximation is good enough to describe the reaction of  $\text{H}_2$  on a metal surface. We neglect the degrees of freedom of the surface atoms and only the  $\text{H}_2$  degrees of freedom (6D) are taken into account. Fig. 2.2a depicts the coordinate system used for the dynamics and Fig. 2.2b the surface unit cell for the Ni(111) system and the high symmetry impact sites.

### 2.2.2 Construction of the PES

For the full (6D) PES construction, self-consistent DFT was used, applying the candidate SRP functionals listed in table 2.1 to try and obtain chemical accuracy. The main idea of SRP-DFT as first proposed by Díaz et al.<sup>4</sup> is that the exchange-correlation (XC) functional is adapted to the system at hand by optimizing the  $\alpha$  parameter in Eq. (2.1)

$$E_{\text{XC}} = \alpha E_{\text{XC}}^1 + (1 - \alpha) E_{\text{XC}}^2. \quad (2.1)$$

Here,  $E_{\text{XC}}^1$  and  $E_{\text{XC}}^2$  are two "standard" (i.e GGA level) XC functionals, of which one generally tends to overestimate the sticking coefficient, and the second tends to underestimate the sticking coefficient. Standard XC functionals used for molecule-surface reactions are the  $\text{PBE}^{10}$  and  $\text{RPBE}^{40}$  functionals. Downsides of the SRP-approach are that the approach is specific to one system, one needs at least one experimental data set to construct an SRP-DF, and the quality of this functional depends on the quality of the experiment.

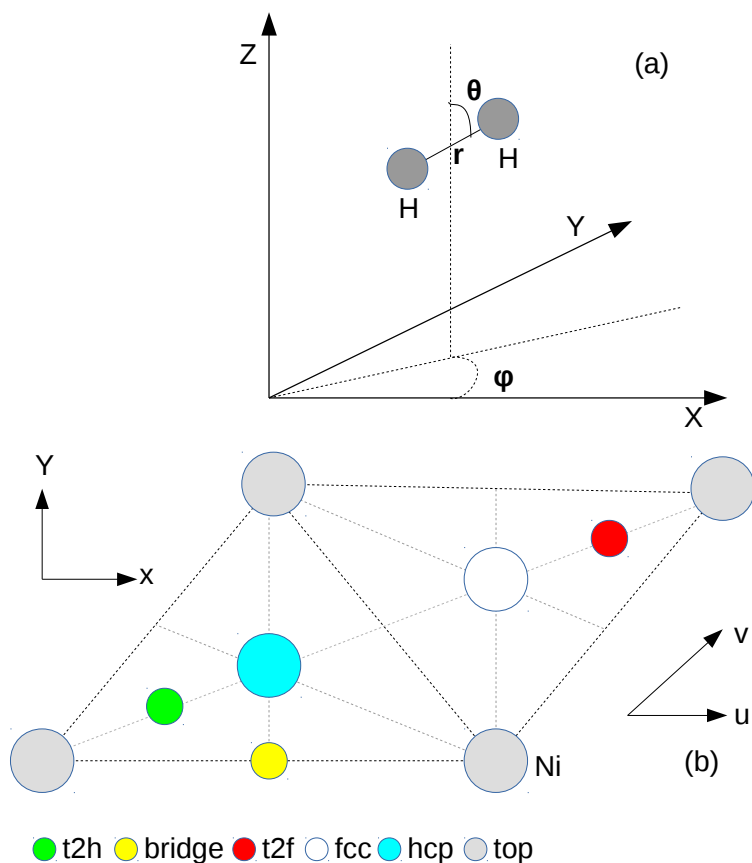


FIGURE 2.2: (a) Coordinate system used to describe the  $H_2$  molecule relative to the static Ni(111) surface. (b) The surface unit cell and sites considered for the Ni(111) surface. The origin ( $X=u=0, Y=v=0, Z=0$ ) of the center of mass coordinates is located in the surface plane at a top site, i.e., at a surface atom.

As found to be necessary for  $\text{CHD}_3$  on  $\text{Ni}(111)$ <sup>41</sup>,  $\text{CHD}_3 + \text{Pt}(111)$ <sup>42,43</sup>,  $\text{H}_2 + \text{Pt}(111)$ <sup>35</sup>, and  $\text{H}_2$  on  $\text{Ru}(0001)$ <sup>44</sup>, in many cases we take the correlation functional to describe the van der Waals interaction using the correlation functional of Dion et al.<sup>36</sup> ( $E_C^{\text{vdW-DF}}$ ) or Lee et al.<sup>37</sup> ( $E_C^{\text{vdW-DF}^2}$ ). These correlation functionals have been shown to improve the description of weakly activated dissociation<sup>44</sup> while maintaining the same accuracy<sup>45</sup> or improving the accuracy<sup>41</sup> for highly activated dissociation systems. The  $\text{PBE}\alpha=0.57\text{-vdW-DF}2$  functional is the SRP-DF for the chemically related  $\text{H}_2 + \text{Pt}(111)$  system<sup>35</sup>, which suggests that it might also work well for  $\text{H}_2 + \text{Ni}(111)$ .

The vdW-DF1 and vdW-DF2 correlational functionals are non-empirical, being based on first principles. With their inclusion, our SRP functional form becomes

$$E_{\text{XC}} = \alpha E_{\text{X}}^1 + (1 - \alpha) E_{\text{X}}^2 + E_{\text{C}}. \quad (2.2)$$

In equation (2.2), the contributing exchange functionals  $E_{\text{X}}$  and the correlation functionals  $E_{\text{C}}$  included in the exchange-correlation functionals we used are specified in Table 2.1.

To solve the Kohn-Sham equations, we used the Quantum Espresso package (QE)<sup>46</sup>. In the calculations to construct PESs, we used the spin-polarized extension of the vdW-DF and vdW-DF2 correlation functional<sup>47</sup> implemented in QE. Furthermore, we implemented the exchange part of the  $\text{SRP}\alpha\text{-vdW-DF}$  (or  $\text{vdW-DF}2$ ) functional through the modified version of the LIBXC exchange-correlation functional library<sup>48</sup>. The electron-ion interaction is described by using the projector augmented wave (PAW) potentials as proposed by Blöchl<sup>49</sup> from the pseudopotential library<sup>50</sup> (version 1.0.0) with the energy cut off for plane wave expansion corresponding to 50 Ry (1 Ry  $\approx$  13.606 eV) with 0.011025 Ry wide Methfessel-Paxton smearing to facilitate the convergence. The Brillouin zone has been sampled with a  $5 \times 5 \times 1$   $\Gamma$ -centered grid of k-points. We used a  $(3 \times 3)$  surface unit cell with a total of 36 Ni atoms, with 18 Å vacuum separating the slab from its first periodic image, and a 4 layers slab.

We first optimized the geometric structure of the Ni slab with the Vienna *ab initio* simulation package (VASP) package<sup>51,52</sup>. First, the bulk fcc lattice constant was determined using a  $24 \times 24 \times 24$   $\Gamma$ -centered grid of k-points. Next, slab relaxation calculations were performed using a  $24 \times 24 \times 1$   $\Gamma$ -centered grid of k-points and the energy cut off for plane wave expansion corresponding to 400 eV and 0.1 eV wide Methfessel-Paxton (or Fermi) smearing for convergence. After having obtained the relaxed slab (see Table S1 of the Supporting Information (SI) of Ref.<sup>53</sup> for the results of the  $\text{PBE-vdW-DF}2$  functional), the convergence of the molecule-surface interaction energy has been tested with respect to the



number of metal layers, cell size, the cut-off energy and the k-point sampling by comparing computed minimum energy barrier heights. The transition state (TS) geometries have been determined using the dimer method as implemented in the VASP transition state tools (VTST) package<sup>54–57</sup>. In the TS search, the surface was frozen in the relaxed 0 K geometry of the bare slab. The optimization of the TS geometries has been stopped once the maximum force on any degree of freedom was smaller than 5 meV/Å. All the TS geometries have been proven to be first order saddle points in the molecular coordinate space through frequency analysis (by checking that one and only one imaginary frequency was found). The barrier height has been computed as  $E_b = E_{TS} - E_{asym}$ ; here  $E_{TS}$  is the absolute energy of the transition state geometry and  $E_{asym}$  is the absolute energy of the system with the molecule in the gas phase. The gas phase geometry consists of the optimized molecule placed in the vacuum far from the surface. For our case, the vacuum distance was 18 Å and the gas phase molecule was taken at 9 Å from the slab. Note that the TS geometries presented in Section III were obtained from the PESs fitted to data computed with QE. We ascertained that the molecule-surface interaction energies calculated with VASP (in convergence tests) were in good agreement with those computed with QE (used for PES fitting and dynamics), see Table S2 of the SI of Ref. <sup>53</sup>.

### 2.2.3 Interpolation of PES

The PESs were interpolated using the corrugation reducing procedure (CRP)<sup>58,59</sup>, with the formula

$$V^{6D}(\vec{r}) = I^{6D}(\vec{r}) + \sum_{i=1}^2 V_i^{3D}(\vec{r}_i) \quad (2.3)$$

in which  $V^{6D}$  is the full 6D PES of the H<sub>2</sub>/surface system,  $\vec{r}$  is the vector of coordinates of the H<sub>2</sub> molecule with respect to the surface,  $I^{6D}$  is the so-called 6D interpolation function of the H<sub>2</sub>/surface system,  $V_i^{3D}$  is the 3D PES of the H/surface system and  $\vec{r}_i$  is the vector of coordinates of the *i*th H atom with respect to the surface. The 3D atom-surface PES is then written as

$$V_i^{3D}(\vec{r}_i) = I_i^{3D}(\vec{r}_i) + \sum_{j=1}^N V^{1D}(R_{ij}) \quad (2.4)$$

where  $I_i^{3D}$  is the 3D interpolation function describing the H/surface system,  $N$  is the number of surface atoms taken into account,  $V^{1D}$  is the 1D functional mimicking the interaction of the H atom with a single surface atom and  $R_{ij}$  is the distance between H atom *i* and surface atom *j*.

The idea behind the CRP is to interpolate the  $I^{6D}$  instead of  $V^{6D}$ , as  $I^{6D}$  is much less corrugated in the  $u$ ,  $v$ ,  $\theta$  and  $\varphi$  degrees of freedom than  $V^{6D}$  is<sup>58</sup>. The  $(u,v)$  coordinate system is a coordinate system in which the surface lattice vectors are taken as unit vectors(Fig. 2.2).

For  $H_2$  on Ni(111), the skewing angle of the coordinate system is  $60^\circ$  (Fig. 2.2b). The interpolation procedure used for the  $C_{3v}$  potential of  $H_2+Ni(111)$  is the same as used in Ref.<sup>44</sup> for  $H_2$  on Ru(0001) and for  $H_2+Cu(111)$  and  $H_2+Pt(111)$ <sup>45</sup>. For the interpolation of the  $I^{6D}$  potential with  $C_{3v}$  symmetry, 29 configurations of  $(u, v, \theta, \varphi)$  are used, spread over six different sites  $(u, v)$ . These sites are shown in Fig. 2.2b. The configurations used in this work are exactly the same as used in Ref.<sup>44</sup>, see also Tables S3 and S4 of the SI of Ref.<sup>44</sup>.

The interpolation is done in several steps: First, for every configuration, the interpolation is performed over the  $r$  and  $Z$  degree of freedom. For this interpolation, a  $15 \times 26$  ( $r \times Z$ ) grid is used, employing a two-dimensional (2D) cubic spline interpolation, where  $r_{min} = 0.4 \text{ \AA}$ ,  $r_{max} = 2.3 \text{ \AA}$ ,  $Z_{min} = 0.25 \text{ \AA}$  and  $Z_{max} = 6.5 \text{ \AA}$ . Then, for every site, the interpolation is performed over the  $\theta$  and  $\varphi$  degrees of freedom using symmetry-adapted products sin and cos functions. Finally, an interpolation over  $u$  and  $v$  is performed, for which again symmetry-adapted products sin and cos functions are used. At long-range, we apply a switching function between  $5.5 \text{ \AA}$  and  $6.5 \text{ \AA}$  from the full 6D potential to a 2D asymptotic gas-surface potential that only depends on  $r$  and  $Z$ , because far away from the surface, the corrugation and anisotropy of the PES are vanishingly small. This asymptotic potential is represented by

$$V^{2D}(r, Z) = V^{\text{ext}}(Z) + V^{\text{gas}}(r) \quad (2.5)$$

where  $V^{\text{ext}}$  is a function describing the dependence of the PES on  $Z$  beyond  $Z = 6.5 \text{ \AA}$  and  $V^{\text{gas}}$  is the interaction at  $Z = Z_{max} = 9 \text{ \AA}$ . For the  $I^{3D}$  interpolation, 10 sites in  $(u, v)$  are used for the potentials with  $C_{3v}$  symmetry. The 10 sites used in this work are exactly the same as used in Ref.<sup>44</sup>. Apart from the top site where 202 points are taken in  $Z$ , for each site 106 points are taken in  $Z$ , with  $Z_{min} = -1.195 \text{ \AA}$  and  $Z_{max} = 9 \text{ \AA}$ . The function  $V^{1D}$  is taken to describe the interaction of the H atom with the surface above the top site, as used previously for the investigation of  $H_2+Cu(111)$ <sup>45</sup>.

## 2.2.4 Dynamics Methods

### 2.2.4.A Quasi-classical Dynamics

We take into account the zero-point energy of  $H_2$  to compute the dynamical observables by using the QCT method<sup>60</sup>. To evaluate the initial state-resolved

reaction probabilities, we placed our molecule initially at  $Z = 9 \text{ \AA}$  with a velocity normal toward the surface that corresponds to a specific initial incidence energy. At this distance, the interaction of the molecule with the surface is essentially zero. For each average beam translational energy, accurate results were obtained with typically 40,000 trajectories. In all cases, the maximum propagation time is 2 ps. To propagate our equation of motions, the Stoer and Bulirsh<sup>61</sup> method was used. The time-independent Schrödinger equation was solved using the Fourier grid Hamiltonian method<sup>62</sup> to determine the bound state rotational-vibrational eigenvalues of gas phase  $\text{H}_2$ . The bond distance and the vibrational velocity of the molecule are randomly sampled from a one-dimensional quasi-classical dynamics calculation of a vibrating  $\text{H}_2$  molecule for the corresponding rovibrational energy<sup>63</sup>. The orientation of the molecule,  $\theta$  and  $\varphi$ , is chosen also based on the selection of the initial rotational state. The magnitude of the classical initial angular momentum is fixed by  $L = \sqrt{j(j+1)}/\hbar$  and its orientation, while constrained by  $\cos \Theta_L = m_j/\sqrt{j(j+1)}$ , is otherwise randomly chosen as described by Wijzenbroek et al.<sup>45</sup>. Here,  $j$  is the rotational quantum number,  $m_j$  the magnetic rotational quantum number and  $\Theta_L$  the angle between the angular momentum vector and the surface normal. Other initial conditions are randomly chosen as described in Ref.<sup>63</sup>.

#### 2.2.4.B Quantum Dynamics

The time-dependent wave packet (TDWP) method was used<sup>64</sup> for the quantum dynamical (QD) calculations. The Fourier representation<sup>65</sup> was used to represent the wave packet in  $Z$ ,  $r$ ,  $X$ , and  $Y$ . We employed a finite basis representation to represent the angular wave function<sup>66,67</sup>. The time-dependent Schrödinger equation was propagated using the split operator method<sup>68</sup>. The initial wave packet is taken as a product of a Gaussian wave packet describing the motion of the molecule towards the surface, a plane wave function for motion parallel to the surface, and a rovibrational wave function to describe the initial vibrational and rotational state of the molecule. The scattering amplitude formalism<sup>69–71</sup> is used to analyse the reflected wave packet at  $Z = Z_\infty$ .  $Z_\infty$  is a value of  $Z$  ( $9 \text{ \AA}$ ) where there is no interaction between the molecule and the surface. An optical potential is used to absorb the reacted( $r$ ) or scattered( $Z$ ) wave packet for large values of  $r$  and  $Z$ <sup>72</sup>. For full details of the method and equations, see Ref.<sup>73</sup>. The parameters used in this work are given in Table S5 of the SI of Ref.<sup>53</sup>.

## 2.2.5 Computation of the Observables

### 2.2.5.A Degeneracy-Averaged reaction probabilities

In our QCT calculation of the reaction probabilities, we considered our molecule dissociated when its H-H distance becomes greater than 2.0 Å. Otherwise, the H<sub>2</sub> molecule is considered to be reflected from the surface to the gas phase when its distance to the surface in Z exceeds 6.5 Å and H<sub>2</sub> has a velocity toward the vacuum. The reaction probability was calculated as the ratio of the number of dissociated trajectories, using the formula

$$P_r = N_r/N_{\text{total}} \quad (2.6)$$

where  $N_{\text{total}}$  is the total number of trajectories and  $N_r$  is the number of reactive trajectories. The degeneracy-averaged reaction probability for a particular initial vibrational state  $\nu$  and rotational state  $j$  can be computed as

$$P_{\text{deg}}(E_i; \nu, j) = \sum_{m_j=0}^j (2 - \delta_{m_j}) P_r(E_i; \nu, j, m_j) / (2j + 1). \quad (2.7)$$

Here,  $P_r$  is the fully initial-state-resolved reaction probability.  $P_r$  can be computed with the TDWP method from

$$P_r(E_i; \nu, j, m_j) = 1 - \sum_{\nu', j', m'_j, n, m} P_{\text{scat}}(E_i; \nu, j, m_j \rightarrow \nu', j', m'_j, n, m) \quad (2.8)$$

$P_{\text{scat}}$  are the state-to-state scattering probabilities from the initial state  $(\nu, j, m_j)$  to the final state  $(\nu', j', m'_j, n, m)$ , where  $n$  and  $m$  are the quantum numbers for diffraction.

### 2.2.5.B Molecular Beam sticking probabilities

When calculating the sticking probabilities using a molecular beam simulation, the properties of the experimental molecular beam should be taken into account. This is done in two steps : Firstly, the monoenergetic reaction probabilities  $R_{\text{mono}}(E_i, T_n)$  are computed through Boltzmann averaging over all rovibrational states populated in the molecular beam with the nozzle temperature  $T_n$  at the collision energy  $E_i$ <sup>45</sup> :

$$R_{\text{mono}}(E_i, T_n) = \sum_{\nu, j} F_B(\nu, j, T_n) P_{\text{deg}}(E_i; \nu, j) \quad (2.9)$$

Here  $F_B$  is the Boltzmann weight of each  $(\nu, j)$  state.

$$F_B(\nu, j, T_n) = \frac{w(j)F(\nu, j, T_n)}{\sum_{\nu', j' \equiv j \pmod{2}} F(\nu', j', T_n)} \quad (2.10)$$

in which

$$F(\nu, j, T_n) = (2j + 1) \exp(-E_{vib}(\nu, j)/k_B T_{vib}) \\ \times \exp(-E_{rot}(\nu, j)/k_B T_{rot}) \quad (2.11)$$

In equation (2.10), the summation runs only over the values of  $j'$  with the same parity as  $j$ . In equation (2.11)  $E_{vib}$  and  $E_{rot}$  are the vibrational and rotational energy, respectively, of the  $(\nu, j)$  state and  $k_B$  is the Boltzmann constant. In these equations, it is assumed that the rotational temperature of the molecules in the beam is lower than the nozzle temperature ( $T_{rot} = 0.8 T_n$ )<sup>74,75</sup> and that the vibrational temperature is equal to the nozzle temperature ( $T_{vib} = T_n$ ). We also assume that the fractions of ortho- and para- $H_2$  and  $D_2$  are equivalent to those in the high-temperature limit, given by  $w(j)$ . For  $H_2$ ,  $w(j)$  is equal to  $\frac{1}{4}$  for even  $j$  and  $\frac{3}{4}$  for odd  $j$ , and for  $D_2$ ,  $w(j)$  is equal to  $\frac{2}{3}$  for even  $j$  and  $\frac{1}{3}$  for odd  $j$ .

Secondly, the experimental spread of incidence energies is taken into account. The monoenergetic reaction probability is averaged over the velocity distribution by<sup>76</sup>

$$R_{beam} = \frac{\int_0^\infty f(v_i; T_n) R_{mono}(E_i; T_n) dv_i}{\int_0^\infty f(v_i; T_n) dv_i} \quad (2.12)$$

Here,  $f(v_i; T_n)$  is the flux-weighted velocity distribution, which is given by<sup>77</sup>

$$f(v_i; T_n) = C v_i^3 \exp[-(v_i - v_0)^2 / \alpha^2] \quad (2.13)$$

In equation (2.13),  $C$  is a constant,  $v_i$  is the velocity of the molecule,  $v_0$  is the stream velocity, and  $\alpha$  is a parameter describing the width of the velocity distribution. The  $v_0$  and  $\alpha$  used in our calculations (Table 2.2) were obtained by fitting the experimental time of flight (TOF) spectra<sup>78</sup> characterising  $H_2$  beams used in the Rendulic group to the function

$$G(t; T_n) = c_1 + c_2 v_i^4 \exp[-(v_i - v_0)^2 / \alpha^2] \quad (2.14)$$

using the Levenberg-Marquardt algorithm<sup>79</sup>.

TABLE 2.2: Parameters used for the molecular beam simulations of H<sub>2</sub> on Ni(111). The parameters were obtained from fits of equation (2.14) to the experimental time of flight spectra<sup>78</sup>. Also presented is the Boltzmann population of the ( $\nu = 0, j = 0$ ) state of H<sub>2</sub> in the beam.

$T_n$ (K)	$\langle E_i \rangle$ (eV)	$c_1$	$c_2 \times 10^{-15}$	$v_0$ (m/s)	$\alpha$ (m/s)	$F_B$ ( $\nu = 0, j = 0, T_n$ )
100	0.035	0.021	0.753	1,832.40	82.31	0.24788
300	0.067	0.009	0.238	2,496.08	239.45	0.15560
500	0.122	0.023	8.069	3,127.77	740.22	0.09853
800	0.153	0.023	5.570	3,352.75	1,005.88	0.06291
1100	0.216	0.041	3.120	3,679.94	1,464.91	0.04589
1400	0.303	0.018	2.172	3,650.40	2,237.06	0.03575
1700	0.392	0.016	57.918	3,320.96	2,998.75	0.02891

## 2.3 Results and Discussion

### 2.3.1 Potential Energy Surfaces

Fig. 2.3 shows, for some selected high symmetry configurations, two-dimensional (2D) cuts through the PESs (also called elbow plots) for the PBE-vdW2 and for the PBE functionals. In all cases, H<sub>2</sub> was oriented parallel to surface. In agreement with the previous work on H<sub>2</sub> on Ru(0001)<sup>44</sup>, the barrier height decreases in the order  $\text{hcp}/\text{fcc} > \text{bridge} > \text{t2h}/\text{t2f} > \text{top}$  (see Table 2.3). The hcp barrier was found to be slightly lower than the fcc barrier. With the PBE-vdW2 functional, the dissociation is activated, in the sense that the transition states have as energies 24 meV and 135 meV for the early barrier and late barrier, respectively, above the top site (Fig. 2.3(a)). With PBE, the dissociation is very weakly activated with the energies of 11 meV for the early and -180 meV for the late barrier (Table 2.3). Non-activated behaviour was observed for the PBE $\alpha$ 0.57-vdW2 functional (see Table S6 of the SI of Ref. <sup>53</sup>) with energies of -50 meV and -27 meV for the early and late top site barriers, respectively. For the other functionals, the dissociation was found to be activated (see Table S6 of the SI of Ref. <sup>53</sup>).

From Fig. 2.3, we can also see that, for the PBE-vdW2 functional, the top and t2f symmetry configurations present two saddle points, with a local minimum in between (Figs. 2.3a and 2.3d). This notable feature is general for all functionals except for the PBE, the SRP48 functional and for SRPB86R-vdW2 where the PES was found to exhibit only one saddle point for the t2f configuration (see Table S6 of the SI of Ref. <sup>53</sup> and Fig. 2.3h). Differences were found with respect to the relative energies of the early and late barriers present in 2D cuts above the top and t2f impact sites. Note that, when using the PBE $\alpha$  functional<sup>38</sup> with  $\alpha$  being the adjustable parameter, if  $\alpha = 1$ , the PBE $\alpha$  functional corresponds to the PBE<sup>10</sup> functional, while for  $\alpha \rightarrow \infty$ , the PBE $\alpha$  functional corresponds to the RPBE<sup>80</sup> functional. For PBE $\alpha$ -vdW2 and SRP $\alpha$ -vdW1 (vdW2), the late barrier

TABLE 2.3: Some selected barrier heights (in eV) and locations ( $r_b, Z_b$ ) (in Å), relative to the gas phase minimum, for the four geometries depicted in Fig. 2.3 and for hcp. Where available, energy barriers have been indicated for the PBE-vdW2 and PBE functionals. All geometries are for the H<sub>2</sub> molecule lying parallel to the surface ( $\theta = 90^\circ$ ).

Parameters	top(early)	top(late)	brg	hcp	fcc	t2f(early)	t2f(late)
$\varphi$	$0^0$	$0^0$	$90^0$	$30^0$	$0^0$	$240^0$	$240^0$
$Z_b^{PBE-vdW2}$	2.083	1.368	1.602	1.519	1.508	1.747	1.304
$Z_b^{PBE}$	2.349	1.372	1.838	1.741	1.731	2.034	-
$r_b^{PBE-vdW2}$	0.763	1.240	0.810	0.843	0.847	0.790	1.021
$r_b^{PBE}$	0.763	1.222	0.794	0.811	0.812	0.777	-
$E_b^{PBE-vdW2}$	0.024	0.135	0.321	0.412	0.427	0.174	0.162
$E_b^{PBE}$	0.011	-0.180	0.179	0.248	0.257	0.089	-

for the top symmetry configuration was found to be higher than the early top site barrier, in contrast with the SRP48, PBE and SRPB86R-vdW2 functionals where the opposite was found (See Table S6 of the SI of Ref.<sup>53</sup>). The latter 3 functionals also correspond to the functionals for which only an early barrier is found on the t2f site.

To gain a deeper understanding of the PESs' features, we also consider here the energetic corrugation, as was done previously<sup>44</sup> in an investigation of H<sub>2</sub> on Ru(0001). The energetic corrugation is defined as the difference between the hcp( $\theta = 90^\circ, \varphi = 30^\circ$ ) barrier height and the earlier top site ( $\theta = 90^\circ, \varphi = 0^\circ$ ) barrier height. The energetic corrugation corresponds to the width of the reaction probability curve for an activated dissociation system<sup>44,81</sup>. It usually corresponds to the range of energies over which the reaction probability increases more or less linearly from an onset energy that is close to the reaction threshold to an energy at which the reaction probability starts to plateau<sup>44</sup>. Fig. 2.4A plots the energetic corrugation against the top site barrier height and Fig. 2.4B depicts the variation of the early barrier height above the top site against the distance to the surface of this early barrier. For the most part, we observe a linear dependence for functionals with the same correlation functional, as seen for PBE $\alpha$ -vdW2, where the corrugation energetic increases with the  $\alpha$  parameter. Specifically, the functionals with higher top barrier heights tend to yield a larger energetic corrugation if they have the same correlation functional. This is the case for the SRP $\alpha$ -vdW2 functionals. The early top site barriers tend to be closer to the surface if van der Waals correlation is used (Fig. 2.4B), and, more generally, the barriers get closer to the surface if PBE correlation is replaced by vdW2 (see Table 2.3) or vdW1 correlation. This is why functionals yielding similar early

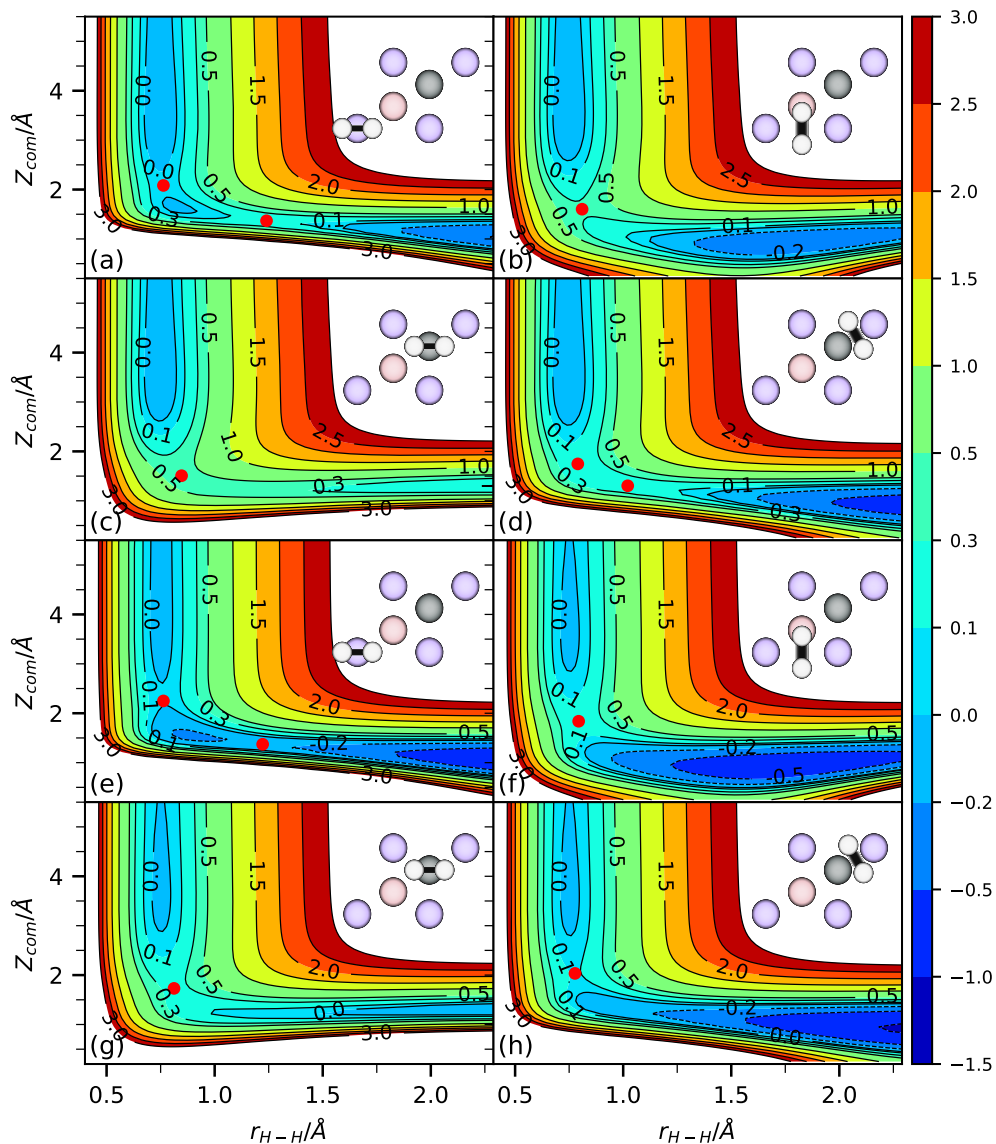


FIGURE 2.3: Elbow plots (i.e:  $V(Z,r)$ ) of  $H_2$  on Ni(111) for four high symmetry configurations with  $H_2$  parallel to the surface ( $\theta=90^\circ$ ) computed with PBE-vdW2[(a), (b), (c) and (d)] and PBE[(e), (f), (g) and (h)] functionals and interpolated with CRP method, for the top( $\varphi=0^\circ$ ), bridge( $\varphi=90^\circ$ ), fcc( $\varphi=0^\circ$ ) and t2f( $\varphi=120^\circ$ ) configurations shown in the insets. Saddle points are indicated by red circles.



top site minimum barriers tend to yield a larger energetic corrugation if they incorporate van der Waals correlation instead of PBE correlation, as also seen in Fig. 2.4A and previously found for  $\text{H}_2 + \text{Ru}(0001)$ . Increasing the  $\alpha$ -parameter makes the functionals more repulsive, leading to early barriers that are further from the surface. The trends observed in Fig. 2.4 were previously found for  $\text{H}_2$  on  $\text{Ru}(0001)$ <sup>44</sup>.

## 2.3.2 Comparison to experiment

In Fig. 2.5, the sticking probabilities ( $S_0$ ) computed with molecular beam simulations for  $\text{H}_2$  dissociating on  $\text{Ni}(111)$  are shown for all functionals used, and compared with the experiments of Rendulic et al.<sup>28</sup>. From panel (a), we see that the  $S_0$  computed with PBE<sup>10</sup> are in reasonable agreement with the sticking coefficients computed in fully classical simulations with PW91<sup>33,34</sup> by Kresse. Differences may be attributed to the different simulation methods used, small differences in the functionals (but note that the PBE functional was designed to reproduce PW91 energies closely<sup>10</sup>), and differences in the input parameters to the DFT calculations. For instance, Kresse performed fully classical simulations, choosing the rovibrational energies according to incidence energy, while we performed QCT simulations with averaging over the beam's translational energy distribution and rovibrational state populations.

The PBE<sup>11</sup> functional overestimates the sticking probability. This clearly indicates that the highest top site barrier found for the PBE PES (11 meV) is too low. On the other hand, the SRP50-vdW2(RPBE:PBE(50:50)vdW2) functional consistently underestimates the measured  $S_0$ . This clearly suggests that the barriers in this PES are too high. Results for the SRP32-vdW2 functional closely resemble those of the SRP50-vdW2 functional and are therefore not shown in Fig. 2.5. If we replace the vdW2 correlation from SRP50-vdW2 by PBE correlation and slightly change the  $\alpha$  parameter (SRP48), both the reaction threshold and the width of the sticking probability curve change. The reaction probability is underestimated for  $E_i < 0.2$  eV and overestimated for  $E_i > 0.2$  eV. If on the other hand we only change the exchange part to a mixture of B86R<sup>39</sup> and RPBE<sup>80</sup> exchange while keeping vdW2 correlation (B86R:RPBE(68:32)vdW2), we obtain a sticking probability curve that is very similar to the one obtained with SRP48. Neither the SRP48 nor the B86r:RPBE(68:32)-vdW2 functional yield good agreement with experiment. Both functionals containing PBE correlation (PBE and SRP48) yield sticking curves that are too steep at the onset to yield good agreement with experiment at the onset of the experimental sticking curves.

As Fig. 2.5(b) shows, the PBE $\alpha = 0.57$ -vdW2 functional also leads to a consistently overestimated sticking probability. The extrapolation of the

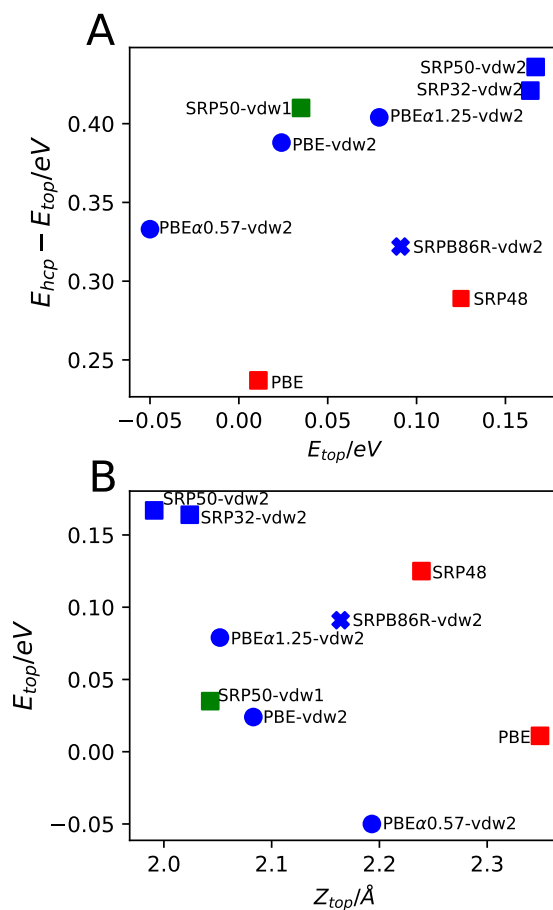


FIGURE 2.4: (A) Energetic corrugation of the potential versus the barrier height associated with the early top site barrier for the constructed PESs for the functionals investigated. (B) Height of the early top to bridge barrier versus the distance of the surface of the early top to bridge barrier for the constructed PESs for the functionals investigated. Results obtained with functionals sharing the same correlation functional expression are shown with the same colour. Results obtained with functionals using a similar expression for the exchange functional in Eq. 2.2 are shown with the same symbol (i.e., blue vdW2, green vdW1, red PBE for correlation; square mix PBE:RPBE, circle PBE $\alpha$ , cross mix B86R:RPBE for exchange).

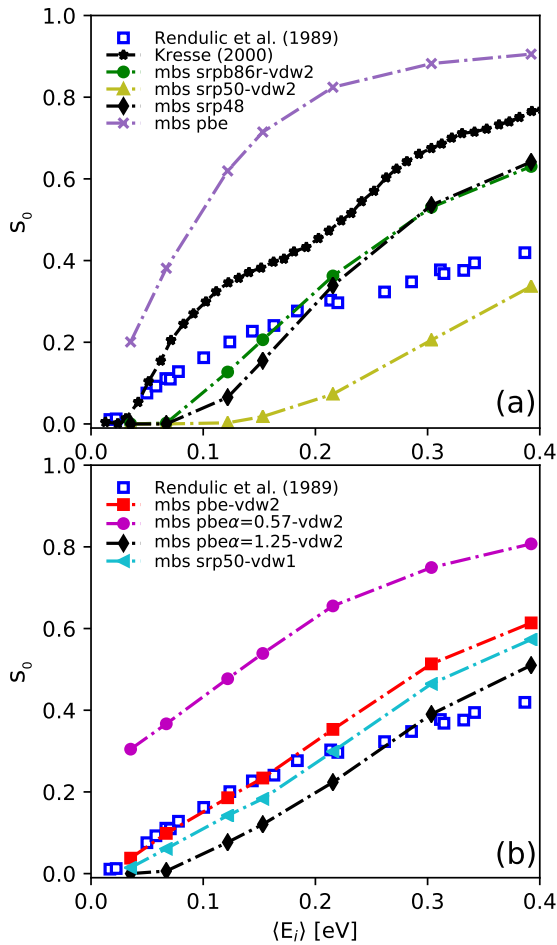


FIGURE 2.5: (a,b) Reaction probability for molecular beams of  $H_2$  dissociating on Ni(111) computed with various functionals, compared to experiment<sup>28</sup>.

computed reaction probability curve to lower incidence energies yields a positive intercept, in agreement with our finding that with this functional reaction is non-activated above the top site, but in disagreement with experiment. The results show that the  $\text{PBE}\alpha = 0.57\text{-vdW2}$  functional is not transferable from  $\text{H}_2 + \text{Pt}(111)$ <sup>35</sup> to  $\text{H}_2 + \text{Ni}(111)$ .

With the  $\text{PBE-vdW2}$  ( $\text{PBE}\alpha = 1.0\text{-vdW2}$ ) PES, excellent agreement with experiment is achieved at the lowest incidence energies (up to 0.2 eV), but the computed  $S_0$  are too high in the higher energy range (0.2-0.4 eV). Nevertheless it is encouraging that the agreement is good for the incidence energy range for which good agreement was found in the experiments of Rendulic et al.<sup>28</sup>, Resch et al.<sup>29</sup>, and of Hayward and Taylor<sup>27</sup>. In particular, we note that replacing PBE correlation with vdW2 correlation in the PBE functional (thus obtaining  $\text{PBE-vdW2}$ ) leads to a sticking curve that has not only the correct onset, but also the correct shape (steepness) for incidence energies up to about 0.2 eV. A similar finding was previously obtained for  $\text{H}_2 + \text{Ru}(0001)$ <sup>44</sup>. From Fig. 2.5(b), we can also see how the computed  $S_0$  curve depends on the  $\alpha$  parameter when using  $\text{PBE}\alpha$  exchange and vdW2 correlation. The  $S_0$  curve shifts to higher  $E_i$  when the  $\alpha$  parameter increases, but the shape of the  $S_0$  curve is basically unchanged. With the  $\text{PBE}\alpha = 1.25\text{-vdW2}$  functional, the computed  $S_0$  are too low for  $E_i$  up to 0.25 eV and too high for  $E_i > 0.3$  eV. Finally, the  $\text{RPBE:PBE}(50:50)\text{vdW1}$  ( $\text{SRP50-vdW1}$ ) functional also gives reasonable agreement with experiment, with the computed  $S_0$  being rather similar to those obtained with the  $\text{PBE-vdW2}$  functional. These two functionals were also found to give good agreement with one another and with experiment for the weakly activated dissociation of  $\text{H}_2$  on  $\text{Ru}(0001)$ <sup>45</sup>. As also found for this system, the  $\text{PBE-vdW2}$  and  $\text{SRP50-vdW1}$  functionals yield a similar minimum barrier height and energetic corrugation (Fig. 2.4A). If we put emphasis on the comparison to the experimental data of Rendulic et al.<sup>28</sup> for energies up to 0.2 eV, the  $\text{PBE-vdW2}$  functional is best, followed closely by the  $\text{SRP50-vdW1}$  functional.

Having arrived at our verdict on which functional is most accurate when comparing to the results of Rendulic et al.<sup>28</sup>, we now perform a more extensive comparison with available experiments to arrive at a verdict on the quality of the  $\text{PBE-vdW2}$  functional for describing  $\text{H}_2 + \text{Ni}(111)$ . In Fig. 2.6 we compare our computed  $S_0$  for this functional to experimental  $S_0$  for normal and off-normal incidence obtained by Rendulic et al.<sup>28</sup> and to experimental  $S_0$  for normal incidence obtained by Resch et al.<sup>29</sup>. As was the case for the normal incidence results obtained by Rendulic et al. (Fig. 2.6b), their results for off-normal incidence (Fig. 2.6c) start to deviate from the computed  $S_0$  for  $E_i > 0.2$  eV. As the  $S_0$  measured by Rendulic et al. obeyed normal energy scaling, this can be taken to suggest that the discrepancies between the  $\text{PBE-vdW2}$  theory and

experiment at  $E_i > 0.2$  eV could be due to differences between the translational energy distributions used in the experiments and in the simulations, a point we will come back to below.

For normal incidence the  $S_0$  computed with PBE-vdW2 are in better agreement with the results of Resch et al. (Fig. 2.6a) than with those of Rendulic et al. (Fig. 2.6b). Both experimental data sets were obtained in the same group (of Rendulic). Assuming the results obtained later to be the most accurate, we will therefore base our verdict on the quality of the PBE-vdW2 functional on the comparison in Fig. 2.6a. We do this in the usual way<sup>13,14,82</sup> by computing the mean absolute deviation (MAD) between theory and experiment, which is computed as the average of the absolute difference in incidence energy between the experimental  $S_0$  and the theoretical sticking probability curve spline interpolated to that value of  $S_0$  (some examples of incidence energy differences are shown in Fig. 2.6). The MAD values and also values of the mean signed difference (MSD) are reported in Table 2.4. As can be seen, the MAD value for the comparison with the normal incidence data of Resch et al. is 26 meV (0.60 kcal/mol), i.e., lower than 1 kcal/mol. Therefore, from this point of view the PBE-vdW2 functional is a candidate SRP density functional for  $H_2 + Ni(111)$ . This statement comes with the following three caveats: (i) Our only criterion for taking the experimental dataset from normal incidence by Resch et al. as the reference data set has been that these data were obtained later in time and in the same group as the data of Rendulic et al., (ii) when the comparison is made with the normal incidence data of Rendulic et al., we do arrive at an MAD value (1.42 kcal/mol) greater than 1 kcal/mol, and (iii) for a candidate SRP-DF to be called a true SRP-DF it should also describe an experiment on  $H_2 + Ni(111)$  to which it was not fitted with chemical accuracy. Here, the experiment of Rendulic et al. for  $\theta = 40^\circ$  does not count, one reason being that it is not independent from the normal incident experiment the PBE-vdW2 functional was fitted to (because normal and off-normal incidence results are related by normal energy scaling<sup>28</sup>).

For the PBE-vdW2 functional to be called an SRP-DF, we think two things should happen: (i) new and well-defined experiments should be carried out on sticking of  $H_2$  to  $Ni(111)$  for  $E_i > 0.2$  eV to clear up the energy dependence of sticking at larger incidence energies, and (ii) the quality of the PBE-vdW2 functional should be confirmed through a successful comparison with another experiment probing the  $H_2$ - $Ni(111)$  interaction. Our present results do suggest that the PBE-vdW2 functional describes the minimum barrier region of the PES accurately. In the next section we will discuss possible explanations of the discrepancies that remain between the PBE-vdW2 theory and the experiments for  $E_i > 0.2$  eV.

TABLE 2.4: MAD and MSD values characterizing the agreement between the  $S_0$  computed with the PBE-vdW2 functional and measured in experiments.

Experiment	MAD (kcal/mol)	MSD (kcal/mol)
Resch et al. <sup>29</sup> , $\theta = 0^0$	0.60	0.60
Rendulic et al. <sup>28</sup> , $\theta = 0^0$	1.42	1.34
Rendulic et al. <sup>28</sup> , $\theta = 40^0$	0.90	0.37

### 2.3.3 Causes for the discrepancies between theory and experiment

To understand the discrepancy between the experiments and the best theoretical (PBE-vdW2) results at the highest energies mentioned above, we discuss four potential sources of error: (i) errors in the experiments; (ii) errors in the simulation of the experiments due to assuming wrong translational energy distributions or nozzle temperatures; (iii) errors in the dynamical model or dynamics method used, and (iv) errors in the PES used.

As we mentioned earlier in our introduction, many sets of experimental data have been published on sticking of  $H_2+Ni(111)$ . The sets of measurements from Rendulic et al.<sup>28</sup>, Resch et al.<sup>29</sup> and Hayward and Taylor<sup>27</sup> are in reasonable agreement with one another for low incidence energies, and the discrepancies between the first two experiments for incidence energies  $> 0.2$  eV may point to problems with the experiments at these energies (Fig. 2.1). As can be seen from the normal incidence results in Figs. 2.6a and 2.6b, at the higher energies better agreement is obtained of the PBE-vdW2 results with the set of  $S_0$  published later by the Rendulic group (in 1993, by Resch et al.). Again assuming the results obtained later in time to be more accurate, this might be taken to suggest that the  $S_0$  measured by Rendulic et al. were too low for  $E_i > 0.2$  eV. This might be related to the translational energy distributions of the beam, as suggested by the observation that our computed  $S_0$  for PBE-vdW2 are also too high for off-normal incidence with  $E_i > 0.2$  eV when comparing to the data of Rendulic et al. (Fig. 2.6c).

In Fig. 2.7, we have also plotted the  $S_0$  measured by Resch et al.<sup>29</sup> for adsorption of  $H_2$  on  $Ni(111)$  covered by 0.02ML potassium. It is clear that at incidence energies  $> 0.25$  eV, the experimental  $S_0$  from Resch et al.<sup>29</sup> for the potassium covered surface reproduce those from Rendulic et al.<sup>28</sup> for the clean surface. As already pointed out, the experimental data from Resch et al.<sup>29</sup> for the clean  $Ni(111)$  surface reproduce our PBE-vdW2 results rather well, except for one point at 0.33 eV. While it may be tempting to attribute the

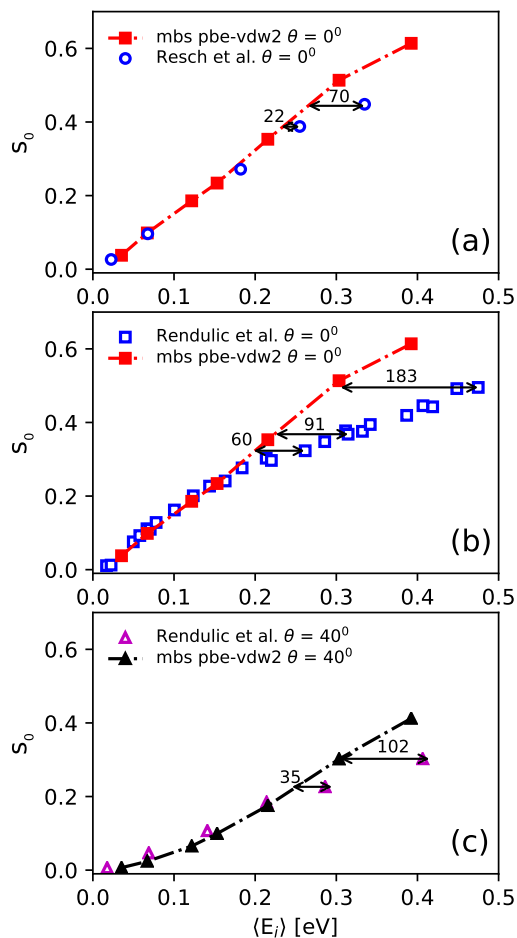


FIGURE 2.6: Sticking probability for molecular beams of  $H_2$  dissociating on Ni(111) computed with PBE-vdW2, compared to experiments<sup>28,29</sup> for  $H_2$  normal and off-normal to Ni(111) surface. The numbers added to the arrows indicates differences in incidence energy between the experimental and interpolated theoretical  $S_0$  in meV.

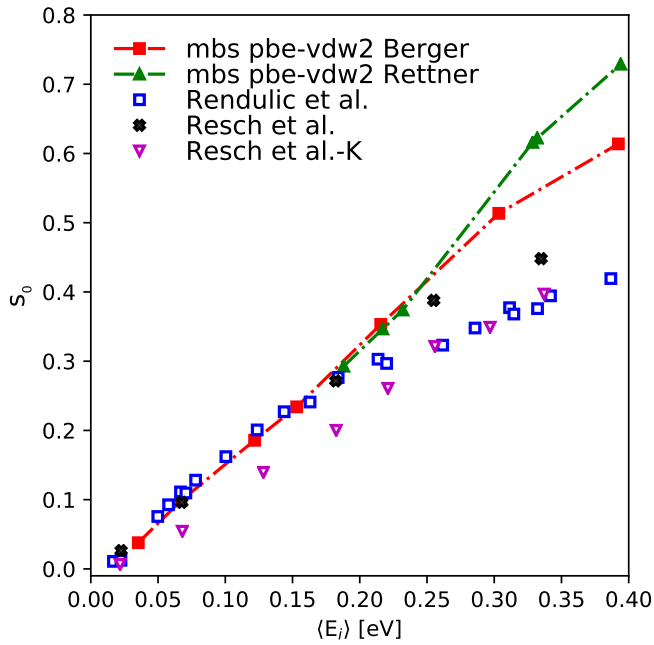


FIGURE 2.7: Comparison of reaction probability for molecular beams of  $H_2$  dissociating on Ni(111) computed with PBE-vdW2 and obtained with parameters from Berger<sup>78</sup> (red square box) and from Rettner<sup>74</sup> (green upper triangle), compared to experiments<sup>28,29</sup> for  $H_2$  normal to Ni(111) surface.



discrepancies of the  $S_0$  computed with PBE-vdW2 with the data of Rendulic et al. to contamination of their nickel sample with K in the experiments by Rendulic et al.<sup>28</sup>, assuming a nickel surface covered by 0.02 ML K would lead to deteriorated agreement between the computed  $S_0$  and the  $S_0$  which would be measured for the covered surface for  $E_i < 0.2$  eV. This suggests that contamination with K in the experiments is not the cause of the discrepancies we try to explain.

We now come to the second point, i.e. possible errors in the simulations of the molecular beam conditions. For neither set of measurements (Refs.<sup>28,29</sup>), the beam conditions have been published. Calculations on  $H_2+Cu(111)$ <sup>4</sup> have shown that the knowledge of the nozzle temperature and parameters characterising the translational energy distribution of the  $H_2$  beam is essential for accurately simulating highly activated reactive scattering of  $H_2$  from metal surfaces. In the absence of specified beam data, and as discussed above, in computing the  $S_0$  discussed so far we have assumed that the beam parameters for  $H_2+Ni(111)$  were the same as those used in other experiments of this group, and obtainable from the Ph.D. thesis of Berger<sup>78</sup>. To investigate the sensitivity of the computed  $S_0$  to the beam parameters, we also tested the beam parameters characterising pure  $H_2$  beams from Rettner et al.<sup>74</sup> published in Refs.<sup>4,83</sup>, which are characteristic of beams with a much narrower energy distribution<sup>4</sup>. As seen in Fig. 2.7, relative to the  $S_0$  computed with the Berger beam parameters, the  $S_0$  computed with the parameters due to Rettner and Auerbach and co-workers are higher for  $E_i > 0.25$  eV. If anything, this suggests that the discrepancy with experiment is not due to simulating beams that are too narrow; rather, the experimental beams might have been broader in incidence energy than the Berger beams we simulated. An alternative explanation for the experimental  $S_0$  being too low at large  $E_i$  is that the data collection time was too large in the King and Wells measurements to determine  $S_0$ , so that the measured  $S_0$  no longer was equal to the initial sticking coefficient, but reflected sticking on an H-precovered surface.

We now turn to point (iii), the question of whether the dynamical method and the model used in our calculations might be responsible for the discrepancies with the experiment at higher incidence energies. We start by evaluating the quality of the QCT method for molecular beam simulations of the sticking probability. Quantum dynamical calculations have been carried out on  $H_2+Ni(111)$  reaction for normal incidence of  $H_2$  in some selected initial rovibrational states. In Fig. 2.8, the degeneracy averaged initial state-resolved reaction probability obtained from QCT calculations is compared to QD results for  $\nu = 0, j = 0$ ;  $\nu = 0, j = 1$  and  $\nu = 0, j = 2$ , for the PBE-vdW2 functional. It is clear that, especially at the lowest energies, some oscillations are present in the QD results. These oscillations may be explained by the fact that the  $H_2$  molecule has extra time to tunnel through the barrier when trapped in a metastable state leading to

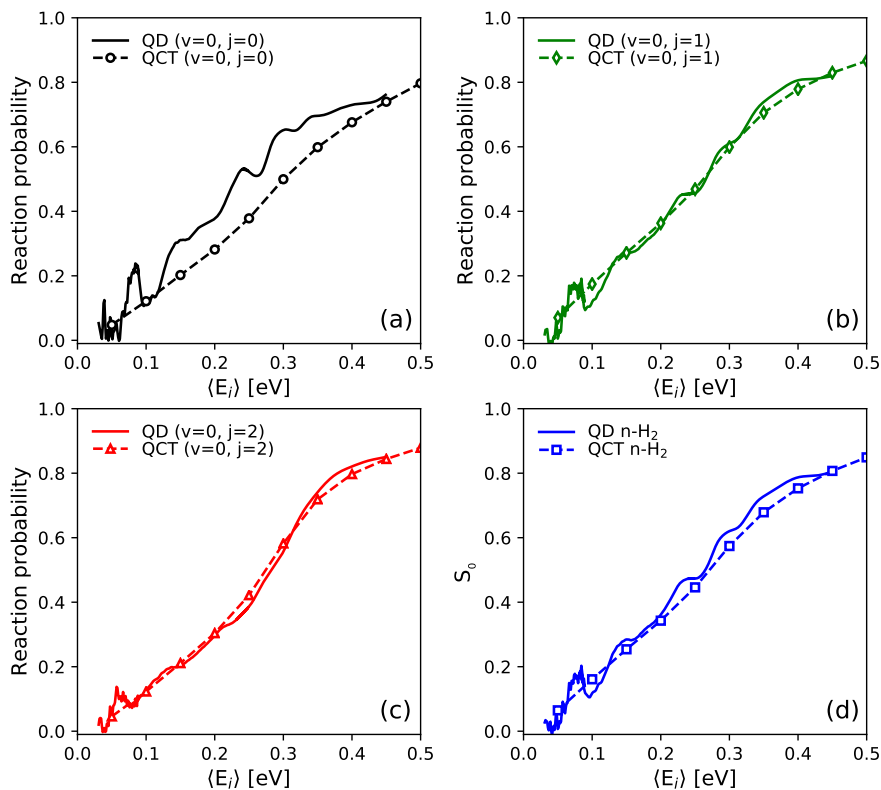


FIGURE 2.8: Comparison between quantum dynamics and quasi-classical trajectory for initial rotational state-resolved reaction probabilities of  $\text{H}_2$  dissociating on Ni(111) computed with PBE-vdW2 (a-c), and comparison of sticking probability for cold  $n\text{-H}_2$  (d).

dissociation at the corresponding energies<sup>84</sup>. Our finding that the oscillations are most pronounced for the ( $\nu = 0, j = 0$ ) state suggests that the trapping leading to the oscillations might be due to the population of excited librational (i.e., hindered rotational) states at the surface.

The agreement between QCT and QD is found to be excellent for the higher rotational states, i.e., for ( $\nu = 0, j = 1$ ) and for ( $\nu = 0, j = 2$ ). For ( $\nu = 0, j = 0$ ), the QCT reaction probabilities underestimate the QD results for several incidence energies. However, we expect the effect on the sticking probability to be small. As Fig. 2.8d shows, most of the difference between the QD and QCT sticking probability would already disappear if the beam simulation were to be performed for cold n-H<sub>2</sub> (25%  $j = 0$  H<sub>2</sub> + 75%  $j = 1$  H<sub>2</sub>). For most nozzle temperatures (incidence energies), the weight of  $j = 0$  H<sub>2</sub> in the beam should actually be much lower than 0.25, as shown in Table 2.2, and this is especially true for  $E_i > 0.2$  eV. Therefore, and because the QCT and the QD results are in good agreement for  $j > 0$ , the discrepancies between theory and experiment for  $E_i > 0.2$  eV should not be due to using the QCT method to compute  $S_0$ .

We next turn to the limitations of the dynamical model. In our calculations with the BOSS model, we have neglected the effects of electron-hole pair excitation. However, calculations<sup>85</sup> on the similar H<sub>2</sub> + Ru(0001) system suggest that the effect of electron-hole pair excitation on the sticking coefficient should be minor. We have also neglected the effect of the surface phonons. Again, calculations<sup>86</sup> on H<sub>2</sub> sticking to Pd(110) and Pd(111) suggest that, at incidence energies  $> 0.2$  eV where the dissociation mechanism on these surfaces becomes activated, the effect of allowing surface atom motion should become negligible. In summary, it is unlikely that the discrepancy between the present theory and the experiments of the Rendulic group is due to the use of the BOSS model in our calculations.

Finally, we come to point (iv), i.e., how PES features might have led to discrepancies between the molecular beam simulation results and the measured sticking coefficients. We first note that the two functionals that gave the best agreement with experiment (PBE-vdW2 and SRP50-vdW1) have a similar minimum barrier height and energetic corrugation. Based on the agreement with experiment we obtained with the PBE-vdW2 functional (see Fig. 2.6), we suggest that the minimum barrier height predicted by the PBE-vdW2 functional is accurate. The comparison with the results of Resch et al. at higher incidence energies suggests that the energetic corrugation of the PES may have been underestimated, assuming the results of Resch et al. to be correct. However, the theory correctly predicted the  $S_0$  measured by Resch et al. up to about 0.3 eV. This suggests that the heights of the barriers at the bridge and hcp and fcc hollow sites computed with PBE-vdW2 may have been too small. If this

would indeed be true, the  $\text{H}_2 + \text{Ni}(111)$  system would be the first example of an  $\text{H}_2 + \text{metal surface}$  system for which the energetic corrugation of the PES is underestimated even when using a functional incorporating van der Waals correlation. For example, the PBE-vdW2 and SRP50-vdW1 functionals gave excellent results for the similar weakly activated  $\text{H}_2 + \text{Ru}(0001)$  reaction<sup>44</sup>.

## 2.4 Conclusions

In this chapter we take a first step to develop a SRP-DF for  $\text{H}_2$  on  $\text{Ni}(111)$ , also investigating if the SRP-DF derived previously for  $\text{H}_2 + \text{Pt}(111)$  is transferable to the system investigated. To address these questions, 6D PESs have been constructed for the dissociation of  $\text{H}_2 + \text{Ni}(111)$  using nine different exchange-correlation functionals. The PESs calculated were then interpolated using the CRP method. To compare with experimentally measured sticking probabilities, quasi-classical trajectory and quantum dynamics calculations have been performed using the BOSS model.

The functionals investigated yield a wide range of barrier heights and barrier positions. The functionals containing van der Waals correlation yield barriers that are closer to the surface and exhibit a larger energetic corrugation than functionals containing PBE correlation, as previously also found for the related  $\text{H}_2 + \text{Ru}(0001)$  early barrier system.

The PBE-vdW2 and RPBE:PBE(50:50)vdW1 functionals describe the sticking experiments performed by the Rendulic group quite well, with PBE-vdW2 giving the best results. From the comparison with the most recent molecular beam experiments performed by the Rendulic group, we conclude that PBE-vdW2 can be considered to be a candidate SRP-DF for  $\text{H}_2 + \text{Ni}(111)$ . However, the  $\text{PBE}\alpha=0.57\text{-vdW2}$  functional, which is a SRP-DF for  $\text{H}_2$  on  $\text{Pt}(111)$  is not a SRP-DF for  $\text{H}_2 + \text{Ni}(111)$ , even though Ni and Pt belong to the same group.

The PBE-vdW2 sticking probabilities are not yet in good agreement with the most recent experiments of the Rendulic group<sup>28</sup> for incidence energies  $> 0.3$  eV. Also, for incidence energies greater than 0.2 eV the  $S_0$  published in an earlier paper of the Rendulic group deviated from the  $S_0$  the group published 4 years later. For incidence energies  $> 0.25$  eV we found that  $S_0$  starts to exhibit a considerable dependence on the beam conditions, so that some of the discrepancies noted could be due to different beam parameters characterizing the experimental beams and the beams simulated in the calculations. Other possible causes of error in the experiments have also been discussed. We consider it unlikely that the discrepancies between theory and experiment are due to using an incorrect dynamical model (BOSS) or dynamics method (QCT). In particular, except perhaps for  $\nu = 0, j = 0$  initial-state resolved reaction probabilities

computed with QCT were in good agreement with QD results, so that QCT should give accurate results for sticking. However, it is possible that the PBE-vdW2 functional yields barriers for dissociation over the bridge and hollow sites that are too low. To resolve this and other questions, we advocate that new and well-defined (with respect to velocity distributions and nozzle temperatures of the beams used) experiments are performed on sticking of H<sub>2</sub> to Ni(111) for incidence energies > 0.2 eV.

## References

- (1) Chorkendorff, I.; Niemantsverdriet, J. W., *Concepts of modern catalysis and kinetics*; Wiley Online Library: 2003; Vol. 138.
- (2) Ertl, G. Primary steps in catalytic synthesis of ammonia. *J. Vac. Sci. Technol., A: Vacuum, Surfaces, and Films* **1983**, *1*, 1247–1253.
- (3) Noyori, R. Synthesizing our future. *Nat. Chem.* **2009**, *1*, 5–6.
- (4) Díaz, C.; Pijper, E.; Olsen, R. A.; Busnengo, H. F.; Auerbach, D. J.; Kroes, G. J. Chemically accurate simulation of a prototypical surface reaction: H<sub>2</sub> dissociation on Cu(111). *Science* **2009**, *326*, 832–834.
- (5) Kroes, G. J. Toward a database of chemically accurate barrier heights for reactions of molecules with metal surfaces. *J. Phys. Chem. Lett.* **2015**, *6*, 4106–4114.
- (6) Kroes, G. J. Computational approaches to dissociative chemisorption on metals: towards chemical accuracy. *Phys. Chem. Chem. Phys.* **2021**, *23*, 8962–9048.
- (7) **Tchakoua, T.**; Gerrits, N.; Smeets, E. W. F.; Kroes, G. J. SBH17: Benchmark Database of Barrier Heights for Dissociative Chemisorption on Transition Metal Surfaces. *J. Chem. Theory Comput.* **2023**, *19*, 245–270.
- (8) Langreth, D. C.; Mehl, M. Beyond the local-density approximation in calculations of ground-state electronic properties. *Phys. Rev. B* **1983**, *28*, 1809.
- (9) Becke, A. D. Density-functional exchange-energy approximation with correct asymptotic behavior. *Phys. Rev. A* **1988**, *38*, 3098.
- (10) Perdew, J. P.; Burke, K.; Ernzerhof, M. Generalized Gradient Approximation Made Simple. *Phys. Rev. Lett.* **1996**, *77*, 3865–3868.
- (11) Hammer, B. Bond activation at monatomic steps: NO dissociation at corrugated Ru(0001). *Phys. Rev. Lett.* **1999**, *83*, 3681.
- (12) Peverati, R.; Truhlar, D. G. An improved and broadly accurate local approximation to the exchange–correlation density functional: The MN12-L functional for electronic structure calculations in chemistry and physics. *PCCP* **2012**, *14*, 13171–13174.

- (13) Migliorini, D.; Chadwick, H.; Nattino, F.; Gutiérrez-González, A.; Dombrowski, E.; High, E. A.; Guo, H.; Utz, A. L.; Jackson, B.; Beck, R. D.; Kroes, G. J. Surface reaction barriometry: methane dissociation on flat and stepped transition-metal surfaces. *J. Phys. Chem. Lett.* **2017**, *8*, 4177–4182.
- (14) Nour Ghassemi, E.; Somers, M.; Kroes, G. J. Test of the transferability of the specific reaction parameter functional for  $\text{H}_2 + \text{Cu}(111)$  to  $\text{D}_2 + \text{Ag}(111)$ . *J. Phys. Chem. C* **2018**, *122*, 22939–22952.
- (15) Boereboom, J.; Wijzenbroek, M.; Somers, M.; Kroes, G. Towards a specific reaction parameter density functional for reactive scattering of  $\text{H}_2$  from  $\text{Pd}(111)$ . *J. Chem. Phys.* **2013**, *139*, 244707.
- (16) Ghassemi, E. N.; Somers, M. F.; Kroes, G. J. Assessment of Two Problems of Specific Reaction Parameter Density Functional Theory: Sticking and Diffraction of  $\text{H}_2$  on  $\text{Pt}(111)$ . *J. Phys. Chem. C* **2019**, *123*, 10406–10418.
- (17) Kroes, G. J. Six-dimensional quantum dynamics of dissociative chemisorption of  $\text{H}_2$  on metal surfaces. *Prog. Surf. Sci* **1999**, *60*, 1–85.
- (18) Groß, A. Reactions at surfaces studied by ab initio dynamics calculations. *Surf. Sci. Rep.* **1998**, *32*, 291–340.
- (19) Kroes, G. J.; Somers, M. F. Six-dimensional dynamics of dissociative chemisorption of  $\text{H}_2$  on metal surfaces. *J. Theor. Comput. Chem.* **2005**, *4*, 493–581.
- (20) Kroes, G. J.; Díaz, C. Quantum and classical dynamics of reactive scattering of  $\text{H}_2$  from metal surfaces. *Chem. Soc. Rev.* **2016**, *45*, 3658–3700.
- (21) Kroes, G. J. Frontiers in surface scattering simulations. *Science* **2008**, *321*, 794–797.
- (22) Kroes, G. J. Towards chemically accurate simulation of molecule–surface reactions. *PCCP* **2012**, *14*, 14966–14981.
- (23) Spiering, P.; Meyer, J. Testing Electronic Friction Models: Vibrational De-excitation in Scattering of  $\text{H}_2$  and  $\text{D}_2$  from  $\text{Cu}(111)$ . *J. Phys. Chem. Lett.* **2018**, *9*, 1803–1808.
- (24) Zhang, Y.; Maurer, R. J.; Guo, H.; Jiang, B. Hot-electron effects during reactive scattering of  $\text{H}_2$  from  $\text{Ag}(111)$ : the interplay between mode-specific electronic friction and the potential energy landscape. *Chem. Sci.* **2019**, *10*, 1089–1097.

- (25) Steinrück, H.; Rendulic, K.; Winkler, A. The sticking coefficient of H<sub>2</sub> on Ni(111) as a function of particle energy and angle of incidence: A test of detailed balancing. *Surf. Sci.* **1985**, *154*, 99–108.
- (26) Robota, H.; Vielhaber, W.; Lin, M.; Segner, J.; Ertl, G. Dynamics of interaction of H<sub>2</sub> and D<sub>2</sub> with Ni(110) and Ni(111) surfaces. *Surf. Sci.* **1985**, *155*, 101–120.
- (27) Hayward, D.; Taylor, A. The variation of the sticking probability of hydrogen and deuterium on Ni(111) with energy and angle of incidence. *Chem. Phys. Lett.* **1986**, *124*, 264–267.
- (28) Rendulic, K.; Anger, G.; Winkler, A. Wide range nozzle beam adsorption data for the systems H<sub>2</sub>/nickel and H<sub>2</sub>/Pd(100). *Surf. Sci.* **1989**, *208*, 404–424.
- (29) Resch, C.; Zhukov, V.; Lugstein, A.; Berger, H.; Winkler, A.; Rendulic, K. Dynamics of hydrogen adsorption on promoter- and inhibitor-modified nickel surfaces. *Chem. Phys.* **1993**, *177*, 421–431.
- (30) Hahn, C., Ph.D. Thesis, Leiden Institute of Chemistry, 2012.
- (31) Bourcet, A.; Tantardini, G. F. A theoretical study of the adsorption dynamics of hydrogen on Ni(111) surface. *J. Electron. Spectrosc. Relat. Phenom.* **1994**, *69*, 55–64.
- (32) Kresse, G. Dissociation and sticking of H<sub>2</sub> on the Ni(111), (100), and (110) substrate. *Phys. Rev. B* **2000**, *62*, 8295–8305.
- (33) Perdew, J. P.; Wang, Y. Accurate and simple analytic representation of the electron-gas correlation energy. *Phys. Rev. B* **1992**, *45*, 13244.
- (34) Perdew, J. P.; Chevary, J. A.; Vosko, S. H.; Jackson, K. A.; Pederson, M. R.; Singh, D. J.; Fiolhais, C. Atoms, molecules, solids, and surfaces: Applications of the generalized gradient approximation for exchange and correlation. *Phys. Rev. B* **1992**, *46*, 6671.
- (35) Ghassemi, E. N.; Wijzenbroek, M.; Somers, M. F.; Kroes, G. J. Chemically accurate simulation of dissociative chemisorption of D<sub>2</sub> on Pt(111). *Chem. Phys. Lett.* **2017**, *683*, 329–335.
- (36) Dion, M.; Rydberg, H.; Schröder, E.; Langreth, D. C.; Lundqvist, B. I. Van der Waals Density Functional for General Geometries. *Phys. Rev. Lett.* **2004**, *92*, 246401.
- (37) Lee, K.; Murray, É. D.; Kong, L.; Lundqvist, B. I.; Langreth, D. C. Higher-accuracy van der Waals density functional. *Phys. Rev. B* **2010**, *82*, 081101.



- (38) Madsen, G. K. H. Functional form of the generalized gradient approximation for exchange: The PBE $\alpha$  functional. *Phys. Rev. B* **2007**, *75*, 195108.
- (39) Becke, A. D. Density-functional thermochemistry. V. Systematic optimization of exchange-correlation functionals. *J. Chem. Phys.* **1997**, *107*, 8554–8560.
- (40) Hammer, B.; Hansen, L. B.; Nørskov, J. K. Improved adsorption energetics within density-functional theory using revised Perdew-Burke-Ernzerhof functionals. *Phys. Rev. B* **1999**, *59*, 7413–7421.
- (41) Nattino, F.; Migliorini, D.; Kroes, G. J.; Dombrowski, E.; High, E. A.; Killelea, D. R.; Utz, A. L. Chemically accurate simulation of a polyatomic molecule-metal surface reaction. *J. Phys. Chem. Lett.* **2016**, *7*, 2402–2406.
- (42) Migliorini, D.; Chadwick, H.; Kroes, G. J. Methane on a stepped surface: Dynamical insights on the dissociation of CHD<sub>3</sub> on Pt(111) and Pt(211). *J. Chem. Phys.* **2018**, *149*, 094701.
- (43) Chadwick, H.; Migliorini, D.; Kroes, G. J. CHD<sub>3</sub> dissociation on Pt(111): A comparison of the reaction dynamics based on the PBE functional and on a specific reaction parameter functional. *J. Chem. Phys.* **2018**, *149*, 044701.
- (44) Wijzenbroek, M.; Kroes, G. J. The effect of the exchange-correlation functional on H<sub>2</sub> dissociation on Ru(0001). *J. Chem. Phys.* **2014**, *140*, 084702.
- (45) Wijzenbroek, M.; Klein, D. M.; Smits, B.; Somers, M. F.; Kroes, G. J. Performance of a Non-Local van der Waals Density Functional on the Dissociation of H<sub>2</sub> on Metal Surfaces. *J. Phys. Chem. A* **2015**, *119*, 12146–12158.
- (46) Giannozzi, P. et al. Advanced capabilities for materials modelling with QUANTUM ESPRESSO. *J. Phys.: Condens. Matter* **2017**, *29*, 465901.
- (47) Thonhauser, T.; Zuluaga, S.; Arter, C. A.; Berland, K.; Schröder, E.; Hyldgaard, P. Spin Signature of Nonlocal Correlation Binding in Metal-Organic Frameworks. *Phys. Rev. Lett.* **2015**, *115*, 136402.
- (48) Marques, M. A.; Oliveira, M. J.; Burnus, T. Libxc: A library of exchange and correlation functionals for density functional theory. *Comput. Phys. Commun.* **2012**, *183*, 2272–2281.
- (49) Blöchl, P. E. Projector augmented-wave method. *Phys. Rev. B* **1994**, *50*, 17953–17979.

- (50) Dal Corso, A. Pseudopotentials periodic table: From H to Pu. *Comput. Mater. Sci.* **2014**, *95*, 337–350.
- (51) Kresse, G.; Hafner, J. Ab initio molecular dynamics for liquid metals. *Phys. Rev. B* **1993**, *47*, 558–561.
- (52) Kresse, G.; Hafner, J. Ab initio molecular-dynamics simulation of the liquid-metal–amorphous-semiconductor transition in germanium. *Phys. Rev. B* **1994**, *49*, 14251–14269.
- (53) **Tchakoua, T**; Smeets, E. W.; Somers, M.; Kroes, G. J. Toward a Specific Reaction Parameter Density Functional for  $\text{H}_2 + \text{Ni}(111)$ : Comparison of Theory with Molecular Beam Sticking Experiments. *J. Phys. Chem. C* **2019**, *123*, 20420–20433.
- (54) Henkelman, G.; Jónsson, H. A dimer method for finding saddle points on high dimensional potential surfaces using only first derivatives. *J. Chem. Phys.* **1999**, *111*, 7010–7022.
- (55) Heyden, A.; Bell, A. T.; Keil, F. J. Efficient methods for finding transition states in chemical reactions: Comparison of improved dimer method and partitioned rational function optimization method. *J. Chem. Phys.* **2005**, *123*, 224101.
- (56) Kästner, J.; Sherwood, P. Superlinearly converging dimer method for transition state search. *J. Chem. Phys.* **2008**, *128*, 014106.
- (57) Xiao, P.; Sheppard, D.; Rogal, J.; Henkelman, G. Solid-state dimer method for calculating solid-solid phase transitions. *J. Chem. Phys.* **2014**, *140*, 174104.
- (58) Busnengo, H.; Salin, A.; Dong, W. Representation of the 6D potential energy surface for a diatomic molecule near a solid surface. *J. Chem. Phys.* **2000**, *112*, 7641–7651.
- (59) Olsen, R. A.; Busnengo, H. F.; Salin, A.; Somers, M. F.; Kroes, G. J.; Baerends, E. J. Constructing accurate potential energy surfaces for a diatomic molecule interacting with a solid surface:  $\text{H}_2 + \text{Pt}(111)$  and  $\text{H}_2 + \text{Cu}(100)$ . *J. Chem. Phys.* **2002**, *116*, 3841–3855.
- (60) Karplus, M.; Porter, R. N.; Sharma, R. Exchange reactions with activation energy. I. Simple barrier potential for  $(\text{H}, \text{H}_2)$ . *J. Chem. Phys.* **1965**, *43*, 3259–3287.
- (61) Stoer, J.; Bulirsch, R., *Introduction to numerical analysis*; Springer Science & Business Media: 1980.

- (62) Marston, C. C.; Balint-Kurti, G. G. The Fourier grid Hamiltonian method for bound state eigenvalues and eigenfunctions. *J. Chem. Phys.* **1989**, *91*, 3571–3576.
- (63) Wijzenbroek, M.; Helstone, D.; Meyer, J.; Kroes, G. J. Dynamics of H<sub>2</sub> dissociation on the close-packed (111) surface of the noblest metal: H<sub>2</sub>+Au(111). *J. Chem. Phys.* **2016**, *145*, 144701.
- (64) Kosloff, R. Time-dependent quantum-mechanical methods for molecular dynamics. *J. Phys. Chem.* **1988**, *92*, 2087–2100.
- (65) Kosloff, D.; Kosloff, R. A Fourier method solution for the time dependent Schrödinger equation as a tool in molecular dynamics. *J. Comput. Phys.* **1983**, *52*, 35–53.
- (66) Corey, G. C.; Lemoine, D. Pseudospectral method for solving the time-dependent Schrödinger equation in spherical coordinates. *J. Chem. Phys.* **1992**, *97*, 4115–4126.
- (67) Lemoine, D. The finite basis representation as the primary space in multidimensional pseudospectral schemes. *J. Chem. Phys.* **1994**, *101*, 10526–10532.
- (68) Feit, M.; Fleck Jr, J.; Steiger, A. Solution of the Schrödinger equation by a spectral method. *J. Comput. Phys.* **1982**, *47*, 412–433.
- (69) Balint-Kurti, G. G.; Dixon, R. N.; Marston, C. C. Time-dependent quantum dynamics of molecular photofragmentation processes. *J. Chem. Soc., Faraday Trans.* **1990**, *86*, 1741–1749.
- (70) Balint-Kurti, G. G.; Dixon, R. N.; Marston, C. C. Grid methods for solving the Schrödinger equation and time dependent quantum dynamics of molecular photofragmentation and reactive scattering processes. *Int. Rev. Phys. Chem.* **1992**, *11*, 317–344.
- (71) Mowrey, R. C.; Kroes, G. J. Application of an efficient asymptotic analysis method to molecule–surface scattering. *J. Chem. Phys.* **1995**, *103*, 1216–1225.
- (72) Vibok, A.; Balint-Kurti, G. Parametrization of complex absorbing potentials for time-dependent quantum dynamics. *J. Phys. Chem.* **1992**, *96*, 8712–8719.
- (73) Pijper, E.; Kroes, G. J.; Olsen, R. A.; Baerends, E. J. Reactive and diffractive scattering of H<sub>2</sub> from Pt(111) studied using a six-dimensional wave packet method. *J. Chem. Phys.* **2002**, *117*, 5885–5898.

- (74) Rettner, C.; Michelsen, H.; Auerbach, D. Quantum-state-specific dynamics of the dissociative adsorption and associative desorption of H<sub>2</sub> at a Cu(111) surface. *J. Chem. Phys.* **1995**, *102*, 4625–4641.
- (75) Gallagher, R. J.; Fenn, J. B. Relaxation rates from time of flight analysis of molecular beams. *J. Chem. Phys.* **1974**, *60*, 3487–3491.
- (76) Díaz, C.; Olsen, R. A.; Auerbach, D. J.; Kroes, G. J. Six-dimensional dynamics study of reactive and non reactive scattering of H<sub>2</sub> from Cu(111) using a chemically accurate potential energy surface. *Phys. Chem. Chem. Phys.* **2010**, *12*, 6499–6519.
- (77) Michelsen, H. A.; Auerbach, D. J. A critical examination of data on the dissociative adsorption and associative desorption of hydrogen at copper surfaces. *J. Chem. Phys.* **1991**, *94*, 7502–7520.
- (78) Berger, H. F., Ph.D. Thesis, Technische Universität Graz, 1992.
- (79) Marquardt, D. W. An Algorithm for Least-Squares Estimation of Non-linear Parameters. *J. Soc. Ind. Appl. Math.* **1963**, *11*, 431–441.
- (80) Perdew, J. P.; Schmidt, K. Jacob's ladder of density functional approximations for the exchange-correlation energy. *AIP Conf. Proc.* **2001**, *577*, 1–20.
- (81) Gross, A.; Hammer, B.; Scheffler, M.; Brenig, W. High-dimensional quantum dynamics of adsorption and desorption of H<sub>2</sub> at Cu(111). *Phys. Rev. Lett.* **1994**, *73*, 3121.
- (82) Ghassemi, E. N.; Smeets, E. W. F.; Somers, M. F.; Kroes, G. J.; Groot, I. M.; Juurlink, L. B.; Füchsel, G. Transferability of the specific reaction parameter density functional for H<sub>2</sub> + Pt(111) to H<sub>2</sub> + Pt(211). *J. Phys. Chem. C* **2019**, *123*, 2973–2986.
- (83) Smeets, E. W. F.; Voss, J.; Kroes, G. J. Specific Reaction Parameter Density Functional Based on the Meta-Generalized Gradient Approximation: Application to H<sub>2</sub>+Cu(111) and H<sub>2</sub>+Ag(111). *J. Phys. Chem. A* **2019**, *123*, 5395–5406.
- (84) Chen, J.-C.; Juanes-Marcos, J. C.; Woittequand, S.; Somers, M. F.; Díaz, C.; Olsen, R. A.; Kroes, G. J. Six-dimensional quasiclassical and quantum dynamics of H<sub>2</sub> dissociation on the c (2× 2)-Ti/Al(100) surface. *J. Chem. Phys.* **2011**, *134*, 114708.
- (85) Füchsel, G.; Schimka, S.; Saalfrank, P. On the role of electronic friction for dissociative adsorption and scattering of hydrogen molecules at a Ru(0001) surface. *J. Phys. Chem. A* **2013**, *117*, 8761–8769.

- (86) Busnengo, H.; Di Césare, M.; Dong, W.; Salin, A. Surface temperature effects in dynamic trapping mediated adsorption of light molecules on metal surfaces: H<sub>2</sub> on Pd (111) and Pd (110). *Phys. Rev. B* **2005**, *72*, 125411.

## SBH17: Benchmark Database of Barrier Heights for Dissociative Chemisorption on Transition Metal Surfaces

This Chapter is based on:

**Tchakoua, T.;** Gerrits, N.; Smeets, E. W. F.; Kroes, G. J. SBH17: Benchmark Database of Barrier Heights for Dissociative Chemisorption on Transition Metal Surfaces. *J. Chem. Theory Comput.* **2023**, *19*, 245–270

### Abstract

Accurate barriers for rate controlling elementary reactions on metal surfaces are key to understanding, controlling, and predicting the rate of heterogeneously catalyzed processes. While barrier heights for gas phase reactions have been extensively benchmarked, dissociative chemisorption barriers for the reactions of molecules on metal surfaces have received much less attention. A first database called SBH10 and containing 10 entries was recently constructed based on the specific reaction parameter approach to density functional theory (SRP-DFT) and more appropriate semi-empirical approaches. We have now constructed a new and improved database (SBH17) containing 17 entries based on SRP-DFT and more appropriate semi-empirical approaches. For this new SBH17 benchmark study, we have tested three algorithms (high, medium, and light) for calculating barrier heights for dissociative chemisorption on metals, which we have named for the amount of computational effort involved in their use. We test the performance of 14 density functionals at the generalized gradient approximation (GGA), GGA+vdW-DF and meta-GGA rungs. Our results show that, in contrast with the previous SBH10 study where the BEEF-vdW-DF2 functional seemed to be most accurate, the work horse functional PBE and the MS2 density functional are the most accurate of the GGA and meta-GGA functionals tested. Of the GGA+vdW functionals tested, the SRP32-vdW-DF1 functional is the

most accurate. Additionally we found that the medium algorithm is accurate enough for assessing the performance of the density functionals tested, while it avoids geometry optimizations of minimum barrier geometries for each density functional tested. The medium algorithm does require metal lattice constants and interlayer distances that are optimized separately for each functional. While these are avoided in the light algorithm, this algorithm is found not to give a reliable description of functional performance. The combination of relative ease of use and demonstrated reliability of the medium algorithm will likely pave the way for incorporation of the SBH17 database in larger databases used for testing new density functionals and electronic structure methods.

### 3.1 Introduction

Heterogeneous catalyzed processes are of large importance to the chemical industry<sup>1</sup>, well-known examples of such processes being ammonia synthesis<sup>2</sup> and steam reforming<sup>3</sup>. In heterogeneously catalyzed processes on metal surfaces, the steps with a high degree of rate control often involve the dissociative chemisorption (DC, the process whereby the interaction of a molecule with a surface leads to the breaking of a bond in the molecule and the formation of two new bonds of the molecular fragments to the surface) of a molecule on the surface<sup>4,5</sup>. Understanding how heterogeneous catalysis works is of huge importance. Our ability to understand the different mechanisms underlying DC on metal surfaces could benefit significantly from the availability of an accurate database for barrier heights of elementary molecule-metal surface reactions. Just like chemisorption energies of (intermediate) reactants and products, accurate barriers for rate controlling elementary reactions are key to understanding, controlling, and predicting the rate of overall heterogeneously catalyzed processes<sup>6-9</sup>.

Ideally, accurate barrier heights could be extracted directly from detailed systematic experiments. However, it is not possible to measure barrier heights for DC directly. An observable that can be measured experimentally and that is strongly related to the barrier height for DC is the sticking probability ( $S_0$ )<sup>10</sup>. The best way to access barrier heights using theory is through a theoretical approach in which potential energy surfaces (PESs) are computed and used in dynamics calculations to evaluate  $S_0$  as a function of average incidence energy<sup>10</sup>. Comparison with experimental  $S_0$ <sup>10-14</sup> will then allow one to evaluate the accuracy of the electronic structure method used to compute the PES for the calculated barrier height<sup>10</sup>. Only when experimental data are reproduced within chemical accuracy (i.e., with errors smaller than 1 kcal/mol<sup>11,12</sup>) to a sufficiently large extent, a claim can be made that the computed barrier height is of high accuracy.

For adsorption bond energies to transition metal surfaces, a database containing 39 entries for use with DFT benchmarking studies has recently been constructed<sup>15</sup>. This database, subsets of it<sup>16,17</sup>, and a slightly extended version<sup>18</sup> of it, have been used in several benchmark DFT studies<sup>15–21</sup>, and a considerably extended database containing 81 entries also exists<sup>22</sup>. Barrier heights for gas phase reaction have been extensively benchmarked<sup>23–26</sup>. However, barriers for DC on metal surfaces have been mapped out to a much smaller extent<sup>10</sup>, and have been little used for benchmark calculations. For many gas phase reactions, it has been possible to use the very accurate CCSD(T)<sup>27</sup> electronic structure method to compute reference values. On the other hand, for molecule-metal surface reactions, until very recently only semi-local density functional theory (DFT)<sup>28</sup> could be used, which is much less accurate. As result, it is not yet known how large the errors in barriers for molecule-metal surface reactions are when using standard exchange-correlation (XC) functionals. For reactions occurring in the gas phase, it is well known that the density functionals (DFs) at the second rung on Jacob's ladder<sup>28,29</sup> (GGA level<sup>30,31</sup>) underestimate barrier heights as a consequence of self-interaction errors<sup>24,32</sup>. An idea of the performance of semi-local functionals on gas phase reaction barriers can be obtained from their performance on the BH206 database<sup>24</sup>, tests showing that application of the best performing MN12-L<sup>33</sup> and N12<sup>34</sup> non-separable meta-GGA and GGA DFs resulted in root mean square deviations of 4.3 and 7.1 kcal/mol, respectively. To overcome this potential problem of the XC functional for molecule-metal surface reactions, the SRP-DFT method<sup>35,36</sup> (which uses weighted averages of two XC functionals) has been adopted for such reactions<sup>11</sup>. This semi-empirical (SE) method has allowed prediction of barrier heights to within chemical accuracy (1 kcal/mol) for specific systems<sup>10</sup>.

Some theoretical studies have been carried out recently in attempts to build databases of barrier heights for molecule-metal surface reactions. The first database (CatApp<sup>37,38</sup>) was built based on DFT calculations using only one functional (RPBE<sup>39</sup>). More recently, a first attempt was made to construct a database of molecule-metal surface reaction barriers for benchmarking purposes<sup>40</sup>. This database, called SHB10, contained 6 entries based on SRP-DFT and 4 entries based on more ad-hoc SE procedures. The SBH10 database was used<sup>40</sup> to test the performance of one DF consisting of GGA exchange and non-local correlation (BEEF-vdW-DF2<sup>16</sup>), one meta-GGA (MS2<sup>41</sup>), and one screened hybrid DF (HSE06<sup>42</sup>). A surprising conclusion was that BEEF-vdW-DF2 performed the best.

With more than 30 000 papers published annually<sup>43</sup>, DFT arguably is the most important electronic structure method for dealing with complex systems. It is therefore important to develop a large enough database that allows testing



the method on barrier heights for molecule-metal surface reactions. As discussed below, accurate SRP-DFT barriers for DC are now available for 14 molecule-metal surface reactions, allowing the former database to be extended with 7 systems if additional results from three more ad-hoc procedures are included as before. In the present chapter, we therefore develop a new and larger database for benchmarking (SBH17), which contains benchmark results for 17 systems. We now also test a much larger number of DFs on this larger database, i.e., 3 GGA-type DFs, 4 meta-GGA DFs, and 7 DFs containing GGA exchange and non-local correlation. In performing these tests, we also take an improved approach over that taken in the previous paper<sup>40</sup>, in which the metal surface was allowed to relax in response to the incoming molecule while computing the barrier height. This approach is flawed in that the metal surface atoms have too little time to respond to the motion of the incoming molecule in the hypersonic molecular beam experiments employed to perform sticking experiments, which are used in the SE procedure to construct SRP DFs<sup>10</sup>.

In performing the tests of the 14 DFs to be discussed below, three different algorithms will be used to compute barrier heights. These algorithms differ in the computational effort that may be required to compute metal lattice constants and metal slabs that have interlayer distances simulating metal surfaces interacting with the vacuum, and to locate the transition state geometry for a specific functional. These three algorithms will be compared among each other for their performance. A new database for molecule-metal surface reaction barriers is of course more likely to be used if it meets the following two demands, which may conflict with one another. When used in testing new functionals or electronic structure methods in general, the algorithm should be as easy and straightforward to use, and require as little computational effort, as possible. At the same time, the algorithm should also still yield reliable results regarding how functionals or new methods perform, because otherwise it would not be useful.

The outline of our chapter is as follows: In Section 3.2, the methods used are explained, beginning with the DFs tested in Section 3.2.1. The description of the SE procedures used to obtain reference values of barrier heights, and the motivation of the use of SRP-DFT are presented in Section 3.2.2, the choice of the reference values is clearly explained in Section 3.2.3, and the details of the algorithms used are described in Section 3.2.4. Computational details are presented in Section 3.2.5. The results are presented in Section 3.3, beginning with the structure of the metals in Section 3.3.1 while Section 3.3.2 presents the DC barriers. The discussion is provided in Section 3.4. The description of the metals with the DFs tested is discussed in Section 3.4.1. The description of the barrier heights to DC is discussed in Section 3.4.2. In this Section, the performance of the algorithms is discussed in Section 3.4.2.A. Subsequently, the

TABLE 3.1: XC functionals tested in this work, and how their exchange and correlation parts are chosen. The type 'GGA-vdW' means that GGA exchange is combined with vdW-DF1<sup>44</sup> or vdW-DF2<sup>45</sup> correlation..

	Name	Type	Exchange	Correlation
1	PBE	GGA	PBE <sup>30</sup>	PBE <sup>30</sup>
2	RPBE	GGA	RPBE <sup>39</sup>	PBE <sup>30</sup>
3	SRP50	GGA	0.50RPBE <sup>39</sup> +0.50PBE <sup>30</sup>	PBE <sup>30</sup>
4	vdW-DF1	GGA+vdW	revPBE <sup>46</sup>	vdW-DF1 <sup>44</sup>
5	vdW-DF2	GGA+vdW	rPW86 <sup>47</sup>	vdW-DF2 <sup>45</sup>
6	PBE-vdW-DF2	GGA+vdW	PBE <sup>30</sup>	vdW-DF2 <sup>45</sup>
7	SRP32-vdW-DF1	GGA+vdW	0.32RPBE <sup>39</sup> +0.68PBE <sup>30</sup>	vdW-DF1 <sup>44</sup>
8	PBE $\alpha$ 57-vdW-DF2	GGA+vdW	PBE $\alpha$ = 0.57 <sup>48</sup>	vdW-DF2 <sup>45</sup>
9	BEEF-vdW-DF2	GGA+vdW	BEEF <sup>16</sup>	BvdW-DF2 <sup>16,44</sup>
10	optPBE-vdW-DF1	GGA-vdW	optPBE <sup>49</sup>	vdW-DF1 <sup>44</sup>
11	revTPSS	meta-GGA	revTPSS <sup>50</sup>	revTPSS <sup>50</sup>
12	SCAN	meta-GGA	SCAN <sup>51</sup>	SCAN <sup>51</sup>
13	MS-B86bl <sup>52</sup>	meta-GGA	MS-B86bl	revTPSS <sup>50</sup>
14	MS2	meta-GGA	MS2 <sup>41</sup>	MS2 <sup>41</sup>

performance of the DFs using the medium algorithm for SBH17 is discussed in Section 3.4.2.B. The dependence of the performance for the barrier heights on the type of system is discussed in 3.4.2.C. The comparison with results for the previous SBH10 database is provided in Section 3.4.2.D. Section 3.4.3 provides a comparison of how the DFs tested perform on the SBH17 database for DC barriers (kinetics) to how they perform for molecular chemisorption (thermochemistry), and to how they perform for gas phase kinetics and thermochemistry. A discussion on future improvements is given in Section 3.4.4. Finally, the conclusions and outlook are given in Section 3.5.

## 3.2 Methods

### 3.2.1 Density functionals tested

The DFs that we have tested on reaction barriers for DC on metal surfaces, as present in our new database discussed below, are listed in Table 3.1. Of these XC DFs, three fall in the GGA<sup>28</sup> category, seven consist of GGA exchange<sup>28</sup> and vdW-DF1<sup>44</sup> or vdW-DF2<sup>45</sup> Rutgers-Chalmers type non-local correlation, and four fall within the meta-GGA<sup>28</sup> category. Here, we will only briefly describe the DFs tested; for details we refer to the original papers.

In the GGA, which is at the second rung of "Jacob's ladder"<sup>28,29</sup>, use is made of the density and its gradient. As discussed by Perdew<sup>28</sup>, at the GGA level a constraint based DF can be made to satisfy a subset of constraints, but not all known constraints. For applications to surface reaction dynamics, to some extent the constraint based PBE and RPBE DFs selected here may be considered to be "at extremes", with PBE<sup>30</sup> often underpredicting and RPBE<sup>39</sup>

often overpredicting reaction barrier heights according to conventional wisdom<sup>10</sup>. The PBE DF<sup>30</sup> is often considered to be a "workhorse" GGA DF, in a sense that it describes a range of properties of molecules and materials with a fair accuracy. The PBE DF was designed<sup>30</sup> to replace the PW91<sup>53</sup> DF, yielding similar results while employing a mathematical framework superior to that of PW91. The RPBE DF is mainly used for molecule-metal surface interactions, and was introduced to correct for the overbinding observed for adsorption of small atoms and molecules to metal surfaces<sup>39</sup> as obtained with the PBE DF. In addition to RPBE and PBE we also test a 50/50 % mixture of these DFs, which is called SRP50 here. The choice of this DF stems from the similar 48/52 % RPBE/PBE mixture providing a chemically accurate description of the well-studied H<sub>2</sub>+Cu(111) system (see also below). We only test 3 GGA DFs here because they suffer from a fundamental drawback: optimizing GGA DFs for their performance of adsorption energies of molecules to metal surfaces goes at the cost of an accurate description of the metal surface itself<sup>54,55</sup>. It has been argued that this problem can be solved with GGA DFs of which the XC DF is non-separable in an exchange and a correlation part<sup>34</sup>, but we do not test such DFs here.

Like the meta-GGA DFs discussed below, GGA DFs are not capable of a reasonably accurate description of the van der Waals interaction. For this reason, and because we are dealing with metals, we have tested seven DFs consisting of GGA exchange and non-local correlation functionals, for which we use either one of two Rutgers-Chalmers correlation functionals, which we call vdW-DF1<sup>44</sup> and vdW-DF2<sup>45</sup>, respectively. These van der Waals DFs were originally designed to be a part of a non-empirical XC DF where the exchange DF was somehow matched to the specific correlation DF<sup>44,45</sup>, and these non-empirical XC DFs, which are both tested here, are simply called vdW-DF1 and vdW-DF2 here. The vdW-DF2 correlation DF has also been incorporated in the so-called BEEF-vdW DF (here called BEEF-vdW-DF2) also tested here, which was semi-empirically fitted to adsorption energies on transition metal surfaces, gas phase reaction barriers, and other properties<sup>16</sup>. The optPBE-vdW-DF1 functional is an example of a DF in which the vdW-DF1 correlation functional has been combined with a semi-empirically adjusted exchange DF, in this case to obtain good interactions of weakly interacting dimers<sup>47</sup>. Finally, the PBE-vdW-DF2, SRP32-vdW-DF1, and PBE $\alpha$ 57-vdW-DF2 are combinations of GGA exchange DFs and vdW-DF1 or vdW-DF2 correlation DFs designed to describe particular DC systems with chemical accuracy, i.e., H<sub>2</sub> + Ru(0001)<sup>56</sup>, CH<sub>4</sub> + Ni(111)<sup>13</sup>, and H<sub>2</sub> + Pt(111)<sup>57</sup>, respectively. These DFs are more fully described in Table 3.1. We note that for all of the DFs incorporating vdW-DF1 or vdW-DF2 discussed here except BEEF-vdW-DF2, the full correlation functional can be written as the sum of correlation

from the local density approximation (LDA) and a non-local functional, which is the non-local part of the vdW-DF1<sup>44</sup> or vdW-DF2<sup>45</sup> DF. For BEEF-vdW-DF2, the full correlation functional is written as a weighted average of the LDA and the semi-local PBE correlation functional (with the sum of the weights equal to 1)<sup>16</sup> plus the non-local part of vdW-DF2<sup>45</sup>. To emphasize this difference, the correlation DF of BEEF-vdW-DF2 is represented by the acronym BvdW-DF2 in Table 3.1.

In the meta-GGA, which is at the third rung of "Jacob's ladder"<sup>28,29</sup>, additional use is made of the kinetic energy density, which is equivalent to the Laplacian of the electron density. Of these, the revTPSS DF<sup>50</sup> was designed to be the workhorse counterpart of the GGA PBE DF. The SCAN DF was designed to enforce all known physical constraints on the DF<sup>51</sup> (this can be done at the meta-GGA level but not at the GGA level<sup>51</sup>). The MS2 functional has two semi-empirically fitted parameters in it, and was designed with the specific aim of accurately describing both metals and molecules<sup>41</sup>. Finally, the MS-B86bl DF has been shown to accurately describe the earlier mentioned H<sub>2</sub> + Cu(111) system, and its design<sup>52</sup> should ensure reasonable accuracy for any system in which H<sub>2</sub> interacts with a metal surface. Again, details on the composition of these XC DFs may be found in Table 3.1.

In hybrid DFs, which are at the fourth rung of Jacob's ladder<sup>28,29</sup>, a fraction of the semi-local exchange in the exchange part of the XC functional is replaced by exact exchange. Screened exact exchange DFs (in which the exact exchange component is switched off at large electron-electron distances) have been used in a few instances in studies of a specific DC system (see e.g. Ref.<sup>58</sup>). However, their use is computationally expensive, and a screened hybrid DF was only used to study 4 of the 10 systems addressed in the SBH10 paper<sup>40</sup>. For this reason, and because their use will be more appropriate once systems are addressed for which electron transfer from the surface to the molecule is likely<sup>58</sup>, we will not test such functionals here.

In rung 5 functionals<sup>28,29</sup> virtual orbitals are added in addition to exact exchange. The random phase approximation (RPA)<sup>59-62</sup> is a well known example of such functionals. The RPA has been used in one specific study of reaction barriers in a DC molecule-metal surface system that we know of<sup>63</sup>, and in a limited number of benchmark studies of molecular adsorption on metal surfaces<sup>17,64</sup>. However, its use is even more computationally expensive than that of hybrid functionals. For this reason, we have not tested the RPA, nor have we tested any other rung 5 DFs.

### 3.2.2 Semi-empirical approaches to obtaining reference values of barrier heights

In determining reference values for barrier heights of gas phase reactions for use in databases, theorists have often benefited from the availability of electronic structure methods and associated algorithms delivering reaction barrier heights with chemical accuracy. For instance, barriers for the NHBTH38 database (a database for 38 non-hydrogen atom transfer reactions) were obtained with an algorithm in which results obtained with the highly accurate CCSD(T)<sup>27</sup> method were extrapolated to the basis set limit<sup>65</sup>. In the construction of the HBTH38 database theorists likewise relied on barrier heights obtained from high level *ab initio* electronic structure methods, although in this case the *ab initio* results were also compared to experiment to extract best guesses (i.e., reference values) of barrier heights<sup>66,67</sup>.

As already noted in the introduction, the situation is quite different in the field of reaction dynamics on metal surfaces. In this field semi-local density functionals are routinely applied to DC reactions occurring on metal surfaces. However, the results are semi-quantitative at best, as one might expect from the performance of these functionals on gas phase reactions<sup>10,56,68,69</sup>. In attempts to do better, the first principles diffusion Monte-Carlo (DMC) method has been used to compute barrier heights for e.g.  $\text{N}_2 + \text{Cu}(111)$ <sup>70</sup> and for  $\text{H}_2 + \text{Mg}(0001)$ <sup>71</sup>,  $\text{Cu}(111)$ <sup>72</sup>, and  $\text{Al}(110)$ <sup>73</sup>. The results for  $\text{H}_2 + \text{Cu}(111)$ <sup>72</sup> suggested that DMC can deliver near chemical accuracy for barrier heights for DC on transition metal surfaces (accuracy better than 2 kcal/mol), in line with results for the HBTH38 and NHBTH38 gas phase reaction barrier databases<sup>10,74,75</sup>. However, chemical accuracy was not yet achieved for this benchmark reaction, and DMC calculations are computationally expensive. Embedded correlated wave function (ECW) calculations based on multi-reference perturbation theory embedded in DFT provided near chemical accuracy for a DC reaction on a simple metal surface ( $\text{O}_2 + \text{Al}(111)$ <sup>76</sup>). However, the computational expense of such calculations is presently too high for molecules interacting with transition metals (TMs), as calculations<sup>77</sup> on  $\text{H}_2 + \text{Cu}(111)$  suggest. Zhao et al. made a positive assessment of their ECW method on the basis of the comparison of the emb-CASPT2 barrier height for DC of  $\text{H}_2$  on  $\text{Cu}(111)$  (0.15 eV)<sup>77</sup> with an "experimental" value<sup>78</sup> from the literature (0.05 eV). However, this value was extracted through an invalid extrapolation procedure (over temperature, to 0 K, see fig.15 of Ref.<sup>78</sup>) in an analysis that was at best approximate for higher temperatures, and was originally meant to make contact with kinetics experiments<sup>78</sup>. The best value of the  $\text{H}_2 + \text{Cu}(111)$  barrier height is however 0.63 eV<sup>11</sup>, and not 0.05 eV.

As argued in most detail in Ref.<sup>10</sup> (to which we refer for these details) accurate

reaction barriers heights for DC reactions on metals are therefore best determined through a SE approach. This approach is best based on supersonic molecular beam experiments that probe the reactivity on the ideal surface, whereas rate measurements usually probe the reaction at (often unknown) defects<sup>79,80</sup>, making the latter experiments less useful for benchmarking purposes<sup>10,81</sup>. The basic idea of the SE SRP-DFT approach used to extract reference barrier heights is to adjust a DF until appropriate dynamics calculations on the basis of that DF yield agreement with measured DC probabilities. The correctness of this procedure can be argued<sup>10</sup> on the basis of the so-called hole model<sup>82</sup>, which essentially states that computed reaction probabilities will be correct if the potential energy surface (and the minimum barrier height extracted from it) is correct. We deem the approach to deliver chemical accuracy because numerous instances have now shown that with appropriate dynamics methods and models measured DC probability curves can be reproduced to within energy shifts less than 1 kcal/mol on the basis of appropriately constructed functionals. Essentially the spirit of the method is not so different from the approach taken to originally construct the HTBH38 gas phase reaction barrier database, which also combined theoretical and experimental information<sup>66,67</sup>. We also recall that in any case a reaction barrier height is not an observable. The procedure to validate a computed barrier height through comparison with an experiment must necessarily take recourse to the use of a measured observable that is as closely related to the barrier height as possible.

The SE SRP-DFT approach discussed above is used for most reactions in the SBH17 database (i.e., for 14 out of 17 cases). With this approach, an appropriate dynamical method and model was used to model supersonic molecular beam experiments in all but one case ( $\text{CH}_4 + \text{Ni}(211)$ , see below)<sup>10</sup>. This means, for instance, that all (or all relevant) molecular degrees of freedom were usually modeled in dynamics calculations. We will discuss the SRP-DFT electronic structure method used for these cases in Section 3.2.2.A below. In the earlier SBH10 database<sup>40</sup>, four systems were introduced for which reference values were derived using experiments and their analysis by a more primitive SE approach. These analyses were carried out before 2009, when SRP-DFT became available<sup>11</sup>. Reference values for three of these systems in our present SBH17 database were inherited from the earlier SBH10 database, which we will briefly discuss in Section 3.2.2.B below. (For one of the four systems ( $\text{CH}_4 + \text{Ni}(211)$ , called 'CH<sub>4</sub>/Ni(111) step' in Ref.<sup>40</sup>, accurate results are now available and we have moved this system to the SRP-DFT part of the database.) As will also be discussed below, it would be good if the reference values for these three systems be replaced in future by more accurate values from for instance SRP-DFT. For each system in the SBH17 database Section 3.2.3 describes what the specific

reference value used for the system is, and how it was derived.

### 3.2.2.A The specific reaction parameter approach to density functional theory (SRP-DFT)

The SRP-DFT method as introduced is a SE method, and was originally applied to reactions in the gas and condensed phases by Truhlar and co-workers<sup>35,36</sup>. SRP-DFT was first applied to DC on a metal surface by Díaz et al<sup>11</sup>. They used an implementation in which the SRP-DF is a weighted average of two GGA DFs according to a mixing parameter  $\mathbf{x}$ . Changing the mixing parameter "tunes" the functional to reproduce  $S_0$ , which is strongly correlated with the minimum barrier height. In the most straightforward approach, a GGA XC DF that underestimates and one that overestimates the barrier height is used:

$$E_{xc}^{SRP-DFT} = \mathbf{x}E_{xc}^{GGA-DF1} + (1 - \mathbf{x})E_{xc}^{GGA-DF2}. \quad (3.1)$$

Standard GGA DFs often used for mixing in applications to molecule-metal surface reactions are the RPBE<sup>39</sup> and PBE<sup>30</sup> functionals discussed in Section 3.2.1. For weakly activated H<sub>2</sub>-metal and for CH<sub>4</sub>-metal systems, the correlation part of the SRP-DF is best substituted by the van der Waals non-local correlation functional of Dion et al<sup>44</sup> (vdW-DF1) or of Lee et al<sup>45</sup> (vdW-DF2), changing equation 3.1 to become:

$$E_{xc}^{SRP-DFT} = \mathbf{x}E_x^{GGA-DF1} + (1 - \mathbf{x})E_x^{GGA-DF2} + E_c^{non-local}. \quad (3.2)$$

In equation 3.2, the mixing parameter only tunes the exchange part of the XC DF in the SRP-DF. Instead of a weighted average of two XC or exchange DFs, one can also use an inherently tunable DF, such as the PBE $\alpha$  exchange DF, in which  $\alpha$  can be adjusted. Using non-local correlation, the equation for the SRP-DF then becomes:

$$E_{xc}^{SRP-DFT} = E_x^{PBE\alpha} + E_c^{non-local}. \quad (3.3)$$

As originally defined, a DF is only considered to be a SRP-DF if after fitting  $\mathbf{x}$  it not only reproduces a particular sticking experiment with chemical accuracy, but also reproduces another experiment on the same system with comparable accuracy<sup>11</sup>. In contrast, if a parameterized DF only reproduces the sticking experiment it was fitted to, it was originally called a candidate SRP-DF<sup>10</sup>. Here we drop this distinction and refer to both categories of DFs as SRP-DFs. Additionally, the SRP-DF can be considered to be transferable if it can reproduce experimental results for a system it was not fitted to<sup>83</sup>. For example, in some cases, the SRP-DF fitted to reproduce molecular beam dissociation

chemisorption experiments for H<sub>2</sub> and D<sub>2</sub> were shown to be transferable among systems in which H<sub>2</sub> interacts with different crystal faces of the same metal<sup>84–86</sup>. One downside of the SE SRP-DFT approach to DC of the molecules on the metal surfaces used so far, in which semi-local exchange DFs are used, is that successful applications of this approach have only been demonstrated to systems for which the difference of the metal work function (WF) and the molecule's electron affinity (EA) is larger than 7 eV. The SRP-DF approach has allowed the construction of chemically accurate barriers for 14 systems<sup>10,85</sup> with (WF-EA) > 7 eV, as shown in Table 3.2 and now discussed further below.

The supersonic molecular beam experiments referred to above need to be modeled with an appropriate dynamical method (e.g., quasi-classical or quantum dynamics) and dynamical model. Here, the latter refers to whether or not all molecular degrees of freedom, the motion of the surface atoms, and electron-hole pair (ehp) excitation are considered<sup>10</sup>. Because dynamics rather than transition state theory is used, and because the surface atoms usually do not have time to respond to the incoming molecule, it makes most sense to tabulate "classical reaction barrier heights". By this we mean barrier heights arising directly from electronic structure calculations without corrections for zero-point energies (zpes) and entropy effects, for the molecule interacting with the "ideal" surface, i.e., with the surface atoms sitting in their equilibrium lattice positions for a classical 0 K surface. The SRP-DFT barriers reported below all are classical barrier heights computed with a SRP-DF or with a PES based on SRP-DFT calculations.

### 3.2.2.B Ad hoc semi-empirical approaches

As noted above, for three systems (CH<sub>4</sub> + Ni(100), CH<sub>4</sub> + Ru(0001), and N<sub>2</sub> + Ru(10 $\bar{1}$ 0)) reference values were taken from the paper on the SBH10 database, and these were extracted using a more primitive SE approach than used in SRP-DFT. As will be detailed below in Section 3.2.3, reduced dimensionality modeling of supersonic molecular beam sticking experiments was used to derive a minimum barrier height for CH<sub>4</sub> + Ni(100). Thermal S<sub>0</sub> measured for N<sub>2</sub> dissociating on Ru(0001) were fitted to an Arrhenius type equation to derive an activation energy for DC at defects, which were considered to be the steps occurring in Ru(10 $\bar{1}$ 0). Finally, an activation energy for CH<sub>4</sub> dissociation on Ru(0001) was derived from associative desorption experiments as described below, invoking detailed balance. Even though activation energies were derived for N<sub>2</sub> and CH<sub>4</sub> dissociation on Ru(10 $\bar{1}$ 0) and Ru(0001), respectively, we felt that the approaches used were too crude to attempt extracting classical minimum barrier heights for these systems by subtracting zpe corrections using known approximate values<sup>40</sup>. Instead we simply use the semi-empirically extracted



TABLE 3.2: Summary of the SBH17 database. Barrier heights (in eV) and the most important co-ordinates defining the barrier geometry are presented. The "site" defines the projection of the molecule's center-of-mass position on the surface,  $r_b$  (in Å) the length of the dissociating bond, and  $Z_b$  (in Å) the distance of the molecule's center-of-mass to the surface. The molecule's orientation is defined by the polar angles of orientation ( $\theta$ ) of the diatomic molecule, or partly defined by the ( $\theta, \varphi$ ) pair of angles giving the polar angle of the breaking CH-bond and the umbrella axis the remaining methyl fragment makes with the surface normal, respectively. Barrier heights obtained from PESs used in the dynamics are marked with an asterisk (\*). For some CH<sub>4</sub>+metal systems the barrier height is also given without residual correction (in brackets, see the text).

$N_s$	System	functional	site	$r_b$	$Z_b$	$\theta$	$\varphi/\beta$	$E_b$
1	H <sub>2</sub> +Cu(111) <sup>11</sup>	SRP43	brg	1.03	1.16	90	90	0.628
2	H <sub>2</sub> +Cu(100) <sup>86</sup>	SRP43	brg	1.23	1.0054	90	90	0.740
3	H <sub>2</sub> +Cu(110) <sup>87</sup>	optPBE-vdW-DF1	short-brg	1.20	0.89	64	90	0.789
4	H <sub>2</sub> +Pt(111) <sup>57</sup>	PBE $\alpha$ 57-vdW-DF2	top(early)	0.769	2.202	90	0	-0.008*
5	H <sub>2</sub> +Pt(211) <sup>84</sup>	PBE $\alpha$ 57-vdW-DF2	top	0.75	2.79	90	90	-0.083*
6	H <sub>2</sub> +Ru(0001) <sup>56</sup>	PBE-vdW-DF2	top(early)	0.751	2.605	90	0	0.004*
7	H <sub>2</sub> +Ni(111) <sup>88</sup>	PBE-vdW-DF2	top(early)	0.763	2.083	90	0	0.024*
8	H <sub>2</sub> +Ag(111) <sup>85</sup>	MS-PBEL-rVV10	brg	1.224	1.157	90	0	1.082*
9	N <sub>2</sub> +Ru(0001) <sup>89</sup>	RPBE	brg	1.741	1.318	84	30	1.840
10	N <sub>2</sub> +Ru(1010) <sup>79,90</sup>	experiment						0.40
11	CH <sub>4</sub> +Ni(111) <sup>13</sup>	SRP32-vdW-DF1	top	1.606	2.176	135.7	164.7	1.015 (1.055)
12	CH <sub>4</sub> +Ni(100) <sup>91</sup>	experiment						0.76
13	CH <sub>4</sub> +Ni(211) <sup>92</sup>	SRP32-vdW-DF1	top	1.632	2.033	126.0		0.699
14	CH <sub>4</sub> +Pt(111) <sup>83</sup>	SRP32-vdW-DF1	top	1.56	2.28	133.4	168.3	0.815 (0.856)
15	CH <sub>4</sub> +Pt(211) <sup>14</sup>	SRP32-vdW-DF1	top	1.53	2.27	133	168	0.559 (0.581)
16	CH <sub>4</sub> +Ir(111) <sup>93</sup>	SRP32-vdW-DF1	top					0.836
17	CH <sub>4</sub> +Ru(0001) <sup>94</sup>	experiment						0.80

activation energies as reference values for the minimum barrier heights for these two systems.

### 3.2.3 The SBH17 database

The systems that constitute our SBH17 benchmark database of barrier heights for DC on transition metal surfaces are listed in Table 3.2. This table contains reference barrier heights and data concerning the barrier geometries for 17 systems. The bulk of the data come from SRP-DFT, such that 14 entries in Table 3.2 may also be viewed as constituting a database that can be named SBH14/SRP. Three entries in Table 3.2 come from more ad-hoc SE approaches, as also discussed in the original SBH10 paper<sup>40</sup>. In this Section we justify our choice of the reference values of the barrier height and our reference geometries, which is important to do especially in cases where conflicting data exists. Note that barrier heights obtained from SRP-DFT are given in eV using 3 significant digits behind the decimal place (i.e., expressed in meV), even though the accuracy

claimed for these numbers is only one kcal/mol  $\approx$  43 meV. This claim is based on the energy shift between the sticking probabilities that were measured and computed on the basis of the SRP DF yielding the minimum barrier height being smaller than 1 kcal/mol<sup>10,11</sup>, as more fully discussed in Section 3.2.2. In expressing barrier heights like this, we follow a rather common practice in computational chemistry, as this will allow other researchers to check whether they can reproduce our numbers. The barrier heights extracted using more ad-hoc approaches (Section 3.2.2.B) have been stated with the amount of significant digits used originally by the scientists providing these benchmark results, and the errors in these reference values may well be larger than 1 kcal/mol. Finally, we note that the average value of the absolute barrier heights of SBH17 is 14.8 kcal/mol.

### 3.2.3.A Dissociative chemisorption of H<sub>2</sub> on transition metals

#### H<sub>2</sub> on Cu(111), Cu(100) and Cu(110)

The DC of H<sub>2</sub> on copper surfaces perhaps represents the most widely studied class of DC systems by both theory<sup>11,85,87,95–97</sup> and experiment<sup>78,97–101</sup>. Being activated systems, in the absence of strong effects of ehp excitation and energy transfer involving phonons<sup>102</sup> on reactive scattering they represent perfect systems for benchmarking electronic structure methods for their capability to accurately predict barriers.

#### H<sub>2</sub> + Cu(111)

The first system for which a SRP-DF was derived for DC on a metal surface was H<sub>2</sub> on Cu(111)<sup>11</sup>, and the first SRP-DF for this system (SRP43) was a weighted average of the PW91<sup>53</sup> (57%) and the RPBE<sup>39</sup> (43%) DF. With the PES developed with this SRP-DF and using the BOSS model quasi-classical trajectory and time-dependent wave packet calculations reproduced measured molecular beam S<sub>0</sub> for H<sub>2</sub> and D<sub>2</sub>, initial-state selected reaction probabilities for H<sub>2</sub><sup>78,99</sup>, and data for rotationally inelastic scattering<sup>103</sup> to within chemical accuracy. Density functional molecular dynamics (DFMD) calculations with the subsequently developed SRP48-DF<sup>104</sup> (48% RPBE<sup>39</sup> and 52% PBE<sup>30</sup>) also accurately reproduced measured<sup>105</sup> rotational quadrupole alignment parameters A<sub>0</sub><sup>(2)</sup>(J), and enabled a chemically accurate description of initial-state selected reaction probabilities of D<sub>2</sub> on Cu(111), after an appropriate re-analysis of the experimental data<sup>95</sup>. Recent studies<sup>87,106</sup> using optPBE-vdW-DF1 exchange combined with non-local vdW-DF1 correlation (re-parameterized PBE for vdW-DF1)<sup>49</sup> also provided a chemically accurate description of S<sub>0</sub> for H<sub>2</sub> and D<sub>2</sub>

on Cu(111). Additionally, three different combinations of GGA exchange DFs with non-local vdW-DF2 correlation<sup>106</sup> allowed chemically accurate descriptions of the reaction of H<sub>2</sub> and D<sub>2</sub> on Cu(111), and the same was true for three newly developed meta-GGA DFs<sup>52</sup>. The barriers reported for the vdW-DF1 and vdW-DF2 combinations and the new meta-GGA DFs were somewhat different from the one obtained with the original SRP43 DF (the SRP48 DF was designed to reproduce the SRP43 energy at the SRP43 barrier geometry<sup>104</sup>). As reference for our benchmark database, the SRP43 barrier height (0.628 eV)<sup>11</sup> will be used. While calculations with some of the other mentioned DFs in cases described the sticking experiments more accurately than SRP48<sup>104</sup> or SRP43<sup>11</sup>, only calculations with the latter 2 DFs reproduced initial-state selected reaction probabilities extracted from associative desorption experiments with chemical accuracy, suggesting that these two DFs should be the DFs best describing H<sub>2</sub>+Cu(111)<sup>106</sup>.

### H<sub>2</sub> + Cu(100)

H<sub>2</sub> on Cu(100) is the second system for which an SRP-DF was demonstrated<sup>86</sup>. The SRP-DF(SRP43<sup>11</sup>) originally developed for H<sub>2</sub> on Cu(111) could also be used to reproduce the measured S<sub>0</sub><sup>98</sup> for H<sub>2</sub> on Cu(100) within the BOSS model<sup>86</sup>. This also represents an example of the transferability that SRP-DFs may exhibit for chemically closely related systems<sup>10</sup>, in this case systems in which the same molecule interacts with different low index faces of the same metal. As reference value for our database we use the value of the barrier height reported for SRP43<sup>86</sup> (0.74 eV).

### H<sub>2</sub> + Cu(110)

In a recent study, effectively a new SRP-DF was demonstrated for H<sub>2</sub> + Cu(110)<sup>87</sup>. The optPBE-vdW-DF1 was used to develop PESs based on embedded atom neural network (EANN) fits for H<sub>2</sub> on Cu(111), Cu(100) and Cu(110) by Jiang and coworkers<sup>87</sup>. Dynamics calculations employing the resulting PES for H<sub>2</sub> + Cu(110) yield a chemically accurate description of molecular beam sticking experiments on H<sub>2</sub> + Cu(110)<sup>107</sup>. The optPBE-vdW-DF1 functional had previously<sup>108</sup> been shown to yield a chemically accurate description of molecular beam sticking experiments on D<sub>2</sub> on Cu(111)<sup>109</sup>. Jiang and co-workers also demonstrated chemically accurate descriptions of sticking experiments on H<sub>2</sub> + Cu(111) and Cu(100). This therefore represents another example of transferability of SRP-DFs among chemically related systems<sup>10</sup>, where one DF (optPBE-vdW-DF1) can be used to model sticking of one and the same molecule on several low index faces

of the same metal. The barrier height reported by Jiang and coworkers for their PES (0.789 eV)<sup>87</sup> will be used as the reference value for our database.

## H<sub>2</sub> on Pt(111) and Pt(211)

### H<sub>2</sub> + Pt(111)

H<sub>2</sub> on Pt(111) is considered as a weakly activated system because of its low minimum barrier height. Three DFs have been found that describe the sticking of D<sub>2</sub> on Pt(111) with chemical accuracy<sup>57,106</sup>. The SRP-DF first developed for D<sub>2</sub> + Pt(111) was the PBE $\alpha$ 57-vdW-DF2 functional (see Section 3.2.2 and Tables 3.1 and 3.2). With this DF measured<sup>110</sup> S<sub>0</sub> for both normal and off-normal incidence of D<sub>2</sub> were reproduced with chemical accuracy<sup>57</sup>. The SRP48<sup>104</sup> and a DF consisting of 68% B86r exchange<sup>111</sup> and 32% RPBE exchange<sup>39</sup> combined with vdW-DF2 correlation<sup>45</sup> (SRPB86r68-vdW-DF2) also both reproduced the measured<sup>110</sup> S<sub>0</sub> for normal incidence with overall chemical accuracy<sup>106</sup>. However, the PBE $\alpha$ 57-vdW-DF2 resulted in the most accurate results near the reaction threshold<sup>57</sup>, suggesting that this DF yields the barrier height with the highest accuracy<sup>106</sup>. Furthermore, recent work has shown that this DF can reproduce experiments of D<sub>2</sub> on chemically related curved Pt crystals with (111) terraces and (100) steps with chemical accuracy<sup>112</sup>. The barrier height reported for PBE $\alpha$ 57-vdW-DF2 was -0.008 eV. We retain this value as the reference value (see Table 3.2), even though it was set to 0.0 eV in the previous SBH10 database<sup>40</sup>.

### H<sub>2</sub> + Pt(211)

The PBE $\alpha$ 57-vdW-DF2 functional developed for H<sub>2</sub> on Pt(111) was also employed to test transferability to H<sub>2</sub> on Pt(211)<sup>84</sup>. This SRP-DF also yields<sup>84</sup> a chemically accurate description of experiments on DC of H<sub>2</sub> and D<sub>2</sub> on the stepped Pt(211) surface<sup>113</sup>. The lowest barrier height found in reduced dimensionality (by finding saddle points in the reduced 2D spaces formed by the elbow plots in figure 4 of Ref.<sup>84</sup>) was -0.083 eV, and this is the value that we use, along with the "top1 ( $\varphi = 90^\circ$ )" geometry defined in Ref.<sup>84</sup>.

### H<sub>2</sub> + Ru(0001)

Like H<sub>2</sub> + Pt(111), H<sub>2</sub> on Ru is a weakly activated system. For this system, two DFs were found<sup>56</sup> to reproduce measured<sup>114</sup> S<sub>0</sub> for H<sub>2</sub> + Ru(0001) with chemical accuracy. These DFs were the PBE-vdW-DF2 functional (see Tables 3.1 and 3.2) and the functional containing 50% PBE<sup>30</sup> and 50% RPBE<sup>39</sup> exchange combined with vdW-DF1 correlation<sup>44</sup> (SRP50-vdW-DF1). The barrier height reported

for both DFs was 0.004 eV. This is the value we use in our database, even though it was set to 0.0 in the previous SBH10 database<sup>40</sup>.

## **H<sub>2</sub> + Ni(111)**

The DC of H<sub>2</sub> on Ni(111) is also weakly activated. Similar to the case of H<sub>2</sub> on Ru(0001), agreement with existing sticking experiments<sup>115,116</sup> was achieved<sup>88</sup> to within chemical accuracy with dynamics calculations based on the PBE-vdW-DF2 functional (see Tables 3.1 and 3.2 and also **Chapter 2**). The PBE-vdW-DF2 calculations for H<sub>2</sub> + Ni(111) were done with the spin-corrected vdW-DF2 functional<sup>117</sup> (spin-vdW-DF2) to take into account the magnetic character of the Ni(111) surface, whereas for all other considered systems the original non-spin corrected vdW-DF1 and vdW-DF2 functionals were used. The barrier height reported is that of the early top site barrier (as also used for H<sub>2</sub> + Pt(111) and Ru(0001)), which is 0.024 eV<sup>88</sup>. In all VASP calculations we perform here, we employ the non-spin corrected vdW-DF1 and vdW-DF2 functionals; however, we note that earlier calculations suggested little influence of the spin-correction on the barrier height computed for CH<sub>4</sub> + Ni(111) with a functional featuring vdW-DF1 correlation<sup>13</sup>. The barrier height we use as the reference value (obtained with PBE-spin-vdW-DF2) in our database is 0.024 eV.

## **H<sub>2</sub> + Ag(111)**

H<sub>2</sub> + Ag(111) is a highly activated system, for which molecular beam sticking experiments were performed by Hodgson and co-workers<sup>118</sup>. Recently it was shown<sup>85</sup> that the measurements<sup>118,119</sup> can be reproduced with chemical accuracy using recently developed made-simple meta-GGA exchange DFs<sup>52</sup> combined with rVV10 non-local correlation<sup>120</sup>. Here we use the barrier height obtained with the functional yielding the best agreement with experiment (MS-PBEL-rVV10)<sup>85</sup> as the reference value for our database (1.082 eV).

### **3.2.3.B N<sub>2</sub> dissociation on Ru surfaces**

#### **N<sub>2</sub> + Ru(0001)**

Ru is well-known as a catalyst for the Haber-Bosch process used to make ammonia, which is a raw material for artificial fertilizer<sup>121</sup>. As noted in the original SBH10 paper<sup>40</sup>, for N<sub>2</sub> + Ru(0001) barrier heights are available from both SRP-DFT<sup>89,122</sup> and from a direct estimate based on experimental results<sup>123</sup>. The directly estimated barrier height based on a laser-assisted associative desorption experiment<sup>123</sup> was 1.8 eV, whereas the calculations based on the RPBE DF

that were found to give a chemically accurate description<sup>89,122</sup> of the best experimentally measured  $S_0$ <sup>124</sup> gave a barrier height of 1.84 eV. Specifically, computed  $S_0$  on the basis of the RPBE DF and a dynamical model in which energy transfer was allowed to surface atom vibrations and ehp excitation gave good agreement<sup>122</sup> with the best estimates of measured  $S_0$ <sup>124</sup>. Table S1 in the supporting information (SI) of Ref.<sup>125</sup> presents data concerning the dependence of the computed barrier height on the pseudo-potentials used for this system. In the calculations presented here we used for both N- and Ru- atoms a hard pseudo-potential, i.e.  $Ru_{pv}$  and  $N_h$ . As the reference value for our database, we will use 1.84 eV, which value was obtained using a hard pseudo-potential for Ru ( $Ru_{pv}$ ) but an ordinary pseudo-potential for N( $N$ )<sup>89</sup> in the DFT calculations performed to produce the PES underlying the good agreement with experiment.

### $N_2 + Ru(10\bar{1}0)$

Because of the absence of SRP-DFT data for  $N_2 + Ru(10\bar{1}0)$ , as was done in the original SBH10 paper<sup>40</sup>, we use a reference value of 0.4 eV for the barrier height. Note that this value actually represents an activation energy obtained from thermal rate measurements on DC of  $N_2$  on Ru(0001)<sup>79,90</sup>, suggesting that the barrier height contains zpe corrections. Another presumption implicitly used in Refs.<sup>79,90</sup>, and therefore in Ref.<sup>40</sup>, is that the activation energy derived from measurements<sup>79,90</sup> on (necessarily defected) Ru(0001) should be the same as the activation energy that would be obtained for Ru(10 $\bar{1}$ 0), i.e., that the steps occurring on the latter surface have the same promoting effect on the reaction on Ru(0001) as do the unspecified defects on Ru(0001).

### 3.2.3.C $CH_4$ dissociation on transition metals

The DC of  $CH_4$  on metal surfaces is important to industry as it constitutes the first step in the steam reforming of natural gas, producing CO, which can be used for alcohol synthesis and for the Fischer-Tropsch process, and hydrogen, which can be used as a fuel and for ammonia production. The dissociation of  $CH_4$  on metal surfaces has been the subject of many theoretical<sup>13,14,91–93,126</sup> and experimental studies<sup>13,14,94,127–136</sup>.

### $CH_4 + Ni(111)$

$CH_4 + Ni(111)$  is the first  $CH_4$  on metal system for which a SRP-DF was derived<sup>13</sup>. The generic expression given by Eq. 3.2 was employed, using a weighted average of the RPBE (32%) and the PBE exchange DFs (68%) combined with non-local vdW-DF1<sup>44</sup>. This SRP-DF (SRP32-vdW-DF1<sup>13</sup>) was fitted to laser-off

experiments performed on  $\text{CHD}_3 + \text{Ni}(111)$  for  $T_N = 600$  and  $650$  K using DFMD calculations. Subsequent DFMD calculations also reproduced measured  $S_0$  for CH-stretch excited  $\text{CHD}_3$  on  $\text{Ni}(111)$  with chemical accuracy. The barrier height that was computed with an appropriate residual energy correction for the vacuum distance was  $1.015$  eV<sup>13</sup> (Table 3.2, see also table S6 of Ref<sup>14</sup>). This is the reference value that should be used for calculations in which  $\text{CH}_4$  is placed far enough from the surface to obtain a value of the asymptotic energy that is converged with respect to the vacuum length<sup>13</sup> (i.e, the value of  $E_b^c$  in table S6 of Ref<sup>14</sup>, see also the discussion in Section 3.1 of the SI to Ref<sup>14</sup>). This is the reference value we use to compare results to that were computed with the GGA and meta-GGA calculations, as with these DFs the asymptotic energy is converged with respect to the vacuum length used in our calculations. For the calculations with vdW-DF1 and vdW-DF2 correlation DFs, we take into account that a correction has to be applied for the fact that in the present calculations the vacuum distance was too short (at  $13$  Å), and the molecule too close to the surface (at  $6$  Å) for these DFs. Instead, for these DFs we use the value of  $E_b^{13}$  quoted in table S6 of Ref<sup>14</sup> (i.e,  $1.055$  eV, see Table 3.2).

### $\text{CH}_4 + \text{Ni}(100)$

Sticking of  $\text{CH}_4$  on  $\text{Ni}(100)$  has been simulated with quantum dynamics calculations explicitly modeling motion in eight molecular degrees of freedom<sup>68</sup>, with QCT calculations<sup>137</sup> and with reaction path Hamiltonian (RPH) calculations<sup>137–141</sup>. In none of these calculations agreement with existing molecular beam experiments was achieved to within chemical accuracy. Therefore, for this system we instead use the same reference value of the barrier height as the value quoted in the previous SBH10 database<sup>40</sup>. However, we note that the earlier paper<sup>40</sup> gave an incomplete explanation of how this value ( $0.76$  eV) of the barrier height was obtained in the paper referenced<sup>91</sup>. The value used refers to the barrier height employed in calculations<sup>91</sup> with a three-dimensional dynamical model augmented with the so-called hole model<sup>82</sup>, which approximately reproduced previously measured  $S_0$ <sup>127</sup>. The value quoted for the minimum barrier height ( $0.76$  eV) is in fact not a minimum barrier height in the model employed in Ref.<sup>91</sup>, but rather the barrier height averaged over the impact points on the surface and the orientations of the dissociating molecule. We will analyze the consequences of this misinterpretation below, and make a recommendation as to whether and how this value should be replaced in a future version of the database.

### CH<sub>4</sub> on Ni(211)

The SRP32-vdW-DF1 developed for CH<sub>4</sub> on Ni(111) has also been used in RPH calculations on sticking of CH<sub>4</sub> + Ni(211)<sup>92</sup>. However, molecular beam sticking experiments are not yet available for this system. A recent study of Guo and Jackson<sup>126</sup> also reported computed thermal S<sub>0</sub> for step and terrace sites calculated for CH<sub>4</sub> on Ni(211) with harmonic and anharmonic transition state theory. It was possible to compare these results to analogous results extracted from experiments on CH<sub>4</sub>+Ni(14 13 13)<sup>142</sup>, which surface also consists of (100) steps and (111) terraces, albeit that the terraces are much wider than on Ni(211). Excellent agreement was obtained for the sticking at the step sites, suggesting that the SRP-DF for CH<sub>4</sub> + Ni(111) should also describe sticking of methane on Ni surfaces consisting of (111) terraces and (100) steps (like Ni(211)) with chemical accuracy. For our benchmark study, we will use therefore as the reference value the minimum barrier height reported by Jackson and coworkers for DC at the steps of Ni(211), which is 0.699 eV.

### CH<sub>4</sub> + Pt(111) and Pt(211)

For the DC of CH<sub>4</sub> on metals, several cases of transferability were observed. DFMD calculations with the SRP32-vdW-DF1 functional developed for CHD<sub>3</sub> on Ni(111) also reproduced molecular beam sticking experiments on CHD<sub>3</sub> + Pt(111) and Pt(211) with chemical accuracy<sup>14</sup>. The barrier heights reported for these two systems, again including a residual energy correction for the short vacuum distance and the short distance of the methane to the surface in the initial state used in the DFMD calculations, are E<sub>b</sub><sup>c</sup> = 0.815 eV<sup>14</sup> and 0.559 eV, and these are the reference values we use when testing GGA and meta-GGA DFs<sup>13,143</sup>. As for CH<sub>4</sub> + Ni(111), for our benchmark purposes, when testing DFs with vdW-DF1 and vdW-DF2 correlation, we will use the values with residual energy correction (0.856 eV and 0.581 eV respectively) as reported by Migliorini et al<sup>14</sup> (table S6 of Ref<sup>14</sup> and table 3 of Ref<sup>143</sup>).

### CH<sub>4</sub> + Ir(111)

As was the case for CH<sub>4</sub> + Ni(211), the SRP32-vdW-DF1 developed for CH<sub>4</sub> + Ni(111) has also been used in RPH dynamics calculations on CH<sub>4</sub> + Ir(111)<sup>93</sup>. The S<sub>0</sub> computed with this method for sticking of CH<sub>4</sub> in its vibrational ground state have been compared with values measured in molecular beam experiments<sup>128,130,136</sup>. An analysis of how these data compare (see fig.67 of Ref<sup>10</sup>) shows that the RPH dynamics calculations reproduce the measured S<sub>0</sub>



with chemical accuracy. For this system we therefore used the barrier height reported by Ref.<sup>93</sup>, which is 0.836 eV, as the reference value.

### CH<sub>4</sub> + Ru(0001)

As already noted in the SBH10 paper<sup>40</sup>, this reference value was extracted from experiments on laser assisted associative desorption (LAAD)<sup>94</sup>. Specifically, the "adiabatic minimum barrier height  $V^*(0)$ " was extracted from the experiments by taking temperature dependent values of the highest CH<sub>4</sub> translational energy observed as a function of the surface temperature ( $T_s$ ), and extrapolating the maximum translational energy observed to  $T_s = 0$  K. While this gave values not too different from the  $V^*(0)$  values extracted in an approximate fashion<sup>94</sup> from earlier molecular beam sticking experiments<sup>129</sup> and from earlier DFT calculations<sup>94,144</sup>, the method used was approximate. Moreover it is clear from the paper<sup>94</sup> that the  $V^*(0)$  value should be interpreted as an activation energy, i.e., in DFT it would be the minimum barrier height with zpe corrections added.

### 3.2.4 Algorithms for computing minimum barrier heights

The minimum barrier height to DC may be computed with DFT as

$$E_b = E_{TS} - E_{asym} \quad . \quad (3.4)$$

Here,  $E_{TS}$  is the energy of the system with the molecule at the transition state (TS) or minimum barrier geometry, and  $E_{asym}$  the energy of the system with the molecule in its equilibrium gas phase geometry, and far enough from the surface that molecule and surface no longer interact with each other. This coincides with an approach that is usually taken to extract barrier heights from PESs used in dynamics calculations. We also suggest that this approach might benefit from cancellation of errors, which might not result if the energies of the reactants (the bare surface and the incoming molecule) are calculated separately, in calculations that might differ in the size of the supercell and k-points used. In any case the asymptotic state will somehow have to be represented in the PES used for the dynamics calculations, so that it makes sense to compute it in the same manner as the minimum barrier height.

Ideally, these geometries would be known to high accuracy from theory or experiment. While this is true for the equilibrium geometry of the small molecules investigated here, and usually also for the structure of the metal surfaces investigated here, it is not true for the transition state geometries. In this sense, the field of molecule-metal surface chemistry differs from that of gas phase chemistry<sup>23–26</sup>, where transition state geometries of at least small

systems are often well known from accurate *ab initio* (CCSD(T)<sup>27</sup>) calculations. When benchmarking electronic structure methods on gas phase systems, the availability of CCSD(T) geometries carries the advantage with it that only single point calculations have to be performed, and that geometry optimizations can be omitted.

This is not the case for calculations on DC on metals. Choices have to be made regarding several issues. These issues are: (i) how to choose the equilibrium gas phase geometry of the molecule, (ii) how to choose the geometry of the molecule in the transition state, and (iii) how to choose the geometry of the metal surface in the TS and asymptotic geometries. In this work we have tested how the results depend on different choices regarding these issues. We have tested this using three algorithms, which we call high, medium, and light according to the computational effort associated with the algorithms.

#### 3.2.4.A Light Algorithm

Calculations with the light algorithm are least expensive as only single point calculations are involved. The following choices are made: (i) the experimental equilibrium geometry of the molecule is used for the asymptotic state, (ii) the TS geometry of the molecule relative to that of the surface is taken as the SRP-DFT geometry of the molecule relative to the metal surface (see Table 3.2), and (iii) the metal surface is built up by simply using the experimental lattice constant at 0 K, without relaxation of the interlayer distances in the slab.

#### 3.2.4.B Medium Algorithm

In the case of medium algorithm, for (ii) the same choice is made for the geometry of the molecule relative to the surface in the system's TS geometry as in the light algorithm. However, for (i) and (iii) different choices are made: the molecule's equilibrium geometry is now computed on the basis of the DF tested, and the lattice constant of the metal surface as well as the relaxed interlayer distances of the metal surface at the interface with the vacuum are now also optimized separately for each functional tested. This takes into account that the lattice constant and the relaxed interlayer distances may depend strongly on the DF tested<sup>145</sup>, while in turn the minimum barrier height may depend rather strongly on the parameters determining the geometry of the metal surface. The dependence of the minimum barrier height on the geometry of the metal surface is relevant to DFMD calculations<sup>146,147</sup>, as incorrect initial geometries of the metal may lead to surface strain, which can in turn affect the barrier height to DC<sup>148</sup>. In the medium as well as in the high algorithm below, the geometry of the metal surface in the TS is taken the same as that in the asymptotic state,

as the metal surface atoms will usually not have time to respond to the fast incoming motion of the molecule in the hypersonic molecular beam experiments to which comparison is made for assessing the accuracy of SRP DFs<sup>10</sup>. We note that for CH<sub>4</sub> the molecule's geometry has only been optimized once, with the RPBE functional, and the RPBE geometry was used with all other DFs. Table S2 of the SI of Ref.<sup>125</sup> shows that this leads to errors no greater than 5 meV.

### 3.2.4.C High Algorithm

The high algorithm differs from the medium algorithm only in that now the TS geometry of the molecule relative to the surface is determined by geometry optimization using the dimer method as implemented in the VASP Transition State Tools (VTST) package<sup>149–152</sup>. As stated above, in the TS search process, the metal surface was kept frozen in its relaxed 0 K geometry. The optimization of the TS geometry of the molecule was stopped when the maximum force on any degree of freedom was smaller than 5 meV/Å. All the TS geometries reported here have been confirmed to be the first-order saddle points in the molecular coordinate space by frequency analysis (by checking that one and only one imaginary frequency was found).

### 3.2.5 Computational details

All the new calculations presented here are performed using the Vienna *ab initio* simulation package<sup>153–156</sup> (Vasp5.4.4). The calculations with DFs incorporating vdW-DF1<sup>44</sup> or vdW-DF2<sup>45</sup> correlation have therefore been performed with the Vasp implementation of these DFs<sup>47</sup>, except the calculations with the BEEF-vdW-DF2 DF<sup>16</sup>, for which the libbeef library<sup>157</sup> was used. Through the way these DFs were implemented, they all inherit the LDA correlation from the PBE DF<sup>30</sup>, which means that the PW92 variant of the LDA correlation<sup>158</sup> is used. All calculations with vdW-DF1 or vdW-DF2 were performed with the algorithm due to Román-Pérez and Soler<sup>159</sup>, which speeds up the evaluation of these DFs. Because of the amount of the calculations that had to be done, the Atomic Simulation Environment (ASE) was used as a convenient interface package<sup>160,161</sup>. Typically, the default projected augmented wave (PAW) pseudo-potentials were used; however, for N<sub>2</sub>+Ru(0001) and N<sub>2</sub>-Ru(1010) we used hard core pseudo-potential: **Ru**<sub>pv</sub> ( a **Z<sub>n</sub>** core pseudo-potential leaving 14 of the electrons of **Ru** in its 4p<sup>6</sup>5s<sup>1</sup>4d<sup>7</sup> configuration to be modeled ) and **N<sub>h</sub>** ( a **H<sub>e</sub>** core pseudo-potential leaving 5 electrons of **N** in its 2s<sup>2</sup>2p<sup>3</sup> configuration to be modeled). For all systems containing a **Ni** surface, spin polarization has been taken into account. A complete description of the input parameters (e.g., number of metal layers in the metal slab, size of the surface unit cell, the plane wave cut-off energy, the

number of k-points, the vacuum distance, etc.) used in this work can be seen in Table S3 of the SI of Ref.<sup>125</sup>. In the optimization of the metal slab, for all systems, we used a  $1 \times 1$  surface unit cell, kept the bottom layer frozen and the upper  $n-1$  layers of the metal surface were allowed to relax. For the 3 systems for which only ad-hoc SE results are available ( $\text{CH}_4 + \text{Ru}(0001)$ ,  $\text{CH}_4 + \text{Ni}(100)$ , and  $\text{N}_2 + \text{Ru}(10\bar{1}0)$ ), the geometries we used for the medium and light algorithms were obtained from the calculations where we used the high algorithm based on the SRP32-vdW-DF1 for  $\text{CH}_4$  on metal systems, and on the RPBE DF for  $\text{N}_2 - \text{Ru}(10\bar{1}0)$ .

## 3.3 Results

### 3.3.1 Structure of the metals

Table 3.3 presents, for all metals in the database, the calculated lattice constants as computed with all DFs tested, comparing with zpe corrected experimental values<sup>162,163</sup>, and also showing the MAE and MSE with respect to the experiment for each DF. The lowest MAEs are found for the meta-GGA DFs, and the highest MAEs for the DFs consisting of GGA exchange but vdW-DF1 or vdW-DF2 correlation, with the vdW-DF2 functional exhibiting the poorest performance. For this property the GGA-DFs are found to be of intermediate accuracy.

Table 3.4 shows, for each DF tested, the computed percentage change of the distance between the top two layers of the relaxed (111) metal surface relative to the ideal bulk interlayer distance, for the (111) surfaces relevant to SBH17, also comparing to the corresponding experimental results. Again, the best results are found with the meta-GGA DFs. For instance, with the revTPSS DF, the correct sign was found for all four metal surfaces for which experimental results are available. The GGA DFs get the sign wrong for Pt(111), while the functionals with vdW-DF1 and vdW-DF2 correlation all get the sign wrong for Ag(111). With the functionals and input parameters used, neither experiment nor other DFT calculations presented in Table 3.4 are quantitatively reproduced.

### 3.3.2 Dissociative chemisorption barriers

To give an idea of the size of the error that may arise from the DF and algorithm used for a particular system, Table 3.5 and Figure 3.1 present the barrier heights computed for  $\text{H}_2 + \text{Cu}(111)$  (the barrier heights for the other systems in the database and geometries can be found in Tables S4 to S19 and Figures S1 to S16 of the SI of Ref.<sup>125</sup>). With the medium algorithm, three DFs (SRP50, revTPSS, and MS-B86bl) yield barrier heights close to the SRP reference value of 0.636

TABLE 3.3: Comparison of metal lattice constants computed in this work with experiment and with other computational results. Lattice constants computed in this work are marked with "†" and listed for each tested DF, also providing other computational results for the DFs tested where available. The experimental values (Exp) have been corrected for zpe effects. The MAE and MSE represent the means of the absolute and signed deviations of the lattice constants computed in this work from the experimental values, for each DF tested. All results are in Å.

	Ag	Ir	Cu	Pt	Ni	Ru		
Exp	4.062 <sup>162</sup>	3.831 <sup>162</sup>	3.597 <sup>162</sup>	3.912 <sup>162</sup>	3.499 <sup>162</sup>	2.703 <sup>163</sup>	4.274 <sup>163</sup>	
Functional								
PBE	4.146 <sup>†</sup>	3.889 <sup>†</sup>	3.624 <sup>†</sup>	3.985 <sup>†</sup>	3.519 <sup>†</sup>	2.722 <sup>†</sup>	4.293 <sup>†</sup>	MAE
	4.152 <sup>162</sup>	3.887 <sup>162</sup>	3.632 <sup>162</sup>	3.985 <sup>162</sup>	3.518 <sup>162</sup>	2.735 <sup>56</sup>	4.304 <sup>56</sup>	0.0506
		3.916 <sup>4</sup>						
		3.873 <sup>165</sup>						
		3.877 <sup>166</sup>						
RPBE	4.201 <sup>†</sup>	3.903 <sup>†</sup>	3.673 <sup>†</sup>	4.010 <sup>†</sup>	3.553 <sup>†</sup>	2.734 <sup>†</sup>	4.315 <sup>†</sup>	0.0824
		3.908 <sup>164</sup>				2.744 <sup>56</sup>	4.325 <sup>56</sup>	
		3.891 <sup>166</sup>						
SRP60	4.173 <sup>†</sup>	3.896 <sup>†</sup>	3.648 <sup>†</sup>	3.997 <sup>†</sup>	3.535 <sup>†</sup>	2.727 <sup>†</sup>	4.304 <sup>†</sup>	0.0678
vdW-DF1	4.226 <sup>†</sup>	3.934 <sup>†</sup>	3.703 <sup>†</sup>	4.052 <sup>†</sup>	3.573 <sup>†</sup>	2.753 <sup>†</sup>	4.338 <sup>†</sup>	0.115
						2.761 <sup>56</sup>	4.351 <sup>56</sup>	
vdW-DF2	4.288 <sup>†</sup>	3.988 <sup>†</sup>	3.775 <sup>†</sup>	4.126 <sup>†</sup>	3.615 <sup>†</sup>	2.791 <sup>†</sup>	4.398 <sup>†</sup>	0.176
		3.987 <sup>166</sup>						
SRP32-vdW-DF1	4.203 <sup>†</sup>	3.928 <sup>†</sup>	3.680 <sup>†</sup>	4.042 <sup>†</sup>	3.558 <sup>†</sup>	2.747 <sup>†</sup>	4.330 <sup>†</sup>	0.100
		3.923 <sup>66</sup>						
PBE-vdW-DF2	4.204 <sup>†</sup>	3.927 <sup>†</sup>	3.681 <sup>†</sup>	4.040 <sup>†</sup>	3.518 <sup>†</sup>	2.747 <sup>†</sup>	4.330 <sup>†</sup>	0.092
						2.754 <sup>56</sup>	4.341 <sup>56</sup>	0.092

Table 3.3 Continued.

	Ag	Ir	Cu	Pt	Ni	Ru		
Exp	4.062 <sup>162</sup>	3.831 <sup>162</sup>	3.597 <sup>162</sup>	3.912 <sup>162</sup>	3.499 <sup>162</sup>	2.703 <sup>163</sup>	4.274 <sup>163</sup>	
Functional								MSE
PBEa67-vdW-DF2	4.173 <sup>†</sup> 4.176 <sup>167</sup>	3.918 <sup>†</sup>	3.653 <sup>†</sup>	4.025 <sup>†</sup> 4.015 <sup>57</sup>	3.537 <sup>†</sup>	2.739 <sup>†</sup>	4.319 <sup>†</sup>	0.0792
BEEF-vdW-DF2	4.196 <sup>†</sup>	3.899 <sup>†</sup>	3.656 <sup>†</sup>	4.014 <sup>†</sup>	3.536 <sup>†</sup>	2.730 <sup>†</sup>	4.306 <sup>†</sup>	0.0782
optPBE-vdW-DF1	4.160 <sup>†</sup>	3.907 <sup>†</sup>	3.641 <sup>†</sup>	4.007 <sup>†</sup>	3.526 <sup>†</sup>	2.730 <sup>†</sup>	4.306 <sup>†</sup>	0.066
revTPSS	4.064 <sup>†</sup>	3.851 <sup>†</sup>	3.561 <sup>†</sup>	3.927 <sup>†</sup>	3.457 <sup>†</sup>	2.700 <sup>†</sup> 2.69 <sup>56</sup>	4.268 <sup>†</sup> 4.246 <sup>56</sup>	0.0244 -0.010
SCAN	4.091 <sup>†</sup>	3.808 <sup>†</sup>	3.580 <sup>†</sup>	3.906 <sup>†</sup>	3.460 <sup>†</sup>	2.696 <sup>†</sup>	4.249 <sup>†</sup>	0.0246 -0.013
MS-B86b1	4.101 <sup>†</sup> 4.092 <sup>52</sup>	3.841 <sup>†</sup>	3.583 <sup>†</sup> 3.583 <sup>52</sup>	3.907 <sup>†</sup> 3.906 <sup>52</sup>	3.472 <sup>†</sup>	2.700 <sup>†</sup>	4.260 <sup>†</sup>	0.0208 -0.001
MS2	4.0745 <sup>†</sup>	3.8407 <sup>†</sup>	3.5543 <sup>†</sup>	3.9115 <sup>†</sup>	3.4498 <sup>†</sup>	2.7002 <sup>†</sup>	4.2631 <sup>†</sup>	0.0248 -0.016

TABLE 3.4: Comparison of computed and measured results characterizing surface relaxation. The relaxation of the interlayer lattice spacing between the upper two layers of the surface relative to the bulk value is given in % for all (111) surfaces relevant to the SBH17 database and for all DFs tested in this work, also comparing to experimental results (Exp) and other DFT results where available. Values computed in this work are marked with a "†".

	Ag	Ir	Cu	Pt	Ni
Exp	-2.5% <sup>168</sup> -0.5% <sup>171</sup>		-1.0% <sup>169</sup> -0.7% <sup>172</sup>	1.1% <sup>170</sup>	-0.07% <sup>169</sup>
			GGA		
PBE	-0.34† -0.20 <sup>145</sup> -0.30 <sup>173</sup>	-2.66†	-0.26† -0.30 <sup>145</sup>	-0.07† 0.90 <sup>145</sup> 0.90 <sup>173</sup>	-1.38†
RPBE	0.38†	-2.58†	-0.47†	-0.05†	-0.80†
SRP50	-0.04†	-2.62†	-0.33†	-0.06†	-1.32†
			GGA+vdW		
vdW-DF1	1.19† 0.10 <sup>167</sup>	-2.37†	-0.38† -0.20 <sup>167</sup>	0.00† 1.30 <sup>167</sup>	-1.26† -1.10 <sup>167</sup>
vdW-DF2	2.24† 0.50 <sup>167</sup>	-1.99†	-1.63† 0.00 <sup>167</sup>	0.31† 1.50 <sup>167</sup>	-1.46† -1.10 <sup>167</sup>
SRP32-vdW-DF1	0.73†	-2.44†	-0.20†	-0.06†	-1.21†
PBE-vdW-DF2	0.77†	-2.42†	-0.13†	-0.07†	0.66†
PBE $\alpha$ 57-vdW-DF2	0.51† 0.00 <sup>167</sup>	-2.14†	-0.02† -0.40 <sup>167</sup>	-0.10† -0.80 <sup>167</sup>	-1.16† -0.80 <sup>167</sup>
BEEF-vdW-DF2	0.54†	-2.51†	-0.09†	0.03†	-1.17†
			meta-GGA		
revTPSS	-0.86†	-2.81†	-0.31†	0.35†	-0.92†
SCAN	-0.95† -0.40 <sup>145</sup>	-2.70†	-0.99† -0.40 <sup>145</sup>	2.39† 2.50 <sup>145</sup>	-1.57†
MS-B86bl	-0.73† -0.50 <sup>52</sup>	-2.76†	-0.85† -1.00 <sup>52</sup>	1.16† 1.00 <sup>52</sup>	-1.00†
MS2	-0.54†	-2.77†	-0.94†	0.4†	-0.96†

eV<sup>11</sup>. However, other DFs yield barriers that are far off the mark, with the largest overestimate (by 0.48 eV) coming from the vdW-DF2 and the largest underestimate (by 0.28 eV) coming from the SCAN functional.

Table 3.6 shows MAEs and MSEs for all algorithms and DFs. To compare the results obtained with different algorithms, the average is always taken over the number of systems for which reliable saddle point geometries could be obtained with the high algorithm for a given DF. As Table 3.6 shows, with the high algorithm reliable saddle point geometries were obtained for 16 systems using the PBE, SRP50, and the MS-B86bl DFs, for 15 systems using the SCAN DF, and for all 17 systems for all remaining DFs. Table 3.6 shows that in general the errors obtained with the medium algorithm are close to those obtained with the high algorithm, which is much more cpu intensive. Interestingly, this was not true for the majority of the meta-GGA DFs: for these DFs the medium and high algorithms only give similar results for the revTPSS DF.

Table 3.7 shows the MAEs and MSEs for all DFs tested with averaging over all 17 systems, using the medium algorithm. With the MSE as accuracy criterion,

TABLE 3.5: Barrier heights for  $\text{H}_2+\text{Cu}(111)$  (in eV) for all the DFs and algorithms tested. Values marked with "CRP" come from an accurate fit of the  $\text{H}_2 + \text{Cu}(111)$  PES to DFT data computed with the DF listed<sup>174</sup>.

Functional	High Algo	Light Algo	Medium Algo	Literature values
		GGA		
PBE	0.478	0.488	0.467	0.484(CRP) <sup>108</sup>
RPBE	0.762	0.819	0.762	0.797(CRP) <sup>174</sup>
SRP50	0.618	0.654	0.616	0.636(SRP48) <sup>174</sup>
		GGA+vdW		
vdW-DF1	1.026	1.102	1.019	1.004(CRP) <sup>174</sup>
vdW-DF2	1.144	1.260	1.117	
PBE-vdW-DF2	0.889	0.952	0.885	0.863(CRP) <sup>174</sup>
SRP32-vdW-DF1	0.863	0.926	0.860	
PBEa57-vdW-DF2	0.736	0.781	0.735	0.72(CRP) <sup>174</sup>
BEEF-vdW-DF2	0.928	0.966	0.925	
optPBE-vdW-DF1	-	-	0.736	
		meta-GGA		
revTPSS	0.667	0.648	0.674	0.605(CRP) <sup>174</sup>
SCAN	0.382	0.334	0.354	0.398(CRP) <sup>174</sup>
MS-B86bl	0.647	0.619	0.634	0.683(CRP) <sup>52</sup>
MS2	0.378	0.340	0.382	

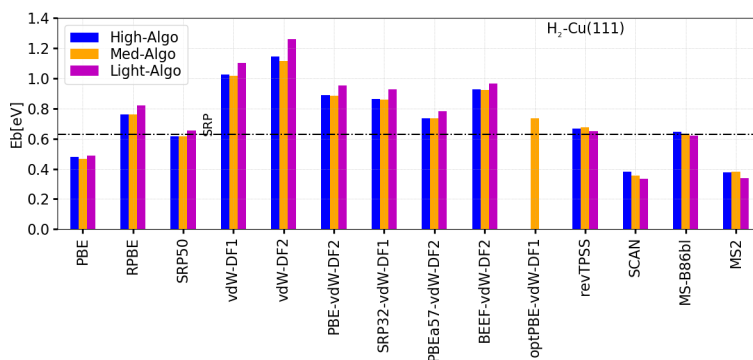


FIGURE 3.1: Performance of the DFs and algorithms tested on the DC of  $\text{H}_2$  on  $\text{Cu}(111)$ . Computed barrier heights are compared with the reference value for this system, which is indicated by the horizontal dot-dashed line (see Table 3.2).

the revTPSS meta-GGA comes out as the best for DC barrier heights. The next three highest-ranked DFs all combine GGA exchange with vdW-DF1 or vdW-DF2 correlation, with the optPBE-DF1 showing the best performance. The PBE DF ranks fifth and is the best performing GGA DF. If the DFs are ranked according to their performance for the MAE the PBE DF actually performs best, with SRP32-vdW-DF2 coming out second, and the MS2 meta-GGA DF ranking third, and thereby outperforming the revTPSS meta-GGA, which now ranks ninth.

Table 3.8 shows the performance of the DFs for the smaller and older SBH10



TABLE 3.6: Performance of the DFs and algorithms tested on the SBH17 database. Mean absolute errors (MAE) and mean signed errors (MSE, both in eV) measure average deviations of the barrier heights computed with each DF and algorithm from the reference values listed in Table 3.2.  $N_{ex}$  represents the number of systems that had to be excluded for specific DFs, and  $N_s$  their numbers (see Table 3.2 and the text).

$N_{ex}$	Functional	Type	High		Med		Light		$N_s$ System missing
			MAE Algo	MSE	MAE Algo	MSE	MAE Algo	MSE	
1	PBE	GGA	0.116	-0.075	0.106	-0.065	0.148	-0.067	
0	RPBE	GGA	0.230	0.230	0.228	0.228	0.263	0.263	5
1	SRP80	GGA	0.126	0.081	0.127	0.085	0.161	0.102	5
0	vdW-DF1	GGA+vdW	0.230	0.230	0.220	0.220	0.297	0.297	
0	vdW-DF2	GGA+vdW	0.329	0.329	0.311	0.311	0.461	0.461	
0	optPBE-vdW-DF1	GGA+vdW	-	-	0.131	-0.033	-	-	
0	PBEa57-vdW-DF2	GGA+vdW	0.139	-0.053	0.124	-0.040	0.135	-0.002	
0	SRP32-vdW-DF1	GGA+vdW	0.127	0.060	0.115	0.057	0.170	0.119	
0	PBE-vdW-DF2	GGA+vdW	0.144	0.109	0.141	0.112	0.191	0.166	
0	BEEF-vdW-DF2	GGA+vdW	0.190	0.190	0.191	0.191	0.228	0.222	
2	SCAN	meta-GGA	0.185	-0.172	0.154	-0.120	0.249	-0.242	5,7
0	revTPSS	meta-GGA	0.147	-0.060	0.146	-0.025	0.165	-0.105	
0	MS2	meta-GGA	0.196	-0.176	0.117	-0.074	0.173	-0.149	
1	MS-B86b1	meta-GGA	0.173	0.157	0.214	0.199	0.191	0.133	5
Average			0.179	0.065	0.166	0.075	0.218	0.092	

TABLE 3.7: Performance of the DFs tested on the SBH17 database using the medium algorithm. The MAE and MSE (in eV) are computed with averaging over all 17 systems. The values of  $r_{MAE}$  and  $r_{|MSE|}$  rank the DFs according to best performance for the MAE and  $|MSE|$  error criteria, respectively.

Functional	Med Algo			
	MAE	$r_{MAE}$	MSE	$r_{ MSE }$
PBE	0.103	1	-0.058	5
RPBE	0.228	13	0.228	13
SRP50	0.125	5	0.085	7
vdW-DF1	0.219	12	0.219	12
vdW-DF2	0.312	14	0.312	14
PBE-vdW-DF2	0.141	8	0.112	9
SRP32-vdW-DF1	0.115	2	0.057	4
PBE $\alpha$ 57-vdW-DF2	0.124	4	-0.040	3
BEEF-vdW-DF2	0.191	10	0.191	10
optPBE-vdW-DF1	0.131	6	-0.033	2
revTPSS	0.146	9	-0.025	1
SCAN	0.140	7	-0.105	8
MS-B86bl	0.210	11	0.195	11
MS2	0.117	3	-0.074	6
Average	0.164		0.076	

database. The three DFs featuring GGA exchange and vdW-DF1 or vdW-DF2 correlation that performed well for the SBH17 database with the absolute value of the MSE as the accuracy criterion again do well, with SRP32-vdW-DF now ranking first. The PBE performance is also consistent, with PBE ranking fifth, but as a GGA DF PBE is now outperformed by SRP50, which takes third place. The DFs performing well in terms of their absolute value of the MSE also do well on the MAE for SBH10.

The top panels of Figure 3.2 presents the correlation of the minimum barrier height of the whole system with the computed lattice constant of the metal for the DFs tested, also comparing to the SE and the experimental values of these parameters, respectively, for  $H_2 + Cu(111)$  and  $CH_4 + Pt(111)$ . The bottom panels show the correlation of the computed minimum barrier height with the distance of the molecule to the surface in the optimized minimum barrier geometry for these two systems. An interesting feature of the revTPSS DF is that it predicts both the lattice constant of the metal and the minimum barrier height with reasonably high accuracy, while the computed distance of the molecule to the metal surface also agrees well with that obtained using the SRP-DFT approach.

Table 3.9 presents the errors made with the medium algorithm for the 8  $H_2$ -metal systems in the database (see also Figs.S17 and S18 of the SI of Ref.<sup>125</sup>). For these systems and with the absolute value of the MSE as accuracy criterion, the PBE GGA DF does best, with the SRP50 DF as the runner up. The three DFs in which GGA exchange was combined with non-local correlation and which did well for SBH17 also do reasonably well for the  $H_2$ -metal reactions. The

TABLE 3.8: Performance of the DFs and algorithms tested on the SBH10 database. Both MAE and MSE (in eV) are calculated by including, and averaging over, the ten systems present in the previous SBH10<sup>40</sup> database. The DFs have been ranked according to the best performance of the high algorithm according to the  $|\text{MSE}|$  criterion. For the BEEF-vdW-DF2 and MS2 DFs we also present the values computed earlier while allowing surface relaxation in the TS<sup>40</sup>.

Functional	Type	High Algo			Med Algo			Light Algo			SBH10 <sup>40</sup> MAE/MSE
		MAE	MSE	MSE	MAE	MSE	MSE	MAE	MSE	MSE	
SRP32-vdW-DF1	GGA+vdW	0.134	0.041	0.041	-0.126	0.034	0.151	0.066			
SRP50	GGA	0.132	0.063	0.063	-0.133	0.067	0.155	0.061			
optPBE-vdW-DF1	GGA+vdW	-	-	0.074	-0.141	-0.074	-	-			
PBEd57-vdW-DF2	GGA+vdW	0.135	-0.076	0.076	-0.132	-0.073	0.143	-0.060			
PBE-vdW-DF2	GGA+vdW	0.142	0.093	0.093	-0.148	0.098	0.163	0.120			
PBE	GGA	0.149	-0.098	0.098	-0.143	-0.091	0.170	-0.112			
revTPSS	meta-GGA	0.198	-0.124	0.124	-0.177	-0.117	0.237	-0.185			
MS-B96bl	meta-GGA	0.196	0.165	0.165	-0.154	-0.123	0.173	0.064			
SCAN	meta-GGA	0.198	-0.178	0.178	-0.179	-0.156	0.253	-0.245			
BEEF-vdW-DF2	GGA+vdW	0.182	0.182	0.182	-0.179	-0.179	0.193	0.183	0.12/-0.03		
MS2	meta-GGA	0.220	-0.188	0.188	-0.171	-0.117	0.223	-0.198	0.36/-0.34		
vdW-DF1	GGA+vdW	0.214	0.214	0.214	-0.211	-0.211	0.256	0.256			
RPBE	GGA	0.223	0.223	0.223	-0.224	-0.224	0.235	0.235			
vdW-DF2	GGA+vdW	0.331	0.331	0.331	-0.324	-0.324	0.435	0.435			
Average		0.189	0.050		-0.174	0.045	0.214	0.047			

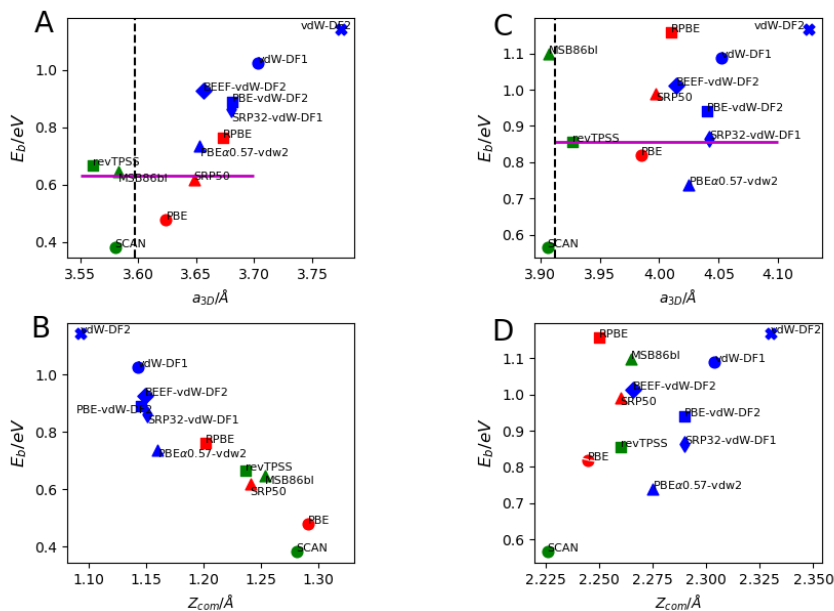


FIGURE 3.2: Correlation of the barrier height for DC with the optimized lattice constant ( $a_{3D}$ ) of the metal (upper panels), and of the barrier height with the distance of the molecule to the surface at the transition state ( $Z_{com}$ ), as computed with all DFs tested in this work. The high algorithm was used. The left panels present results for  $H_2 + Cu(111)$  and the right panels for  $CH_4 + Pt(111)$ . The vertical black dashed lines in the upper panels represent the experimental lattice constants, and the horizontal magenta solid lines the reference values of the barrier heights.

same is true for revTPSS which came out as best for SBH17, but is not best for the  $H_2$ -metal systems. Table 3.10 presents the errors made with the medium algorithm for the 2  $N_2$ -metal systems in the database (see also Figs.S19 and S20 of the SI of Ref. 125). For these systems, DFs that did well for SBH17 generally are not very good. MS-B86bl, BEEF-vdW-DF2 and RPBE perform best for the  $N_2$ -metal systems. Table 3.11 presents the errors made with the medium algorithm for the 7  $CH_4$ -metal systems in the database (see also Figs.S21 and S22 of the SI of Ref. 125). The DFs that did well for SBH17 also do reasonably well for the  $CH_4 +$  metal systems. However, for the latter category SCAN is now the best performing DF using the MSE as accuracy criterion. Using the MAE as accuracy criterion, the best  $CH_4$ -metal results are obtained with the SRP32-vdW-DF1, PBE, and revTPSS DFs, respectively.

TABLE 3.9: Performance of the DFs tested on the 8 H<sub>2</sub>-metal systems present in the SBH17 database using the medium algorithm. The MAE and MSE (in eV) are computed with averaging over all 8 systems. The values of  $r_{MAE}$  and  $r_{|MSE|}$  rank the DFs according to best performance for the MAE and  $|MSE|$  error criteria, respectively.

Functional	Med Algo			
	MAE	$r_{MAE}$	MSE	$r_{ MSE }$
PBE	0.080	2	-0.049	1
RPBE	0.167	10	0.167	10
SRP50	0.070	1	0.063	2
vdW-DF1	0.264	13	0.264	13
vdW-DF2	0.290	14	0.290	14
PBE-vdW-DF2	0.174	11	0.174	11
SRP32-vdW-DF1	0.152	9	0.147	9
PBE $\alpha$ 67-vdW-DF2	0.090	5	0.071	3
BEEF-vdW-DF2	0.227	12	0.227	12
optPBE-vdW-DF1	0.096	6	0.091	6
revTPSS	0.086	4	0.086	5
SCAN	0.121	7	-0.117	7
MS-B86bl	0.128	8	0.128	8
MS2	0.084	3	-0.084	4
Average	0.145		0.104	

TABLE 3.10: Performance of the DFs tested on the 2 N<sub>2</sub>-metal systems present in the SBH17 database using the medium algorithm. The MAE and MSE (in eV) are computed with averaging over all 2 systems. The values of  $r_{MAE}$  and  $r_{|MSE|}$  rank the DFs according to best performance for the MAE and  $|MSE|$  error criteria, respectively.

Functional	Med Algo			
	MAE	$r_{MAE}$	MSE	$r_{ MSE }$
PBE	0.409	10	-0.409	10
RPBE	0.088	3	0.088	4
SRP50	0.157	6	-0.157	6
vdW-DF1	0.048	2	0.048	3
vdW-DF2	0.372	8	0.372	8
PBE-vdW-DF2	0.123	5	-0.123	5
SRP32-vdW-DF1	0.217	7	-0.217	7
PBE $\alpha$ 67-vdW-DF2	0.378	9	-0.378	9
BEEF-vdW-DF2	0.026	1	0.026	2
optPBE-vdW-DF1	0.434	11	-0.434	11
revTPSS	0.723	14	-0.723	14
SCAN	0.525	13	-0.525	13
MS-B86bl	0.102	4	-0.024	1
MS2	0.454	12	-0.454	12
Average	0.290		-0.208	

TABLE 3.11: Performance of the DFs tested on the 7 CH<sub>4</sub>-metal systems present in the SBH17 database using the medium algorithm. The MAE and MSE (in eV) are computed with averaging over all 7 systems. The values of  $r_{MAE}$  and  $r_{|MSE|}$  rank the DFs according to best performance for the MAE and  $|MSE|$  error criteria, respectively.

Functional	Med Algo			
	MAE	$r_{MAE}$	MSE	$r_{ MSE }$
PBE	0.045	2	-0.016	2
RPBE	0.336	14	0.336	14
SRP50	0.177	9	0.177	9
vdW-DF1	0.218	11	0.218	11
vdW-DF2	0.319	12	0.319	12
PBE-vdW-DF2	0.108	8	0.108	8
SRP32-vdW-DF1	0.040	1	0.032	3
PBE $\alpha$ 57-vdW-DF2	0.090	7	-0.071	7
BEEF-vdW-DF2	0.196	10	0.196	10
optPBE-vdW-DF1	0.086	6	-0.060	6
revTPSS	0.05	3	0.047	5
SCAN	0.077	5	-0.007	1
MS-B86bl	0.333	13	0.333	13
MS2	0.059	4	0.046	4
Average	0.153		0.121	

Table 3.12 shows the MAEs and the MSEs for the 17 systems investigated here, where now the averaging is done over the DFs. For both the medium and the high algorithms, the largest MAEs are found for the H<sub>2</sub> + Ag(111), N<sub>2</sub> + Ru(10 $\bar{1}$ 0), and CH<sub>4</sub> + Ni(100) systems. If results for these 3 systems are left out (leading to the database SBH14-3SBER, i.e., SBH17 with the 3 systems with the biggest errors removed), the MAEs and MSEs obtained with averaging over the systems now come out as shown in Table 3.13. As can be seen, omitting the systems for which the largest errors are made does not lead to large changes in the conclusions: according to the MSE criterion, revTPSS comes still out as best, followed by the same three DFs made up of GGA-exchange and non-local correlation (although now with a slightly different order), and PBE (see Tables 3.7 and 3.13). Omitting the three systems for which reference barrier heights came from an ad-hoc SE analysis rather than from SRP-DFT (resulting in the SBH14-SRP database) also does not yield large differences: the revTPSS and optPBE-vdW1 DFs still come out as the two best ranking DFs according to the  $|MSE|$  accuracy criterion (see Tables 3.7 and 3.13). Finally, the correlation of the signed error with (WF-EA) is shown in Figures 3.3, 3.4, and 3.5 for the GGA-DFs, the DFs consisting of GGA exchange and vdW-DF1 or vdW-DF2 correlation, and the meta-GGAs tested here, respectively. A weak correlation seems to be present, with the GGA and meta-GGA DFs producing lower (higher) signed errors for systems with lower (higher) (WF-EA).

## 3.4 Discussion

With the large amount of data here considered, a full analysis is beyond the scope of this chapter. Instead, in the discussion below we will focus on (i) the description of the metal, and (ii) how well the different algorithms do for describing the barriers for DC for the new database. Having determined an optimal algorithm, we then discuss (iii) how the different DFs perform overall for the new SBH17 database, and (iv) how this depends on the three different types of systems in our database. Then, we (v) compare to new and old results for the earlier SBH10 database. We also (vi) compare to the performance of DFs with earlier results for molecular chemisorption, and for gas phase reaction kinetics and thermochemistry. Finally, we also discuss future improvements and extensions of our database.

### 3.4.1 Description of the metal

The trends in how accurately the tested DFs describe the lattice constants of the metals investigated here (Ag, Ir, Cu, Pt, Ni, and Ru), as revealed through Table 3.3, agree well with earlier work done on different sets of bulk solids. For instance, the RPBE DF is known to overestimate lattice constants more than the PBE DF<sup>16,175</sup>, and it makes sense that the lattice constant computed with their 50/50 weighted average (SRP50) falls in between. It is also known that the vdW-DF1 and vdW-DF2 DFs substantially overestimate lattice constants, and much more so than PBE, but that the performance of optPBE-vdW-DF1 is similar to that of PBE, in agreement with Table 3.3<sup>16,47</sup>. Our finding that BEEF-vdW-DF2 performs somewhat worse than optPBE-vdW-DF1 is likewise in agreement with earlier findings<sup>16</sup>, and the same is true for the earlier finding that PBE $\alpha$ 57-vdW-DF2 and optPBE-vdDF1 perform similarly for lattice constants<sup>106</sup>. The SRP32-vdW-DF1 and PBE-vdW-DF2 DFs, which to our knowledge have not been widely tested on solids yet, show a performance that is just a little better than that of vdW-DF1 and vdW-DF2.

Our finding that the four meta-GGA DFs tested here are better for lattice constants than PBE is likewise in agreement with earlier work. This has been confirmed in Refs.<sup>16,175</sup> for revTPSS and in Refs.<sup>175,176</sup> for SCAN. Tran et al.<sup>175</sup> found a similarly good performance for MS2 as for revTPSS and SCAN, in agreement with Table 3.3. Finally, like MS2<sup>41</sup> the MS-B86b1<sup>52</sup> was developed to perform like the PBEsol<sup>54</sup> GGA for metals, and its resulting good performance for metals is in agreement with earlier findings<sup>106</sup>.

Interlayer distances computed with the tested DFs (Table 3.4) are not always in good agreement with experimental values and with literature values obtained

with the same DFs. This is not any reason for concern: converging the values of interlayer distances requires thicker slabs (a larger number of layers, of the order of eight or more<sup>145,173</sup>) than needed for converging reaction barrier heights (typically 4 or 5). As the focus in this work is on reaction barrier heights, no attempts were made to compute interlayer distances that were converged with slab thickness.

## 3.4.2 Description of barrier heights to DC

### 3.4.2.A Preferred algorithm

Table 3.6 can be used to select the optimal algorithm for testing DFs on reaction barrier heights for DC. In selecting this algorithm we also take into account that, for a typical system, the high algorithm requires more "human time", and roughly an order of magnitude more cpu time than the medium algorithm, due to the need to find the saddle point geometry corresponding to the DF tested and the system described. The light algorithm requires even less "human time" than the medium algorithm, as the lattice constant(s) of the metal and the geometry of the metal slab representing the surface also do not need to be optimized for each metal and metal surface, respectively. However, the light algorithm is not much less cpu-intensive than the medium algorithm.

Table 3.6 suggests the use of the medium algorithm for the following two reasons. The first reason is that for all GGA DFs, for all DFs combining GGA exchange with non-local correlation, and for revTPSS the medium algorithm leads to results that hardly differ from the results of the much more expensive high algorithm. In contrast, the light algorithm leads to results that differ considerably from those of the medium algorithm, i.e., higher MAEs and MSEs. This result suggests that, at least for now and while DFs are developed that yield a simultaneously good description of interaction energies and metal structure, the medium algorithm should be used. Figure 3.2 suggests an explanation: for GGA DFs, and apparently also for the DFs combining GGA exchange with non-local correlation, the predicted barrier height and metal lattice constant are correlated, with higher barriers corresponding to larger lattice constants, which has been known for some time<sup>54,55</sup>. Apparently reaction barrier heights are then best computed with the metal surface appropriately relaxed with the DF tested (as done in the high and medium algorithms), which may be related to the observation that reaction barrier heights may be strongly affected by lattice strain<sup>148</sup>. We note that the problem that with GGA DFs barrier heights are usually correctly predicted at the cost of overestimated lattice constants may in principle be solved by resorting to a meta-GGA DF, as the use of the kinetic energy density allows the DF to distinguish between metallic and covalent



TABLE 3.12: Overall accuracy achieved for each system in the SBH17 database with the algorithms tested. For a given system, mean absolute errors (MAE) and mean signed errors (MSE, both in eV) measure average deviations of the barrier heights computed using the DFs tested in this work from the reference values listed in Table 3.2. The averaging is done over the DFs, so that large deviations are likely to be indicative of inaccurate reference values.

System	High Algo		Med Algo		Light Algo	
	MAE	MSE	MAE	MSE	MAE	MSE
H <sub>2</sub> /Cu111	0.205	0.104	0.197	0.098	0.245	0.133
H <sub>2</sub> /Cu100	0.218	0.115	0.209	0.118	0.240	0.101
H <sub>2</sub> /Cu110	0.205	0.104	0.165	0.120	0.286	0.171
H <sub>2</sub> /Ag111	0.339	0.334	0.335	0.330	0.380	0.375
H <sub>2</sub> /Pt211	0.126	-0.048	0.054	0.048	0.056	0.056
H <sub>2</sub> /Pt111	0.125	0.124	0.084	0.082	0.135	0.132
H <sub>2</sub> /Ru0001	0.074	-0.008	0.039	0.016	0.046	0.028
H <sub>2</sub> /Ni111	0.075	0.028	0.063	0.049	0.078	0.059
N <sub>2</sub> /Ru0001	0.230	-0.138	0.231	-0.141	0.318	-0.203
N <sub>2</sub> /Ru1010	0.340	-0.259	0.349	-0.275	0.400	-0.293
CH <sub>4</sub> /Ni100	0.264	0.264	0.266	0.266	0.270	0.270
CH <sub>4</sub> /Ni111	0.144	0.091	0.132	0.100	0.182	0.132
CH <sub>4</sub> /Ni211	0.126	0.058	0.120	0.090	0.134	0.045
CH <sub>4</sub> /Pt111	0.155	0.098	0.146	0.084	0.280	0.246
CH <sub>4</sub> /Pt211	0.118	0.024	0.117	0.068	0.164	-0.032
CH <sub>4</sub> /Ru0001	0.152	0.142	0.157	0.144	0.187	0.176
CH <sub>4</sub> /Ir111	0.124	0.084	0.131	0.094	0.239	0.221
Average	0.177	0.065	0.164	0.076	0.214	0.095

bonding<sup>177</sup>. This should also explain why the correlation observed in the upper two panels of Figure 3.2 between lattice constant and barrier height is not observed for the meta-GGA DFs.

The second reason to use the medium algorithm is simply that it produces the lowest averaged MAE when the MAEs of the barrier heights are averaged over all DFs tested (Table 3.6). The simplest explanation being that the medium algorithm allows the best description of the reaction barrier height, Occam’s razor then suggests the use of the medium algorithm. From now on, our discussion will therefore focus on results obtained with the medium algorithm.

### 3.4.2.B Performance of DFs for SBH17 with medium algorithm

If we take the absolute value of the MSE as the accuracy criterion, of the DFs tested the revTPSS meta-GGA comes out as best with a |MSE| of 25 meV, which corresponds to 0.58 kcal/mol (see also Table 3.7). Of the five best performing DFs, three are made of GGA exchange and non-local correlation, and the DF ranked fifth is the PBE GGA DF. Both the revTPSS and PBE DFs may be described as non-empirical, constraint-based DFs, and interestingly both have been cast as general purpose, workhorse functionals.

TABLE 3.13: Density functional performance on two smaller databases with 14 barrier heights in them. SBH14-3SBER was obtained from SBH17 by removing the 3 systems yielding the largest MAE when averaging over all DFs tested (see Table 12). SBH14-SRP only contains the 14 systems for which reference values of barrier heights were obtained from SRP-DFT. For each database,  $r_{MAE}$  and  $r_{|MSE|}$  rank the DFs according to best performance for the MAE and  $|MSE|$  criterion, respectively. All errors are in eV.

Database	SBH14-3SBER			SBH14-SRP		
Density functional	MAE	$r_{MAE}$	$r_{ MSE }$	MAE	$r_{MAE}$	$r_{ MSE }$
PBE	0.074	1-2	5	0.074	1	4
SRP50	0.098	7	7	0.098	3	7
RPBE	0.208	13	13	0.210	12	12
vdW-DF1	0.191	11	11	0.219	13	13
vdW-DF2	0.267	14	14	0.294	14	14
PBE-vdW-DF2	0.107	8	9	0.128	9	9
SRP32-vdW-DF1	0.074	1-2	3	0.103	4-5	6
PBEc57-vdW-DF2	0.091	5	4	0.112	7	3
BEF-vdW-DF2	0.163	10	10	0.189	11	11
optPBE-vdW-DF1	0.093	6	2	0.114	8	1
revTPSS	0.089	4	1	0.103	4-5	2
SCAN	0.108	9	8	0.107	6	8
MS-B86b1	0.196	12	12	0.186	10	10
MS2	0.086	3	6	0.085	2	5

The MAE is probably the best accuracy criterion, as this quantity tells us by how much the barrier height we compute with a given DF will typically be off from the real value. According to this criterion, the PBE DF comes out best, with a MAE of 0.103 eV (2.4 kcal/mol). With this criterion revTPSS comes out as ninth, with a MAE of 0.146 eV (3.4 kcal/mol). The MS2 DF now comes out as the best meta-GGA DF (MAE = 0.117 eV = 2.7 kcal/mol). The highest ranked GGA+vdW DF now is SRP32-vdW-DF1, which has a second overall ranking (MAE = 0.115 eV = 2.7 kcal/mol).

The major conclusions regarding the accuracy of DFs for the type of DC reactions on SBH17 are robust in the sense that if we remove the three systems from the database that lead to the largest errors (leading to the SBH14-3SBER database) the order of the best performing DFs remains more or less the same. As Table 3.13 shows, revTPSS is still the best in terms of MSEs, and PBE still ranks first in terms of MAEs (although now together with SRP32-vdW-DF2). The best five performing DFs in terms of MSEs and the best three in terms of MAEs remain the same (compare Tables 3.7 and 3.13).

The major conclusions regarding DF accuracy also remain unchanged if we use the SBH14-SRP instead of the SBH17 database (compare Tables 3.7 and 3.13). For instance, the PBE DF remains the best performing DF according to the MAE criterion. SRP32-vdW-DF1 ranks second according to this criterion for SBH17, and still fourth (together with revTPSS) for SBH14-SRP; MS2 ranks third for SBH17, and second for SBH14-SRP. Removing the three systems for which reference barrier heights were obtained using an ad-hoc SE approach does lead to considerably smaller absolute values of the MAE, e.g. 74 meV (1.7 kcal/mol) for PBE under SBH14-SRP vs. 103 meV (2.4 kcal/mol) under SBH17. This suggests that the conclusions regarding DF performance on DC barrier heights in SBH17 would be even more favorable than now obtained if the reference values for the three systems discussed were to be replaced with more accurate SRP-DFT values. The following two observations provide additional evidence that the reference values for at least two of the three systems left out in SBH14-SRP are inaccurate: (i) the SRP32-vdW-DF1 functional, which performs so well for CH<sub>4</sub> + metal surface systems, shows a comparatively poor performance on CH<sub>4</sub> + Ni(100) (Table 3.11 and Fig. 3.4), and (ii) the PBE DF, which shows the lowest MAE for SBH17, shows a larger error on the N<sub>2</sub> + Ru(10 $\bar{1}$ 0) system than on any other system (Fig. 3.3).

If we compare trends found for barriers for DC on metals to trends found for gas phase reaction barriers, a number of important differences stand out. First of all, the MAEs tend to be smaller for DC barriers than for gas phase reaction barriers. To give an example: the MAE of the PBE DF for the BH76 database for hydrogen atom transfer and non-hydrogen atom transfer reactions

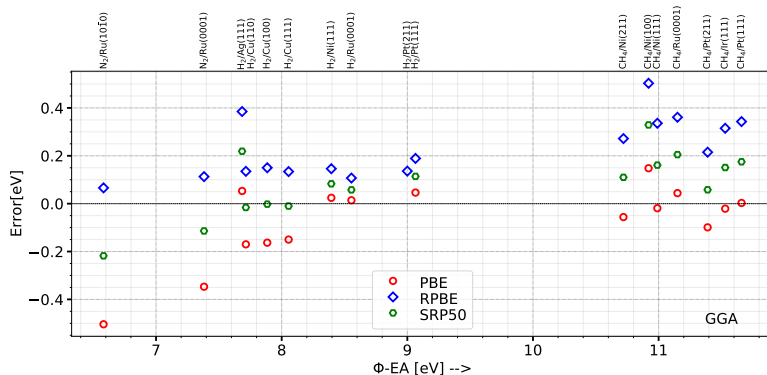


FIGURE 3.3: Correlation between the signed error and the difference of the work function of the metal surface  $\Phi$  and the electron affinity EA of the molecule for all the systems investigated. The results are for the high algorithm, for the GGA DFs tested.

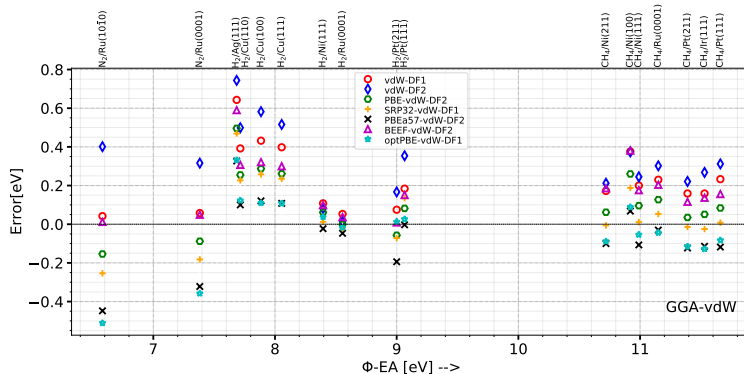


FIGURE 3.4: Correlation between the signed error and the difference of the work function of the metal surface  $\Phi$  and the electron affinity EA of the molecule for all the systems investigated. The results are for the high algorithm, for the GGA-vdW-DF1,2 DFs tested.

is 8.9 kcal/mol<sup>26</sup>, while the MAE found here is 2.4 kcal/mol. It is important to note that this difference does not arise from the barrier heights being much larger for the BH76 database: the average over the absolute values of the barrier heights is 18.6 kcal/mol for BH76<sup>23</sup>, which is not much larger than for SBH17 (14.8 kcal/mol). Second, while RPBE clearly outperforms PBE for gas phase reactions<sup>24,26,178</sup>, the opposite is the case for the DC barriers we consider here. Thirdly, and most importantly: while the PBE and RPBE DFs both systematically underestimate gas phase reaction barrier heights<sup>178</sup>, here we find that the RPBE DF systematically overestimates reaction barrier heights,

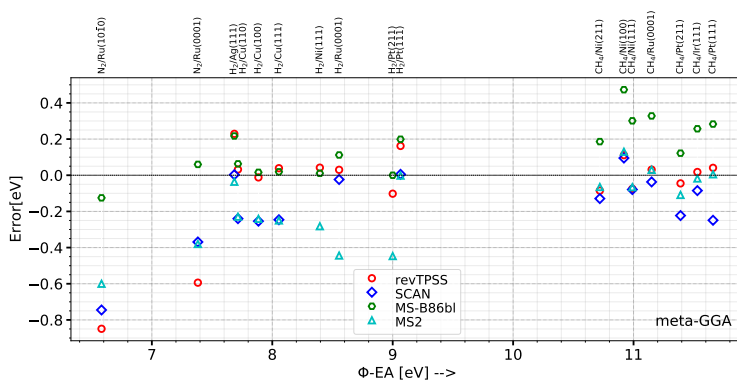


FIGURE 3.5: Correlation between the signed error and the difference of the work function of the metal surface  $\Phi$  and the electron affinity EA of the molecule for all the systems investigated. The results are for the high algorithm, for the meta-GGA DFs tested.

while the PBE DF neither systematically underestimates nor systematically overestimates DC barriers for the systems we consider. We consider this last point a key point, which should be a telltale concerning semi-local DFT and fundamental differences between gas phase reactions and DC on metals. For this we note that the deficiency of semi-local DFT for gas phase reactions has often been rationalized in terms of the delocalization error of Yang and co-workers<sup>179–181</sup>. The following hand waving explanation has been put forward for explaining the comparatively good performance of semi-local DFT for DC barriers in the systems in the database<sup>13</sup>: of the electrons responsible for the formation of bonds between the molecular fragments and the surface, the ones coming from the molecule become more delocalized in the transition state, but the opposite is true for the electrons coming from the metal, which are quite delocalized to start with. This leads to error cancellation. A weakness of this explanation is that it is hard to see how it can be tested or falsified, and more research is needed to clarify the origin of the differences between the performance of semi-local DFT for reaction kinetics in the gas phase and on metal surfaces.

Considering specific DFs, we note that, as found in other studies of molecules interacting with metal surfaces<sup>52,182</sup>, the maximally constrained meta-GGA DF SCAN does not outperform the PBE GGA DF for DC barriers, showing a similar performance to the revTPSS DF for the MAE. The somewhat weak performance of SCAN for adsorption of molecules on metal surfaces has been attributed to density driven errors<sup>182</sup>. The MS2 meta-GGA DF performs reasonably well for DC barriers, ranking third according to the MAE criterion, with a MAE of 0.117 eV (2.7 kcal/mol). The MS86bl DF, which has been constructed in such a way

that its performance should be biased in favor of systems containing hydrogen<sup>52</sup>, is the meta-GGA DF performing least well for DC barriers here.

Of the DFs built from GGA exchange and non-local correlation, the optPBE-vdW-DF1, the SRP32-vdW-DF1, and the PBE $\alpha$ 57-vdW-DF2 DFs perform quite well here, ranking among the best 4 according to the MSE and among the best 6 according to the MAE criterion. For the SRP32-vdW-DF1 and the PBE $\alpha$ 57-vdW-DF2 DFs this is not so surprising as they are known to be SRP-DFs for some of the systems in our database (see Table 3.2). However, the optPBE-vdW-DF1 DF was first developed to obtain an improved description of weak interactions<sup>49</sup>, and only later was this DF shown to accurately model systems in which H<sub>2</sub> interacts with copper surfaces<sup>87,108</sup>. The original vdW-DF1 and vdW-DF2 DFs do not exhibit a very good performance for DC, ranking 12<sup>th</sup> and 14<sup>th</sup> on both accuracy criteria. PBE-vdW-DF2 exhibits a reasonable performance. The performance of BEEF-vdW-DF2 would seem to be disappointing as well, as it seemed to perform much better in the earlier tests on the SBH10 database<sup>40</sup>. This issue will be further considered below.

### 3.4.2.C Dependence on the type of system

The performance of the tested DFs on H<sub>2</sub>-metal systems (Table 3.9) does not contain great surprises. The SRP50 DF performs better on this sub-database than on SBH17, but this is no great surprise as this DF is close to the SRP48 DF, which is an SRP-DF for H<sub>2</sub> + Cu(111)<sup>104</sup>. The SRP32-vdW-DF is also less good for the H<sub>2</sub>-metal sub-database than for SBH17, which may be explained from this DF being an SRP-DF for several CH<sub>4</sub> + metal systems, while it performs poorly for DC of H<sub>2</sub> on Cu and Ag surfaces (see Table 3.2 and Fig. 3.4).

The performance of the tested DFs on N<sub>2</sub>-metal systems (Table 3.10) is rather different from that on the SBH17 database. Specifically, the best four performing DFs for N<sub>2</sub>-metal systems (MS-B86bl, BEEF-vdW-DF2, vdW-DF1, and RPBE according to both the MSE and MAE criteria) show a rather poor overall performance on SBH17. The origin of this discrepancy is not entirely clear. However, there appears to be a weak correlation between the MSE of a given functional and (WF-EA) (see Figures 3.3-3.5). A trend that may be discerned is that the MSE increases with the (WF-EA). The N<sub>2</sub>-metal systems have a low (WF-EA), and lie on one of the outer edges of the range of (WF-EA) spanned by the systems investigated here (see Figures 3.3-3.5). These two observations together perhaps explain why the DFs that come out best for N<sub>2</sub>-metal systems do not do well for SBH17 as a whole: for many of the systems in the database with higher (WF-EA), these DFs will produce much higher unsigned errors.

Finally coming to the CH<sub>4</sub>-metal systems (Table 3.11) the only real surprise is that SCAN performs quite well for these systems. The good performance of SCAN for systems with high (WF-EA) (see Figures 3.3-3.5) is consistent with the explanation that for this DF errors in molecule-metal surface interactions are density driven: for the methane-metal systems, little if no electron transfer will occur from the metal surface to the molecule. This would suggest that errors associated with electron delocalization and self-interaction should be small<sup>58</sup>, which would in turn suggest that density driven errors should be small.

#### 3.4.2.D Comparison to present and previous results for SBH10

To allow a better comparison between the results for the present SBH17 and the older SBH10 database, in Table 3.14 we compare the MAEs obtained for both databases for the 9 DFs that performed best for SBH17 according to the MAE accuracy criterion. In Table 3.14 we also show how these DFs ranked according to both the MAE and the MSE accuracy criterion in both databases.

The comparison shows that, on the whole, not much changes when comparing our new results for SBH10 to our new results for SBH17. Only in one case is the MSE changed by more than 1 kcal/mol ( $\sim 43$  meV), i.e., for the meta-GGA MS2 functional (by 54 meV). The second largest change occurred for the GGA PBE DF (40 meV), and the third largest change for the meta-GGA revTPSS DF (by 31 meV). In all three cases the MAE is increased going from SBH17 to SBH10. Inspection of Figs 3.3 and 3.5 suggests that for these 3 DFs the discrepancy could to a large extent be due to the larger weight of the N<sub>2</sub>-metal systems in the SBH10 database (20 %) compared to that in the SBH17 database (12 %), as the three DFs mentioned all perform rather poorly for the systems containing N<sub>2</sub>.

Finally, there is the matter of how the old results for SBH10<sup>40</sup> compare to the new results for SBH10, and for SBH17. The old study compared results for three DFs where each is a representative of a specific class of DFs, i.e., rung 2 (GGA) exchange with vdW-DF2 correlation (BEEF-vdW-DF2), rung 3 exchange and rung 3 correlation (MS2), and a rung 4, screened hybrid DF (HSE06)<sup>42</sup>. With the latter DF, only results were obtained for the H<sub>2</sub> metal systems. For this reason, and because we did not test any rung 4 DFs here, we will not discuss the old HSE06 results here.

First comparing the old SBH10 to the new SBH10 results here (see Table 3.8), fairly large differences are noted for the two DFs tested. The old results showed a somewhat better performance for the BEEF-vdW-DF2 DF (MAE, MSE = 0.12, 0.03 eV) than here obtained (MAE, MSE = 0.18, 0.18 eV for the medium algorithm, see also Table 3.8). On the other hand the old results showed a

TABLE 3.14: Comparison of DF performance on the SBH17 and SBH10 databases. For the nine DFs that performed best for SBH17 according to the MAE (eV) criterion, a comparison is made with their performance for the SBH10 database. For this, the rank  $r_{MAE}$  of the DF is presented according to the MAE (eV) criterion for both SBH17 and SBH10, as well as the MAE (eV) for the DF for each database. The last column lists the ranks  $r_{|MSE|}$  according to the MSE (eV) as accuracy criterion, for both SBH17 and SBH10 (with  $r_{|MSE|}$  for the latter given in brackets). All results are for the medium algorithm.

DF	$r_{MAE}$ SBH17	MAE SBH17	MAE SBH17	$r_{MAE}$ SBH10	MAE SBH10	$r_{ MSE }$
PBE	1	0.103	0.103	5	0.143	5 (5)
SRP32-vdW-DF1	2	0.115	0.115	1	0.126	4 (1)
MS2	3	0.117	0.117	8	0.171	6 (7)
PBE $\alpha$ 57-vdW-DF2	4	0.124	0.124	2	0.132	3 (3)
SRP50	5	0.125	0.125	3	0.133	7 (2)
optPBE-vdW-DF1	6	0.131	0.131	4	0.141	2 (4)
SCAN	7	0.140	0.140	7	0.179	8 (10)
PBE-vdW-DF2	8	0.141	0.141	6	0.148	9 (6)
revTPSS	9	0.146	0.146	9	0.177	1 (7)



considerably worse performance for the MS2 DF (MAE, MSE = 0.36, -0.34 eV) than here obtained (MAE, MSE = 0.17, -0.12 eV for the medium algorithm, see also Table 3.6). The explanation for this difference is as follows. A shortcoming of the method to compute barrier heights in the older work was that the metal surface was allowed to relax in the presence of the molecule for 9 of the 10 systems in the database in the calculation of the transition state energy. From a physical point of view, this is incorrect when interpreting the outcome of supersonic molecular beam experiments, where the molecule comes in fast and the surface atoms do not have time to respond to its presence<sup>10</sup>. Using this incorrect procedure should lead to an underestimate of the classical barrier height relative to SRP-DFT or experimentally estimated values obtained from supersonic molecular beam sticking experiments, which should reflect the situation where the surface atoms have not relaxed in response to the incoming molecule. How this affects the results for a given DF depends on its MSE. The BEEF-vdW-DF2 DF has a small positive MSE for SBH10 with the old algorithm, which should then go up with the new algorithm, as should the MAE. This explains the worse performance of BEEF-vdW-DF2 for SBH10 with the newer and better algorithm (as Figure 3.6 shows, barrier heights increase with the new algorithm, the reason being that the TS energy comes out higher because the surface is not allowed to relax). The MS2 DF has a large negative MSE for SBH10 with the old algorithm, which should then become smaller but still negative with the new algorithm, and this should lead to a smaller MAE, as indeed observed.

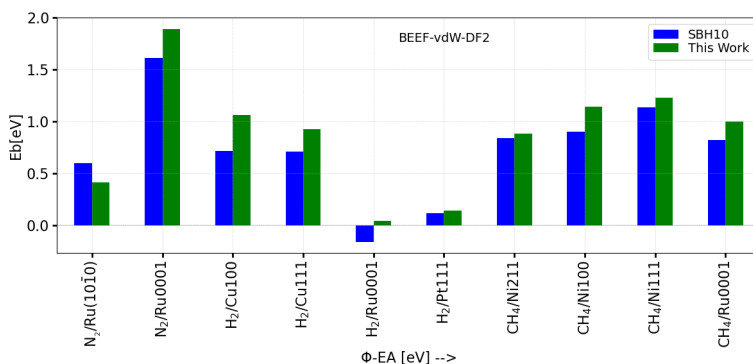


FIGURE 3.6: Comparison of barrier heights computed with the BEEF-vdW-DF2 DF for the systems in the SBH10 database, allowing the surface to relax in the TS (SBH10, results from Ref.<sup>40</sup>) and using the medium algorithm, in which the surface is held fixed at the metal-vacuum interface geometry (This work).

We now compare the old SBH10 to the new SBH17 results. The old results showed a somewhat better performance for the BEEF-vdW-DF2 DF (MAE,

MSE = 0.12, 0.03 eV) than here obtained for SBH17 (MAE, MSE = 0.19, 0.19 eV, medium algorithm, see also Table 3.7). On the other hand the old SBH10 results showed a considerably worse performance for the MS2 DF (MAE, MSE = 0.36, -0.34 eV) than here obtained for SBH17 (MAE, MSE = 0.12, -0.07 eV, medium algorithm, see also Table 3.7). In contrast to the older SBH10 work, we thus find a better performance of the MS2 DF than of the BEEF-vdW-DF2 DF. However, this better performance could in principle reflect the smaller proportion of N<sub>2</sub>-metal systems in SBH17 than in SBH10. If it turns out that, as discussed above in Section 3.4.2.B, MS2 also systematically underestimates barrier heights for N<sub>2</sub>-metal systems, then the performance of this DF for a more balanced database (which should contain more N<sub>2</sub>-metal systems relative to H<sub>2</sub>- and CH<sub>4</sub>-metal systems than now is the case) could be somewhat worse than now found. However, our results do not support the conclusion that might be drawn from the older SBH10 work that meta-GGA functionals systematically underestimate reaction barrier heights for DC on metals: this is not true for revTPSS (MSE = -25 meV), for MS2, and even for SCAN (MAE = 140 meV, MSE = -105 meV, see Table 3.7), and it is certainly not true for MS-B86bl (MSE = 195 meV). Our new study also does not support the idea that meta-GGA DFs should be worse for DC on metals than GGA DFs.

### 3.4.3 Comparison to results for adsorption and to gas phase results

In Table 3.15 our new results for SBH17 are compared to results for adsorption of molecules to metal surfaces, focusing on strong molecule-metal surface interactions, i.e., on chemisorption. The data we compare to come from calculations on the CE26 database<sup>18</sup> and from calculations on the CE21b database<sup>183</sup>, where the latter may be viewed as a sub-database of the former. We use the MAE (or, if not available, the RMSE) as the accuracy criterion, and the DFs are listed in order of increasingly RMSE for the CE26 database. The most important observation that can be made is that the DFs that perform best for DC barrier heights (a kinetic property) usually are not best for chemisorption energies (a thermochemical property), and vice versa. To give a few examples: PBE performs best for DC barriers in SBH17, but ranks sixth of the DFs listed in Table 3.15 for chemisorption energies. Similarly, the three best DFs for chemisorption (BEEF-vdW-DF2, vdW-DF1, and RPBE) did not perform particularly well for dissociation barriers, ranking 10<sup>th</sup>, 12<sup>th</sup>, and 13<sup>th</sup> among the 14 DFs tested on SBH17. A DF performing reasonably well on both chemisorption and DC is MS2, which ranks 4<sup>th</sup> for chemisorption and 3<sup>rd</sup> for DC barriers in Table 3.15, and may be said to yield the best overall performance on molecule-metal surface

interactions. On the basis of the results in Table 3.15 we do not agree with the statement that "a functional that predicts chemisorption energies accurately can also predict barrier heights with comparable accuracy"<sup>18</sup>. In Ref.<sup>18</sup> this conclusion referred to the BEEF-vdW-DF2, which performs well for chemisorption and performed well in the earlier tests on DC of Ref.<sup>40</sup>. However, as shown here its performance for barrier heights is not particularly good if the metal surface is treated appropriately (see Section 3.4.2.B), which was not the case in Ref.<sup>40</sup>.

In Table 3.16 kinetic data coming from barrier height databases (the present SBH17 results for surface reactions, and BH76 and BH206 for gas phase reactions) and thermochemical data (the CE26 results for chemisorption at metal surfaces, and AE6 for atomization energies and TCE for "easy" thermochemical gas phase interactions) are compared for a selection of the GGA and meta-GGA DFs tested here. We see that some of the observations for surface reactions also hold for gas phase interactions. For example, the functional that of PBE and RPBE is best for gas phase reaction barriers (RPBE in BH76 and BH206) is not necessarily best for gas phase thermochemistry (with RPBE outperformed by PBE for the large TCE database, although not for the small AE6 database). For the databases listed in Table 3.16, MS2 has the best overall performance. A striking observation is that RPBE is good for chemisorption (for which it was optimized<sup>39</sup>) while PBE is good for DC barrier heights (for which it was not optimized), as already noted above. In Section 3.4.2 the point that RPBE is better than PBE for gas phase reactions but not for metal surface reactions was already discussed. The revTPSS DF exhibits a fairly robust performance for all the databases in Table 3.16. SCAN is robust for the gas phase databases, poor for chemisorption, but rather good for DC barriers.

### 3.4.4 Future improvements

On the basis of the above, we see the following possible improvements of the present database for DC barriers on metals, and for testing DFs on the database.

First, we suggest that in future the entries in the database are as much as possible based on SRP-DFT, and not on more ad-hoc SE procedures. This would require dynamics calculations with trial DFs on  $\text{CH}_4 + \text{Ru}(0001)$  and  $\text{CH}_4 + \text{Ni}(100)$ , for which molecular beam experiments are already available<sup>91,129</sup>, and new experiments and dynamics calculations on  $\text{N}_2 + \text{Ru}(10\bar{1}0)$ , for which molecular beam sticking experiments are, to our knowledge, not yet available. As noted above our comparison between MAEs computed with PBE for SBH17 and SBH14-SRP suggests that replacing the reference values with SRP-DFT values for the three systems mentioned is likely to lead to smaller MAEs for a thus improved version of the SBH17 database. Second, we suggest that the database

TABLE 3.15: DF performance for kinetics and thermochemistry of molecules reacting with metal surfaces. Errors for adsorption energies as present in the CE21b<sup>183</sup>, and CE26<sup>18</sup> databases are compared to MAEs computed for DC barriers for the new SBH17 database, for the DFs for which results were provided in the chemisorption databases.

All errors are in eV.

DF	Database	CE21b		CE26		SBH17	
	Type DF	MAE	MSE	RMSE	MSE	MAE	Rank
BEEF-vdW-DF2	GGA+vdW	-	-	0.21	0.0	0.19	10
vdW-DF1	GGA+vdW	-	-	0.21	0.09	0.22	12
RPBE	GGA	0.15	0.07	0.23	0.09	0.23	13
MS2	meta-GGA	-	-	0.27	-0.15	0.12	3
vdW-DF2	GGA+vdW	-	-	0.29	0.15	0.31	14
PBE	GGA	0.30	-0.28	0.31	-0.19	0.10	1
revTPSS	meta-GGA	0.30	-0.28	0.31 <sup>a</sup>	-	0.15	9
SCAN	meta-GGA	0.47	-0.46	0.45	-0.39	0.14	7
optPBE-vdW-DF1	GGA+vdW	-	-	0.54	-0.42	0.13	6

<sup>a</sup> Inferred from PBE value for CE26 and similar performance of PBE and revTPSS on the MAE in CE21b.

TABLE 3.16: DF performance for kinetics and thermochemistry of molecules reacting with metal surfaces, and for gas phase chemistry. Comparison of performance of a selection of GGA and meta-GGA DFs for gas phase and metal-surface interactions. Unless indicated otherwise with explicit references the data come from the present results for the SBH17 database (this work), and works presenting data for the BH76 database<sup>26</sup>, the BH206 database<sup>24</sup>, the CE26 database<sup>18</sup>, the AE6 database<sup>183</sup>, and the TCE database<sup>24</sup>. All errors in eV.

DF	Database Type DF	SBH17 MAE	BH76 MAE	BH206 RMSE	CE26 RSME	AE6 MAE	TCE RMSE
PBE	GGA	0.10	0.43	0.40	0.31	1.02	0.40
MS2	meta-GGA	0.12	0.27 <sup>184</sup>	0.27	0.27	0.19 <sup>185</sup>	0.29
SCAN	meta-GGA	0.14	0.34 <sup>51</sup>	0.33	0.45	0.15	0.23
revTPSS	meta-GGA	0.15	0.35	0.32	0.31	0.28	0.27
RPBE	GGA	0.23	0.34	0.33	0.23	0.42	0.42

be extended with additional N<sub>2</sub>-metal systems. It may be possible to do this by semi-empirically fitting SRP-DFs to supersonic molecular beam sticking data on N<sub>2</sub> + Fe(111)<sup>186,187</sup>, W(110)<sup>188,189</sup>, and W(100)<sup>189–192</sup>. Adding these data is desirable to make the database more balanced, as it is now dominated by data for DC of H<sub>2</sub> and CH<sub>4</sub> on metal surfaces. Also, it would show whether our results for the MS2 DF are robust to addition of more N<sub>2</sub>-metal systems to the database, for which this DF did not perform so well, and the same holds for the optPBE-vdW-DF1 and PBE DFs.

On the longer term, it should be necessary to extend the database with systems for which the charge transfer energy, which equals (WF-EA), is less than 7 eV. As noted in Ref.<sup>58</sup>, DFs with semi-local exchange would appear to systematically overestimate the reactivity of such systems, suggesting that DFs with screened exact exchange are required for a good description. Examples of systems for which molecular beam sticking data are available include e.g. H<sub>2</sub>O + Ni(111)<sup>193</sup>, HCl + Au(111)<sup>194</sup>, and O<sub>2</sub> + Al(111)<sup>195,196</sup>, Ag(110)<sup>197,198</sup>, Cu(100)<sup>199</sup>, and Cu(111)<sup>200</sup>. Inclusion of such systems in the database would certainly alter the view of the performance of DFs for DC on metal surfaces, where the view offered in the present work is specific to systems with (WF-EA) > 7 eV, the only exception being N<sub>2</sub> + Ru(1010).

Finally, of course a far larger number of DFs exists than here tested. While we could mention specific DFs here that would be nice to test, this might not do justice to others, as several DFs exist (see e.g. the DFs tested in Refs.<sup>23,24,26</sup>). However, a particular DF we would like to mention is the new machine learned DF DM21<sup>201</sup>. Even though this DF has not been trained on interactions involving transition metals, it would be good to see how it performs on SBH17. It would also be good to test recently developed functionals combining screened exact exchange with vdW-DF1 and vdW-DF2 correlation<sup>202,203</sup>, which may work especially well for the representative database we envisage. We advocate that such future benchmark tests would also incorporate calculations employing the CE26 database for chemisorption on metals<sup>18</sup>.

Last but not least, it would also be good to mention something we would like to keep the same for now. A nice conclusion from the present work is that benchmarking of DFs on the SBH17 database can be done with the "medium algorithm". While this requires some additional work to what is needed for benchmarking DFs on kinetic and thermochemical data on chemical reactions, the overall extra effort required (of determining the lattice constant of the 6 metals present in the database for each DF, and the interlayer relaxation of the metal slabs of the 12 different metal surfaces used here) is manageable. For this reason, we also hope that others will start using the SBH17 database, and that it will be incorporated in the larger databases that are now used for extensive

benchmarks of gas phase reactions<sup>23,24,26</sup>, which unfortunately do not yet include data for reactions on metal surfaces.

### 3.5 Conclusions and outlook

We have presented a new database with barrier heights for DC on metal surfaces that can be used for benchmarking electronic structure methods. The new database is called SBH17 and contains barriers for 17 systems, including 8 H<sub>2</sub> metal systems, 2 N<sub>2</sub> metal systems, and 7 CH<sub>4</sub> metal systems. For 16 systems (WF-EA) exceeds 7 eV. The barrier heights come from SRP-DFT (14 systems) and from more ad-hoc SE procedures (3 systems). The new database is meant to replace an older database (SBH10) that contained barriers for 10 of the 17 systems now treated.

We have tested 14 DFs on the new database, of which three were GGA DFs, 4 meta-GGA DFs, and 7 DFs containing GGA exchange and vdW-DF1 or vdW-DF2 non-local correlation. We first tested how the performance of these DFs depend on the algorithm or procedure used. Three different algorithms were tested, which were labeled “high”, “medium” and “light” according to the investment of computer time that was required for the calculation. In the algorithm that is the best compromise between accuracy and invested computer time (the medium algorithm), for each DF tested one computes the lattice constant of the metals in the database. Next, for each DF tested, for each metal surface in the database one performs a relaxation of the interlayer distances between the top layers. Then, for each system in the database and for each DF the barrier height is computed on the basis of two single point calculations. One of these calculations is for a geometry where the molecule is in the gas phase, and one for a geometry where the molecule is in the saddle-point geometry with respect to the surface obtained from the previous calculations. This saddle point geometry is either the one previously obtained from an SRP-DFT calculation (if the barrier height comes from SRP-DFT) or from a calculation with a functional that is expected to perform best (if the barrier height is a guess based on more approximate SE procedure).

Of the DFs tested, the meta-GGA DFs perform best at describing the metal, followed by PBE and optPBE-DF1. When the MAE is taken as the accuracy criterion, the workhorse PBE GGA DF performs best on the SBH17 database, with a MAE of 2.4 kcal/mol. Other top performers are the MS2 meta-GGA functional and two functionals consisting of GGA exchange and non-local correlation (SRP32-vdW-DF1 and PBE $\alpha$ 57-vdW-DF2). Surprisingly, none of the DFs tested systematically underestimates reaction barriers for DC on metals, in contrast to findings for gas phase reactions. This finding should

be a telltale on the origin of flaws of semi-local DFs for gas phase reaction barriers, and differences between gas phase reactions and DC reactions on metals, suggesting further research on these topics.

Our results for the accuracy of the DFs for DC barriers are robust to the extent that their ranking according to MAE is rather insensitive to removing the three systems yielding the biggest errors in the database, to removing the three systems for which reference barrier heights were obtained with an ad-hoc SE analysis, and to applying the functionals to the older SBH10 database. Improving SBH17 by ensuring that all reference barrier heights come from SRP-DFT is likely to reduce the MAEs of the best performing functionals considerably, e.g. to an error less than 2 kcal/mol for PBE. We obtain different results regarding the relative accuracy of the MS2 and BEEF-vdW-DF2 functionals than obtained in an earlier study of the SBH10 database, which we attribute to an incorrect treatment of the surface atoms in the transition states in the earlier study.

For the sub-databases with H<sub>2</sub>-metal systems, N<sub>2</sub>-metal systems, and CH<sub>4</sub>-metal systems, rankings are obtained that differ from the overall ranking for the complete database. The SRP50-DF (the 50/50 mixture of the PBE and RPBE GGA DFs) performs best for H<sub>2</sub>-metal systems. BEEF-vdW-DF2 performs best for N<sub>2</sub>-metal systems, and SRP32-vdW-DF1 for CH<sub>4</sub>-metal systems.

The DFs performing best for DC barriers (i.e., kinetics) are not the ones that perform best for databases (CE26, CE21b) of chemisorption energies on metals (i.e., thermochemistry). This trend is paralleled in the performance of DFs on databases for kinetics (BH76, BH206) and thermochemistry (AE6, TCE) in the gas phase. The meta-GGA MS2 DF is the functional with the best overall performance for DC barriers and chemisorption energies on metals. Of the five GGA and meta-GGA DFs considered for their performance on 6 databases for kinetics and thermochemistry on metal surfaces and in the gas phase (PBE, RPBE, revTPSS, MS2, and SCAN) again MS2 showed the best overall performance.

Future improvements of the present database include replacing estimates of barrier heights from ad-hoc SE procedures with SRP-DFT values, adding data for the underrepresented N<sub>2</sub>-metal systems, and extending the databases with systems for which (WF-EA) is less than 7 eV. Chemically accurate barriers for the latter category of systems do not yet exist, and obtaining them may require a fundamentally different approach than the SE SRP-DFT approach forming the basis of the present database. Adding such systems should be important because they include systems relevant to sustainable chemistry (e.g., oxygen containing molecules like water and methanol), and because conclusions regarding the performance of DFs for the more general database also including such systems might be different from the present conclusions. In spite of the

present limitations of the database we hope that the new database finds its way into benchmark tests of new and already existing DFs, as it is rather odd that such tests do not yet include the type of reactions that arguably is most important for producing chemicals.



## References

- (1) Noyori, R. Synthesizing our future. *Nat. Chem.* **2009**, *1*, 5–6.
- (2) Ertl, G. Primary steps in catalytic synthesis of ammonia. *J. Vac. Sci. Technol., A: Vacuum, Surfaces, and Films* **1983**, *1*, 1247–1253.
- (3) Chorkendorff, I.; Niemantsverdriet, J. W., *Concepts of modern catalysis and kinetics*; Wiley Online Library: 2003; Vol. 138.
- (4) Wolcott, C. A.; Medford, A. J.; Studt, F.; Campbell, C. T. Degree of rate control approach to computational catalyst screening. *J. Catal.* **2015**, *330*, 197–207.
- (5) Sabbe, M. K.; Reyniers, M.-F.; Reuter, K. First-principles kinetic modeling in heterogeneous catalysis: an industrial perspective on best-practice, gaps and needs. *Catal. Sci. Technol.* **2012**, *2*, 2010–2024.
- (6) Honkala, K.; Hellman, A.; Remediakis, I.; Logadottir, A.; Carlsson, A.; Dahl, S.; Christensen, C. H.; Nørskov, J. K. Ammonia synthesis from first-principles calculations. *science* **2005**, *307*, 555–558.
- (7) Campbell, C. T. The degree of rate control: a powerful tool for catalysis research. *ACS Catal.* **2017**, *7*, 2770–2779.
- (8) Nørskov, J. K.; Abild-Pedersen, F.; Studt, F.; Bligaard, T. Density functional theory in surface chemistry and catalysis. *Proc. Natl. Acad. Sci. U.S.A* **2011**, *108*, 937–943.
- (9) Medford, A. J.; Wellendorff, J.; Vojvodic, A.; Studt, F.; Abild-Pedersen, F.; Jacobsen, K. W.; Bligaard, T.; Nørskov, J. K. Assessing the reliability of calculated catalytic ammonia synthesis rates. *Science* **2014**, *345*, 197–200.
- (10) Kroes, G. J. Computational approaches to dissociative chemisorption on metals: towards chemical accuracy. *Phys. Chem. Chem. Phys.* **2021**, *23*, 8962–9048.
- (11) Díaz, C.; Pijper, E.; Olsen, R. A.; Busnengo, H. F.; Auerbach, D. J.; Kroes, G. J. Chemically accurate simulation of a prototypical surface reaction: H<sub>2</sub> dissociation on Cu(111). *Science* **2009**, *326*, 832–834.
- (12) Kroes, G. J. Toward a database of chemically accurate barrier heights for reactions of molecules with metal surfaces. *J. Phys. Chem. Lett.* **2015**, *6*, 4106–4114.

- (13) Nattino, F.; Migliorini, D.; Kroes, G. J.; Dombrowski, E.; High, E. A.; Killelea, D. R.; Utz, A. L. Chemically accurate simulation of a polyatomic molecule-metal surface reaction. *J. Phys. Chem. Lett.* **2016**, *7*, 2402–2406.
- (14) Migliorini, D.; Chadwick, H.; Nattino, F.; Gutiérrez-González, A.; Dombrowski, E.; High, E. A.; Guo, H.; Utz, A. L.; Jackson, B.; Beck, R. D.; Kroes, G. J. Surface reaction barriometry: methane dissociation on flat and stepped transition-metal surfaces. *J. Phys. Chem. Lett.* **2017**, *8*, 4177–4182.
- (15) Wellendorff, J.; Silbaugh, T. L.; Garcia-Pintos, D.; Nørskov, J. K.; Bligaard, T.; Studt, F.; Campbell, C. T. A benchmark database for adsorption bond energies to transition metal surfaces and comparison to selected DFT functionals. *Surf. Sci.* **2015**, *640*, 36–44.
- (16) Wellendorff, J.; Lundgaard, K. T.; Møgelhøj, A.; Petzold, V.; Landis, D. D.; Nørskov, J. K.; Bligaard, T.; Jacobsen, K. W. Density functionals for surface science: Exchange-correlation model development with Bayesian error estimation. *Phys. Rev. B* **2012**, *85*, 235149.
- (17) Schmidt, P. S.; Thygesen, K. S. Benchmark database of transition metal surface and adsorption energies from many-body perturbation theory. *J. Phys. Chem. C* **2018**, *122*, 4381–4390.
- (18) Mallikarjun Sharada, S.; Karlsson, R. K. B.; Maimaiti, Y.; Voss, J.; Bligaard, T. Adsorption on transition metal surfaces: Transferability and accuracy of DFT using the ADS41 dataset. *Phys. Rev. B* **2019**, *100*, 035439.
- (19) Duanmu, K.; Truhlar, D. G. Validation of density functionals for adsorption energies on transition metal surfaces. *J. Chem. Theory. Comp.* **2017**, *13*, 835–842.
- (20) Hensley, A. J.; Ghale, K.; Rieg, C.; Dang, T.; Anderst, E.; Studt, F.; Campbell, C. T.; McEwen, J.-S.; Xu, Y. DFT-based method for more accurate adsorption energies: an adaptive sum of energies from RPBE and vdW density functionals. *J. Phys. Chem. C* **2017**, *121*, 4937–4945.
- (21) Mahlberg, D.; Sakong, S.; Forster-Tonigold, K.; Groß, A. Improved DFT adsorption energies with semiempirical dispersion corrections. *J. Chem. Theory. Comp.* **2019**, *15*, 3250–3259.
- (22) Silbaugh, T. L.; Campbell, C. T. Energies of formation reactions measured for adsorbates on late transition metal surfaces. *J. Phys. Chem. C* **2016**, *120*, 25161–25172.

- (23) Goerigk, L.; Hansen, A.; Bauer, C.; Ehrlich, S.; Najibi, A.; Grimme, S. A look at the density functional theory zoo with the advanced GMTKN55 database for general main group thermochemistry, kinetics and noncovalent interactions. *Phys. Chem. Chem. Phys.* **2017**, *19*, 32184–32215.
- (24) Mardirossian, N.; Head-Gordon, M. Thirty years of density functional theory in computational chemistry: an overview and extensive assessment of 200 density functionals. *Mol. Phys.* **2017**, *115*, 2315–2372.
- (25) Morgante, P.; Peverati, R. ACCDB: A collection of chemistry databases for broad computational purposes. *J. Comput. Chem.* **2019**, *40*, 839–848.
- (26) Peverati, R.; Truhlar, D. G. Quest for a universal density functional: the accuracy of density functionals across a broad spectrum of databases in chemistry and physics. *Philos. Trans. R. Soc., A* **2014**, *372*, 20120476.
- (27) Raghavachari, K.; Trucks, G. W.; Pople, J. A.; Head-Gordon, M. A fifth-order perturbation comparison of electron correlation theories. *Chem. Phys. Lett.* **1989**, *157*, 479–483.
- (28) Perdew, J. P. Climbing the ladder of density functional approximations. *MRS bull.* **2013**, *38*, 743–750.
- (29) Perdew, J. P.; Schmidt, K. Jacob's ladder of density functional approximations for the exchange–correlation energy, in *Density Functional Theory and its Application to Materials*, edited by V. van Doren, C. van Alsenoy, and P. Geerlings. *AIP Conf. Proc.* **2001**, *577*, 1–20.
- (30) Perdew, J. P.; Burke, K.; Ernzerhof, M. Generalized Gradient Approximation Made Simple. *Phys. Rev. Lett.* **1996**, *77*, 3865–3868.
- (31) Hammer, B. H. L. B.; Hansen, L. B.; Nørskov, J. K. Improved adsorption energetics within density-functional theory using revised Perdew-Burke-Ernzerhof functionals. *Phys. Rev. B* **1999**, *59*, 7413–7421.
- (32) Mori-Sánchez, P.; Cohen, A. J.; Yang, W. Many-electron self-interaction error in approximate density functionals. *J. Chem. Phys.* **2006**, *125*, 201102.
- (33) Peverati, R.; Truhlar, D. G. An improved and broadly accurate local approximation to the exchange–correlation density functional: The MN12-L functional for electronic structure calculations in chemistry and physics. *Phys. Chem. Chem. Phys.* **2012**, *14*, 13171–13174.
- (34) Peverati, R.; Truhlar, D. G. Exchange–correlation functional with good accuracy for both structural and energetic properties while depending only on the density and its gradient. *J. Chem. Theory Comput.* **2012**, *8*, 2310–2319.

- (35) Chuang, Y.-Y.; Radhakrishnan, M. L.; Fast, P. L.; Cramer, C. J.; Truhlar, D. G. Direct dynamics for free radical kinetics in solution: Solvent effect on the rate constant for the reaction of methanol with atomic hydrogen. *J. Phys. Chem. A* **1999**, *103*, 4893–4909.
- (36) Chakraborty, A.; Zhao, Y.; Lin, H.; Truhlar, D. G. Combined valence bond-molecular mechanics potential-energy surface and direct dynamics study of rate constants and kinetic isotope effects for the  $\text{H} + \text{C}_2\text{H}_6$  reaction. *J. Chem. Phys.* **2006**, *124*, 044315.
- (37) <http://sunecat.slac.stanford.edu/catapp/>.
- (38) Hummelshøj, J. S.; Abild-Pedersen, F.; Studt, F.; Bligaard, T.; Nørskov, J. K. CatApp: a web application for surface chemistry and heterogeneous catalysis. *Angew. Chem., Int. Ed.* **2012**, *51*, 272–274.
- (39) Hammer, B.; Hansen, L. B.; Nørskov, J. K. Improved adsorption energetics within density-functional theory using revised Perdew-Burke-Ernzerhof functionals. *Phys. Rev. B* **1999**, *59*, 7413–7421.
- (40) Mallikarjun Sharada, S.; Bligaard, T.; Luntz, A. C.; Kroes, G. J.; Nørskov, J. K. SBH10: A benchmark database of barrier heights on transition metal surfaces. *J. Phys. Chem. C* **2017**, *121*, 19807–19815.
- (41) Sun, J.; Haunschild, R.; Xiao, B.; Bulik, I. W.; Scuseria, G. E.; Perdew, J. P. Semilocal and hybrid meta-generalized gradient approximations based on the understanding of the kinetic-energy-density dependence. *J. Chem. Phys.* **2013**, *138*, 044113.
- (42) Krukau, A. V.; Vydrov, O. A.; Izmaylov, A. F.; Scuseria, G. E. Influence of the exchange screening parameter on the performance of screened hybrid functionals. *J. Chem. Phys.* **2006**, *125*, 224106.
- (43) Pribram-Jones, A.; Gross, D. A.; Burke, K. DFT: A theory full of holes? *Annu. Rev. Phys. Chem.* **2015**, *66*, 283–304.
- (44) Dion, M.; Rydberg, H.; Schröder, E.; Langreth, D. C.; Lundqvist, B. I. Van der Waals Density Functional for General Geometries. *Phys. Rev. Lett.* **2004**, *92*, 246401.
- (45) Lee, K.; Murray, É. D.; Kong, L.; Lundqvist, B. I.; Langreth, D. C. Higher-accuracy van der Waals density functional. *Phys. Rev. B* **2010**, *82*, 081101.
- (46) Zhang, Y.; Yang, W. Comment on “Generalized Gradient Approximation Made Simple”. *Phys. Rev. Lett.* **1998**, *80*, 890–890.
- (47) Klimeš, J.; Bowler, D. R.; Michaelides, A. Van der Waals density functionals applied to solids. *Phys. Rev. B* **2011**, *83*, 195131.

- (48) Madsen, G. K. H. Functional form of the generalized gradient approximation for exchange: The PBE $\alpha$  functional. *Phys. Rev. B* **2007**, *75*, 195108.
- (49) Klimeš, J.; Bowler, D. R.; Michaelides, A. Chemical accuracy for the van der Waals density functional. *J. Phys. Condens. Matter* **2009**, *22*, 022201.
- (50) Perdew, J. P.; Ruzsinszky, A.; Csonka, G. I.; Constantin, L. A.; Sun, J. Workhorse Semilocal Density Functional for Condensed Matter Physics and Quantum Chemistry. *Phys. Rev. Lett.* **2009**, *103*, 026403.
- (51) Sun, J.; Ruzsinszky, A.; Perdew, J. P. Strongly Constrained and Appropriately Normed Semilocal Density Functional. *Phys. Rev. Lett.* **2015**, *115*, 036402.
- (52) Smeets, E. W. F.; Voss, J.; Kroes, G. J. Specific Reaction Parameter Density Functional Based on the Meta-Generalized Gradient Approximation: Application to H<sub>2</sub>+Cu(111) and H<sub>2</sub>+Ag(111). *J. Phys. Chem. A* **2019**, *123*, 5395–5406.
- (53) Perdew, J. P.; Chevary, J. A.; Vosko, S. H.; Jackson, K. A.; Pederson, M. R.; Singh, D. J.; Fiolhais, C. Atoms, molecules, solids, and surfaces: Applications of the generalized gradient approximation for exchange and correlation. *Phys. Rev. B: Condens. Matter Mater. Phys.* **1992**, *46*, 6671–6687.
- (54) Perdew, J. P.; Ruzsinszky, A.; Csonka, G. I.; Vydrov, O. A.; Scuseria, G. E.; Constantin, L. A.; Zhou, X.; Burke, K. Restoring the density-gradient expansion for exchange in solids and surfaces. *Phys. Rev. Lett.* **2008**, *100*, 136406.
- (55) Schimka, L.; Harl, J.; Stroppa, A.; Grüneis, A.; Marsman, M.; Mitterdorfer, F.; Kresse, G. Accurate surface and adsorption energies from many-body perturbation theory. *Nat. Mater.* **2010**, *9*, 741–744.
- (56) Wijzenbroek, M.; Kroes, G. J. The effect of the exchange-correlation functional on H<sub>2</sub> dissociation on Ru(0001). *J. Chem. Phys.* **2014**, *140*, 084702.
- (57) Ghassemi, E. N.; Wijzenbroek, M.; Somers, M. F.; Kroes, G. J. Chemically accurate simulation of dissociative chemisorption of D<sub>2</sub> on Pt(111). *Chem. Phys. Lett.* **2017**, *683*, 329–335.

- (58) Gerrits, N.; Smeets, E. W. F.; Vuckovic, S.; Powell, A. D.; Doblhoff-Dier, K.; Kroes, G. J. Density functional theory for molecule–metal surface reactions: When does the generalized gradient approximation get it right, and what to do if it does not. *J. Phys. Chem. Lett.* **2020**, *11*, 10552–10560.
- (59) Langreth, D.; Perdew, J. The gradient approximation to the exchange–correlation energy functional: A generalization that works. *Solid State Commun.* **1979**, *31*, 567–571.
- (60) Langreth, D. C.; Perdew, J. P. Theory of nonuniform electronic systems. I. Analysis of the gradient approximation and a generalization that works. *Phys. Rev. B* **1980**, *21*, 5469–5493.
- (61) Furche, F. Molecular tests of the random phase approximation to the exchange–correlation energy functional. *Phys. Rev. B* **2001**, *64*, 195120.
- (62) Harl, J.; Schimka, L.; Kresse, G. Assessing the quality of the random phase approximation for lattice constants and atomization energies of solids. *Phys. Rev. B* **2010**, *81*, 115126.
- (63) Karlicky, F.; Lazar, P.; Dubecky, M.; Otyepka, M. Random phase approximation in surface chemistry: Water splitting on iron. *J. Chem. Theory. Comp.* **2013**, *9*, 3670–3676.
- (64) Olsen, T.; Patrick, C. E.; Bates, J. E.; Ruzsinszky, A.; Thygesen, K. S. Beyond the RPA and GW methods with adiabatic xc-kernels for accurate ground state and quasiparticle energies. *Npj Comput. mater* **2019**, *5*, 1–23.
- (65) Zhao, Y.; González-García, N.; Truhlar, D. G. Benchmark database of barrier heights for heavy atom transfer, nucleophilic substitution, association, and unimolecular reactions and its use to test theoretical methods. *J. Phys. Chem. A* **2005**, *109*, 2012–2018.
- (66) Lynch, B. J.; Fast, P. L.; Harris, M.; Truhlar, D. G. Adiabatic connection for kinetics. *J. Phys. Chem. A* **2000**, *104*, 4811–4815.
- (67) Zhao, Y.; Lynch, B. J.; Truhlar, D. G. Multi-coefficient extrapolated density functional theory for thermochemistry and thermochemical kinetics. *Phys. Chem. Chem. Phys.* **2005**, *7*, 43–52.
- (68) Shen, X.; Zhang, Z.; Zhang, D. H. Eight-dimensional quantum dynamics study of CH<sub>4</sub> and CD<sub>4</sub> dissociation on Ni(100) surface. *J. Phys. Chem. C* **2016**, *120*, 20199–20205.
- (69) Farjamnia, A.; Jackson, B. The dissociative chemisorption of CO<sub>2</sub> on Ni (100): A quantum dynamics study. *J. Chem. Phys.* **2017**, *146*, 074704.

- (70) Hoggan, P. E.; Bouferguène, A. Quantum Monte Carlo for activated reactions at solid surfaces: Time well spent on stretched bonds. *Int. J. Quantum Chem.* **2014**, *114*, 1150–1156.
- (71) Pozzo, M.; Alfè, D. Hydrogen dissociation on Mg (0001) studied via quantum Monte Carlo calculations. *Phys. Rev. B* **2008**, *78*, 245313.
- (72) Doblhoff-Dier, K.; Meyer, J.; Hoggan, P. E.; Kroes, G. J. Quantum Monte Carlo calculations on a benchmark molecule–metal surface reaction: H<sub>2</sub>+ Cu (111). *J. Chem. Theory Comput.* **2017**, *13*, 3208–3219.
- (73) Powell, A. D.; Kroes, G. J.; Doblhoff-Dier, K. Quantum Monte Carlo calculations on dissociative chemisorption of H<sub>2</sub>+ Al (110): minimum barrier heights and their comparison to DFT values. *J. Chem. Phys.* **2020**, *153*, 224701.
- (74) Zhou, X.; Wang, F. Barrier heights of hydrogen-transfer reactions with diffusion quantum monte carlo method. *J. Comput. Chem.* **2017**, *38*, 798–806.
- (75) Krongchon, K.; Busemeyer, B.; Wagner, L. K. Accurate barrier heights using diffusion Monte Carlo. *J. Chem. Phys.* **2017**, *146*, 124129.
- (76) Yin, R.; Zhang, Y.; Libisch, F.; Carter, E. A.; Guo, H.; Jiang, B. Dissociative chemisorption of O<sub>2</sub> on Al (111): dynamics on a correlated wave-function-based potential energy surface. *J. Phys. Chem. Lett.* **2018**, *9*, 3271–3277.
- (77) Zhao, Q.; Zhang, X.; Martirez, J. M. P.; Carter, E. A. Benchmarking an embedded adaptive sampling configuration interaction method for surface reactions: H<sub>2</sub> desorption from and CH<sub>4</sub> dissociation on Cu (111). *J. Chem. Theory. Comput.* **2020**, *16*, 7078–7088.
- (78) Rettner, C.; Michelsen, H.; Auerbach, D. Quantum-state-specific dynamics of the dissociative adsorption and associative desorption of H<sub>2</sub> at a Cu(111) surface. *J. Chem. Phys.* **1995**, *102*, 4625–4641.
- (79) Dahl, S.; Logadottir, A.; Egeberg, R. C.; Larsen, J. H.; Chorkendorff, I.; Törnqvist, E.; Nørskov, J. K. Role of steps in N<sub>2</sub> activation on Ru(0001). *Phys. Rev. Lett.* **1999**, *83*, 1814–1817.
- (80) Zambelli, T.; Wintterlin, J.; Trost, J.; Ertl, G. Identification of the " active sites" of a surface-catalyzed reaction. *Science* **1996**, *273*, 1688–1690.
- (81) Klippenstein, S. J.; Pande, V. S.; Truhlar, D. G. Chemical kinetics and mechanisms of complex systems: a perspective on recent theoretical advances. *J. Am. Chem. Soc.* **2014**, *136*, 528–546.

- (82) Karikorpi, M.; Holloway, S.; Henriksen, N.; Nørskov, J. K. Dynamics of molecule-surface interactions. *Surf. Sci.* **1987**, *179*, L41–L48.
- (83) Migliorini, D.; Chadwick, H.; Kroes, G. J. Methane on a stepped surface: Dynamical insights on the dissociation of CHD<sub>3</sub> on Pt(111) and Pt(211). *J. Chem. Phys.* **2018**, *149*, 094701.
- (84) Ghassemi, E. N.; Smeets, E. W. F.; Somers, M. F.; Kroes, G. J.; Groot, I. M.; Juurlink, L. B.; Füchsel, G. Transferability of the specific reaction parameter density functional for H<sub>2</sub> + Pt(111) to H<sub>2</sub> + Pt(211). *J. Phys. Chem. C* **2019**, *123*, 2973–2986.
- (85) Smeets, E. W. F.; Kroes, G. J. Performance of Made Simple Meta-GGA Functionals with rVV10 Nonlocal Correlation for H<sub>2</sub>+ Cu(111), D<sub>2</sub>+Ag(111), H<sub>2</sub>+Au(111), and D<sub>2</sub>+Pt(111). *J. Phys. Chem. C* **2021**, *125*, 8993–9010.
- (86) Sementa, L.; Wijzenbroek, M.; Van Kolck, B. J.; Somers, M. F.; Al-Halabi, A.; Busnengo, H. F.; Olsen, R. A.; Kroes, G. J.; Rutkowski, M.; Thewes, C., et al. Reactive scattering of H<sub>2</sub> from Cu(100): comparison of dynamics calculations based on the specific reaction parameter approach to density functional theory with experiment. *J. Chem. Phys.* **2013**, *138*, 044708.
- (87) Zhu, L.; Zhang, Y.; Zhang, L.; Zhou, X.; Jiang, B. Unified and transferable description of dynamics of H<sub>2</sub> dissociative adsorption on multiple copper surfaces via machine learning. *Phys. Chem. Chem. Phys.* **2020**, *22*, 13958–13964.
- (88) **Tchakoua, T**; Smeets, E. W.; Somers, M.; Kroes, G. J. Toward a Specific Reaction Parameter Density Functional for H<sub>2</sub>+ Ni(111): Comparison of Theory with Molecular Beam Sticking Experiments. *J. Phys. Chem. C* **2019**, *123*, 20420–20433.
- (89) Shakouri, K.; Behler, J.; Meyer, J.; Kroes, G. J. Accurate neural network description of surface phonons in reactive gas-surface dynamics: N<sub>2</sub>+ Ru(0001). *J. Phys. Chem. Lett.* **2017**, *8*, 2131–2136.
- (90) Dahl, S.; Törnqvist, E.; Chorkendorff, I. Dissociative adsorption of N<sub>2</sub> on Ru(0001): a surface reaction totally dominated by steps. *J. Catal.* **2000**, *192*, 381–390.
- (91) Luntz, A. CH<sub>4</sub> dissociation on Ni(100): Comparison of a direct dynamical model to molecular beam experiments. *J. Chem. Phys.* **1995**, *102*, 8264–8269.



- (92) Guo, H.; Menzel, J. P.; Jackson, B. Quantum dynamics studies of the dissociative chemisorption of CH<sub>4</sub> on the steps and terraces of Ni(211). *J. Chem. Phys.* **2018**, *149*, 244704.
- (93) Jackson, B. Direct and trapping-mediated pathways to dissociative chemisorption: CH<sub>4</sub> dissociation on Ir (111) with step defects. *J. Chem. Phys.* **2020**, *153*, 034704.
- (94) Mortensen, H.; Diekhöner, L.; Baurichter, A.; Luntz, A. C. CH<sub>4</sub> dissociation on Ru(0001): A view from both sides of the barrier. *J. Chem. Phys.* **2002**, *116*, 5781–5794.
- (95) Nattino, F.; Genova, A.; Guijt, M.; Muzas, A. S.; Díaz, C.; Auerbach, D. J.; Kroes, G. J. Dissociation and recombination of D<sub>2</sub> on Cu(111): Ab initio molecular dynamics calculations and improved analysis of desorption experiments. *J. Chem. Phys.* **2014**, *141*, 124705.
- (96) Smeets, E. W. F.; Füchsel, G.; Kroes, G. J. Quantum dynamics of dissociative chemisorption of H<sub>2</sub> on the Stepped Cu(211) Surface. *J. Phys. Chem. C* **2019**, *123*, 23049–23063.
- (97) Chadwick, H.; Somers, M. F.; Stewart, A. C.; Alkoby, Y.; Carter, T. J. D.; Butkovicova, D.; Alexandrowicz, G. Stopping molecular rotation using coherent ultra-low-energy magnetic manipulations. *Nat. Commun.* **2022**, *13*.
- (98) Anger, G.; Winkler, A.; Rendulic, K. Adsorption and desorption kinetics in the systems H<sub>2</sub>/Cu(111), H<sub>2</sub>/Cu(110) and H<sub>2</sub>/Cu(100). *Surf. Sci.* **1989**, *220*, 1–17.
- (99) Berger, H.; Leisch, M.; Winkler, A.; Rendulic, K. A search for vibrational contributions to the activated adsorption of H<sub>2</sub> on copper. *Chem. Phys. Lett.* **1990**, *175*, 425–428.
- (100) Michelsen, H.; Rettner, C.; Auerbach, D.; Zare, R. Effect of rotation on the translational and vibrational energy dependence of the dissociative adsorption of D<sub>2</sub> on Cu(111). *J. Chem. Phys.* **1993**, *98*, 8294–8307.
- (101) Kaufmann, S.; Shuai, Q.; Auerbach, D. J.; Schwarzer, D.; Wodtke, A. M. Associative desorption of hydrogen isotopologues from copper surfaces: characterization of two reaction mechanisms. *J. Chem. Phys.* **2018**, *148*, 194703.
- (102) Kroes, G. J.; Díaz, C. Quantum and classical dynamics of reactive scattering of H<sub>2</sub> from metal surfaces. *Chem. Soc. Rev.* **2016**, *45*, 3658–3700.

- (103) Hodgson, A.; Samson, P.; Wight, A.; Cottrell, C. Rotational excitation and vibrational relaxation of H<sub>2</sub> ( $\nu=1$ ,  $J=0$ ) Scattered from Cu(111). *Phys. Rev. Lett.* **1997**, *78*, 963–966.
- (104) Nattino, F.; Díaz, C.; Jackson, B.; Kroes, G. J. Effect of surface motion on the rotational quadrupole alignment parameter of D<sub>2</sub> reacting on Cu(111). *Phys. Rev. Lett.* **2012**, *108*, 236104.
- (105) Hou, H.; Guldin, S.; Rettner, C.; Wodtke, A.; Auerbach, D. The stereodynamics of a gas-surface reaction. *Science* **1997**, *277*, 80–82.
- (106) Smeets, E. W.; Kroes, G. J. Designing new SRP density functionals including non-local vdW-DF2 correlation for H<sub>2</sub>+Cu(111) and their transferability to H<sub>2</sub>+Ag(111), Au(111) and Pt(111). *Phys. Chem. Chem. Phys.* **2021**, *23*, 7875–7901.
- (107) Berger, H. F.; Rendulic, K. D. An investigation of vibrationally assisted adsorption: the cases H<sub>2</sub>/Cu(110) and H<sub>2</sub>/Al(110). *Surf. Sci.* **1991**, *253*, 325–333.
- (108) Wijzenbroek, M.; Klein, D. M.; Smits, B.; Somers, M. F.; Kroes, G. J. Performance of a non-local van der Waals density functional on the dissociation of H<sub>2</sub> on metal surfaces. *J. Phys. Chem. A* **2015**, *119*, 12146–12158.
- (109) Michelsen, H. A.; Rettner, C. T.; Auerbach, D. J. State-specific dynamics of D<sub>2</sub> desorption from Cu(111): the role of molecular rotational motion in activated adsorption-desorption dynamics. *Phys. Rev. Lett.* **1992**, *69*, 2678–2681.
- (110) Luntz, A. C.; Brown, J. K.; Williams, M. D. Molecular beam studies of H<sub>2</sub> and D<sub>2</sub> dissociative chemisorption on Pt(111). *J. Chem. Phys.* **1990**, *93*, 5240–5246.
- (111) Hamada, I. van der Waals density functional made accurate. *Phys. Rev. B* **2014**, *89*, 121103.
- (112) Gerrits, N. Accurate Simulations of the Reaction of H<sub>2</sub> on a Curved Pt Crystal through Machine Learning. *J. Phys. Chem. Lett.* **2021**, *12*, 12157–12164.
- (113) Groot, I. M. N.; Kleyn, A. W.; Juurlink, L. B. F. The energy dependence of the ratio of step and terrace reactivity for H<sub>2</sub> dissociation on stepped platinum. *Angew. Chem., Int. Ed.* **2011**, *50*, 5174–5177.
- (114) Groot, I. M. N.; Ueta, H.; Van der Niet, M. J. T. C.; Kleyn, A. W.; Juurlink, L. B. F. Supersonic molecular beam studies of dissociative adsorption of H<sub>2</sub> on Ru(0001). *J. Chem. Phys.* **2007**, *127*, 244701.

- (115) Resch, C.; Zhukov, V.; Lugstein, A.; Berger, H.; Winkler, A.; Rendulic, K. Dynamics of hydrogen adsorption on promoter- and inhibitor-modified nickel surfaces. *Chem. Phys.* **1993**, *177*, 421–431.
- (116) Rendulic, K.; Anger, G.; Winkler, A. Wide range nozzle beam adsorption data for the systems H<sub>2</sub>/nickel and H<sub>2</sub>/Pd(100). *Surf. Sci.* **1989**, *208*, 404–424.
- (117) Thonhauser, T.; Zuluaga, S.; Arter, C. A.; Berland, K.; Schröder, E.; Hyldgaard, P. Spin Signature of Nonlocal Correlation Binding in Metal-Organic Frameworks. *Phys. Rev. Lett.* **2015**, *115*, 136402.
- (118) Cottrell, C.; Carter, R. N.; Nesbitt, A.; Samson, P.; Hodgson, A. Vibrational state dependence of D<sub>2</sub> dissociation on Ag(111). *J. Chem. Phys.* **1997**, *106*, 4714–4722.
- (119) Murphy, M.; Hodgson, A. Role of surface thermal motion in the dissociative chemisorption and recombinative desorption of D<sub>2</sub> on Ag(111). *Phys. Rev. Lett.* **1997**, *78*, 4458–4461.
- (120) Sabatini, R.; Gorni, T.; De Gironcoli, S. Nonlocal van der Waals density functional made simple and efficient. *Phys. Rev. B* **2013**, *87*, 041108.
- (121) Smil, V. Detonator of the population explosion. *Nature* **1999**, *400*, 415–415.
- (122) Spiering, P.; Shakouri, K.; Behler, J.; Kroes, G. J.; Meyer, J. Orbital-dependent electronic friction significantly affects the description of reactive scattering of N<sub>2</sub> from Ru(0001). *J. Phys. Chem. Lett.* **2019**, *10*, 2957–2962.
- (123) Diekhöner, L.; Mortensen, H.; Baurichter, A.; Luntz, A. Laser assisted associative desorption of N<sub>2</sub> and CO from Ru(0001). *J. Chem. Phys.* **2001**, *115*, 3356–3373.
- (124) Diekhöner, L.; Mortensen, H.; Baurichter, A.; Jensen, E.; Petrunin, V. V.; Luntz, A. C. N<sub>2</sub> dissociative adsorption on Ru(0001): The role of energy loss. *J. Chem. Phys.* **2001**, *115*, 9028–9035.
- (125) **Tchakoua, T.**; Gerrits, N.; Smeets, E. W. F.; Kroes, G. J. SBH17: Benchmark Database of Barrier Heights for Dissociative Chemisorption on Transition Metal Surfaces. *J. Chem. Theory Comput.* **2023**, *19*, 245–270.
- (126) Guo, H.; Jackson, B. Methane dissociation on stepped Ni surfaces resolved by impact site, collision energy, vibrational state, and lattice distortion. *J. Chem. Phys.* **2019**, *150*, 204703.

- (127) Holmblad, P. M.; Wambach, J.; Chorkendorff, I. Molecular beam study of dissociative sticking of methane on Ni(100). *J. Chem. Phys.* **1995**, *102*, 8255–8263.
- (128) Seets, D. C.; Reeves, C. T.; Ferguson, B. A.; Wheeler, M. C.; Mullins, C. B. Dissociative chemisorption of methane on Ir(111): Evidence for direct and trapping-mediated mechanisms. *J. Chem. Phys.* **1997**, *107*, 10229–10241.
- (129) Larsen, J. H.; Holmblad, P. M.; Chorkendorff, I. Dissociative sticking of CH<sub>4</sub> on Ru(0001). *J. Chem. Phys.* **1999**, *110*, 2637–2642.
- (130) Moiraghi, R.; Lozano, A.; Peterson, E.; Utz, A.; Dong, W.; Busnengo, H. F. Nonthermalized precursor-mediated dissociative chemisorption at high catalysis temperatures. *J. Phys. Chem. Lett.* **2020**, *11*, 2211–2218.
- (131) Juurlink, L. B. F.; McCabe, P. R.; Smith, R. R.; DiCologero, C. L.; Utz, A. L. Eigenstate-resolved studies of gas-surface reactivity: CH<sub>4</sub> ( $\nu$  3) dissociation on Ni(100). *Phys. Rev. Lett.* **1999**, *83*, 868–871.
- (132) Beck, R. D.; Maroni, P.; Papageorgopoulos, D. C.; Dang, T. T.; Schmid, M. P.; Rizzo, T. R. Vibrational mode-specific reaction of methane on a nickel surface. *Science* **2003**, *302*, 98–100.
- (133) Smith, R. R.; Killelea, D. R.; DelSesto, D. F.; Utz, A. L. Preference for vibrational over translational energy in a gas-surface reaction. *Science* **2004**, *304*, 992–995.
- (134) Killelea, D. R.; Campbell, V. L.; Shuman, N. S.; Utz, A. L. Bond-selective control of a heterogeneously catalyzed reaction. *Science* **2008**, *319*, 790–793.
- (135) Yoder, B. L.; Bisson, R.; Beck, R. D. Steric effects in the chemisorption of vibrationally excited methane on Ni(100). *Science* **2010**, *329*, 553–556.
- (136) Dombrowski, E.; Peterson, E.; Del Sesto, D.; Utz, A. L. Precursor-mediated reactivity of vibrationally hot molecules: Methane activation on Ir(111). *Catal. Today* **2015**, *244*, 10–18.
- (137) Mastromatteo, M.; Jackson, B. The dissociative chemisorption of methane on Ni(100) and Ni(111): Classical and quantum studies based on the reaction path Hamiltonian. *J. Chem. Phys.* **2013**, *139*, 194701.
- (138) Nave, S.; Jackson, B. Vibrational mode-selective chemistry: methane dissociation on Ni(100). *Phys. Rev. B* **2010**, *81*, 233408.
- (139) Jackson, B.; Nave, S. The dissociative chemisorption of methane on Ni(100): Reaction path description of mode-selective chemistry. *J. Chemical Phys.* **2011**, *135*, 114701.

- (140) Nave, S.; Tiwari, A. K.; Jackson, B. Dissociative chemisorption of methane on Ni and Pt surfaces: mode-specific chemistry and the effects of lattice motion. *J. Phys. Chem. A* **2014**, *118*, 9615–9631.
- (141) Jackson, B.; Nattino, F.; Kroes, G. J. Dissociative chemisorption of methane on metal surfaces: tests of dynamical assumptions using quantum models and ab initio molecular dynamics. *J. Chem. Phys.* **2014**, *141*, 054102.
- (142) Abild-Pedersen, F.; Lytken, O.; Engbæk, J.; Nielsen, G.; Chorkendorff, I.; Nørskov, J. K. Methane activation on Ni(111): Effects of poisons and step defects. *Surf. Sci* **2005**, *590*, 127–137.
- (143) Migliorini, D.; Chadwick, H.; Nattino, F.; Gutiérrez-González, A.; Dombrowski, E.; High, E. A.; Guo, H.; Utz, A. L.; Jackson, B.; Beck, R. D., et al. Correction to “Surface Reaction Barriometry: Methane Dissociation on Flat and Stepped Transition-Metal Surfaces”. *J. Phys. Chem. Lett.* **2019**, *10*, 661–662.
- (144) Ciobica, I.; Frechard, F.; Van Santen, R.; Kleyn, A.; Hafner, J. A DFT study of transition states for C-H activation on the Ru(0001) surface. *J. Phys. Chem. B* **2000**, *104*, 3364–3369.
- (145) Patra, A.; Bates, J. E.; Sun, J.; Perdew, J. P. Properties of real metallic surfaces: Effects of density functional semilocality and van der Waals nonlocality. *Proc. Natl. Acad. Sci.* **2017**, *114*, E9188–E9196.
- (146) Mondal, A.; Wijzenbroek, M.; Bonfanti, M.; Díaz, C.; Kroes, G. J. Thermal lattice expansion effect on reactive scattering of H<sub>2</sub> from Cu(111) at T<sub>s</sub> = 925 K. *J. Phys. Chem. A* **2013**, *117*, 8770–8781.
- (147) Marashdeh, A.; Casolo, S.; Sementa, L.; Zacharias, H.; Kroes, G. J. Surface temperature effects on dissociative chemisorption of H<sub>2</sub> on Cu(100). *J. Phys. Chem. C* **2013**, *117*, 8851–8863.
- (148) Sakong, S.; Groß, A. Dissociative adsorption of hydrogen on strained Cu surfaces. *Surf. Sci.* **2003**, *525*, 107–118.
- (149) Henkelman, G.; Jónsson, H. A dimer method for finding saddle points on high dimensional potential surfaces using only first derivatives. *J. Chem. Phys.* **1999**, *111*, 7010–7022.
- (150) Heyden, A.; Bell, A. T.; Keil, F. J. Efficient methods for finding transition states in chemical reactions: Comparison of improved dimer method and partitioned rational function optimization method. *J. Chem. Phys.* **2005**, *123*, 224101.

- (151) Kästner, J.; Sherwood, P. Superlinearly converging dimer method for transition state search. *J. Chem. Phys.* **2008**, *128*, 014106.
- (152) Xiao, P.; Sheppard, D.; Rogal, J.; Henkelman, G. Solid-state dimer method for calculating solid-solid phase transitions. *J. Chem. Phys.* **2014**, *140*, 174104.
- (153) Kresse, G.; Hafner, J. Ab initio molecular dynamics for liquid metals. *Phys. Rev. B* **1993**, *47*, 558–561.
- (154) Kresse, G.; Hafner, J. Ab initio molecular-dynamics simulation of the liquid-metal–amorphous-semiconductor transition in germanium. *Phys. Rev. B* **1994**, *49*, 14251–14269.
- (155) Kresse, G.; Furthmüller, J. Efficiency of ab-initio total energy calculations for metals and semiconductors using a plane-wave basis set. *Comput. Mater. Sci.* **1996**, *6*, 15–50.
- (156) Kresse, G.; Furthmüller, J. Efficient iterative schemes for ab initio total-energy calculations using a plane-wave basis set. *Phys. Rev. B* **1996**, *54*, 11169.
- (157) <http://github.com/vossjo/libbeef>.
- (158) Perdew, J. P.; Wang, Y. Accurate and simple analytic representation of the electron-gas correlation energy. *Phys. Rev. B* **1992**, *45*, 13244.
- (159) Román-Pérez, G.; Soler, J. M. Efficient implementation of a van der Waals density functional: application to double-wall carbon nanotubes. *Phys. Rev. Lett.* **2009**, *103*, 096102.
- (160) Bahn, S. R.; Jacobsen, K. W. An object-oriented scripting interface to a legacy electronic structure code. *Comput. Sci. Eng.* **2002**, *4*, 56–66.
- (161) Larsen, A. H.; Mortensen, J. J.; Blomqvist, J.; Castelli, I. E.; Christensen, R.; Dułak, M.; Friis, J.; Groves, M. N.; Hammer, B.; Hargus, C., et al. The atomic simulation environment—a Python library for working with atoms. *J. Phys.: Condens. Matter* **2017**, *29*, 273002.
- (162) Haas, P.; Tran, F.; Blaha, P. Calculation of the lattice constant of solids with semilocal functionals. *Phys. Rev. B* **2009**, *79*, 085104.
- (163) Arblaster, J. W. Crystallographic properties of ruthenium. *Platinum Met. Rev.* **2013**, *57*, 127–136.
- (164) Qi, Q.; Wang, X.; Chen, L.; Li, B. Methane dissociation on Pt(111), Ir(111) and PtIr(111) surface: A density functional theory study. *Appl. Surf. Sci.* **2013**, *284*, 784–791.

- (165) Moiraghi, R.; Lozano, A.; Busnengo, H. F. Theoretical study of the dissociative adsorption of methane on Ir(111): The role of steps and surface distortions at high temperatures. *J. Phys. Chem. C* **2016**, *120*, 3946–3954.
- (166) Zhou, X.; Jiang, B.; Guo, H. Corrections to “Dissociative Chemisorption of Methane on Stepped Ir(332) Surface: Density Functional Theory and Ab Initio Molecular Dynamics Studies”. *J. Phys. Chem. C* **2019**, *123*, 31298–31298.
- (167) Smeets, E. W. F.; Kroes, G. J. Designing new SRP density functionals including non-local vdW-DF2 correlation for H<sub>2</sub>+Cu(111) and their transferability to H<sub>2</sub>+Ag(111), Au(111) and Pt(111). *Phys. Chem. Chem. Phys.* **2021**, *23*, 7875–7901.
- (168) Statiris, P.; Lu, H.; Gustafsson, T. Temperature dependent sign reversal of the surface contraction of Ag(111). *Phys. Rev. Lett.* **1994**, *72*, 3574–3577.
- (169) Okazawa, T.; Takeuchi, F.; Kido, Y. Enhanced and correlated thermal vibrations of Cu(111) and Ni(111) surfaces. *Phys. Rev. B* **2005**, *72*, 075408.
- (170) Adams, D. L.; Nielsen, H. B.; Van Hove, M. A. Quantitative analysis of low-energy-electron diffraction: Application to Pt(111). *Phys. Rev. B* **1979**, *20*, 4789–4806.
- (171) Soares, E. A.; Leatherman, G. S.; Diehl, R. D.; Van Hove, M. A. Low-energy electron diffraction study of the thermal expansion of Ag(111). *Surf. Sci.* **2000**, *468*, 129–136.
- (172) Lindgren, S.; Walldén, L.; Rundgren, J.; Westrin, P. Low-energy electron diffraction from Cu(111): Subthreshold effect and energy-dependent inner potential; surface relaxation and metric distances between spectra. *Phys. Rev. B* **1984**, *29*, 576.
- (173) Singh-Miller, N. E.; Marzari, N. Surface energies, work functions, and surface relaxations of low-index metallic surfaces from first principles. *Phys. Rev. B* **2009**, *80*, 235407.
- (174) Wijzenbroek, M. Hydrogen dissociation on metal surfaces, Ph.D. Thesis, Leiden Institute of Chemistry, 2016.
- (175) Tran, F.; Stelzl, J.; Blaha, P. Rungs 1 to 4 of DFT Jacob’s ladder: Extensive test on the lattice constant, bulk modulus, and cohesive energy of solids. *J. Chem. Phys.* **2016**, *144*, 204120.

- (176) Zhang, G.-X.; Reilly, A. M.; Tkatchenko, A.; Scheffler, M. Performance of various density-functional approximations for cohesive properties of 64 bulk solids. *New J. Phys.* **2018**, *20*, 063020.
- (177) Sun, J.; Marsman, M.; Ruzsinszky, A.; Kresse, G.; Perdew, J. P. Improved lattice constants, surface energies, and CO desorption energies from a semilocal density functional. *Physical Review B* **2011**, *83*, 121410.
- (178) Yang, K.; Zheng, J.; Zhao, Y.; Truhlar, D. G. Tests of the rpbe, revpbe,  $\tau$ -hcthyb,  $\omega$  b 97 xd, and mohlyp density functional approximations and 29 others against representative databases for diverse bond energies and barrier heights in catalysis. *J. Chem. Phys.* **2010**, *132*, 164117.
- (179) Zhang, Y.; Yang, W. A challenge for density functionals: Self-interaction error increases for systems with a noninteger number of electrons. *J. Chem. Phys.* **1998**, *109*, 2604–2608.
- (180) Cohen, A. J.; Mori-Sánchez, P.; Yang, W. Insights into current limitations of density functional theory. *Science* **2008**, *321*, 792–794.
- (181) Li, C.; Zheng, X.; Su, N. Q.; Yang, W. Localized orbital scaling correction for systematic elimination of delocalization error in density functional approximations. *Natl. Sci. Rev.* **2018**, *5*, 203–215.
- (182) Patra, A.; Peng, H.; Sun, J.; Perdew, J. P. Rethinking CO adsorption on transition-metal surfaces: Effect of density-driven self-interaction errors. *Phys. Rev. B* **2019**, *100*, 035442.
- (183) Garza, A. J.; Bell, A. T.; Head-Gordon, M. Nonempirical meta-generalized gradient approximations for modeling chemisorption at metal surfaces. *J. Chem. Theory Comput.* **2018**, *14*, 3083–3090.
- (184) Yu, H.; He, X.; Li, S.; Truhlar, D. G. MN15: A Kohn–Sham global-hybrid exchange–correlation density functional with broad accuracy for multi-reference and single-reference systems and noncovalent interactions. *Chem. Sci.* **2016**, *7*, 5032–5051.
- (185) Furness, J. W.; Sun, J. Enhancing the efficiency of density functionals with an improved iso-orbital indicator. *Phys. Rev. B* **2019**, *99*, 041119.
- (186) Rettner, C. T.; Stein, H. Effect of vibrational energy on the dissociative chemisorption of N<sub>2</sub> on Fe(111). *J. Chem. Phys.* **1987**, *87*, 770–771.
- (187) Rettner, C. T.; Stein, H. Effect of translational energy on the chemisorption of N<sub>2</sub> on Fe(111): Activated dissociation via a precursor state. *Phys. Rev. Lett.* **1987**, *59*, 2768–2771.



- (188) Pfnür, H. E.; Rettner, C. T.; Lee, J.; Madix, R. J.; Auerbach, D. J. Dynamics of the activated dissociative chemisorption of N<sub>2</sub> on W(110): A molecular beam study. *J. Chem. Phys.* **1986**, *85*, 7452–7466.
- (189) Rettner, C. T.; Schweizer, E. K.; Stein, H. Dynamics of the chemisorption of N<sub>2</sub> on W(100): Precursor-mediated and activated dissociation. *J. Chem. Phys.* **1990**, *93*, 1442–1454.
- (190) Rettner, C. T.; Schweizer, E. K.; Stein, H.; Auerbach, D. J. Role of surface temperature in the precursor-mediated dissociative chemisorption of N<sub>2</sub> on W(100). *Phys. Rev. Lett.* **1988**, *61*, 986–989.
- (191) Rettner, C. T.; Stein, H.; Schweizer, E. K. Effect of collision energy and incidence angle on the precursor-mediated dissociative chemisorption of N<sub>2</sub> on W(100). *J. Chem. Phys.* **1988**, *89*, 3337–3341.
- (192) Beutl, M.; Rendulic, K. D.; Castro, G. R. Does the rotational state of a molecule influence trapping in a precursor? An investigation of N<sub>2</sub>/W(100), CO/FeSi(100) and O<sub>2</sub>/Ni(111). *Surf. Sci.* **1997**, *385*, 97–106.
- (193) Hundt, P. M.; Jiang, B.; van Reijzen, M. E.; Guo, H.; Beck, R. D. Vibrationally promoted dissociation of water on Ni(111). *Science* **2014**, *344*, 504–507.
- (194) Gerrits, N.; Geweke, J.; Smeets, E. W. F.; Voss, J.; Wodtke, A. M.; Kroes, G. J. Closing the Gap Between Experiment and Theory: Reactive Scattering of HCl from Au(111). *J. Phys. Chem. C* **2020**, *124*, 15944–15960.
- (195) Österlund, L.; Zoric-Acute, I.; Kasemo, B. Dissociative sticking of O<sub>2</sub> on Al(111). *Phys. Rev. B* **1997**, *55*, 15452–15455.
- (196) Kurahashi, M.; Yamauchi, Y. Steric effect in O<sub>2</sub> sticking on Al(111): Preference for parallel geometry. *Phys. Rev. Lett.* **2013**, *110*, 246102.
- (197) Raukema, A.; Butler, D. A.; Kleyn, A. W. The interaction of oxygen with the Ag(110) surface. *J. Phys.: Condens. Matter* **1996**, *8*, 2247–2263.
- (198) Kurahashi, M. Chemisorption of aligned O<sub>2</sub> on Ag(110). *J. Chem. Phys.* **2019**, *151*, 084702.
- (199) Hall, J.; Saksager, O.; Chorkendorff, I. Dissociative chemisorption of O<sub>2</sub> on Cu(100). Effects of mechanical energy transfer and recoil. *Chem. Phys. Lett.* **1993**, *216*, 413–417.
- (200) Minniti, M.; Farías, D.; Perna, P.; Miranda, R. Enhanced selectivity towards O<sub>2</sub> and H<sub>2</sub> dissociation on ultrathin Cu films on Ru(0001). *J. Chem. Phys.* **2012**, *137*, 074706.

- (201) Kirkpatrick, J.; McMorrow, B.; Turban, D. H.; Gaunt, A. L.; Spencer, J. S.; Matthews, A. G. D. G.; Obika, A.; Thiry, L.; Fortunato, M.; Pfau, D., et al. Pushing the frontiers of density functionals by solving the fractional electron problem. *Science* **2021**, *374*, 1385–1389.
- (202) Shukla, V.; Jiao, Y.; Frostenson, C. M.; Hyldgaard, P. vdW-DF-ahcx: a range-separated van der Waals density functional hybrid. *J. Phys.: Condens. Matter* **2021**, *34*, 025902.
- (203) Shukla, V.; Jiao, Y.; Lee, J.-H.; Schröder, E.; Neaton, J. B.; Hyldgaard, P. Accurate Nonempirical Range-Separated Hybrid van der Waals Density Functional for Complex Molecular Problems, Solids, and Surfaces. *Phys. Rev. X* **2022**, *12*, 041003.

# 4

## Simulating Highly Activated Sticking of H<sub>2</sub> on Al(110): Quantum versus quasi-classical dynamics

This Chapter is based on:

**Tchakoua, T.;** Powell, A. D.; Gerrits, N.; Somers, M. F.; Doblhoff-Dier, K.; Busnengo, H. F.; Kroes, G. J. Simulating highly activated sticking of H<sub>2</sub> on Al(110): Quantum versus quasi-classical dynamics. *J. Phys. Chem. C* **2023**, *127*, 1932–7447

4

Chapter

### Abstract

We evaluate the importance of quantum effects on the sticking of H<sub>2</sub> on Al(110), for conditions that are close to those of molecular beam experiments that have been done on this system. Calculations with the quasi-classical trajectory (QCT) method and with quantum dynamics (QD) are performed using a model in which only motion in the six molecular degrees of freedom is allowed. The potential energy surface used has a minimum barrier height close to the value recently obtained with quantum Monte-Carlo. Monte-Carlo averaging over the initial rovibrational states allowed the QD calculations to be done with an order of magnitude smaller computational expense. The sticking probability curve computed with QD is shifted to lower energies relative to the QCT curve by 0.21 to 0.05 kcal/mol, with the highest shift obtained for the lowest incidence energy. Quantum effects are therefore expected to play a small role in calculations that would evaluate the accuracy of electronic structure methods for determining the minimum barrier height to dissociative chemisorption for H<sub>2</sub> + Al(110) on the basis of the standard procedure for comparing results of theory with molecular beam experiments.

## 4.1 Introduction

The dissociative chemisorption (DC) of molecules on metal surfaces is of high practical interest, as the transition state (TS) of the DC reaction is often a rate-limiting state in overall heterogeneously catalyzed processes<sup>1,2</sup> (such as ammonia production<sup>3</sup> and steam reforming<sup>4</sup>), and most chemicals are made through heterogeneous catalysis<sup>5</sup>. It is therefore important to be able to compute accurate barriers for DC on metals with electronic structure methods, and to test the ability of density functional theory (DFT) to compute such barriers accurately. With more than 30,000 papers published annually<sup>6</sup>, DFT is probably the most important electronic structure method applied to complex systems. While DFT has been tested extensively on databases of gas phase reaction barriers<sup>7-10</sup>, tests<sup>11-13</sup> on databases of barrier heights for DC on metals<sup>11,12</sup> are still scarce.

Unfortunately, reaction barrier heights are not observables<sup>14</sup>. The way to validate the capability of electronic structure methods to accurately compute barrier heights is therefore to compute an observable that strongly depends on the barrier height<sup>14</sup>. For DC on metals, this is the sticking probability ( $S_0$ ), which can be measured in a supersonic molecular beam experiment<sup>14,15</sup>, as can be argued on the basis of the hole-model<sup>16</sup>. The validation procedure therefore also requires dynamics calculations to be performed with an appropriate dynamical model and dynamical method<sup>14</sup>. In this procedure, the electronic structure method is used to generate the forces acting on the atoms (either directly in *ab initio* molecular dynamics or density functional molecular dynamics calculations or indirectly from a potential energy surface that was fitted to *ab initio* data)<sup>14</sup>. If such calculations yield a  $S_0$  curve that is in good agreement with a high quality experiment, and if the dynamical model and method used were of high enough accuracy, the minimum barrier height computed with the electronic structure method should be an accurate value of the TS energy, also allowing its use for benchmarking purposes<sup>11,12,14</sup>.

For DC of  $H_2$  on a metal surface, with few exceptions<sup>17</sup> experiments measure  $S_0$ , or effectively the DC probability, as an average over both the velocity distribution of the molecular beam and the rovibrational states populated in the beam at the nozzle temperature ( $T_n$ ) used in the experiments<sup>18-27</sup>. With  $H_2$  being the lightest molecule one might think that the sticking in such experiments should be highly influenced by quantum effects like tunneling, and that this should be especially true if the barrier to DC is high. However, this is not necessarily true. For instance, on the basis of experiments on DC of  $H_2$  on Cu(111) it has been argued that at low incidence energies ( $E_i$ ) the reaction is dominated by vibrationally excited  $H_2$  in its  $\nu=1$  or even its  $\nu=2$  state, where  $\nu$  is

the vibrational quantum number<sup>21</sup>. With averaging over the rovibrational states, the question then becomes: is the sticking dominated by "classical", i.e., over the barrier reaction of H<sub>2</sub> in highly excited vibrational and/or rotational states, or are quantum effects like tunneling highly important because most molecules that react are in low vibrational and rotational states with high Boltzmann populations, and their reaction is dominated by tunneling? In other words, to compute S<sub>0</sub>, does the quasi-classical trajectory (QCT) method<sup>28,29</sup> suffice, or should one use a quantum dynamical (QD) method, like the time-dependent wave packet (TDWP) method<sup>30,31</sup>? So far, existing evidence for H<sub>2</sub> reacting on Cu(111)<sup>32</sup> and Cu(211)<sup>33</sup> suggests that quantum effects are not of large importance for S<sub>0</sub> down to 0.01 or even to 0.001. Evidence concerning DC of H<sub>2</sub> or D<sub>2</sub> in specific single initial rovibrational states in some cases does suggest large differences between quantum and quasi-classical dynamics calculations<sup>34–40</sup>, but as already indicated most experimental results for DC of H<sub>2</sub> on metals represent averages over several rovibrational states. Additionally, in molecular beam experiments the importance of quantum effects may depend on how wide the translational energy distributions of the beams are, as molecules in the high energy tail of a beam might react more readily through a classical mechanism.

Here the question we raised above (how important are quantum effects on the sticking of H<sub>2</sub> on metal surfaces) is addressed for the DC of H<sub>2</sub> on Al(110). There are several reasons for addressing this system. First, this system is representative of H<sub>2</sub>-metal DC reactions with a very high minimum barrier (i.e., > 1 eV)<sup>41</sup>, as also found in e.g. H<sub>2</sub> + Ag(111)<sup>32,42,43</sup> and H<sub>2</sub> + Au(111)<sup>32,43,44</sup>. Second, this reaction has been investigated in experiments<sup>20,45</sup> for which the velocity distributions used can be derived from actual time-of-flight (TOF) distributions and other experimental information that has been published<sup>45</sup>. This information has been used successfully to accurately model experiments on the sticking of H<sub>2</sub> and D<sub>2</sub> on Cu(111)<sup>46,47</sup>, Cu(100)<sup>47,48</sup>, and Cu(110)<sup>47</sup> also investigated with these beams. Finally, the H<sub>2</sub> + Al(110) system is currently being used to investigate the performance of a new first-principles based version of the specific reaction parameter (SRP) approach to DFT (SRP-DFT) in quasi-classical dynamics calculations. For the actual comparison with experiment that we intend to publish shortly (A.D. Powell et al., to be published), it will be important to know the importance of quantum effects, which are the focus of this study. Comparison with experiments is not yet the aim here, as this would also require inclusion of surface atom motion and electron-hole pair (ehp) excitation, which is beyond the scope of the present chapter. In view of the usual way of validating an electronic structure method for barrier heights of DC (i.e., by computing the energy shift between a computed and a measured sticking probability curve<sup>14,46</sup>), the central question we will address is: To what extent may quantum effects be expected

to shift the computed sticking probability curve for  $\text{H}_2 + \text{Al}(110)$  along the incidence energy axis? While we address this question for  $\text{H}_2 + \text{Al}(110)$ , our results may also be relevant to the modeling of existing experiments on DC of  $\text{H}_2$  on  $\text{Ag}(111)$ <sup>24</sup>, or sticking experiments yet to be performed for  $\text{H}_2 + \text{Au}(111)$ .

Our **Chapter** is organized as follows: First, we describe the theoretical methods used in this work in Section 4.2. Section 4.2.1 describes the dynamical model and Section 4.2.2 the DFT method used to generate the electronic structure data describing the molecule-surface interaction. The corrugation reducing procedure<sup>49</sup> used to interpolate the DFT data to generate a global PES is described in Section 4.2.3. Section 4.2.4 describes how we compute  $S_0$ , the observable obtained in hyperthermal molecular beam experiments. The QD and the QCT methods that are used to obtain  $S_0$  for  $\text{H}_2 + \text{Al}(110)$  are described in Sections 4.2.5.A and 4.2.5.B, respectively. In Section 4.3, the results of the calculations are shown and discussed. Section 4.3.1 describes the computed PES, and Section 4.3.2 presents the  $S_0$  computed with QD and with the QCT method, and their comparison. In Section 4.3.3 an attempt is made to underpin the size of the quantum effects predicted with an analysis of the QCT results and the characteristics of the molecular beams we simulate. Conclusions are provided in Section 4.4.

## 4.2 Method

### 4.2.1 Dynamical model

In all calculations (in the QD and in the QCT calculations), the Born-Oppenheimer static surface (BOSS) model<sup>14</sup> has been used. Within this model the surface atoms are kept fixed in their ideal lattice positions and ehp excitation is neglected. Only the motion in the six  $\text{H}_2$  degrees of freedom (6D) is taken into account. Specifically, the molecular coordinates  $X$ ,  $Y$ , and  $Z$  describe the motion of the molecule's center of mass, where  $Z$  is the molecule-surface distance and  $X$ ,  $Y$  describe the lateral positions (see Figs. 4.1A and 4.1B). Furthermore, the H-H bond distance is given by  $r$  and the angular orientation of  $\text{H}_2$  by the polar angle  $\theta$  the  $\text{H}_2$  bond makes with the surface normal and the azimuthal angle  $\varphi$  that the projection of the molecule's bond axis on the surface makes with the X-axis (see Figs. 4.1A and 4.1B). Fig. 4.1A also shows the  $\text{Al}(110)$  surface unit cell and the high symmetry impact sites top, long-bridge, short-bridge, hollow, and the site we call the C-site.

As discussed below the slab we used to model the Al surface mimics an ideal surface at a surface temperature ( $T_s$ ) of 220 K. We note that, with the way the slab has been set-up for 220K, we only include the effects of thermal expansion<sup>50</sup>.

Presently we exclude the effect of the forms of corrugation that surface motion can introduce in a real surface at 220K, and the effect of energy transfer between the molecule and the surface atoms<sup>50-52</sup>.

QCT calculations using the static corrugation model on the activated DC of H<sub>2</sub> and D<sub>2</sub> on Cu(111) at T<sub>s</sub> = 120 K found little effect of the mentioned additional corrugation for S<sub>0</sub> values as low as 10<sup>-3</sup> (see Fig.13 of Ref.<sup>51</sup>). Likewise, density functional molecular dynamics (DFMD) calculations and QCT calculations investigating DC of D<sub>2</sub> on Cu(111) found no detectable effect (within the statistical accuracy of the DFMD calculations) of the mentioned additional corrugation and of energy transfer at T<sub>s</sub> = 120 K for S<sub>0</sub> ≥ 10<sup>-2</sup> (see Fig.S1 of Ref.<sup>53</sup>). Given that DC of H<sub>2</sub> on Al(110) is associated with even lower reaction probabilities<sup>20</sup>, that the measurements on this system were performed at a somewhat higher T<sub>s</sub> (220 K), and that the mass ratio between H and Al should be more conducive to energy transfer according to the Baule model<sup>54</sup> than that between H and Cu, these effects might become more important for the system under investigation here. We believe however that for the current comparison between QD and QCT using a molecular beams of H<sub>2</sub> that we simulate, these effects are not so relevant, although presently this is based on speculation and the answer may depend on whether the thermal motion may promote reactivity through tunneling by modulating the barrier height to DC<sup>55,56</sup>. To our knowledge, work on how surface atom motion might affect the tunneling contribution to DC of H<sub>2</sub> has not yet been performed. However, as stated previously, the effect of phonons will be considered in future work with quasi-classical dynamics (A.D. Powell et al., to be published).

### 4.2.2 DFT Method

Calculations of the H<sub>2</sub>-Al(110) molecule surface interaction were performed using Kohn-Sham DFT<sup>57,58</sup>. The density functional (DF)  $E_{xc}^{SRP71-vdW2}$  used can be written as

$$E_{xc}^{SRP71-vdW2} = 0.29E_x^{PBE} + 0.71E_x^{RPBE} + E_c^{vdW-DF2}. \quad (4.1)$$

It contains 29% PBE<sup>59</sup> exchange and 71% RPBE<sup>60</sup> exchange, while the correlation part of the exchange-correlation functional was taken as the Rutgers-Chalmers vdW-DF2 correlation functional<sup>61</sup>. As will be described in detail elsewhere (A.D. Powell et al., to be published), with this DF an accurate fit is obtained of the barrier heights computed with diffusion MonteCarlo (DMC) for six barrier geometries of H<sub>2</sub> + Al(110)<sup>41</sup>. For example, with the DF of Eq. 4.1 a transition state (TS) energy of 25.4 kcal/mol is obtained, which is in

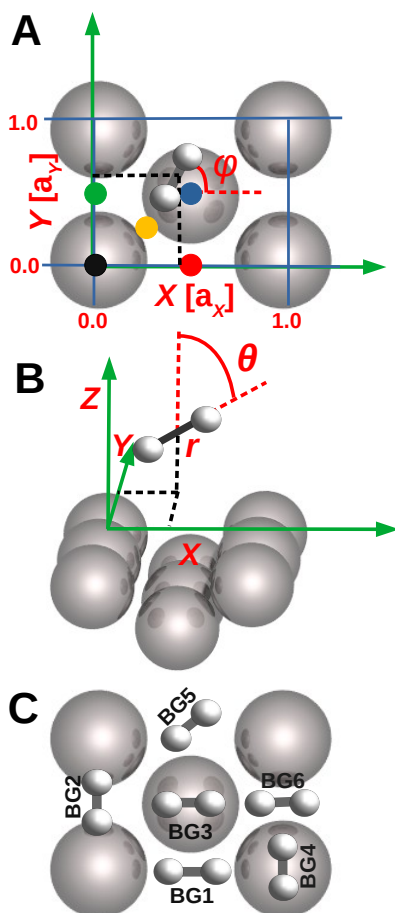


FIGURE 4.1: Top view (A) and side view (B) of the surface unit cell of Al(110), illustrating the six coordinates describing the geometry of the  $H_2$ -Al(110) system in the BOSS model, and (C) the six barrier geometries BG1-BG6. In (A) the black, green, red, blue, and yellow solid circles denote the top, short-bridge, long-bridge, hollow, and C site, respectively.



good agreement with the DMC value of 25.1 kcal/mol<sup>41</sup>. More details of the comparison with DMC data will be provided elsewhere.

In the plane wave DFT calculations the Al(110) surface has been represented using a 10 layer thick Al slab. Details of how the slab was set up and adjusted to represent an Al(110) surface in which the atoms occupy the ideal lattice positions at 220 K are presented in Sections S1 and S3 of the Supporting Information (SI) of Ref.<sup>62</sup>. A  $(3 \times 3)$  surface unit cell was used, leading to a total of 90 Al atoms. A vacuum distance of 16.0 Å was used to separate the slab from its first periodic images in the supercell approach employed. The core electrons have been treated using pseudo-potentials within the projector augmented wave method<sup>63,64</sup> (details are also presented in the SI of Ref.<sup>62</sup>). The energy cutoff for the plane wave expansion was 540 eV. The Brillouin zone has been sampled with a  $8 \times 8 \times 1$   $\Gamma$ -centered grid of k-points. Convergence was facilitated using first order Methfessel-Paxton smearing<sup>65</sup> with a width parameter of 0.1 eV. These input parameters to the plane wave DFT calculations have been established on the basis of convergence tests described in Section S2 of the SI of Ref.<sup>62</sup>. The calculations for the PES have been performed with a user-modified version of the Vienna ab initio simulation package<sup>63,66</sup> (Vasp5.4.4) that allows calculations with a weighted average of the exchange parts of the PBE and RPBE DFs.

### 4.2.3 Interpolation of PES

The H<sub>2</sub>-surface PES was interpolated using the corrugation reducing procedure (CRP)<sup>49</sup>, with the formula

$$I_{6D}(X, Y, Z, r, \theta, \varphi) = V_{6D}(X, Y, Z, r, \theta, \varphi) - R_{3D}(X_A, Y_A, Z_A) - R_{3D}(X_B, Y_B, Z_B) \quad (4.2)$$

in which  $V_{6D}$  is the full 6D PES of the H<sub>2</sub>/surface system,  $I_{6D}$  is the so-called 6D interpolation function of the H<sub>2</sub>/surface system,  $R_{3D}$  is the 3D PES of the H/surface system and  $(X_D, Y_D, Z_D)$  are the Cartesian coordinates of H-atom  $D = A$  or  $B$ . Equation 4.2 recognizes that most of the corrugation and the anisotropy of the H<sub>2</sub>-surface interaction is due to the interaction of the closest H-atom to the surface, so that subtracting the H-atom - surface interactions from the full H<sub>2</sub> - surface interaction  $V_{6D}$  leads to the much smoother interpolation function  $I_{6D}$ <sup>49</sup>. The three-dimensional (3D) atom-surface PES is in turn written as

$$R_{3D}(X, Y, Z) = I_{3D}(X, Y, Z) + \sum_j V_P(R_i). \quad (4.3)$$

Equation 4.3 recognizes that a smoother function (the 3D interpolation function  $I_{3D}$ ) can be obtained by subtracting from the corrugated H-surface interaction the sum of pair interactions  $V_P(R_i)$ , where the  $R_i$  are the distances of the H-atom to the nearest surface atoms labeled by  $i$ .

The interpolation procedure used for the PES of  $H_2+Al(110)$  is the same as used for  $H_2$  on  $Cu(110)$  in Ref.<sup>67</sup>, where the procedure has been described in detail, albeit with respect to a coordinate system that was rotated relative to that in Fig. 4.1A by  $90^\circ$ . For the interpolation of  $I_{3D}$ , 22 configurations of  $(X, Y, \theta, \varphi)$  are used, spread over five different sites  $(X, Y)$ , i.e., the top site, the hollow site, the long-bridge site, the short-bridge site, and a site located halfway between the top and the hollow sites which is called the C-site (See Fig. 4.1). These configurations are identical to the configurations described in Ref.<sup>67</sup>.

The interpolation is done in several steps: First, for every configuration, the interpolation is performed over the  $r$  and  $Z$  degree of freedom. For this interpolation, a  $22 \times 17$  ( $r \times Z$ ) grid is used, employing a two-dimensional (2D) cubic spline interpolation, over the range in  $r$  defined by  $r_{min} = 0.4 \text{ \AA}$  and  $r_{max} = 2.55 \text{ \AA}$  and the range in  $Z$  defined by  $Z_{min} = 0.0 \text{ \AA}$  and  $Z_{max} = 4.0 \text{ \AA}$ . Then, for every site, the interpolation is performed over the  $\theta$  and  $\varphi$  degrees of freedom using symmetry-adapted products of sine and cosine functions. Finally, an interpolation over  $X$  and  $Y$  is performed, for which again symmetry-adapted products of sine and cosine functions are used. At long-range, we apply a switching function between  $3.5 \text{ \AA}$  and  $4.0 \text{ \AA}$  from the full 6D potential to a 2D asymptotic gas-surface potential that only depends on  $r$  and  $Z$ , because far away from the surface, the corrugation and anisotropy of the PES are vanishingly small. This asymptotic potential is represented by

$$V_{2D}(r, Z) = V_{\text{ext}}(Z) + V_{\text{gas}}(r) \quad (4.4)$$

where  $V_{\text{ext}}$  is a function closely describing the dependence of the PES on  $Z$  beyond  $Z = 3.5 \text{ \AA}$  for the BG6 geometry (see Fig. 4.1C), and  $V_{\text{gas}}$  defines the H-H interaction calculated with  $H_2$  positioned in the middle of the vacuum. Between  $Z = 3.5$  and  $4.0 \text{ \AA}$   $V_{\text{ext}}(Z)$  is positioned more or less halfway between the extremes of the full 6D interaction potential computed with the 22 different configurations (combinations of impact site and orientation), these extremes being apart by no more than 26 meV for  $Z = 3.5 \text{ \AA}$ , and by no more than 8 meV for  $Z = 4 \text{ \AA}$ . For the interpolation of  $I_{3D}$ , the same 9 sites in  $(X, Y)$  are used for the H-surface interaction as used in Ref.<sup>67</sup>. The function  $V_P(R_i)$  describes the interaction of an H atom with the surface above the top site, as used previously for the investigation of  $H_2 + Cu(110)$ <sup>67</sup>.

#### 4.2.4 Calculations of observables

The sticking probability measured in a molecular beam experiment can be computed using<sup>14,37,46</sup>

$$S_0(E_{av}; T_n) = \frac{\int_0^\infty f(v; T_n) S_{\text{mon}}(E_i; T_n) dv}{\int_0^\infty f(v; T_n) dv} \quad (4.5)$$

In Eq. 4.5,  $E_{av}$  is the average collision energy, and  $S_{\text{mon}}(E_i; T_n)$  is an intermediate quantity, which may be called the monochromatic sticking probability. To compute the sticking probability this quantity needs to be averaged over the velocity distribution, which can be written as<sup>68,69</sup>

$$f(v; T_n) dv = C v^3 \exp[-(v - v_0)^2 / \alpha^2] dv. \quad (4.6)$$

Here,  $v$  is the molecule's velocity towards the surface that is related to the incidence energy by  $E_i = \frac{1}{2} m v^2$ ,  $m$  being the mass of the molecule, and the parameters characterizing the velocity distribution of the beam are the stream velocity  $v_0$  and the width parameter  $\alpha$ , while  $C$  is a normalization parameter. The beam parameters used are given in Table 4.1. These parameters were taken from Ref.<sup>46</sup> (i.e., they were taken from Tables S5 and S6 of that paper), in which they were obtained by performing fits of TOF spectra and from a plot of the speed ratio vs. the average incidence energy. The TOF spectra and the plot referred to were taken from the PhD thesis of Berger<sup>45</sup>, which describes experiments on  $\text{H}_2$  colliding with  $\text{Cu}(111)$  as well as the experiments on  $\text{H}_2 + \text{Al}(110)$  we will compare with in future (A.D. Powell et al., to be published). The monochromatic sticking probability can be computed using

$$S_{\text{mon}}(E_i, T_n) = \sum_{\nu, j} F_{\text{B}}(\nu, j, T_n) R_{\nu, j}(E_i) \quad (4.7)$$

Here,  $j$  is the rotational quantum number. The Boltzmann weight is given by

$$F_{\text{B}}(\nu, j, T_n) = \frac{w(j) F(\nu, j, T_n)}{\sum_{\nu'=0, j'=0}^{\nu_{\text{max}}, j_{\text{max}}} w(j') F(\nu', j', T_n)} \quad (4.8)$$

in which

$$F(\nu, j, T_n) = (2j + 1) \exp(-E_{\text{vib}}(\nu, j)) / k_B T_n \exp(-E_{\text{rot}}(\nu, j)) / 0.8 k_B T_n \quad (4.9)$$

In Eq. 4.7  $R_{\nu, j}(E_i)$  is the degeneracy averaged reaction probability, i.e., the average over the  $(2j + 1)$  fully initial state resolved reaction probabilities  $R_{\nu, j, m_j}(E_i)$ , where  $m_j$  is the magnetic rotational quantum number (the projection

of  $j$  on the surface normal). In Eq. (4.8), the summation runs only over the values of  $j'$  with the same parity as  $j$ . In equation (4.9)  $E_{vib}$  and  $E_{rot}$  are the vibrational and rotational energy, respectively, of the  $(\nu, j)$  state and  $k_B$  is the Boltzmann constant. In these equations, it is assumed that the rotational temperature of the molecules is 0.8 times the nozzle temperature ( $T_{rot} = 0.8T_n$ )<sup>21,70,71</sup> and that the vibrational temperature is equal to the nozzle temperature ( $T_{vib}=T_n$ )<sup>21,70</sup>. We assume that the fractions of ortho and para-H<sub>2</sub> and D<sub>2</sub> are equal to those in the high-temperature limit, and given by  $w(j)$ . Then for H<sub>2</sub>,  $w(j)$  is equal to  $\frac{1}{4}$  for even  $j$  and  $\frac{3}{4}$  for odd  $j$ .

It is rather trivial to rewrite Eqs. 4.7-4.9 in terms of the fully initial-state resolved reaction probabilities. We will nevertheless provide the equations as it makes it easier to explain the procedure we use for averaging over rovibrational states in the QD calculations below. The equations are:

$$S_{\text{mon}}(E_i, T_n) = \sum_{\nu=0}^{\nu_{\text{max}}} \sum_{j=0}^{j_{\text{max}}} \sum_{m_j=0}^j F_{\text{Bm}}(\nu, j, T_n) R_{\nu, j, m_j}(E_i) \quad (4.10)$$

$$F_{\text{Bm}}(\nu, j, T_n) = \frac{w(j)w_m(m_j)F_m(\nu, j, T_n)}{\sum_{\nu'=0}^{\nu_{\text{max}}} \sum_{j'=0}^{j_{\text{max}}} \sum_{m'_j=0}^{j'} w(j')w_m(m'_j)F_m(\nu', j', T_n)} \quad (4.11)$$

$$F_m(\nu, j, T_n) = \exp(-E_{vib}(\nu, j)/k_B T_n) \exp(-E_{rot}(\nu, j)/0.8k_B T_n) \quad (4.12)$$

In having the sum over  $m_j$  from 0 to  $+j$  in Eqs. 4.10 and 4.11, we have used that  $R_{\nu, j, -m_j}(E_i)(E_i) = R_{\nu, j, m_j}(E_i)$ , which we take into account through the weight factor  $w_m(m_j) = (2 - \delta_{m_j, 0})$  in Eq. 4.11.

The integration in Eq. 4.5 and the summation in Eq. 4.7 or Eq. 4.10 can be performed in different ways. In QCT calculations the computation of reaction or sticking probabilities always involves the selection of initial conditions using a Monte-Carlo integration (or Monte-Carlo averaging) procedure. If this procedure is to be used in the computation of initial sticking probabilities to select e.g. the impact site and the initial orientation of the molecule, one might as well use Monte-Carlo integration throughout in the procedure to compute  $S_0$ . In this often used procedure, which may be referred to as "full Monte-Carlo averaging" (FMC),  $S_0$  is computed in a single calculation with the use of a Monte-Carlo averaging procedure in which the initial velocity of the molecule and the initial rovibrational state are selected according to the initial conditions. This is done on the basis of an appropriate statistical procedure involving random number generation, effectively using Eqs. 4.5 and 4.10. If, on the other hand, the

TDWP method is used to compute  $S_0$  it makes much more sense to compute the integral in Eq. 4.5 by performing a Riemann sum, because the TDWP method yields reaction probabilities over a range of closely spaced energies instead of one energy at a time<sup>30</sup>. In this case the normal procedure is to obtain results for a range of vibrational states running from  $\nu=0$  to  $\nu_{max}$ , and from  $j = 0$  to  $j_{max}$ , where  $j_{max}$  may depend on  $\nu$ , and one can use either Eqs. 4.5 and 4.7 or Eqs. 4.5 and 4.10. Because in this procedure Monte-Carlo averaging is used in neither the integration over incident velocity nor the averaging over initial states, we call this procedure "no Monte Carlo averaging" (NMC). As we are performing QD calculations and comparing QCT calculations to QD (TDWP), the procedure last mentioned (NMC) is the default procedure we typically follow in QCT calculations. A full quantum-classical comparison could then involve a very large number of QD calculations, i.e., for as many states as used in the NMC quasi-classical procedure. Fortunately, as we will show, it is also possible to use a partial Monte-Carlo averaging procedure (PMC), in which the sum in Eq. 4.10 is performed using Monte-Carlo averaging over initial rovibrational states. Specifically, rewriting Eqs. 4.10 and 4.11 we can then perform the sum over a much smaller number of  $N_{sel}$  states:

$$S_{\text{mon}}(E_i, T_n) = \sum_{k=1}^{N_{sel}} F_{\text{Bmk}}(\nu(k), j(k), T_n) R_{\nu(k), j(k), m_j(k)}(E_i) \quad (4.13)$$

$$F_{\text{Bmk}}(\nu(k), j(k), T_n) = \frac{w(j)w_m(m_j)F_m(\nu(k), j(k), T_n)}{\sum_{k=1}^{N_{sel}} w(j'(k))w_m(m'_j(k))F_m(\nu'(k), j'(k), T_n)} \quad (4.14)$$

Equations 4.13 and 4.14 state that in the PMC procedure we used, each rovibrational state ( $\nu, j, m_j \geq 0$ ) included in the sum is *selected* with equal weight (i.e., without taking into account the weight factors in Eq. 4.12 and 4.14) for performing a QCT or QD calculation of  $R_{\nu, j, m_j}(E_i)$ . Here, each state can only be selected once. The weights in Eqs. 4.12 and 4.14 are of course taken into account in computing  $S_0$  through Eq. 4.13, but the  $N_{sel}$  number of selected ( $\nu, j, m_j \geq 0$ ) states all had an equal chance to be selected for use as an initial state in a dynamics calculation.

An important point is that in principle  $N_{sel}$ , and the actual rovibrational states selected, should be the same in all beam simulations to take advantage of the feature of TDWP calculations that they provide results for a range of incidence energies, but for only one initial rovibrational state<sup>72</sup>. Varying  $N_{sel}$  or keeping it the same but using different initial rovibrational states would lead

one to either discard quantum dynamics results that are available anyhow or to perform a needlessly high number of computationally expensive QD calculations.

To keep  $N_{sel}$  as low as possible in view of the computational cost of QD calculations, the following procedure was used. For a given number of  $N_{sel}$ , the states to be used are generated, and the PMC value of  $S_0$ , i.e.,  $S_0(\text{PMC})$ , is computed with QCT. If within a reasonable number of trials we find that  $|S_0(\text{PMC}) - S_0(\text{NMC})|/S_0(\text{NMC}) < 0.1$  for the beam condition corresponding to the lowest average value of  $E_i$ , then the value of  $N_{sel}$  and the corresponding batch of states is accepted as yielding representative values for  $S_0$ . Here an assumption has been that while statistical fluctuations might lead to somewhat larger relative errors in the PMC sticking probabilities than 0.1 at somewhat higher average energies, these larger relative errors should still be of a moderate size, e.g., they should not exceed 0.2 (20%). We say this even though we assume that the reaction should be determined by the lowest amount of rovibrational states at the lowest energy beam condition, making it critical to use a high enough value of  $N_{sel}$  to ensure that at least some of these states are sampled. It should then be possible to obtain fairly accurate values of  $S_0$  at all relevant average incidence energies with the TDWP method on the basis of the same states in the PMC procedure with a much smaller computational effort. Below we will show that  $N_{sel} = 35$  is already small enough for this purpose, while calculations on 319 ( $\nu, j, m_j \geq 0$ ) states would have been necessary with the  $\nu_{max}$  and  $j_{max}$  parameters used in the NMC procedure (these parameters are collected in Table 4.2). An assumption used in this work is that with the rovibrational states thus selected we can also obtain QD results that are representative of NMC QD results, i.e., of the QD results that would be obtained performing QD calculations for all 319 states explicitly.

TABLE 4.1: Parameters used for the molecular beam simulations of  $\text{H}_2$  on  $\text{Al}(110)$ .

$T_n(\text{K})$	$\langle E_i \rangle (\text{kcal/mol})$	$v_0(\text{m/s})$	$\alpha(\text{m/s})$
1100	5.10	3679	1525
1400	7.89	3578	2550
1700	9.36	3265	3103
1120	6.00	3500	1996
1330	7.15	3555	2342
1580	8.49	3219	2903

In both the NMC and PMC procedures using the QCT method, we perform Riemann sums to evaluate Eq. 4.5 in a procedure in which calculations are carried out for  $E_i$  in the range 0.05 - 3.05 eV. Cubic spline interpolation is carried out to

TABLE 4.2: The  $j_{max}$  parameters determining for which rovibrational states  $R_{\nu,j,m_j}$  was taken into account in the NMC and FMC QCT calculations.

	NMC	FMC
$\nu$	$j_{max}$	$j_{max}$
0	15	20
1	13	20
2	11	20
3	-	20

obtain the initial-state selected reaction probabilities for intermediate energies, and extrapolation is carried out to obtain the  $R_{\nu,j,m_j}$  for  $E_i < 0.05$  eV. Tests showed that the upper bound in Eq. 4.5 can be replaced by a value of the velocity corresponding to  $E_i = 2.20$  eV, although the actual upper bound corresponded to 3.05 eV. QD calculations were only carried out up to  $E_i = 1.05$  eV; to obtain QD results, for higher values of  $E_i$  we simply used the QCT reaction probabilities computed for these energies.

## 4.2.5 Dynamics Methods

### 4.2.5.A Quantum Dynamics

The time-dependent wave packet (TDWP) method<sup>30</sup> as implemented in our in-house code<sup>31,36</sup> was used to solve the time-dependent Schrödinger equation (TDSE):

$$i\hbar \frac{d\Psi(\mathbf{Q}; t)}{dt} = \hat{H}(\mathbf{Q})\Psi(\mathbf{Q}; t) \quad (4.15)$$

In Eq.(4.15) the 6 molecular coordinates described in Section 4.2.1 are given by  $\mathbf{Q}$ .  $\Psi(\mathbf{Q}; t)$  is the time-dependent nuclear wave function of the system and  $\hat{H}(\mathbf{Q})$  is the time-independent Hamiltonian given by

$$\hat{H}(\mathbf{Q}) = -\frac{\hbar^2}{2m} \hat{\nabla}^2 - \frac{\hbar^2}{2\mu} \frac{\partial^2}{\partial r^2} + \frac{1}{2\mu r^2} \hat{J}^2(\theta, \varphi) + V(\mathbf{Q}) \quad (4.16)$$

Here,  $\mu$  is the reduced mass of  $\text{H}_2$ ,  $\hat{\nabla}$  and  $\hat{J}$  are the Nabla operator acting on the center-of mass coordinates of the molecule and the angular momentum operator, and  $V(\mathbf{Q})$  is the 6D interpolated CRP PES.

To solve the TDSE, an initial wave function is set up as a product of a Gaussian wave packet  $u(Z_0, k_0^Z)$  centered on  $Z_0$  with average momentum  $k_0^Z$ , a two-dimensional plane wave function  $\phi(k_0^X, k_0^Y)$  for motion along  $X$  and  $Y$ , a

vibrational wave function  $\psi_{\nu,j}(r)$ , and a rotational wave function  $Y_{j,m_j}(\theta, \varphi)$  of incident  $\text{H}_2$ :

$$\Psi(\mathbf{Q}, t = 0) = u(Z; Z_0, k_0^Z) \phi(k_0^X, k_0^Y) \psi_{\nu,j}(r) Y_{j,m_j}(\theta, \varphi) \quad (4.17)$$

In Eq. 4.17, the two-dimensional plane wave function and the Gaussian wave packet are defined as

$$\phi(k_0^X, k_0^Y) = e^{i(k_0^X X_0 + k_0^Y Y_0)} \quad (4.18)$$

$$u(Z_0, k_0^Z) = \frac{1}{\sqrt{2\pi}} \int_0^\infty dk b(k; Z_0, k_0^Z) e^{ikZ} \quad (4.19)$$

with

$$b(k; Z_0, k_0^Z) = \left( \frac{2\sigma^2}{\pi} \right)^{\frac{1}{4}} e^{-\sigma^2(k_0^Z - k)} e^{i(k_0^Z - k)Z_0}. \quad (4.20)$$

Here,  $\sigma$  is the width of the wave packet for motion in  $Z$  centered around the initial average momentum  $k_0^Z$ , and  $k_0^X$  and  $k_0^Y$  are the initial momenta for motion along  $X$  and  $Y$ , which are taken equal to zero here to describe normal incidence. As described in more detail in the SI of Ref.<sup>62</sup> the width  $\sigma$  is chosen in such a way that 90% of the Gaussian wave packet is placed in an energy range  $E_i \in [E_{min}, E_{max}]$ , and four of these energy ranges are used to generate results between  $E_i = 0.05$  and 1.05 eV. In the expression for the time-dependent wave function, a Fourier representation was used to represent the dependence of the wave function on  $Z$ ,  $r$ ,  $X$ , and  $Y$ . Fast Fourier transforms were used to evaluate the action of the corresponding kinetic energy operators on the wave function<sup>73</sup>. We employed a finite basis representation to represent the angular part of the wave function<sup>74,75</sup>. Eq.( 4.15) is solved numerically using the split operator method<sup>76</sup> using a time step  $\Delta t$ . A complex absorbing potential (CAP, actually, a negative imaginary potential of quadratic order<sup>77</sup>) is used to absorb the reacted and scattered wave packet for large values of  $r$  and  $Z$ , respectively. For high incidence energies relative to the reaction threshold the scattered fraction of the wave function is analyzed through the scattering amplitude formalism<sup>78,79</sup>, after which state-to-state scattering probabilities  $P_{sc}$  can be obtained from the squares of the S-matrix elements<sup>31,36</sup>. Summing the  $P_{sc}$  and subtracting from 1 then yields the fully initial-state resolved reaction probability  $R_{\nu,j,m_j}(E_i)$ .

For incidence energies just above and below the reaction threshold for the initial  $(\nu, j)$  state we have used the flux analysis method<sup>80,81</sup> to compute  $R_{\nu,j,m_j}(E_i)$  more directly, by analyzing the reactive flux through the five-dimensional surface at a large enough and fixed value of  $r = r_{fl} = 6.55 a_0 \approx 3.47 \text{ \AA}$ . This H-H



distance is far beyond that of the barriers to DC for the system investigated (see Section 4.2.5.B below) but lower than the value where the CAP absorbing the reacted part of the wave packet is turned on (see Table S4 of the SI of Ref.<sup>62</sup>). Also, we have checked that using this value yields results equal to those of the scattering amplitude formalism in the regime where results of the latter method are not affected by resonances. We found that the calculation of the state-to-state scattering probabilities (and, thereby, of the  $R_{\nu,j,m_j}(E_i)$ ) at  $E_i$  near the reaction threshold may be hampered by the formation of meta-stable states located in the entrance channel when using the scattering matrix formalism. This was not the case with the flux-analysis formalism, presumably because these entrance channel states do not affect the reaction due to the high barrier (of about 1 eV) to the reaction; instead, they only affect the scattering back to the gas phase.

The input parameters to the TDWP calculations were selected on the basis of convergence tests. These parameters are discussed in Section S4 of the SI of Ref.<sup>62</sup> and provided in Table S4 of the SI of Ref.<sup>62</sup>.

#### 4.2.5.B Quasi-classical dynamics

In performing the classical dynamics calculations we always impart the zero-point energy to the vibration of H<sub>2</sub>, i.e., we use the QCT method<sup>28,29</sup>. To evaluate the initial state-resolved reaction probabilities, we placed our molecule initially at  $Z = 8.0$  Å with a velocity normal toward the surface that corresponds to a specific initial incidence energy. At this distance, the interaction of the molecule with the surface is essentially zero. For each initial rovibrational state modeled calculations were performed for fixed incidence energies in the range 0.05 - 3.05 eV. For each energy and initial rovibrational state, typically  $N_T = 500,000$  trajectories were computed. In all cases, the maximum propagation time is 2 ps. In the calculations using the FMC procedure,  $N_T = 190,000,000$  trajectories were run for each initial condition. In the FMC procedure states with  $\nu$  up to 3 were included, and the  $j_{max}$  values employed with the vibrational states are listed in Table 4.2.

To solve the equation of motions, the Bulirsch-Stoer method was used<sup>82,83</sup>. As in the TDWP calculations, the time-independent Schrödinger equation (TISE) was solved using the Fourier grid Hamiltonian method<sup>84</sup> to determine the bound state rotational-vibrational eigenvalues of gas phase H<sub>2</sub>. The bond distance and the vibrational velocity of the molecule are randomly sampled from a one-dimensional quasi-classical dynamics calculation of a vibrating H<sub>2</sub> molecule for the corresponding rovibrational energy<sup>44</sup>. The orientation of the molecule, specified by  $\theta$  and  $\varphi$ , is chosen based on the selection of the initial rotational state. The magnitude of the classical initial angular momentum is fixed by  $L = \sqrt{j(j+1)}/\hbar$

and its orientation, while constrained by  $\cos \Theta_L = m_j / \sqrt{j(j+1)}$ , is otherwise randomly chosen as described by Wijzenbroek et al.<sup>85</sup>. Here,  $j$  is the rotational quantum number,  $m_j$  the magnetic rotational quantum number and  $\Theta_L$  the angle between the angular momentum vector and the surface normal. Other initial conditions are randomly chosen as described in Ref.<sup>44</sup>. Reaction is defined to occur if the H-H distance becomes longer than 2.2 Å. The initial state-selected reaction probability can be computed as

$$R_{\nu,j,m_j}(E_i) = \sqrt{\frac{N_r}{N_T}} \quad (4.21)$$

where  $N_r$  is the number of reacted trajectories. The statistical error in the computed reaction probability, which defines a 68% confidence interval, can be computed as

$$\sigma = \sqrt{\frac{R(1-R)}{N_T}} \quad (4.22)$$

The reaction probabilities can be used to compute  $S_0$  using Eqs.4.5 and 4.7 or 4.5 and 4.13 as described above in Section 4.2.4.

## 4.3 Results and discussion

### 4.3.1 The fitted potential energy surface

The accuracy of our CRP 6D potential has been checked by comparing the interpolated results to the raw DFT data. Fig. 4.2 shows, for six selected high symmetry configurations (BG1-BG6, called TS1-TS6 in table 5 of Ref.<sup>41</sup>, "BG" stands for "barrier geometry"), two-dimensional (2D) cuts through the PES (also called elbow plots). In all cases, H<sub>2</sub> was oriented parallel to the surface. The CRP reproduces the DFT data quite well. Moreover, the 2D minimum energy paths (MEPs) obtained with the CRP are in close agreement with the DFT results as shown in the same figure. Furthermore, a quantitative comparison between the CRP and the DFT results is shown in Table 4.3 for all the BGs represented in Fig. 4.2. As can be seen, the barrier heights and geometries derived from the CRP are in excellent agreement with the raw DFT results. The mean absolute deviation (MAD) associated with the six barrier heights is just 0.24 kcal/mol.

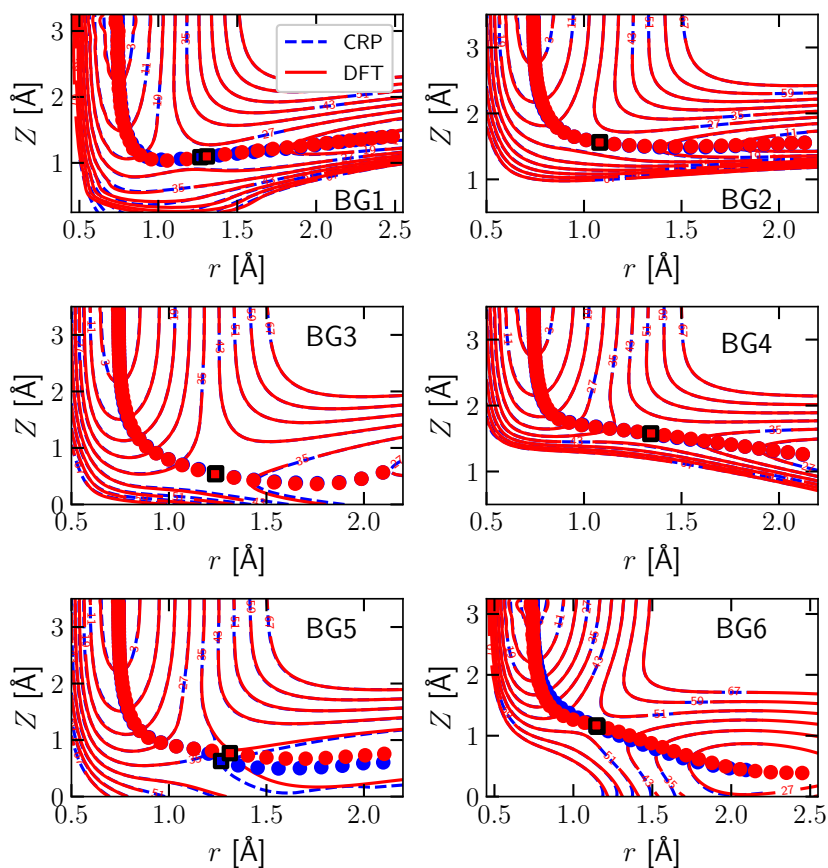


FIGURE 4.2: Elbow plots of the H<sub>2</sub>-Al(110) PES as directly calculated with DFT (red solid lines) and fitted with the CRP (blue dashed lines). The blue numbers label the contour lines of the PES. Red (blue) circles indicate the minimum energy path from reactants to product as computed directly with DFT (obtained from the CRP fit). The red (blue) square indicates the position of the barrier in 2D as computed with DFT (interpolated with the CRP). Results are given for the six barrier geometries indicated in Fig. 4.1C and investigated in Ref. <sup>41</sup>.

TABLE 4.3: Comparison between CRP and DFT of the barrier heights (in kcal/mol) and locations ( $r_b$ ,  $Z_b$ ) (in Å), relative to the gas phase minimum, for all the six BGs (table 5 Ref.<sup>41</sup>). All geometries are for the H<sub>2</sub> molecule lying parallel to the surface ( $\theta = 90^\circ$ ). Also indicated are the signed errors between DFT and CRP ( $\Delta E = E_b^{CRP} - E_b^{DFT}$ ).

Adsorption Site	BG1	BG2	BG3	BG4	BG5	BG6
$Z_b^{DFT}$	1.08	1.56	0.54	1.57	0.77	1.15
$Z_b^{CRP}$	1.08	1.56	0.55	1.57	0.63	1.15
$r_b^{DFT}$	1.22	1.08	1.24	1.34	1.31	1.15
$r_b^{CRP}$	1.26	1.08	1.24	1.34	1.27	1.15
$E_b^{DFT}$	25.3	24.8	37.5	37.8	34.8	49.4
$E_b^{CRP}$	25.40	24.78	37.73	38.03	35.60	49.44
$\Delta E$	0.10	-0.02	0.23	0.24	0.80	0.05

### 4.3.2 Sticking probabilities computed with quantum and quasi-classical methods, and their comparison

As a "sanity check", we first performed a comparison of the  $S_0$  computed with the NMC procedure and the FMC procedure. The results show that the  $\nu_{max}$  and the ( $j_{max}$ ,  $\nu = 0-2$ ) values used in the NMC procedure (see Table 4.2) were high enough to yield, for the range of molecular beam conditions investigated here, values of  $S_0$  that are accurate enough for our purposes (see Fig.S1 of the SI of Ref.<sup>62</sup>).

We next investigated the accuracy of the PMC procedure by comparing QCT results obtained with the NMC and the PMC procedures (see Fig.4.3). Even though the decisions on which number of states to be included, and which states to be included in the PMC procedure were taken only on the basis of the results for the lowest  $E_i$ , we find that the PMC results are accurate enough for our purpose for all average  $E_i$ . The absolute value of the relative error was 1.6% for  $\langle E_i \rangle = 5.1$  kcal/mol (meeting our requirement that it should be lower than 10%), 15.9% for  $\langle E_i \rangle = 6.0$  kcal/mol, and decreased monotonically from 7.4% for  $\langle E_i \rangle = 7.1$  kcal/mol to 1.6% for  $\langle E_i \rangle = 9.4$  kcal/mol (meeting our requirement that it should in no case be higher than 20%). The non-monotonic dependence of the relative error on average incidence energy can be attributed to statistics: the selected batch of states is good for  $\langle E_i \rangle \geq 7.1$  kcal/mol, good enough for the lower value of 6.0 kcal/mol, and perhaps by chance it is excellent for the lowest value (5.1 kcal/mol), where the reactivity should be dominated by the smallest amount of rovibrational states that are thermally populated. We conclude that the value of  $N_{sel}$  (35) is high enough for our purposes, and that the batch of rovibrational states selected is good enough to yield representative QCT

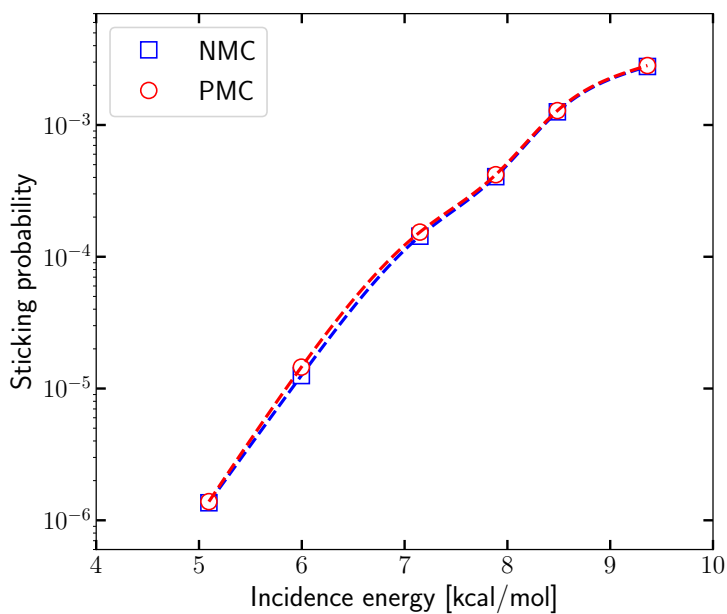


FIGURE 4.3: Sticking probabilities computed with the QCT method using averaging over all 319  $\nu = 0, 1,$  and  $2$  ( $\nu, j, m_j$ ) states ("NMC") and Monte-Carlo averaging over only 35 such states ("PMC").

results, and that it should therefore in principle suffice to base the QD-QCT comparison on the results for this batch of rovibrational states only.

We compare  $R_{\nu,j,m_j}(E_i)$  computed with QD and QCT dynamics for three initial rovibrational states (with  $\nu = 0, 1$ , and  $2$ , respectively, with these 3 states contributing to the  $S_0$  computed with the PMC procedure) in Figs.4.4A-4.4C. The trends we see in typical comparisons of QD and QCT results for specific initial rovibrational states are exemplified in this plot. We usually see that the differences between the  $R_{\nu,j,m_j}(E_i)$  computed with QD and QCT dynamics become increasingly small for  $E_i$  increasing and approaching the reaction threshold for the specific initial rovibrational state. This reaction threshold is close to  $\approx 23.8$  kcal/mol = 1.03 eV for the ( $\nu=0, j=2$ ) state for which results are presented in Fig.4.4A, the minimum barrier height of the CRP potential being 24.8 kcal/mol), while it is lower for the other initial states included in the sum of Eq.4.10, which have higher rovibrational energies. At lower energies we typically see QD reaction probabilities that are higher than the QCT results, which we attribute to tunneling. The opposite is also sometimes observed (see the result in Fig.4.4A for the highest  $E_i$ ), which is most likely due to artificial zero point energy conversion (in the QCT method conservation of zero-point energy during the trajectory is not guaranteed<sup>29</sup>).

Figure 4.5 shows the effect of the type of differences typically observed between QD and QCT values of  $R_{\nu,j,m_j}(E_i)$  for particular individual ( $\nu, j, m_j$ ) states (see Fig. 4.4) on the  $S_0$  curves computed with QD and with QCT dynamics. Especially at low  $\langle E_i \rangle$  the QD  $S_0$  are considerably larger than their QCT counterparts (by 80% and 32% at  $\langle E_i \rangle = 5.1$  and 6 kcal/mol, respectively, decreasing to only 5% at 9.4 kcal/mol). As a result, the QD  $S_0$  curve is shifted towards lower values of the average incidence energy than the QCT curve, with the value of the energy shift decreasing towards larger  $\langle E_i \rangle$ . As a result of the decreasing value, the difference in the curves cannot really be quantified well with the single average value of the energy shift (0.11 kcal/mol). The computed energy shifts are substantially smaller than the accepted criterion of chemical accuracy (which is 1.0 kcal/mol). Nevertheless it should still be good to correct for quantum effects and artifacts of the QCT method (i.e., zero-point energy conversion lack of quantization once a trajectory has been started) once comparisons with experiments are made to enable maximally reliable conclusions regarding the accuracy of the electronic structure approach used to generate the PES in the dynamics. However, it is important to note that quantum corrections to the sticking curve are not likely to have a big effect on the evaluation of the accuracy of an electronic structure method through the usual procedure, in which computed and measured sticking probability curves are obtained and the accuracy of the barrier is judged on the basis of the energy shift between these

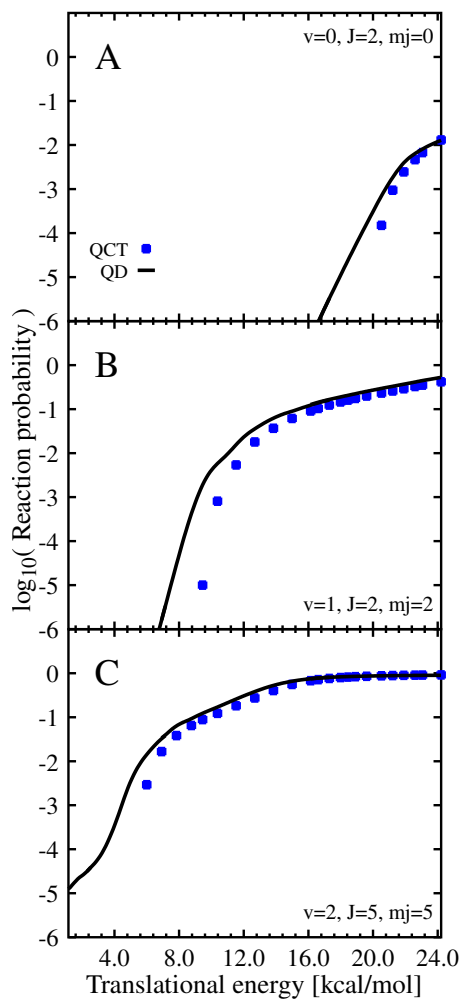


FIGURE 4.4:  $R_{\nu,j,m_j}(E_i)$  computed with QD (black line) and QCT (blue squares) dynamics are compared for three different initial rovibrational states, of which one with  $\nu=0$ , one with  $\nu=1$ , and one with  $\nu=2$ .

curves<sup>14,46,86,87</sup>.

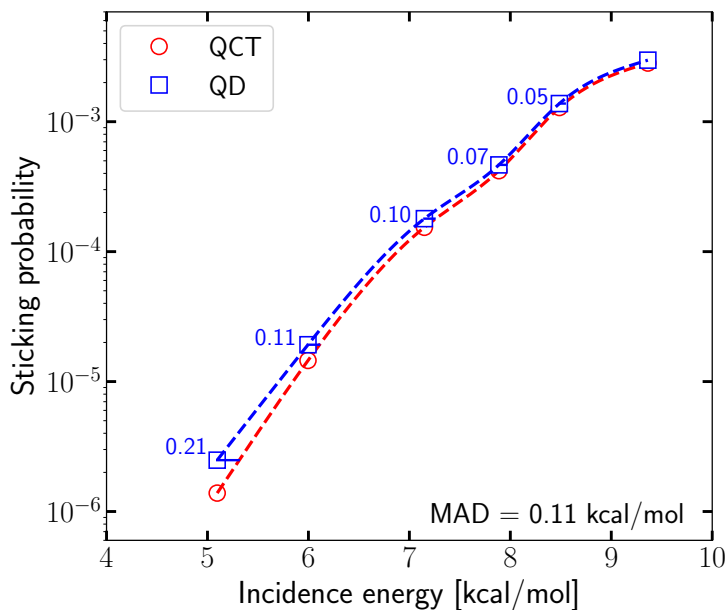


FIGURE 4.5: Sticking probabilities computed with QD (blue squares) and with QCT (red circles) dynamics using the PMC procedure are compared. The distances along the energy axis (in kcal/mol) between the QD sticking probabilities and the spline interpolated QCT sticking curve are also presented in blue.

### 4.3.3 Analysis of the size of the quantum effects on the sticking: role of vibration and incidence energy

It is interesting to note that the energy shifts between the QD and QCT curves in Fig. 4.5 appear as rather small, and that from this point of view the quantum effects on the sticking probability appear to be rather small at  $E_i$  much smaller than the minimum barrier to DC (24.8 kcal/mol). To explain this, we have analyzed our NMC QCT results in some detail. We have looked at the effect of the distributions of the initial vibrational state of  $H_2$  and of its  $E_i$ , where both are ultimately governed by the  $T_n$  used in the experiments using pure beams, as employed for  $H_2 + Al(110)$ <sup>20</sup>. Figure 4.6 shows the percentage contribution to  $S_0$  of  $H_2$  in specific initial vibrational states for the average incidence energies investigated here. At the lowest  $\langle E_i \rangle$  (5.1 eV) the sticking is dominated by  $\nu=1$   $H_2$ , and the sticking of  $\nu=2$   $H_2$  is much more important than the sticking of  $\nu=0$   $H_2$ . The reaction of  $\nu=1$   $H_2$  also dominates the sticking at  $\langle E_i \rangle =$



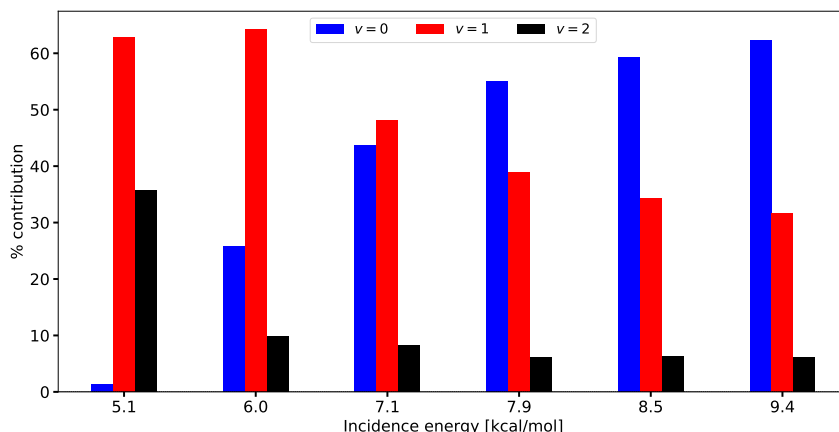


FIGURE 4.6: Histogram of the percentage contributions to  $S_0$  of  $H_2$  in its  $\nu=0$  (blue bars on the left),  $\nu=1$  (green bars in the middle), and  $\nu=2$  (red bars on the right) vibrational states to the sticking at the six different average incidence energies shown.

6.0 and 7.15 eV, and it remains important even at higher  $E_i$ . Part of the reason for the small quantum effects as perceived here may therefore be that a small fraction of the  $H_2$  molecules is incident in high initial vibrational states, which may help them to react in a classical "over the barrier" fashion without the need for tunneling. We note that experiments were able to show that the activated sticking of  $H_2$  on Cu(111) is dominated by DC of  $H_2$  in its  $\nu=1$  state, and at very low  $E_i$  by DC of  $H_2$  in its  $\nu=2$  state<sup>21</sup>, and this might likewise explain why differences between QCT and QC values of  $S_0$  were found to be small for this system as well<sup>32</sup>. Similarly, calculations on experiments on  $D_2 + Ag(111)$  (with an even higher barrier of 31.8 kcal/mol) suggested that the sticking in this system should be dominated by  $\nu=3$   $D_2$  for  $\langle E_i \rangle = 11.2$  kcal/mol<sup>88</sup>. Note that the extent to which the sticking in DC on a surface is dominated by the contribution of the molecule in a particular vibrational state should also depend on the distribution of the translational energy of the incident beam, and not just on the characteristics of the DC system itself.

The role of  $E_i$  is addressed in more detail Fig.4.7. For three values of  $T_n$  (corresponding to  $\langle E_i \rangle = 5.1, 7.9,$  and  $9.4$  kcal/mol) the percentage contribution to the sticking of  $H_2$  in a particular vibrational state  $\nu$  is shown of the  $H_2$  molecules incident in four ranges of  $E_i$ , which are indicated in eV. The minimum barrier height in the PES (24.8 kcal/mol) is approximately equal to 1.08 eV. At  $\langle E_i \rangle = 7.9,$  and  $9.4$  kcal/mol most  $\nu=0$  molecules react with  $E_i$  in excess of the TS energy (i.e., at  $E_i > 1.10$  eV), and most  $\nu=1$  molecules

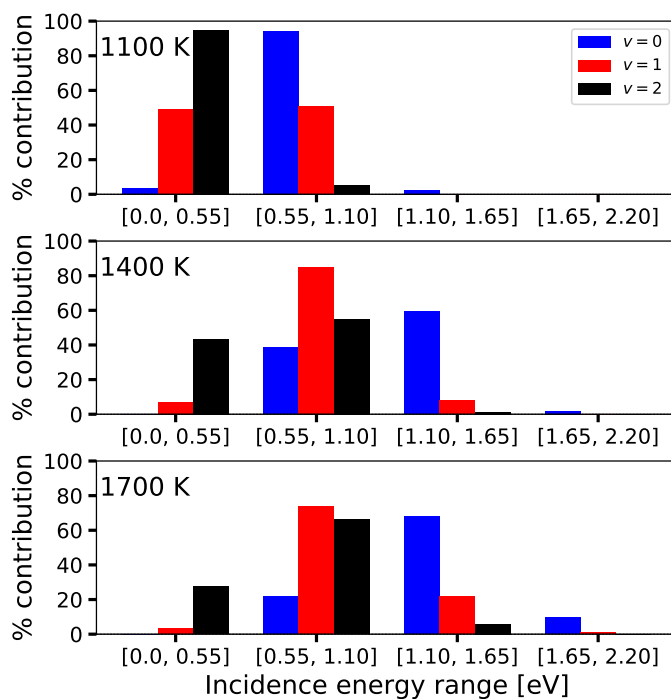


FIGURE 4.7: Histogram of the percentage contributions of  $\text{H}_2$  incident in four ranges of incidence energies to the reaction of  $\text{H}_2$  in a particular initial vibrational state  $\nu$ , for  $\nu=0$  (red bars on the left),  $\nu=1$  (green bars in the middle), and  $\nu=2$  (blue bars on the right) in the sticking at three different nozzle temperatures.

react with  $E_i > 0.55$  eV. At these conditions most of the  $\nu=0$  molecules that react in the QCT calculations are thus able to do so in a classical fashion with an incidence energy that exceeds the classical barrier height. That they are able to do so is related to the widths of the translational energy distributions in the experiments. As Fig.4.8 shows, the 1400 and 1700 K beams still have a considerable fraction (relative to the computed values of  $S_0$ , see Fig.4.3) of molecules in them with  $E_i$  exceeding the classical barrier height of 24.8 kcal/mol.

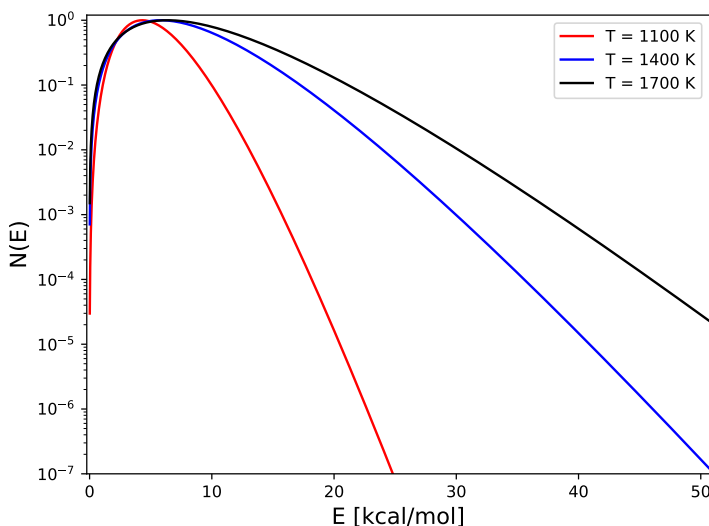


FIGURE 4.8: Flux-weighted translational energy distributions corresponding to the velocity distribution expression of Eq.4.6, as determined from Ref<sup>45</sup>. for the conditions corresponding to  $T_n = 1100, 1400,$  and  $1700$  K ( $\langle E_i \rangle = 5.1, 7.9,$  and  $9.4$  kcal/mol).

The distributions have been rescaled to make their maximum coincide with 1.0.

Whereas at  $\langle E_i \rangle = 7.9,$  and  $9.4$  kcal/mol most  $\nu=0$  molecules react with  $E_i > 1.1$  eV, most  $\nu=1$  and  $\nu=2$  molecules react at smaller  $E_i$  under these conditions (see Fig.4.7). The extent to which the sticking is dominated by the DC of  $H_2$  in a particular vibrational state, and how this is related to incidence energy, depends on how efficiently pre-exciting the vibration of  $H_2$  promotes reaction relative to enhancing  $E_i$ . This can be expressed by the vibrational efficacy, which can be defined through<sup>22,37</sup>

$$\eta_\nu(R) = \frac{E_i^{\nu-1}(R) - E_i^\nu(R)}{E_{vib}(\nu) - E_{vib}(\nu-1)} \quad (4.23)$$

In Eq.4.23,  $E_i^\nu(R)$  is the incidence energy for which  $R_{\nu,j=0}(E_i)$  first becomes equal to  $R$ , and  $E_{vib}(\nu)$  is the vibrational energy of the molecule in the state

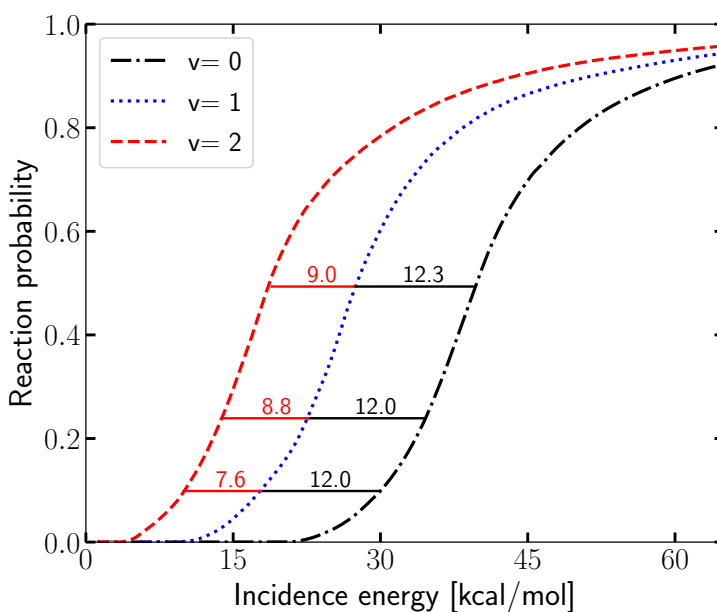


FIGURE 4.9: The initial-state selected reaction probability for the  $(\nu, j=0)$  state of  $\text{H}_2$  is shown as a function of  $E_i$  for  $\nu=0, 1,$  and  $2$ , indicating energy spacings between the curves (in kcal/mol) for values of the reaction probability of 0.1, 0.25, and 0.5.

$\nu$ . To illustrate the vibrational efficacy in the  $\text{H}_2 + \text{Al}(110)$  system, we show  $R_{\nu,j=0}(E_i)$  in Fig. 4.9 for  $\nu = 0, 1, \text{ and } 2$ , and vibrational efficacies are presented in Table 4.4. For  $\nu=1$  the vibrational efficacy exceeds 1, although it is smaller than the vibrational efficacy computed for  $D_2$  on  $\text{Ag}(111)$  for  $R = 0.24$ , which was equal to 1.37<sup>88</sup>. As also discussed for  $D_2 + \text{Ag}(111)$  in Ref.<sup>88</sup> and analyzed in detail in Ref.<sup>89</sup>, vibrational efficacies  $> 1$  show that, in the lower vibrational state (here in  $\nu=0$ ), the molecule has to come in at such high  $E_i$  in order to react that it cannot follow the minimum energy path and skids off it<sup>90,91</sup>. As a result, it must cross the "mountain pass" from the reactant to the product "valley" at a higher point than the optimum, lowest one. This effect has previously been called the bobsled effect<sup>92</sup>. The high efficiency with which  $\nu=1$   $\text{H}_2$  is able to react on  $\text{Al}(110)$  helps with explaining why quantum effects on the sticking in this system are so small for low  $S_0$ : thanks to the high vibrational efficacy  $\nu=1$   $\text{H}_2$  can react in a classical over the barrier type fashion at relatively low incidence energies. An additional reason that quantum effects on the sticking should be relatively small for the experiments performed by Rendulic and co-workers is that the translational energy distributions of their molecular beams are broad<sup>45</sup>, also when compared to  $\text{H}_2$  beams used by other groups, as discussed in Refs.<sup>46,93</sup>. As a result, especially at higher  $T_n$  a sizeable fraction of the incident molecules in the high-energy tail of the beam have a high enough  $E_i$  to react in in a classical fashion.

TABLE 4.4: Vibrational efficacies for DC of  $\text{H}_2$  on  $\text{Al}(110)$ .

	$\eta_\nu(R = 0.1)$	$\eta_\nu(R = 0.25)$	$\eta_\nu(R = 0.5)$
$\nu=0$	1.01	1.01	1.03
$\nu=1$	0.67	0.78	0.80

## 4.4 Conclusions

We evaluate the accuracy of the QCT method, or, alternatively, the importance of quantum effects for the sticking of  $\text{H}_2$  on  $\text{Al}(110)$ , for conditions that should be close to the conditions under which molecular beam experiments have been done on this system<sup>20</sup>. For this purpose, QCT and QD calculations have been done with the BOSS model on a PES obtained with DFT, which exhibits a minimum barrier height close to that recently obtained with QMC calculations<sup>41</sup>. To keep the number of QD calculations to be performed small, a procedure (PMC) was used in which Monte-Carlo averaging over the initial rovibrational

states of H<sub>2</sub> was employed. This procedure allowed the quasi-classical calculation of sticking probabilities with a relative error < 7.5% for 5 of the six initial conditions investigated, and of 16% for one of these conditions, at approximately an order of magnitude less computation time.

The sticking probabilities computed with QD using the PMC procedure exceed the ones computed with the QCT method by 80 and 30% for the two beam conditions corresponding to the lowest incidence energies (5.1 and 6.0 kcal/mol), decreasing to only 5% for the highest incidence energy of 9.4 kcal/mol. The sticking probability curve computed with QD is shifted to lower energies relative to the QCT curve by 0.21 to 0.05 kcal/mol, with the highest shift obtained for the lowest incidence energy. These "quantum effects" may be viewed as being rather small for molecular beam sticking experiments in which the average incidence energies (5.1-8.5 kcal/mol) are much smaller than the minimum barrier height of the system investigated (24.8 kcal/mol). The smallness of the quantum effects are explained on the basis of the large vibrational efficacy of the system ( $> 1$  for  $\nu=1$ ) and on the broadness of the translational energy distributions of the molecular beams used in the experiments we address, which mean that sticking can take place through DC of vibrationally excited molecules in the high incidence energy tails of the molecular beams. We conclude that "quantum effects" are not expected to play a major role in calculations that would evaluate the accuracy of electronic structure methods for determining the minimum barrier height to DC for H<sub>2</sub> + Al(110) on the basis of existing molecular beam experiments, as the verdict would depend on the energy shift between the computed and the measured sticking probability curve. However, for maximum reliability of the conclusions on accuracy it would still be good to take the quantum effects into account, as the maximum shift (0.21 kcal/mol) is not negligible on the scale of "chemical accuracy" (1 kcal/mol).

## References

- (1) Wolcott, C. A.; Medford, A. J.; Studt, F.; Campbell, C. T. Degree of rate control approach to computational catalyst screening. *J. Catal.* **2015**, *330*, 197–207.
- (2) Sabbe, M. K.; Reyniers, M.-F.; Reuter, K. First-principles kinetic modeling in heterogeneous catalysis: an industrial perspective on best-practice, gaps and needs. *Catal. Sci. Technol.* **2012**, *2*, 2010–2024.
- (3) Ertl, G. Primary steps in catalytic synthesis of ammonia. *J. Vac. Sci. Technol., A: Vacuum, Surfaces, and Films* **1983**, *1*, 1247–1253.
- (4) Chorkendorff, I.; Niemantsverdriet, J. W., *Concepts of modern catalysis and kinetics*; Wiley Online Library: 2003; Vol. 138.
- (5) Noyori, R. Synthesizing our future. *Nat. Chem.* **2009**, *1*, 5–6.
- (6) Pribram-Jones, A.; Gross, D. A.; Burke, K. DFT: A theory full of holes? *Annu. Rev. Phys. Chem.* **2015**, *66*, 283–304.
- (7) Goerigk, L.; Hansen, A.; Bauer, C.; Ehrlich, S.; Najibi, A.; Grimme, S. A look at the density functional theory zoo with the advanced GMTKN55 database for general main group thermochemistry, kinetics and noncovalent interactions. *Phys. Chem. Chem. Phys.* **2017**, *19*, 32184–32215.
- (8) Mardirossian, N.; Head-Gordon, M. Thirty years of density functional theory in computational chemistry: an overview and extensive assessment of 200 density functionals. *Mol. Phys.* **2017**, *115*, 2315–2372.
- (9) Morgante, P.; Peverati, R. ACCDB: A collection of chemistry databases for broad computational purposes. *J. Comput. Chem.* **2019**, *40*, 839–848.
- (10) Peverati, R.; Truhlar, D. G. Quest for a universal density functional: the accuracy of density functionals across a broad spectrum of databases in chemistry and physics. *Philos. Trans. R. Soc., A* **2014**, *372*, 20120476.
- (11) Mallikarjun Sharada, S.; Bligaard, T.; Luntz, A. C.; Kroes, G. J.; Nørskov, J. K. SBH10: A benchmark database of barrier heights on transition metal surfaces. *J. Phys. Chem. C* **2017**, *121*, 19807–19815.
- (12) **Tchakoua, T.**; Gerrits, N.; Smeets, E. W. F.; Kroes, G. J. SBH17: Benchmark Database of Barrier Heights for Dissociative Chemisorption on Transition Metal Surfaces. *J. Chem. Theory Comput.* **2023**, *19*, 245–270.
- (13) Araujo, R. B.; Rodrigues, G. L.; Dos Santos, E. C.; Pettersson, L. G. Adsorption energies on transition metal surfaces: towards an accurate and balanced description. *Nature Commun.* **2022**, *13*, 1–14.

- (14) Kroes, G. J. Computational approaches to dissociative chemisorption on metals: towards chemical accuracy. *Phys. Chem. Chem. Phys.* **2021**, *23*, 8962–9048.
- (15) Klippenstein, S. J.; Pande, V. S.; Truhlar, D. G. Chemical kinetics and mechanisms of complex systems: a perspective on recent theoretical advances. *J. Am. Chem. Soc.* **2014**, *136*, 528–546.
- (16) Karikorpi, M.; Holloway, S.; Henriksen, N.; Nørskov, J. K. Dynamics of molecule-surface interactions. *Surf. Sci.* **1987**, *179*, L41–L48.
- (17) Gostein, M.; Sitz, G. O. Rotational state-resolved sticking coefficients for H<sub>2</sub> on Pd (111): testing dynamical steering in dissociative adsorption. *J. Chem. Phys.* **1997**, *106*, 7378–7390.
- (18) Anger, G.; Winkler, A.; Rendulic, K. Adsorption and desorption kinetics in the systems H<sub>2</sub>/Cu(111), H<sub>2</sub>/Cu(110) and H<sub>2</sub>/Cu(100). *Surf. Sci.* **1989**, *220*, 1–17.
- (19) Berger, H.; Leisch, M.; Winkler, A.; Rendulic, K. A search for vibrational contributions to the activated adsorption of H<sub>2</sub> on copper. *Chem. Phys. Lett.* **1990**, *175*, 425–428.
- (20) Berger, H. F.; Rendulic, K. D. An investigation of vibrationally assisted adsorption: the cases H<sub>2</sub>/Cu(110) and H<sub>2</sub>/Al(110). *Surf. Sci.* **1991**, *253*, 325–333.
- (21) Rettner, C.; Michelsen, H.; Auerbach, D. Quantum-state-specific dynamics of the dissociative adsorption and associative desorption of H<sub>2</sub> at a Cu(111) surface. *J. Chem. Phys.* **1995**, *102*, 4625–4641.
- (22) Michelsen, H.; Rettner, C.; Auerbach, D.; Zare, R. Effect of rotation on the translational and vibrational energy dependence of the dissociative adsorption of D<sub>2</sub> on Cu(111). *J. Chem. Phys.* **1993**, *98*, 8294–8307.
- (23) Luntz, A. C.; Brown, J. K.; Williams, M. D. Molecular beam studies of H<sub>2</sub> and D<sub>2</sub> dissociative chemisorption on Pt(111). *J. Chem. Phys.* **1990**, *93*, 5240–5246.
- (24) Cottrell, C.; Carter, R. N.; Nesbitt, A.; Samson, P.; Hodgson, A. Vibrational state dependence of D<sub>2</sub> dissociation on Ag(111). *J. Chem. Phys.* **1997**, *106*, 4714–4722.
- (25) Groot, I. M. N.; Ueta, H.; Van der Niet, M. J. T. C.; Kleyn, A. W.; Juurlink, L. B. F. Supersonic molecular beam studies of dissociative adsorption of H<sub>2</sub> on Ru(0001). *J. Chem. Phys.* **2007**, *127*, 244701.



- (26) Cao, K.; van Lent, R.; Kleyn, A.; Juurlink, L. A molecular beam study of D<sub>2</sub> dissociation on Pt (111): Testing SRP-DFT calculations. *Chem. Phys. Lett.* **2018**, *706*, 680–683.
- (27) Füchsel, G.; Cao, K.; Er, S.; Smeets, E. W.; Kleyn, A. W.; Juurlink, L. B.; Kroes, G. J. Anomalous Dependence of the Reactivity on the Presence of Steps: Dissociation of D<sub>2</sub> on Cu (211). *J. Phys. Chem. Lett.* **2018**, *9*, 170–175.
- (28) Karplus, M.; Porter, R. N.; Sharma, R. Exchange reactions with activation energy. I. Simple barrier potential for (H, H<sub>2</sub>). *J. Chem. Phys.* **1965**, *43*, 3259–3287.
- (29) Porter, R. N.; Raff, L. M. In *Dynamics of molecular collisions, Part B*, W. H. Miller, Ed. Plenum: New York; Springer: 1976, pp 1–52.
- (30) Kosloff, R. Time-dependent quantum-mechanical methods for molecular dynamics. *J. Phys. Chem.* **1988**, *92*, 2087–2100.
- (31) Pijper, E.; Kroes, G. J.; Olsen, R. A.; Baerends, E. J. Reactive and diffractive scattering of H<sub>2</sub> from Pt(111) studied using a six-dimensional wave packet method. *J. Chem. Phys.* **2002**, *117*, 5885–5898.
- (32) Smeets, E. W. F.; Kroes, G. J. Designing new SRP density functionals including non-local vdW-DF2 correlation for H<sub>2</sub>+Cu(111) and their transferability to H<sub>2</sub>+Ag(111), Au(111) and Pt(111). *Phys. Chem. Chem. Phys.* **2021**, *23*, 7875–7901.
- (33) Smeets, E. W. F.; Füchsel, G.; Kroes, G. J. Quantum dynamics of dissociative chemisorption of H<sub>2</sub> on the Stepped Cu(211) Surface. *J. Phys. Chem. C* **2019**, *123*, 23049–23063.
- (34) Groß, A. Reactions at surfaces studied by ab initio dynamics calculations. *Surf. Sci. Rep.* **1998**, *32*, 291–340.
- (35) Kroes, G. J. Six-dimensional quantum dynamics of dissociative chemisorption of H<sub>2</sub> on metal surfaces. *Prog. Surf. Sci.* **1999**, *60*, 1–85.
- (36) Kroes, G. J.; Somers, M. F. Six-dimensional dynamics of dissociative chemisorption of H<sub>2</sub> on metal surfaces. *J. Theor. Comput. Chem.* **2005**, *4*, 493–581.
- (37) Kroes, G. J.; Díaz, C. Quantum and classical dynamics of reactive scattering of H<sub>2</sub> from metal surfaces. *Chem. Soc. Rev.* **2016**, *45*, 3658–3700.
- (38) Busnengo, H.; Crespos, C.; Dong, W.; Rayez, J.; Salin, A. Classical dynamics of dissociative adsorption for a nonactivated system: The role of zero point energy. *J. Chem. Phys.* **2002**, *116*, 9005–9013.

- (39) Busnengo, H. F.; Pijper, E.; Somers, M.; Kroes, G.; Salin, A.; Olsen, R.; Lemoine, D.; Dong, W. Six-dimensional quantum and classical dynamics study of  $\text{H}_2$  ( $\nu=0$ ,  $J=0$ ) scattering from Pd(111). *Chem. Phys. Lett.* **2002**, *356*, 515–522.
- (40) Liu, Q.; Zhang, L.; Li, Y.; Jiang, B. Ring Polymer Molecular Dynamics in Gas–Surface Reactions: Inclusion of Quantum Effects Made Simple. *J. Phys. Chem. Lett.* **2019**, *10*, 7475–7481.
- (41) Powell, A. D.; Kroes, G. J.; Doblhoff-Dier, K. Quantum Monte Carlo calculations on dissociative chemisorption of  $\text{H}_2$ + Al (110): minimum barrier heights and their comparison to DFT values. *J. Chem. Phys.* **2020**, *153*, 224701.
- (42) Jiang, B.; Guo, H. Six-dimensional quantum dynamics for dissociative chemisorption of  $\text{H}_2$  and  $\text{D}_2$  on Ag (111) on a permutation invariant potential energy surface. *Phys. Chem. Chem. Phys.* **2014**, *16*, 24704–24715.
- (43) Smeets, E. W. F.; Kroes, G. J. Performance of Made Simple Meta-GGA Functionals with rVV10 Nonlocal Correlation for  $\text{H}_2$ + Cu(111),  $\text{D}_2$ +Ag(111),  $\text{H}_2$ +Au(111), and  $\text{D}_2$ +Pt(111). *J. Phys. Chem. C* **2021**, *125*, 8993–9010.
- (44) Wijzenbroek, M.; Helstone, D.; Meyer, J.; Kroes, G. J. Dynamics of  $\text{H}_2$  dissociation on the close-packed (111) surface of the noblest metal:  $\text{H}_2$ + Au(111). *J. Chem. Phys.* **2016**, *145*, 144701.
- (45) Berger, H. F., Ph.D. Thesis, Technische Universitat Graz, 1992.
- (46) Díaz, C.; Pijper, E.; Olsen, R. A.; Busnengo, H. F.; Auerbach, D. J.; Kroes, G. J. Chemically accurate simulation of a prototypical surface reaction:  $\text{H}_2$  dissociation on Cu(111). *Science* **2009**, *326*, 832–834.
- (47) Zhu, L.; Zhang, Y.; Zhang, L.; Zhou, X.; Jiang, B. Unified and transferable description of dynamics of  $\text{H}_2$  dissociative adsorption on multiple copper surfaces via machine learning. *Phys. Chem. Chem. Phys.* **2020**, *22*, 13958–13964.
- (48) Sementa, L.; Wijzenbroek, M.; van Kolck, B.; Somers, M.; Al-Halabi, A.; Busnengo, H. F.; Olsen, R. A.; Kroes, G. J.; Rutkowski, M. J.; Thewes, C.; Kleimeier, N. F.; Zacharias, H. Reactive scattering of  $\text{H}_2$  from Cu(100): comparison of dynamics calculations based on the specific reaction parameter approach to density functional theory with experiment. *J. Chem. Phys.* **2013**, *138* 4, 044708.

- (49) Busnengo, H.; Salin, A.; Dong, W. Representation of the 6D potential energy surface for a diatomic molecule near a solid surface. *J. Chem. Phys.* **2000**, *112*, 7641–7651.
- (50) Mondal, A.; Wijzenbroek, M.; Bonfanti, M.; Díaz, C.; Kroes, G. J. Thermal lattice expansion effect on reactive scattering of H<sub>2</sub> from Cu(111) at T<sub>s</sub> = 925 K. *J. Phys. Chem. A* **2013**, *117*, 8770–8781.
- (51) Wijzenbroek, M.; Somers, M. F. Static surface temperature effects on the dissociation of H<sub>2</sub> and D<sub>2</sub> on Cu(111). *J. Chem. Phys.* **2012**, *137*, 054703.
- (52) Smits, B.; Litjens, L. G.; Somers, M. F. Accurate Description of the Quantum Dynamical Surface Temperature Effects on the Dissociative Chemisorption of H<sub>2</sub> from Cu (111). *J. Chem. Phys.* **2022**, *156*, 214706.
- (53) Nattino, F.; Díaz, C.; Jackson, B.; Kroes, G. J. Effect of surface motion on the rotational quadrupole alignment parameter of D<sub>2</sub> reacting on Cu(111). *Phys. Rev. Lett.* **2012**, *108*, 236104.
- (54) Sexl, T. Ergänzung zu B. Baule "Theoretische Behandlung der Erscheinungen in verdünnten Gasen". *Annalen der Physik* **1926**, *385*, 515–523.
- (55) Bonfanti, M.; Díaz, C.; Somers, M. F.; Kroes, G. J. Hydrogen dissociation on Cu(111): the influence of lattice motion. Part I. *Phys. Chem. Chem. Phys.* **2011**, *13*, 4552–4561.
- (56) Bonfanti, M.; Somers, M. F.; Díaz, C.; Busnengo, H. F.; Kroes, G. J. 7D quantum dynamics of H<sub>2</sub> scattering from Cu(111): the accuracy of the phonon sudden approximation. *Z. Phys. Chem.* **2013**, *227*, 1397–1420.
- (57) Hohenberg, P.; Kohn, W. Inhomogeneous electron gas. *Phys. Rev.* **1964**, *136*, B864–B871.
- (58) Kohn, W.; Sham, L. J. Self-consistent equations including exchange and correlation effects. *Phys. Rev.* **1965**, *140*, A1133–A1138.
- (59) Perdew, J. P.; Burke, K.; Ernzerhof, M. Generalized Gradient Approximation Made Simple. *Phys. Rev. Lett.* **1996**, *77*, 3865–3868.
- (60) Hammer, B. H. L. B.; Hansen, L. B.; Nørskov, J. K. Improved adsorption energetics within density-functional theory using revised Perdew-Burke-Ernzerhof functionals. *Phys. Rev. B* **1999**, *59*, 7413–7421.
- (61) Lee, K.; Murray, É. D.; Kong, L.; Lundqvist, B. I.; Langreth, D. C. Higher-accuracy van der Waals density functional. *Phys. Rev. B* **2010**, *82*, 081101.

- (62) **Tchakoua, T.**; Powell, A. D.; Gerrits, N.; Somers, M. F.; Doblhoff-Dier, K.; Busnengo, H. F.; Kroes, G. J. Simulating highly activated sticking of H<sub>2</sub> on Al(110): Quantum versus quasi-classical dynamics. *J. Phys. Chem. C* **2023**, *127*, 1932–7447.
- (63) Kresse, G.; Joubert, D. From ultrasoft pseudopotentials to the projector augmented-wave method. *Phys. Rev. B* **1999**, *59*, 1758–1775.
- (64) Blöchl, P. E. Projector augmented-wave method. *Phys. Rev. B* **1994**, *50*, 17953–17979.
- (65) Methfessel, M. P. A. T.; Paxton, A. T. High-precision sampling for Brillouin-zone integration in metals. *Phys. Rev. B* **1989**, *40*, 3616–3621.
- (66) Kresse, G.; Furthmüller, J. Efficient iterative schemes for ab initio total-energy calculations using a plane-wave basis set. *Phys. Rev. B* **1996**, *54*, 11169.
- (67) Salin, A. Theoretical study of hydrogen dissociative adsorption on the Cu (110) surface. *J. Chem. Phys.* **2006**, *124*, 104704.
- (68) Michelsen, H. A.; Auerbach, D. J. A critical examination of data on the dissociative adsorption and associative desorption of hydrogen at copper surfaces. *J. Chem. Phys.* **1991**, *94*, 7502–7520.
- (69) Auerbach, D. Atomic and Molecular Beam Methods. *G. Scoles, Oxford Univ. Press, New York* **1988**, Vol. 1, 362–379.
- (70) Rendulic, K.; Anger, G.; Winkler, A. Wide range nozzle beam adsorption data for the systems H<sub>2</sub>/nickel and H<sub>2</sub>/Pd(100). *Surf. Sci.* **1989**, *208*, 404–424.
- (71) Gallagher, R. J.; Fenn, J. B. Rotational relaxation of molecular hydrogen. *J. Chem. Phys.* **1974**, *60*, 3492–3499.
- (72) Kosloff, R. Time-dependent quantum-mechanical methods for molecular dynamics. *J. Phys. Chem. C* **1988**, *92*, 2087–2100.
- (73) Kosloff, D.; Kosloff, R. A Fourier method solution for the time dependent Schrödinger equation as a tool in molecular dynamics. *J. Comput. Phys.* **1983**, *52*, 35–53.
- (74) Corey, G. C.; Lemoine, D. Pseudospectral method for solving the time-dependent Schrödinger equation in spherical coordinates. *J. Chem. Phys.* **1992**, *97*, 4115–4126.
- (75) Lemoine, D. The finite basis representation as the primary space in multidimensional pseudospectral schemes. *J. Chem. Phys.* **1994**, *101*, 10526–10532.

- (76) Feit, M.; Fleck Jr, J.; Steiger, A. Solution of the Schrödinger equation by a spectral method. *J. Comput. Phys.* **1982**, *47*, 412–433.
- (77) Vibok, A.; Balint-Kurti, G. Parametrization of complex absorbing potentials for time-dependent quantum dynamics. *J. Phys. Chem.* **1992**, *96*, 8712–8719.
- (78) Balint-Kurti, G. G.; Dixon, R. N.; Marston, C. C. Grid methods for solving the Schrödinger equation and time dependent quantum dynamics of molecular photofragmentation and reactive scattering processes. *Int. Rev. Phys. Chem.* **1992**, *11*, 317–344.
- (79) Mowrey, R. C.; Kroes, G. J. Application of an efficient asymptotic analysis method to molecule–surface scattering. *J. Chem. Phys.* **1995**, *103*, 1216–1225.
- (80) Neuhauser, D.; Baer, M.; Judson, R. S.; Kouri, D. J. The application of time-dependent wavepacket methods to reactive scattering. *Comput. Phys. Commun.* **1991**, *63*, 460–481.
- (81) Zhang, D. H.; Zhang, J. Z. Full-dimensional time-dependent treatment for diatom–diatom reactions: The  $\text{H}_2 + \text{OH}$  reaction. *J. Chem. Phys.* **1994**, *101*, 1146–1156.
- (82) Stoer, J.; Bulirsch, R., *Introduction to numerical analysis*; Springer Science & Business Media: 1980.
- (83) Bulirsch, R.; Stoer, J. Numerical treatment of ordinary differential equations by extrapolation methods. *Numer. Math* **1966**, *8*, 1–13.
- (84) Marston, C. C.; Balint-Kurti, G. G. The Fourier grid Hamiltonian method for bound state eigenvalues and eigenfunctions. *J. Chem. Phys.* **1989**, *91*, 3571–3576.
- (85) Wijzenbroek, M.; Klein, D. M.; Smits, B.; Somers, M. F.; Kroes, G. J. Performance of a Non-Local van der Waals Density Functional on the Dissociation of  $\text{H}_2$  on Metal Surfaces. *J. Phys. Chem. A* **2015**, *119*, 12146–12158.
- (86) Nattino, F.; Migliorini, D.; Kroes, G. J.; Dombrowski, E.; High, E. A.; Killelea, D. R.; Utz, A. L. Chemically accurate simulation of a polyatomic molecule-metal surface reaction. *J. Phys. Chem. Lett.* **2016**, *7*, 2402–2406.

- (87) Migliorini, D.; Chadwick, H.; Nattino, F.; Gutiérrez-González, A.; Dombrowski, E.; High, E. A.; Guo, H.; Utz, A. L.; Jackson, B.; Beck, R. D.; Kroes, G. J. Surface reaction barriometry: methane dissociation on flat and stepped transition-metal surfaces. *J. Phys. Chem. Lett.* **2017**, *8*, 4177–4182.
- (88) Nour Ghassemi, E.; Somers, M.; Kroes, G. J. Test of the transferability of the specific reaction parameter functional for  $\text{H}_2 + \text{Cu}(111)$  to  $\text{D}_2 + \text{Ag}(111)$ . *J. Phys. Chem. C* **2018**, *122*, 22939–22952.
- (89) Gerrits, N.; Shakouri, K.; Behler, J.; Kroes, G. J. Accurate probabilities for highly activated reaction of polyatomic molecules on surfaces using a high-dimensional neural network potential:  $\text{CHD}_3 + \text{Cu}(111)$ . *J. Phys. Chem. Lett.* **2019**, *10*, 1763–1768.
- (90) Díaz, C.; Olsen, R. A note on the vibrational efficacy in molecule-surface reactions. *J. Chem. Phys.* **2009**, *130*, 094706.
- (91) Smith, R. R.; Killelea, D. R.; DelSesto, D. F.; Utz, A. L. Preference for vibrational over translational energy in a gas-surface reaction. *Science* **2004**, *304*, 992–995.
- (92) Levine, R. *Molecular Reaction Dynamics*, Cambridge University Press, 2005.
- (93) Ghassemi, E. N.; Somers, M. F.; Kroes, G. J. Assessment of Two Problems of Specific Reaction Parameter Density Functional Theory: Sticking and Diffraction of  $\text{H}_2$  on  $\text{Pt}(111)$ . *J. Phys. Chem. C* **2019**, *123*, 10406–10418.

# 5

## Constructing Mixed Density Functionals for Describing Dissociative Chemisorption on Metal Surfaces: Basic Principles

This Chapter is based on:

**Tchakoua, T.;** Jansen, T.; van Nies, Y.; van den Elshout, R.; van Boxmeer, B. A. B.; Poort, S. P.; Ackermans, M. G.; Beltrão, G. S.; Hildebrand, S. A.; Beekman, S. E. J.; van der Drift, T.; Kaart, S.; Santić, A.; Somers, M. F.; Kroes, G. J. Constructing mixed density functionals for describing dissociative chemisorption on metal surfaces: some basic principles. *J. Phys. Chem. C* **Submitted**

### Abstract

We investigate the ability of mixed, parameterized density functionals combining exchange at the generalized gradient approximation (GGA) level with either GGA or non-local correlation to reproduce barrier heights for dissociative chemisorption on metal surfaces. For this, seven expressions of such mixed density functionals are tested on a database consisting of results for 16 systems taken from a recently published slightly larger database called SBH17. Three expressions are derived that exhibit high tunability and use correlation functionals that are either of the GGA form or of two limiting non-local forms also describing the attractive van der Waals interaction in an approximate way. We also find that, for mixed density functionals incorporating GGA correlation, the optimum fraction of repulsive GGA exchange obtained with a specific GGA density functional is correlated with the charge-transfer parameter, which is equal to the difference of the work function of the metal surface and the electron affinity of the molecule.

## 5.1 Introduction

Transition states formed by the barriers to dissociative chemisorption (DC) can exert a high degree of rate control over the rates of heterogeneously catalyzed reactions proceeding over metal surfaces<sup>1,2</sup>, such as ammonia production<sup>3,4</sup> and steam reforming<sup>5</sup>. It is therefore important to describe such barriers accurately. As discussed in several recent papers<sup>6,7</sup> (see also **Chapter 3**), it is not yet possible to use non-empirical present-day electronic structure theory to compute barriers for DC on metal surfaces with guaranteed chemical accuracy (errors  $\leq 1$  kcal/mol), although the development of an approach based on diffusion Monte-Carlo certainly holds promise in this respect<sup>8</sup>. Instead, success with achieving a chemically accurate description of DC on metals has so far been based on a semi-empirical approach<sup>6,9</sup>. Here, the specific reaction parameter (SRP) approach to density functional theory (DFT) is used to compute a potential energy surface (PES)<sup>9-15</sup> or to construct forces used in direct dynamics calculations<sup>16-19</sup>, and an empirical parameter in the functional used is tuned to achieve agreement between calculated and measured DC or "sticking" probabilities, as now documented extensively elsewhere<sup>6</sup>.

While the SRP-DFT approach has already been highly successful, it is also important to recognize that there have been some inadequacies in the approach used so far. An important shortcoming has been that the approach to picking an expression for the SRP functional has been rather ad hoc<sup>9-19</sup>. Approaches used so far have been (i) to take a weighted average of two exchange correlation (XC) functionals within the generalized gradient approximation (GGA)<sup>9,10</sup>, (ii) to take a weighted average of two exchange (X) functionals within the GGA and to combine the resulting X functional with a GGA correlation (C) functional<sup>20</sup>, (iii) as in (ii), but use a non-local C functional<sup>13,14,18,19</sup> also approximately describing the attractive van der Waals interaction<sup>21,22</sup> (see also **Chapter 2**), (iv) to take a GGA exchange functional that was designed to be tunable<sup>23</sup> and to combine it with non-local van der Waals correlation<sup>11,12</sup>, and (v) to use meta-GGA functionals either with semi-local correlation<sup>24</sup> or in combination with non-local correlation<sup>15</sup>.

The time is now ripe to address some basis issues in SRP functional construction, such as (i) can we use a generic expression of the density functional (DF) in such a way that the DF will usually work, and (ii) might it be possible to pick the expression in such a way that the tuning parameter (the "specific reaction parameter") can be made to correlate with a specific property of the system. Two recent and closely related developments ensure that the time is now right. The first is that a new database of dissociative chemisorption barrier heights has recently become available, which has been called the SBH17 database<sup>7</sup> (see also



**Chapter 3**). The database holds reference values of barrier heights to DC for 17 systems, in which  $\text{H}_2$ ,  $\text{N}_2$ , or  $\text{CH}_4$  dissociates over a metal surface. For 14 of these systems the barrier height was determined using SRP-DFT, while for 3 systems a more ad-hoc semi-empirical procedure was used to extract a barrier height from a comparison between theory and experiment<sup>7</sup> (see also **Chapter 3**). In a second development<sup>25</sup> it has become clear that the SRP-DFT approach based on GGA exchange functionals has its limits. So far this approach has only been successful for systems in which the charge transfer parameter  $\Delta E_{CT} = \text{WF} - \text{EA} > 7 \text{ eV}$ <sup>25</sup>. Here WF is the work function of the metal and EA is the electron affinity of the molecule. The SBH17 database therefore mostly contains systems for which this condition has been obeyed, which is the case for 16 out of the 17 systems<sup>7</sup>. For systems with  $\Delta E_{CT} < 7 \text{ eV}$  the use of even one of the most repulsive GGA X DFs, i.e., RPBE<sup>26</sup>, typically leads to underestimated barrier heights<sup>25</sup>.

Here we test several mixed DF expressions to see if we can derive one that works for all or most systems in the recently published database<sup>7</sup> we use here. We also test the suggestion implicit in Ref.<sup>25</sup> that the fraction of RPBE exchange needed in a mixed functional correlates with the value of the charge transfer parameter  $\Delta E_{CT}$  described above. Our Chapter is set up as follows: In Section 5.2, the Method Section, we give a short description of the database we use, which is essentially our previously published database with one system removed from it, in Section 5.2.1. Section 5.2.2 describes the DFs tested and Section 5.2.3 gives computational details. Section 5.3 presents our results, and conclusions are drawn in Section 5.4.

## 5.2 Methods

### 5.2.1 The SBH16 database

The DFs described in Section 5.2.2 have been tested on what we here call the SBH16 database, which is the recently described SBH17 database<sup>7</sup> (see also **Chapter 3**) with the  $\text{H}_2 + \text{Pt}(211)$  system removed from it. The reason that we left out the  $\text{H}_2 + \text{Pt}(211)$  system described here is that the results for this system are not that different from those for the  $\text{H}_2 + \text{Pt}(111)$  system also contained in the SBH17 system, so that not so much is to be gained by adding results for the  $\text{H}_2 + \text{Pt}(211)$  system to the results here presented. The SBH17 database holds results for 8  $\text{H}_2 + \text{metal surface}$  systems (SBH16 for 7 such systems), 2  $\text{N}_2 + \text{metal surface}$  systems, and 7  $\text{CH}_4 + \text{metal}$  systems. The reference values of the barrier heights for these systems and the most important geometrical parameters determining the barrier geometry of the molecule relative to the surface are all

presented in table 2 of Ref.<sup>7</sup> (see also table 3.2 of **Chapter 3**). **Chapter 3** also provides the references to the papers in which fuller descriptions of the barrier geometries and of how they were derived may be obtained.

A few details regarding the SBH17 database are important to this Chapter. One is that the barrier heights and geometries are in principle defined best for the 14 out of the 17 systems (13 in SBH16), for which the reference values were obtained with SRP-DFT. Results for three systems ( $\text{CH}_4 + \text{Ni}(100)$ ,  $\text{CH}_4 + \text{Ru}(0001)$ , and  $\text{N}_2 + \text{Ru}(10\bar{1}0)$ ) were obtained with more ad hoc semi-empirical procedures, as discussed in detail in **Chapter 3**. The result that, of the three systems for which on average the largest errors were found with the density functionals tested, two systems were among the systems for which more ad hoc semi-empirical procedures were used (i.e.,  $\text{CH}_4 + \text{Ru}(0001)$ , and  $\text{N}_2 + \text{Ru}(10\bar{1}0)$ ) is consistent with the lower accuracy anticipated for the ad hoc procedure (the third system for which the DFs tested were least accurate on average was  $\text{H}_2 + \text{Ag}(111)$ ). Finally, a useful number characterizing the SBH16 database is the average value of the absolute values of the barrier heights contained in it, which is 0.687 eV (15.9 kcal/mol).

## 5.2.2 Mixed density functional expressions

The XC part of DFs used as SRP-DFs have typically been taken as mixtures of the X and C components of standard XC DFs. This has the advantage that constraints enforced in constraint-based X and C DFs can also be enforced in SRP-DFs<sup>27</sup>. Based on previous experience, we test the following expressions for the exchange-correlation part of the mixed DFs:

$$E_{\text{XC}}^{\text{SRP}\mathbf{x}} = \mathbf{x}E_{\text{X}}^{\text{RPBE}} + (1 - \mathbf{x})E_{\text{X}}^{\text{PBE}} + E_{\text{C}}^{\text{PBE}} \quad (5.1)$$

$$E_{\text{XC}}^{\text{SRP}\mathbf{x}\text{sol}\mathbf{x}} = \mathbf{x}E_{\text{X}}^{\text{RPBE}} + (1 - \mathbf{x})E_{\text{X}}^{\text{PBEsol}} + E_{\text{C}}^{\text{PBE}} \quad (5.2)$$

$$E_{\text{XC}}^{\text{SRP}\mathbf{x}\text{-vdW}1} = \mathbf{x}E_{\text{X}}^{\text{RPBE}} + (1 - \mathbf{x})E_{\text{X}}^{\text{PBE}} + E_{\text{C}}^{\text{vdW-DF1}} \quad (5.3)$$

$$E_{\text{XC}}^{\text{SRP}\mathbf{x}\text{-vdW}2} = \mathbf{x}E_{\text{X}}^{\text{RPBE}} + (1 - \mathbf{x})E_{\text{X}}^{\text{PBE}} + E_{\text{C}}^{\text{vdW-DF2}} \quad (5.4)$$

$$E_{\text{XC}}^{\text{SRP}\mathbf{x}\text{sol}\mathbf{x}\text{-vdW}2} = \mathbf{x}E_{\text{X}}^{\text{RPBE}} + (1 - \mathbf{x})E_{\text{X}}^{\text{PBEsol}} + E_{\text{C}}^{\text{vdW-DF2}} \quad (5.5)$$

and

$$E_{\text{XC}}^{\text{SRP}\mathbf{x}\text{-vdW}1\text{-ext}} = E_{\text{XC}}^{\text{SRP}\mathbf{x}\text{-vdW}1}, \quad \text{if } \mathbf{x} \geq 0. \quad (5.6a)$$

$$E_{\text{XC}}^{\text{SRP}\mathbf{x}\text{-vdW}1\text{-ext}} = E_{\text{X}}^{\text{PBE}\alpha} + E_{\text{C}}^{\text{vdW-DF1}}, \quad \text{if } \mathbf{x} = (-1 + \alpha) < 0. \quad (5.6b)$$

and

$$E_{XC}^{SRP\mathbf{x}-vdW2-ext} = E_{XC}^{SRP\mathbf{x}-vdW2}, \quad \text{if } \mathbf{x} \geq 0. \quad (5.7a)$$

$$E_{XC}^{SRP\mathbf{x}-vdW2-ext} = E_X^{PBE\alpha} + E_C^{vdW-DF2}, \quad \text{if } \mathbf{x} = (-1 + \alpha) < 0. \quad (5.7b)$$

The  $E_{XC}^{SRP\mathbf{x}}$  DF of Eq.5.1 has been used to arrive at a reparameterized SRP DF for  $H_2 + Cu(111)$ <sup>20</sup>, the original version being a weighted average of the RPBE<sup>26</sup> and PW91<sup>28</sup> DFs<sup>9</sup>. In the limit  $\mathbf{x} = 0$  the DF defined by Eq.5.1 corresponds to the PBE<sup>29</sup> DF, and in the limit  $\mathbf{x} = 1$  it corresponds to the RPBE DF (which has the PBE C DF as the correlation part of its exchange-correlation functional<sup>26</sup>). The PBE DF may be seen as a faster and easier-to-evaluate version of PW91<sup>29</sup>. Choosing Eq.5.1 in attempts to derive an SRP DF for a DC-on-metal-surface system is in accordance with conventional wisdom that PBE often under-predicts and RPBE often over-predicts the barrier height for DC on a metal surface<sup>6</sup>.

A drawback of using Eq.5.1 is that with PBE the barrier height for DC on a metal surface may also be overestimated in specific cases, even though this DF has a negative mean signed error (MSE) of -58 meV for the SBH17 database<sup>7</sup>. For this database, overestimated (though often not by much) barrier heights were observed for a few weakly activated or non-activated  $H_2$ -metal systems ( $H_2 + Pt(111)$ ,  $Pt(211)$ , and  $Ru(0001)$ ), for  $H_2 + Ag(111)$ , and for a few  $CH_4 +$  metal surface systems ( $CH_4 + Ni(100)$ ,  $Pt(211)$ , and  $Ru(0001)$ ). To avoid this we replaced the X DF of PBE by the X DF of PBEsol<sup>30</sup>, which tends to yield lower barriers, this way obtaining the  $E_{XC}^{SRP\mathbf{x}sol}$  mixed DF of Eq.5.2. It should be noted that for  $\mathbf{x} = 0$   $E_{XC}^{SRP\mathbf{x}sol}$  does not equal the PBEsol functional, which employs the same expression for the C functional as PBE but uses a different value of a coefficient in it to balance the C part of PBEsol against its X part<sup>30</sup>. However, as we will show the use of  $E_{XC}^{SRP\mathbf{x}sol}$  comes with the advantage that where necessary it yields lower barrier heights for DC on metals than  $E_{XC}^{SRP\mathbf{x}}$ , and thus  $E_{XC}^{SRP\mathbf{x}sol}$  is more tunable than  $E_{XC}^{SRP\mathbf{x}}$ . Below, we will call the  $\mathbf{x} = 0$  limit of  $E_{XC}^{SRP\mathbf{x}sol}$  PBEsolc, to distinguish it from PBEsol.

A drawback of both Eqs.5.1 and 5.2 is that the attractive van der Waals interaction between molecule and surface is not described with a GGA correlation functional, even though this may be necessary for weakly activated DC of  $H_2$  on metals (where the barrier is usually at a fairly large molecule-surface distance so that a proper description of the van der Waals interaction may be important in spite of its weakness<sup>11,12</sup>) or for  $CH_4$  dissociating on a metal surface<sup>18,19</sup>. For this reason we also test the DFs of the forms  $E_{XC}^{SRP\mathbf{x}-vdW1}$  of Eq.5.3 and

$E_{XC}^{SRP\mathbf{x}-vdW2}$  of Eq.5.4, which contain the vdW-DF1 C functional<sup>21</sup> and the vdW-DF2 C functional<sup>22</sup>, respectively. The  $E_{XC}^{SRP\mathbf{x}-vdW1}$  functional has been used successfully to describe supersonic molecular beam experiments on CH<sub>4</sub> + Ni(111)<sup>18</sup>, Pt(111)<sup>19</sup>, and Pt(211)<sup>19</sup> and on H<sub>2</sub> + Ru(0001)<sup>13</sup>. The  $E_{XC}^{SRP\mathbf{x}-vdW2}$  functional has been used successfully to describe H<sub>2</sub> + Ru(0001)<sup>13</sup> and Ni(111)<sup>14</sup> (see also **Chapter 2**).

The DFs described by Eqs. 5.3 and 5.4 may have a similar problem as the DF described by Eq.5.1, i.e., that the barrier height is already overestimated with  $\mathbf{x} = 0$ , including PBE exchange only. For instance, the SRP-DF found for H<sub>2</sub> + Pt(111)<sup>11</sup> and Pt(211)<sup>12</sup> is given by  $E_{XC}^{PBE\alpha=0.57,vdW2} = E_X^{PBE\alpha=0.57} + E_C^{vdW-DF2}$ , where  $E_X^{PBE\alpha=0.57}$  is the inherently tunable PBE $\alpha$  X DF<sup>23</sup>, with  $\alpha = 0.57$ . As discussed by the developer of the PBE $\alpha$  X functional<sup>23</sup>, PBE $\alpha=1$  corresponds to the PBE functional, while PBE $\alpha=0.52$  is very similar to the X part of the WC functional<sup>31</sup>, which like PBEsol<sup>30</sup> was developed with a view to a better description of the solid state. The  $E_{XC}^{SRP\mathbf{x}-vdW2}$  with  $\mathbf{x} = 0$  (only PBE exchange) overestimates the barrier height for almost all systems in the SBH17 database. For this reason we have also tested the DF  $E_{XC}^{SRP\mathbf{x}sol-vdW2}$  of Eq.5.5, which for  $\mathbf{x} = 0$  consists of PBEsol exchange and the vdW-DF2 correlation functional. In this limit this DF is expected to yield low barriers like  $E_{XC}^{PBE\alpha=0.57,vdW2}$ .

To increase the tunability of a mixed DF expression like given by Eqs.5.1, 5.3, and 5.4, PBE exchange can be replaced by PBEsol exchange, as done in Eq.5.2 to obtain a better tunable DF than the DF of Eq.5.1, and in Eq.5.5 to obtain a better tunable DF than the DF of Eq.5.4. An alternative already implicitly used in the construction of SRP-DFs is to replace PBE exchange by PBE $\alpha$  exchange with  $\alpha < 1$ , as done to obtain  $E_{XC}^{SRP\mathbf{x}-vdW1-ext}$  of Eq.5.6 (which should be more tunable than  $E_{XC}^{SRP\mathbf{x}-vdW1}$  of Eq.5.3) and to obtain  $E_{XC}^{SRP\mathbf{x}-vdW2-ext}$  of Eq.5.7 (which should be more tunable than  $E_{XC}^{SRP\mathbf{x}-vdW2}$  of Eq.5.4). We have not made use of the possibility of the PBE $\alpha$  functional to interpolate between PBE and RPBE exchange, as the PBE $\alpha$  X functional corresponds to the RPBE X functional only in the limit  $\alpha \rightarrow \infty$ , which is a rather awkward limit to work with, and less preferred to a situation where switching from PBE to RPBE exchange can be performed by switching a parameter continuously from 0 to 1, as can be done in Eqs. 5.1, 5.3, and 5.4.

The DFs of Eqs. 5.1-5.5, 5.6a, and 5.7a have been evaluated for  $\mathbf{x} = 0$ ,  $n\Delta\mathbf{x}$  with  $n=1-9$ , and, and, and 1.0, modifying  $\mathbf{x}$  by steps  $\Delta\mathbf{x}$  equal to 0.1. The DFs of Eqs.5.6b and 5.7b have been evaluated for  $\alpha=0.57$  ( $\mathbf{x} = -0.43$ ),  $\alpha=0.70$  ( $\mathbf{x} = -0.30$ ), and  $\alpha=0.85$  ( $\mathbf{x} = -0.15$ ). For each system the best value of  $\mathbf{x}$  was defined for the DFs given by Eqs.5.1-5.7 as described in more detail below. If for the

resulting  $\mathbf{x}$  we have  $0.0 \leq \mathbf{x} \leq 1.0$  for a DF defined by one of the Eqs.5.1-5.5 the interpolation was successful and the DF expression can be used for the system considered. Similarly, if for the resulting  $\mathbf{x}$  we have  $-0.43 \leq \mathbf{x} \leq 1.0$  for a DF defined by one of the Eqs.5.6-5.7 the interpolation was successful and the DF expression can be used for the system considered. Otherwise, extrapolation was used, and the corresponding generic DF was found not to be able to describe the system successfully.

### 5.2.3 Computational details

The minimum barrier height is computed as

$$E_b = E_{TS} - E_{asym}. \quad (5.8)$$

In Eq.5.8  $E_{TS}$  is the energy of the system (molecule + surface) at the minimum barrier geometry, while  $E_{asym}$  is the energy of the system with the molecule in its equilibrium geometry at a distance from the surface such that molecule and surface no longer interact. In the so-called medium algorithm that we use, which is defined and explained in detail in **Chapter 3**, the surface is set up following DFT geometry optimizations of the bulk lattice (to determine the bulk lattice constant(s) with the DF used) and of the metal slab representing the surface (to determine interlayer spacings in the metal surface slab exposed to vacuum according to the DF used). The geometry of the molecule relative to the surface is taken from earlier SRP-DFT calculations as described in **Chapter 3** (see also table 3.2 of that Chapter). In the asymptotic geometry the equilibrium distance of the molecule is likewise computed with the DF tested<sup>7</sup>. A crucial point is that the surface is not allowed to relax with respect to the incoming molecule in the calculation of  $E_{TS}$ . A minor difference with **Chapter 3** is that in the present work the geometry optimization of the bulk representing the surface was done using the geometry optimization method implemented in VASP. In the earlier calculations of **Chapter 3**, a parabola was fitted to the energy of the bulk as a function of the lattice constant, and minimization used to establish the bulk lattice constant. The new approach led to small differences in the values of the barrier heights (of 10 meV or less) with respect to the early results when available for the particular DF tested.

All DFT calculations were performed with a user-modified version of the Vienna ab initio simulation package<sup>32-35</sup> (VASP5.4.4). We also used the Atomic Simulation Environment (ASE)<sup>36,37</sup> as a convenient interface package. All calculations using the vdW-DF1 or vdW-DF2 C functionals were done with the algorithm of Román-Pérez and Soler<sup>38</sup> to speed up their evaluation. All other details regarding the calculations (concerning the pseudo-potentials used, the

handling of spin-polarization in systems containing Ni, the number of metal layers in the slab representing the surface, the size of the surface unit cell, etc.) are the same as in **Chapter 3**, to which we refer for these details.

## 5.3 Results and discussion.

### 5.3.1 Equilibrium lattice constants computed with mixed density functionals

Equilibrium lattice constants computed with the mixed density functional expressions not incorporating the van der Waals interaction are shown in Table 5.A.1 of the Appendix, stepping through  $\boldsymbol{x}$  in SRP $\boldsymbol{x}$  and SRP $\boldsymbol{x}$ sol in steps of 0.1 (results for the other mixed DFs not shown). Comparing with zero-point energy corrected experimental values we obtain the usual result that the PBE DF somewhat underestimates and that RPBE overestimates lattice constants<sup>39,40</sup>. The PBEsolc DF (we recall that PBEsolc is the name we use for the DF with PBEsol exchange and PBE correlation) tends to somewhat underestimate the lattice constant. The PBEsol DF would be expected to do rather well for the lattice constant<sup>40</sup> and we suspect that PBEsolc somewhat underperforms as using PBE correlation with PBEsol exchange should lead to a somewhat unbalanced functional<sup>30</sup>. One might of course vary  $\boldsymbol{x}$  in the SRP $\boldsymbol{x}$ sol DF to obtain the correct lattice constant, but this is not likely to lead to the correct barrier height as GGA DFs yielding good molecule-surface interaction energies tend to overestimate metal lattice constants<sup>30,41</sup>.

### 5.3.2 Performance of limiting forms of the mixed density functionals

To get an impression of how the mixed density functional expressions will perform as generic expressions for fitting SRP functionals, it is a good idea to look at how their limiting forms perform and compare. For this we first consider the limiting forms of the mixed expressions not using van der Waals correlation functionals, i.e., SRP $\boldsymbol{x}$  (Eq.5.1) and SRP $\boldsymbol{x}$ sol (Eq.5.2), which are PBE and RPBE, and PBEsolc (we recall that this is the name we use for the DF with PBEsol exchange and PBE correlation) and RPBE. Figure 5.1 shows that for each system in the SBH16 database the barrier height obtained with PBE is lower than that obtained with RPBE, which correlates well with the finding that PBE often underestimates while RPBE often overestimates barrier heights<sup>6</sup>. Also, for each system in the SBH16 database the barrier height obtained with PBEsolc is lower than that obtained with PBE, suggesting that for the purpose of

fitting barrier heights the SRP $\boldsymbol{x}$ sol expression will be tunable over a wider range than the SRP $\boldsymbol{x}$  expression. The barrier heights computed with the PBEsolc, PBE, and RPBE functionals may also be found in Table 5.A.2 of the Appendix.

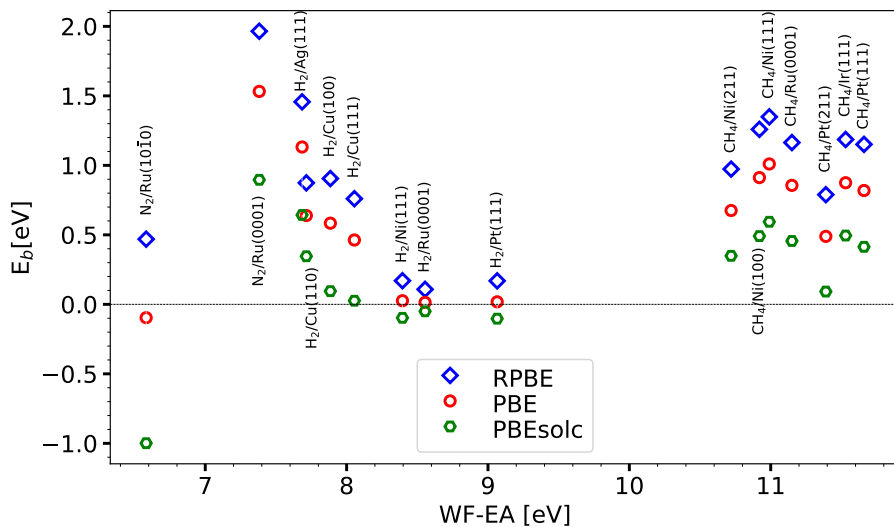


FIGURE 5.1: The barrier heights  $E_b$  computed with the PBEsolc, the PBE, and the RPBE DFs are shown as a function of the charge transfer parameter for the 16 systems present in the SBH16 database.

Barrier heights obtained for each system in the SBH16 database with the limiting forms of the SRP $\boldsymbol{x}$  (Eq.5.1), SRP $\boldsymbol{x}$ vdW1 (Eq.5.3), and SRP $\boldsymbol{x}$ -vdW2 (Eq.5.4) expressions are shown in Fig.5.2 for PBE, PBE-vdW1 and PBE-vdW2, and in Fig.5.3 for RPBE, RPBE-vdW1, and RPBE-vdW2. Whether PBE or PBE-vdW1 yields the lowest barrier height is seen to depend on the value of  $\Delta E_{CT}$ : for  $\Delta E_{CT} \leq 8.055$  eV, PBE yields the lowest barrier height, while for  $\Delta E_{CT} \geq 8.395$  eV, PBE-vdW1 yields the lowest barrier height. While this might look odd, one should remember that the correlation part of the vdW-DF1 functional is not just a van der Waals term that is added to an energy expression excluding the attractive dispersion interaction (e.g., the PBE energy). Rather, the vdW-DF1 correlation functional is a different correlation functional than the PBE correlation functional. There is thus no a priori reason that the PBE-vdW1 energy should always be lower than the PBE energy, or vice versa. Furthermore, the barrier obtained with PBE-vdW2 is almost always higher than that obtained with both PBE-vdW1 and PBE (only for  $\text{H}_2 + \text{Ru}(0001)$  is the barrier higher for PBE-vdW1 than for PBE-vdW2). The findings for RPBE, RPBE-vdW1,

and RPBE-vdW2 (Fig.5.3) are analogous to those for PBE, PBE-vdW1, and PBE-vdW2 (Fig.5.2). The barrier heights computed with the PBE, PBE-vdW1, PBE-vdW2 and RPBE functionals may be found in Table 5.A.2 of the Appendix, and the barrier heights computed with the RPBE-vdW1 and RPBE-vdW2 functionals may be found in Table 5.A.3 of the Appendix.

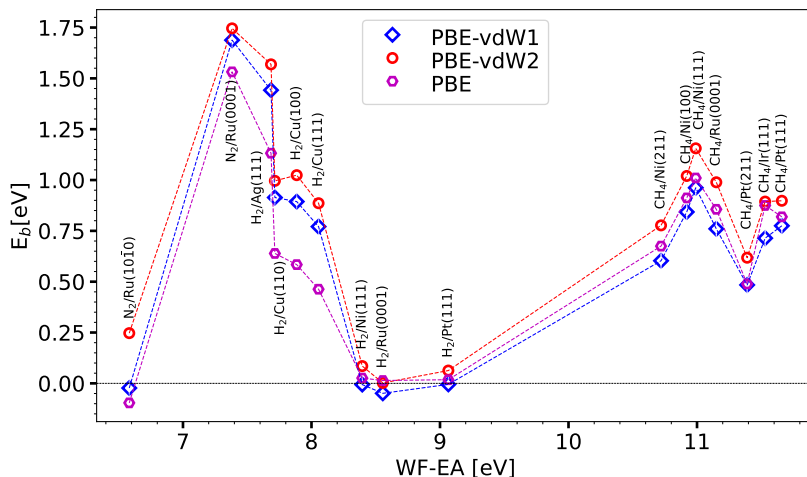


FIGURE 5.2: The barrier heights  $E_b$  computed with the PBE, the PBE-vdW1, and the PBE-vdW2 DFs are shown as a function of the charge transfer parameter for the 16 systems present in the SBH16 database.

Barrier heights obtained for each system in the SBH16 database with the lower-limit-forms of the SRP $\boldsymbol{x}$ sol (Eq.5.2) and SRP $\boldsymbol{x}$ sol-vdW2 (Eq.5.5) expressions are shown in Fig.5.4 for PBEsolc and PBEsolc-vdW2. As can be seen the barriers obtained with PBEsolc-vdW2 are always higher than those obtained with PBEsolc, suggesting that the SRP $\boldsymbol{x}$ sol-vdW2 DF may be slightly less tunable than the SRP $\boldsymbol{x}$ sol DF, which yields very low barriers. The barrier heights computed with the PBEsolc functional may be found in Table 5.A.2 of the Appendix, and the barrier heights computed with the PBEsolc-vdW2 functional may be found in Table 5.A.3 of the Appendix.

Finally, barrier heights obtained with the PBE $\alpha$ -vdW1 and PBE $\alpha$ -vdW2 DFs are compared in Fig.5.A.1 of the Appendix for  $\alpha = 0.57$ , which is the lowest value of  $\alpha$  used here. Figure 5.A.1 shows that the PBE $\alpha$ -vdW1 DF consistently yields lower barrier heights than the PBE $\alpha$ -vdW2 DF with  $\alpha = 0.57$ . This suggests that the PBE $\alpha$ -vdW1 DF is a better tunable mixed DF than the PBE $\alpha$ -vdW2



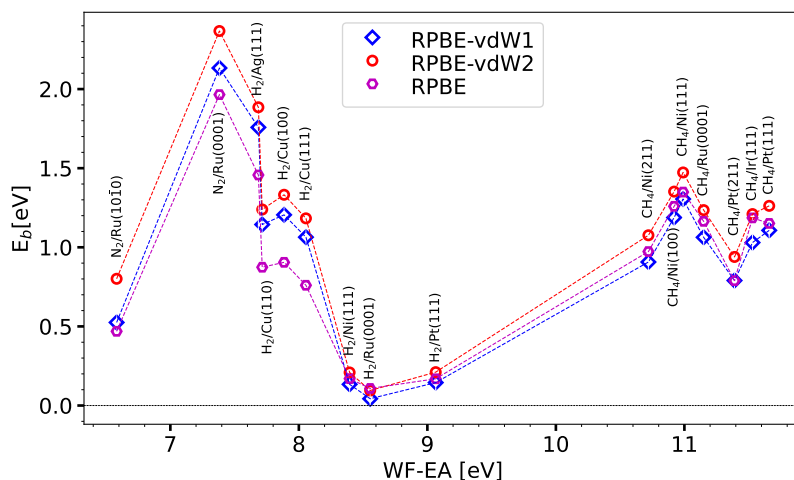


FIGURE 5.3: The barrier heights  $E_b$  computed with the RPBE, the RPBE-vdW1, and the RPBE-vdW2 DFs are shown as a function of the charge transfer parameter for the 16 systems present in the SBH16 database.

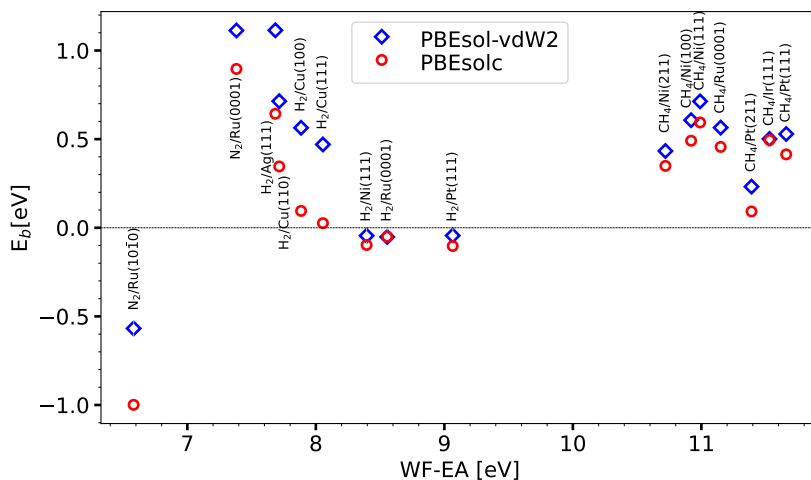


FIGURE 5.4: The barrier heights  $E_b$  computed with the PBEsolc and the PBEsol-vdW2 DFs are shown as a function of the charge transfer parameter for the 16 systems present in the SBH16 database.

DF, as the RPBE-vdW1 and RPBE-vdW2 DFs overestimate the barrier height

for each system in the SBH16 database (see the discussion of Table 5.1 below).

Table 5.1 shows mean absolute errors (MAEs) and mean signed errors (MSEs) for the SBH16 database, also comparing to the previous SBH17 results for those DFs that have previously been tested on this database<sup>7</sup>. Here the error for a specific system is defined as the difference between the barrier height computed here and the reference value tabulated in Ref.<sup>7</sup> for that system. As can be seen the MAEs and MSEs computed here for SBH16 differ from previous results known from SBH17 by no more than 10 meV, underscoring the reliability of the results presented here. As previously found, the PBE DF is the best performing DF in terms of the MAE, the MAE being lowest for the PBE DF. Importantly for this study, the DFs serving as upper limits for mixed DFs here (RPBE for SRP $\mathbf{x}$  of Eq.5.1 and SRP $\mathbf{x}$ sol of Eq.5.2, RPBE-vdW1 for SRP $\mathbf{x}$ -vdW1 of Eq.5.3 and for SRP $\mathbf{x}$ -vdW1-ext of Eqs.5.6, and RPBE-vdW2 for SRP $\mathbf{x}$ vdW2 of Eq.5.4, SRP $\mathbf{x}$ sol-vdW2 of Eq.5.5, and SRP $\mathbf{x}$ -vdW2-ext of Eq.5.7) all have their MSEs equal to their MAEs, suggesting that these DFs all systematically overestimate the barrier height. This is actually a good quality of a functional that is meant to serve as the upper-limit-form of a mixed DF. The PBEsolc DF, which is the lower-limit-form of the SRP $\mathbf{x}$ sol DF of Eq.5.2, shows a MSE that is equal to minus its MAE, suggesting that this DF systematically underestimates the barrier height. This is a good quality of a functional that is meant to serve as the lower-limit-form of a mixed DF, and in view of the behavior of the RPBE DF we expect that the SRP $\mathbf{x}$ sol DF of Eq.5.2 will perform well as a generic expression for reproducing barrier heights by tuning its  $\mathbf{x}$ -parameter. Unfortunately PBE (the lower-limit-form of SRP $\mathbf{x}$  of Eq.5.1), PBE-vdW1 (the lower limit of SRP $\mathbf{x}$ -vdW1 of Eq.5.3), PBE-vdW2 (the lower limit of SRP $\mathbf{x}$ -vdW2 of Eq.5.4), PBEsol-vdW2 (the lower limit of SRP $\mathbf{x}$ solvdW2 of Eq.5.5), PBE $\alpha$ 57-vdW1 (the lower limit of SRP $\mathbf{x}$ -vdW1-ext of Eqs.5.6) and PBE $\alpha$ 57-vdW2 (the lower limit of SRP $\mathbf{x}$ -vdW2-ext of Eqs.5.7) all have that their MSE is not equal to minus their MAE, meaning that these DFs do not systematically underestimate the barrier height for the systems in SBH17. Of these DFs, on the basis of the correspondence between their MAE and the negative of their MSE, PBEsol-vdW2 and PBE $\alpha$ 57-vdW1 are expected to function best as lower-limit-forms, and consequently the mixed DFs SRP $\mathbf{x}$ sol-vdW2 and SRP $\mathbf{x}$ -vdW1-ext are also expected to perform well as tunable mixed DFs.

### 5.3.3 Performance of mixed density functionals as tunable SRP DFs

Figure 5.5 illustrates how we find the optimal value of  $\mathbf{x}$  for each mixed DF by showing how this was done for the particular examples of the H<sub>2</sub> + Cu(111) and

TABLE 5.1: Performance of the DFs that represent limiting forms of the mixed density functionals tested on the SBH16 database using the medium algorithm. The mean absolute errors (MAE's) and the mean signed errors (MSE's) are presented in eV for all density functionals investigated here. For the density functionals for which these results are available we also present MAE's and MSE's computed previously for the closely related SBH17 database<sup>7</sup>.

Functional	Med Algo			
	MAE	MSE	MAE-SBH17	MSE-SBH17
PBE	0.107	-0.065	0.103	-0.058
RPBE	0.235	0.235	0.228	0.228
PBEsolc	0.458	-0.458	-	-
PBEsol-vdW-DF2	0.269	-0.265	-	-
PBE-vdW-DF1	0.128	-0.020	-	-
PBE-vdW-DF2	0.148	0.117	0.141	0.112
PBE $\alpha$ 57-vdW-DF1	0.209	-0.185	-	-
PBE $\alpha$ 57-vdW-DF2	0.132	-0.042	0.124	-0.040
RPBE-vdW-DF1	0.278	0.278	-	-
RPBE-vdW-DF2	0.424	0.424	-	-
Average	0.239	0.002	-	-

CH<sub>4</sub> + Pt(111) systems using the mixed DFs SRP $\boldsymbol{x}$  and SRP $\boldsymbol{x}$ sol of Eqs. 5.1 and 5.2. As Figs. 5.5A and 5.5B show the barrier height obtained with a mixed DF typically depends linearly on  $\boldsymbol{x}$ . This means that the optimal value of  $\boldsymbol{x}$  can be found using linear interpolation, i.e., from the point where the linearly interpolated barrier height curves (the sloping red and black lines) intersect the horizontal blue line representing the reference value of the barrier height. If  $\boldsymbol{x}$  does not fall between the limits of the mixed DF (0 and 1 for the expressions of Eqs. 5.1-5.5, and -0.43 and 1 for Eqs. 5.6 and 5.7) a value of  $\boldsymbol{x}$  can be found by extrapolation. We have not tested whether the DFs that may be obtained by extrapolation lead to reasonable values of the minimum barrier height; we would not recommend their use. However, the values of  $\boldsymbol{x}$  obtained in this way may be used in the calculation of the correlation coefficients discussed in the next Section.

Figures 5.6 and 5.7 show the optimal  $\boldsymbol{x}$  coefficients computed for the SRP $\boldsymbol{x}$  and SRP $\boldsymbol{x}$ sol DFs of Eqs. 5.1 and 5.2, respectively, as a function of  $\Delta E_{CT}$ . These coefficients are also listed for each DF in Table 5.A.4. Figure 5.6 shows that obtaining the optimum value of  $\boldsymbol{x}$  for the SRP $\boldsymbol{x}$  DF required extrapolation to negative values for several H<sub>2</sub>-metal surface and CH<sub>4</sub>-metal surface systems. The use of this mixed DF is therefore not guaranteed to yield a useful SRP DF for systems like the ones investigated here. From the point of view of tunability the opposite is true for the SRP $\boldsymbol{x}$ sol DF, for which we obtained a value of  $\boldsymbol{x}$  falling between 0 and 1 for all systems in the SBH16 database (see Figs. 5.6-5.7).

Figure 5.8 shows the optimal  $\boldsymbol{x}$  coefficients computed for the SRP $\boldsymbol{x}$ sol-vdW2 DF of Eq. 5.5 as a function of  $\Delta E_{CT}$ . These coefficients are also listed for this

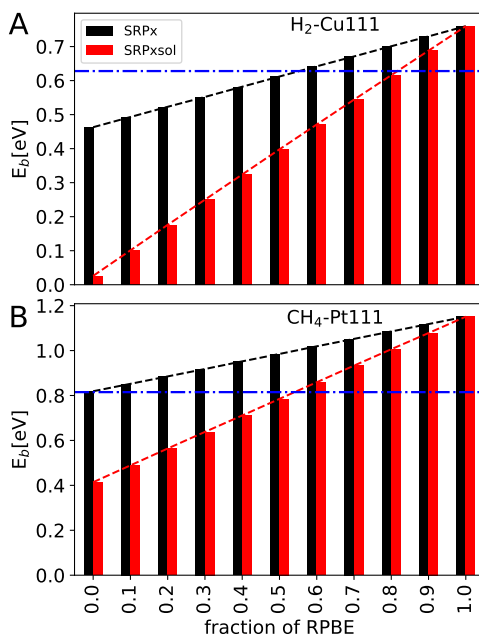


FIGURE 5.5: The barrier heights computed with the SRP $x$  DF (black bars) and the SRP $x$ sol DF (red bars) is shown as a function of the fraction of RPBE exchange  $x$ , (A) for  $H_2 + Cu(111)$  (upper panel) and (B)  $CH_4 + Pt(111)$  (lower panel). Blue horizontal lines indicate the reference value of the barrier height for these systems<sup>7</sup>. The black and red dashed lines linearly interpolate the barrier height as a function of  $x$  for the SRP $x$  and the SRP $x$ sol DFs, respectively. The optimal value of  $x$  is equal to the value of  $x$  for which these lines intersect the blue lines.

DF in Table 5.A.5. Figure 5.8 shows that obtaining the optimum value of  $x$  for the SRP $x$ sol-vdW2 DF only required extrapolation to a negative value for  $H_2 + Ag(111)$ . This system was classified as problematic in the SBH17 study, with all DFs tested there yielding large MAEs for this system<sup>7</sup>. While we conclude that the use of this mixed DF is not guaranteed to yield a useful SRP DF for systems like the ones investigated here, we find that it performs rather well, and that it can probably be used if a SRP DF is desired with vdW-DF2 correlation in it. Note that, when coupled to their original partner exchange functionals<sup>21,22</sup>, the vdW-DF2 functional<sup>22</sup> yields a better description of the S22 database binding energies of gas phase dimers (MAE of 22 meV)<sup>22</sup> than the vdW-DF1 functional<sup>22</sup> (MAE of 41 meV)<sup>21</sup>. However, the vdW-DF1 functional<sup>21</sup> generally yields a better description of bulk solids<sup>42</sup> than the vdW-DF2 functional<sup>22</sup>.

Figure 5.9 shows the optimal  $x$  coefficients computed for the SRP $x$ vdW1-ext DF of Eq.5.6 as a function of  $\Delta E_{CT}$ . These coefficients are also listed in

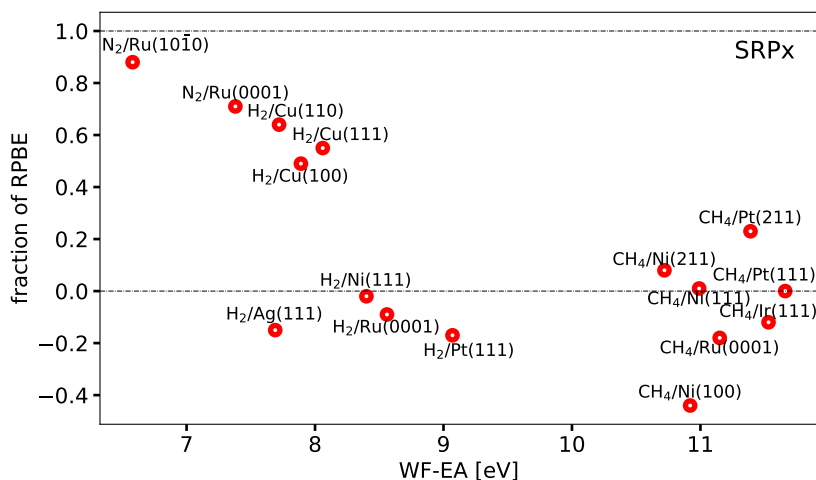


FIGURE 5.6: The optimum fraction of RPBE exchange  $\alpha$  is shown as a function of  $\Delta E_{CT}$  for the SRP $\alpha$  DF (Eq.5.1). Values falling between the two horizontal dot-dashed black lines could be obtained by the interpolation procedure illustrated in Figure 5.5.

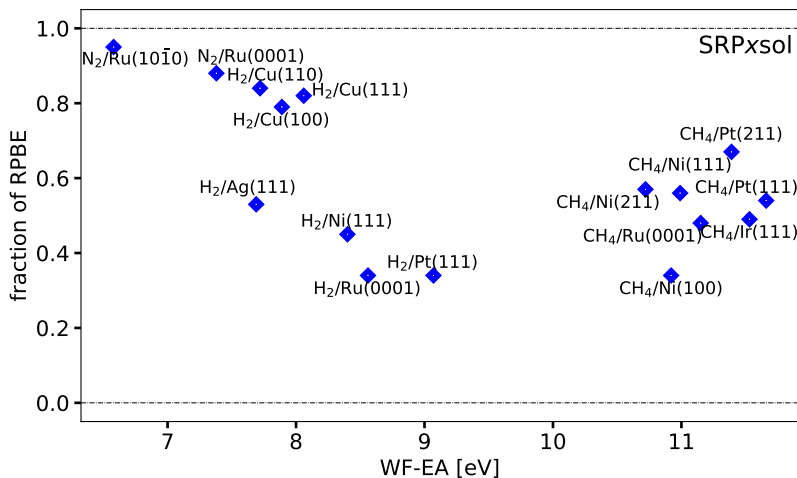


FIGURE 5.7: The optimum fraction of RPBE exchange  $\alpha$  is shown as a function of  $\Delta E_{CT}$  for the SRP $\alpha$ sol DF (Eq.5.2). Values falling between the two horizontal dot-dashed black lines could be obtained by the interpolation procedure illustrated in Figure 5.5.

Table 5.A.5. Figure 5.9 shows that obtaining the optimum value of  $\boldsymbol{x}$  for the SRP $\boldsymbol{x}$ -vdW1-ext DF only required extrapolation to a negative value for H<sub>2</sub> + Cu(110) and H<sub>2</sub> + Ag(111). The latter system was classified as problematic in the SBH17 study, with all DFs tested there yielding large MAEs for this system<sup>7</sup>. The use of the SRP $\boldsymbol{x}$ -vdW1-ext DF mixed DF is not guaranteed to yield a useful SRP DF for systems like the ones investigated here, but we find that it performs rather well just like SRP $\boldsymbol{x}$ sol-vdW-DF2, and the SRP $\boldsymbol{x}$ -vdW1-ext can be used if a SRP-DF is desired with vdW-DF1 correlation in it. As noted above, when partnered with their original exchange functionals vdW-DF1 yields better descriptions of bulk solids, while vdW-DF2 tends to be better for binding energies of gas phase dimers.

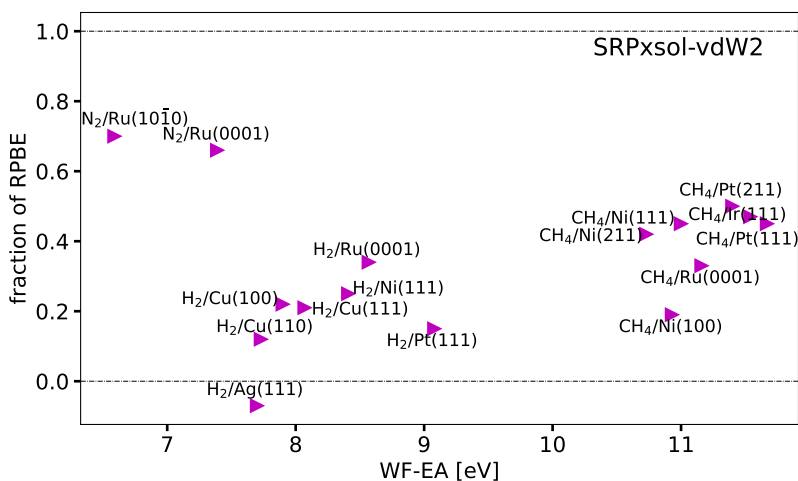


FIGURE 5.8: The optimum fraction of RPBE exchange  $\boldsymbol{x}$  is shown as a function of  $\Delta E_{CT}$  for the SRP $\boldsymbol{x}$ sol-vdW2 DF (Eq.5.5). Values falling between the two horizontal dot-dashed black lines could be obtained by the interpolation procedure illustrated in Figure 5.5.

Figures 5.A.2, 5.A.3, and 5.A.4 show the optimal  $\boldsymbol{x}$  coefficients computed for the SRP $\boldsymbol{x}$ -vdW1, SRP $\boldsymbol{x}$ -vdW2, and SRP $\boldsymbol{x}$ -vdW2-ext DFs of Eqs. 5.3, 5.4, and 5.7, respectively, as a function of  $\Delta E_{CT}$ . These coefficients are also listed for each DF in Tables 5.A.4 and 5.A.5. Figures 5.A.2-5.A.4 show that obtaining the optimum value of  $\boldsymbol{x}$  for these three mixed DFs required extrapolation to negative values for several H<sub>2</sub>-metal surface and in most cases also for several CH<sub>4</sub>-metal surface systems, with SRP $\boldsymbol{x}$ -vdW2 performing particularly poorly. The above suggests that these three mixed DFs, and especially SRP $\boldsymbol{x}$ -vdW2,

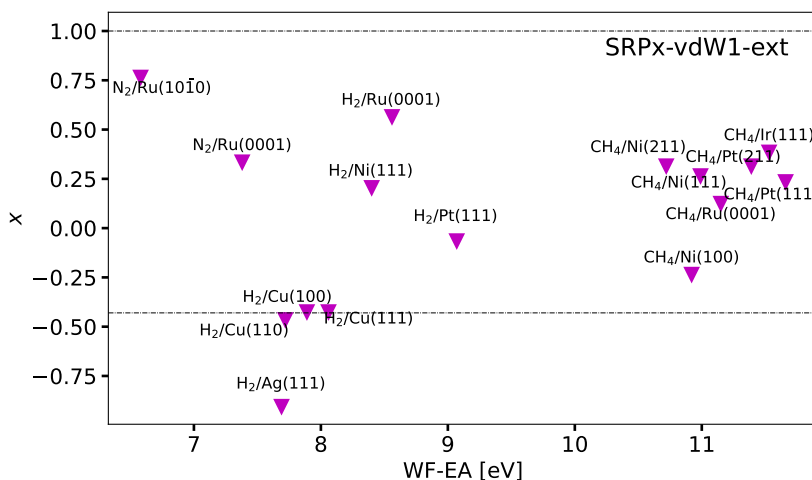


FIGURE 5.9: The optimum mixing parameter  $x$  is shown as a function of  $\Delta E_{CT}$  for the SRP $x$ -vdW1-ext DF (Eq.5.6). Values falling between the two horizontal dot-dashed black lines could be obtained by the interpolation procedure illustrated in Figure 5.5.

should perhaps not be the first choice for deriving a new SRP-DF for a system like the ones present in the SBH16 database.

### 5.3.4 Correlation of the mixing parameter with the charge transfer parameter

Table 5.2 shows correlation coefficients (or Pearson product-moment correlation coefficients)<sup>43</sup>  $r_{xy}$  describing the correlation between the charge transfer parameter taken as independent variable and the mixing coefficient  $x$  taken as dependent variable, for the seven mixed DFs tested here. Including all systems, the  $r_{xy}$  are clearly negative for the SRP $x$  and the SRP $x$ sol DFs. The same is true for these DFs if only the H<sub>2</sub>-metal systems are considered, and for these systems the  $r_{xy}$  values get close to the value of -1 indicating a nearly perfect linear relationship if the H<sub>2</sub> + Ag(111) system, for which the reference barrier height is somewhat suspect, is not considered. For CH<sub>4</sub> metal systems the values of  $r_{xy}$  only take on negative values if the CH<sub>4</sub> + Ru(0001) and Ni(100) systems, for which the reference barrier heights are also somewhat suspect, are not considered, and these values are small in absolute value.

The finding of negative correlation coefficients as observed here for the SRP $x$  and SRP $x$ sol DFs is what we expected to see, for several reasons. First of all, the MAE of the RPBE DF was previously found to increase from 88 to 167 to 336

TABLE 5.2: Correlation coefficients computed for the dependence of the optimum fraction of RPBE exchange  $\alpha$  on the charge transfer parameter for the mixed DFs tested. Computed correlation coefficients are provided for the 7 H<sub>2</sub>-metal surface systems present in the SBH16 database, the 6 H<sub>2</sub>-metal surface systems obtained once H<sub>2</sub> + Ag(111) is removed, the 7 CH<sub>4</sub>-metal surface systems in the SBH16 database, the 5 CH<sub>4</sub>-metal surface systems that remain after CH<sub>4</sub> + Ru(0001) and Ni(100) are removed, the 16 systems (All-16) present in the SBH16 database, and the 12 systems (All-12) that remain after the 3 systems already mentioned and N<sub>2</sub> + Ru(1010) are removed.

type SRP	All-16	All-12	7 H <sub>2</sub> -metal	6 H <sub>2</sub> -metal	7 CH <sub>4</sub> -metal	5 CH <sub>4</sub> -metal
SRP $\alpha$	-0.648	-0.617	-0.584	-0.927	0.211	-0.239
SRP $\alpha$ sol	-0.543	-0.409	-0.761	-0.91	0.228	-0.174
SRP $\alpha$ -vdW-DF1	0.264	0.528	0.752	0.684	0.362	0.003
SRP $\alpha$ -vdW-DF2	0.205	0.483	0.751	0.695	0.500	0.801
SRP $\alpha$ sol-vdW-DF2	0.147	0.447	0.473	0.209	0.483	0.609
SRP $\alpha$ -vdW-DF1-ext	0.236	0.521	0.716	0.627	0.361	0.003
SRP $\alpha$ -vdW-DF2-ext	0.148	0.423	0.741	0.671	0.420	0.428



meV going from N<sub>2</sub>-metal systems to H<sub>2</sub>-metal systems to CH<sub>4</sub>-metal systems<sup>7</sup>, respectively, i.e., going from small values of the charge transfer parameter to large values (see e.g. Table 5.A.2 and Fig.5.6 for how the charge transfer parameter varies with the type of system). The opposite is true for the PBE DF, where the MAE was found to decrease from 409 to 80 to 45 meV going from N<sub>2</sub>-metal systems to H<sub>2</sub>-metal systems to CH<sub>4</sub>-metal systems<sup>7</sup>, respectively. Second, tests on several systems suggest that for systems characterized by charge transfer parameters less than 7 eV even RPBE exchange is not repulsive enough to avoid underestimating the barrier height<sup>25</sup>. However, it is also clear that when all three types of systems are considered the correlation is not that strong, suggesting that when a mixed functional with a fraction of PBE correlation is used the optimum mixing coefficient also depends on other properties of the system than the charge transfer parameter. In this context we note that  $r_{xy}$  for all systems decreases in absolute value if the four systems with suspect reference values (N<sub>2</sub> + Ru(10 $\bar{1}$ 0), CH<sub>4</sub> + Ru(0001), CH<sub>4</sub> + Ni(100), and H<sub>2</sub> + Ag(111))<sup>7</sup> are excluded from the SBH16 database (see Table 5.2), which would not be expected if  $\mathbf{x}$  would only depend on the charge transfer parameter and the relationship would be linear.

The computed values of the correlation coefficients for the DFs incorporating van der Waals correlation are rather different from the values calculated for SRP $\mathbf{x}$  and SRP $\mathbf{x}$ sol, which incorporate PBE correlation. Restricting ourselves to the mixed DFs that exhibit high tunability, i.e., SRP $\mathbf{x}$ sol-vdW2 and SRP $\mathbf{x}$ -vdW1-ext, we see that the former one only exhibits positive correlation coefficients, and that the latter one exhibits correlation coefficients that are either positive or close to zero. The reason for the different values of the correlation coefficients of SRP $\mathbf{x}$  and SRP $\mathbf{x}$ sol on the one hand (mostly negative) and the other DFs incorporating van der Waals correlation on the other hand (mostly positive) are not clear at this stage; the difference is rather puzzling.

## 5.4 Conclusions and outlook.

We have investigated the tunability of several expressions for mixed density functionals, in which a mixing parameter  $\mathbf{x}$  can be tuned to enable the mixed DF to reproduce the reference value of the barrier height to dissociative chemisorption of a molecule on a metal surface. The mixed functionals are tested on the barriers collected in the database we call SBH16, which is equal to the previous SBH17 database in **chapter 3** with the H<sub>2</sub> + Pt(211) system removed from it.

Increasing the fraction of RPBE exchange incorporated in the mixed DFs leads to higher barriers. All mixed DFs tested are well tunable towards higher barriers, as their limiting forms (RPBE, RPBE-vdW1, and RPBE-vdW2) all systematically overestimate the barrier height for the systems in the SBH16

database. It turns out that the biggest challenge to finding a perfectly tunable mixed DF for describing the SBH16 database is to obtain a mixed DF expression with a good lower-energy form, which consistently underestimates barrier heights for systems like the ones present in SBH16. This goal is fully met with the mixed SRP $\mathbf{x}$ sol DF that uses PBE correlation and a mixture of PBEsol and RPBE exchange. The mixed SRP $\mathbf{x}$ sol-vdW2 DF could describe the minimum barrier height of 15 of the 16 systems using vdW-DF2 correlation, while the mixed SRP $\mathbf{x}$ -vdW1 DF could do so for 14 of the 16 systems using vdW-DF1 correlation. Being able to use mixed DFs with different correlation functionals may be important to obtaining a SRP DF for a particular system because reproducing the minimum barrier height is a necessary, but not a sufficient condition for reproducing measured sticking (or dissociative chemisorption) probabilities, as now used for validating SRP functionals and barrier heights: It is also necessary to provide a description of how the barrier height varies when the molecule's impact site on the surface and its orientation relative to the surface is changed, and this variation may depend strongly on the correlation functional used<sup>6,13,27</sup>.

We also tested whether and how the mixing coefficient of the mixed DFs is correlated with the charge transfer parameter describing the system, i.e., the difference between the work function of the metal surface and the electron affinity of the molecule. The answer depends on which mixed DF is used. For the SRP $\mathbf{x}$  and SRP $\mathbf{x}$ sol DFs, which both use PBE correlation, we found that the optimum fraction of RPBE exchange decreases with the charge transfer parameter, as could be expected on the basis of earlier results. However, the opposite relationship and weaker correlation was found for the mixed DFs using vdW-DF1 or vdW-DF2 correlation. The reason for this difference is not clear.

The results presented here point to several new lines of research. First of all the results underscore the need to obtain better reference values for the H<sub>2</sub> + Ag(111), CH<sub>4</sub> + Ru(0001), and CH<sub>4</sub> + Ni(100) systems. For all mixed DFs the optimized mixing coefficients for these systems appear as outliers when plotted as a function of the charge transfer parameter, and removing these systems from the database leads to correlation coefficients with an increased absolute value for the mixed SRP $\mathbf{x}$  and SRP $\mathbf{x}$ sol DFs for the H<sub>2</sub>-metal surface and the CH<sub>4</sub>-metal surface systems.

A small improvement over using the SRP $\mathbf{x}$ sol mixed DF could be to use a DF that simply mixes the RPBE and the PBEsol exchange-correlation functionals. This would avoid the use of an exchange correlation functional with unbalanced exchange and correlation at the lower  $\mathbf{x}=0$  end of the spectrum, i.e., PBEsolc.

When it comes to designing mixed functionals incorporating vdW-DF1 or vdW-DF2 correlation, another idea worth testing might be to investigate mixtures of weakly repulsive GGA exchange DFs that are appropriate matches for the vdW1

and vdW2 correlation functionals with the rather repulsive<sup>44</sup> exchange functionals combined with these C functionals in the original vdW-DF1<sup>21</sup> and vdW-DF2<sup>22</sup> DFs. Examples of such exchange functionals have been incorporated in the C09<sup>45</sup> and CX<sup>46</sup> vdW functionals, and other exchange functionals mentioned in Ref.<sup>44</sup>. Another idea would be to explore mixtures of repulsive meta-GGA DFs (such as MS-B86bl<sup>24</sup>) and attractive meta-GGA DFs (such as SCAN<sup>47</sup>) that tend to overestimate respectively underestimate barriers to dissociative chemisorption of molecules on metals<sup>7</sup>. It would also be of interest to investigate the performance of mixtures of, or parameterized forms of screened hybrid functionals such as HSE06<sup>48</sup> and screened hybrid functionals incorporating van der Waals correlation<sup>44,49</sup>. However, it might be most productive to test such hybrid functionals once a database becomes available that also incorporates good reference values of barrier heights for systems characterized by charge transfer parameters  $< 7$  eV, such as  $O_2 + Ag(111)$ <sup>25</sup> and  $HCl + Au(111)$ <sup>50</sup>. Such systems presently defy an accurate description based on DFs incorporating GGA exchange<sup>25,50,51</sup>.

## 5.A Appendix Tables and Figures

TABLE 5.A.1: Measured zero-point-energy-corrected and computed equilibrium lattice constants  $a$  of the fcc metals Ag, Cu, Ir, Ni, and Pt, and  $a$  and  $c$  of the hcp metal Ru are presented. The computed values have been calculated with the SRP $\alpha$  and SRP $\alpha$ sol DFs varying  $\alpha$  by steps  $\Delta\alpha$  of 0.1.

Metal	Ag	Cu	Ir	Ni	Pt	Ru	
	$a$	$a$	$a$	$a$	$a$	$a$	$c$
Experimental	4.062 <sup>52</sup>	3.597 <sup>52</sup>	3.831 <sup>52</sup>	3.499 <sup>52</sup>	3.912 <sup>52</sup>	2.703 <sup>53</sup>	4.274 <sup>53</sup>
SRP $\alpha$							
PBE	4.147	3.635	3.873	3.518	3.968	2.721	4.293
$\alpha=0.1$	4.153	3.639	3.874	3.521	3.970	2.722	4.295
$\alpha=0.2$	4.159	3.644	3.875	3.524	3.972	2.723	4.297
$\alpha=0.3$	4.165	3.648	3.877	3.528	3.974	2.725	4.299
$\alpha=0.4$	4.172	3.652	3.878	3.531	3.976	2.726	4.301
$\alpha=0.5$	4.178	3.657	3.880	3.535	3.979	2.727	4.303
$\alpha=0.6$	4.185	3.661	3.882	3.539	3.981	2.728	4.305
$\alpha=0.7$	4.191	3.666	3.883	3.542	3.983	2.730	4.307
$\alpha=0.8$	4.198	3.670	3.885	3.546	3.985	2.731	4.308
$\alpha=0.9$	4.205	3.675	3.886	3.550	3.988	2.732	4.310
RPBE	4.213	3.679	3.888	3.553	3.990	2.733	4.312
SRP $\alpha$ sol							
PBEsol	4.035	3.559	3.822	3.454	3.902	2.683	4.237
$\alpha=0.1$	4.051	3.570	3.828	3.464	3.910	2.688	4.244
$\alpha=0.2$	4.067	3.581	3.834	3.473	3.918	2.693	4.252
$\alpha=0.3$	4.083	3.593	3.841	3.482	3.927	2.698	4.260
$\alpha=0.4$	4.099	3.604	3.847	3.492	3.935	2.704	4.268
$\alpha=0.5$	4.117	3.616	3.854	3.502	3.944	2.709	4.275
$\alpha=0.6$	4.134	3.628	3.860	3.512	3.953	2.714	4.283
$\alpha=0.7$	4.152	3.641	3.867	3.522	3.962	2.719	4.290
$\alpha=0.8$	4.172	3.653	3.874	3.532	3.971	2.723	4.298
$\alpha=0.9$	4.192	3.666	3.881	3.543	3.980	2.728	4.305
RPBE	4.213	3.679	3.888	3.553	3.990	2.733	4.312

TABLE 5.A.2: Calculated barrier heights  $E_b$  computed with limiting forms of the mixed DFs are shown for the 16 systems present in the SBH16 database, as calculated for the PBE, the RPBE, the PBEsolc, the PBE-vdW1, the PBE-vdW2, and the PBE $\alpha$ -vdW1 DF with  $\alpha=0.57$ . Also presented are the values of the charge excitation parameter  $\Delta E_{CT}=\text{WF-EA}$ . The systems are arranged with the charge transfer parameter increasing from top to bottom.

System	$E_b^{PBE}$	$E_b^{RPBE}$	$E_b^{PBEsolc}$	$E_b^{PBE-vdW1}$	$E_b^{PBE-vdW2}$	$E_b^{PBE\alpha-vdW1}$	WF-EA
N <sub>2</sub> +Ru(1010)	-0.096	0.469	-0.999	-0.023	0.247	-0.314	6.582
N <sub>2</sub> +Ru(0001)	1.532	1.965	0.896	1.688	1.746	1.314	7.382
H <sub>2</sub> +Ag(111)	1.132	1.457	0.643	1.442	1.569	1.275	7.685
H <sub>2</sub> +Cu(110)	0.639	0.874	0.346	0.914	0.996	0.792	7.715
H <sub>2</sub> +Cu(100)	0.584	0.905	0.095	0.894	1.024	0.731	7.885
H <sub>2</sub> +Cu(111)	0.463	0.760	0.026	0.771	0.886	0.617	8.055
H <sub>2</sub> +Ni(111)	0.026	0.170	-0.097	-0.006	0.085	-0.076	8.395
H <sub>2</sub> +Ru(0001)	0.014	0.108	-0.050	-0.049	0.002	-0.096	8.555
H <sub>2</sub> +Pt(111)	0.018	0.169	-0.103	-0.005	0.063	-0.079	9.065
CH <sub>4</sub> +Ni(211)	0.675	0.973	0.349	0.603	0.777	0.448	10.72
CH <sub>4</sub> +Ni(100)	0.912	1.259	0.491	0.843	1.020	0.664	10.92
CH <sub>4</sub> +Ni(111)	1.010	1.349	0.594	0.962	1.156	0.785	10.99
CH <sub>4</sub> +Ru(0001)	0.856	1.164	0.456	0.760	0.989	0.603	11.15
CH <sub>4</sub> +Pt(211)	0.489	0.789	0.092	0.484	0.618	0.316	11.39
CH <sub>4</sub> +Ir(111)	0.875	1.186	0.495	0.714	0.894	0.550	11.53
CH <sub>4</sub> +Pt(111)	0.819	1.151	0.414	0.775	0.898	0.604	11.66

TABLE 5.A.3: Calculated barrier heights  $E_b$  computed with limiting forms of the mixed DFs are shown for the 16 systems present in the SBH16 database, as calculated for the the PBE $\alpha$ -vdW1 DF with  $\alpha=0.57$ , the RPBE-vdW1 DF, the RPBE-vdW2 DF, and the PBEsol-vdW2 DF. Also presented are the values of the charge excitation parameter  $\Delta E_{CT}=\text{WF-EA}$ . The systems are arranged with the charge transfer parameter increasing from top to bottom.

System	$E_b^{PBE\alpha-vdW2}$	$E_b^{RPBE-vdW1}$	$E_b^{RPBE-vdW2}$	$E_b^{PBEsol-vdW2}$	WF-EA
N <sub>2</sub> +Ru(1010)	-0.044	0.525	0.801	-0.568	6.582
N <sub>2</sub> +Ru(0001)	1.529	2.133	2.367	1.113	7.382
H <sub>2</sub> +Ag(111)	1.403	1.758	1.885	1.114	7.685
H <sub>2</sub> +Cu(110)	0.887	1.144	1.239	0.714	7.715
H <sub>2</sub> +Cu(100)	0.859	1.205	1.332	0.564	7.885
H <sub>2</sub> +Cu(111)	0.736	1.064	1.183	0.470	8.055
H <sub>2</sub> +Ni(111)	-0.002	0.134	0.209	-0.045	8.395
H <sub>2</sub> +Ru(0001)	-0.044	0.043	0.095	-0.052	8.555
H <sub>2</sub> +Pt(111)	-0.012	0.145	0.211	-0.044	9.065
CH <sub>4</sub> +Ni(211)	0.613	0.907	1.076	0.433	10.72
CH <sub>4</sub> +Ni(100)	0.829	1.188	1.352	0.607	10.92
CH <sub>4</sub> +Ni(111)	0.949	1.305	1.473	0.713	10.99
CH <sub>4</sub> +Ru(0001)	0.775	1.063	1.235	0.565	11.15
CH <sub>4</sub> +Pt(211)	0.474	0.790	0.939	0.232	11.39
CH <sub>4</sub> +Ir(111)	0.730	1.030	1.210	0.501	11.53
CH <sub>4</sub> +Pt(111)	0.726	1.107	1.262	0.529	11.66

TABLE 5.A.4: The optimal mixing coefficient  $\boldsymbol{x}$  is shown for the mixed DFs SRP $\boldsymbol{x}$ , SRP $\boldsymbol{x}$ sol, SRP $\boldsymbol{x}$ -vdW1, and SRP $\boldsymbol{x}$ -vdW2. Also presented are the values of the charge excitation parameter  $\Delta E_{CT}$ =WF-EA. The systems are arranged with the charge transfer parameter increasing from top to bottom.

System	WF-EA	SRP $\boldsymbol{x}$	SRP $\boldsymbol{x}$ sol	SRP $\boldsymbol{x}$ -vdW1	SRP $\boldsymbol{x}$ -vdW2
N <sub>2</sub> + Ru(1010)	6.582	0.88	0.95	0.77	0.27
N <sub>2</sub> + Ru(0001)	7.382	0.71	0.88	0.34	0.01
H <sub>2</sub> + Ag(111)	7.685	-0.15	0.53	-1.14	-1.55
H <sub>2</sub> + Cu(110)	7.715	0.64	0.84	-0.55	-0.91
H <sub>2</sub> + Cu(100)	7.885	0.49	0.79	-0.49	-0.91
H <sub>2</sub> + Cu(111)	8.055	0.55	0.82	-0.49	-0.88
H <sub>2</sub> + Ni(111)	8.395	-0.02	0.45	0.21	-0.42
H <sub>2</sub> + Ru(0001)	8.555	-0.09	0.34	0.57	0.02
H <sub>2</sub> + Pt(111)	9.065	-0.17	0.34	-0.02	-0.48
CH <sub>4</sub> + Ni(211)	10.72	0.08	0.57	0.32	-0.24
CH <sub>4</sub> + Ni(100)	10.92	-0.44	0.34	-0.24	-0.76
CH <sub>4</sub> + Ni(111)	10.99	0.01	0.56	0.27	-0.26
CH <sub>4</sub> + Ru(0001)	11.15	-0.18	0.48	0.13	-0.44
CH <sub>4</sub> + Pt(211)	11.39	0.23	0.67	0.32	-0.14
CH <sub>4</sub> + Ir(111)	11.53	-0.12	0.49	0.39	-0.18
CH <sub>4</sub> + Pt(111)	11.66	0.00	0.54	0.24	-0.17

TABLE 5.A.5: The optimal mixing coefficient  $\boldsymbol{x}$  is shown for the mixed DFs SRP $\boldsymbol{x}$ sol-vdW2, SRP $\boldsymbol{x}$ -vdW1-ext, and SRP $\boldsymbol{x}$ -vdW2-ext. Also presented are the values of the charge excitation parameter  $\Delta E_{CT}$ =WF-EA. The systems are arranged with the charge transfer parameter (see Table 5.A.4) increasing from top to bottom.

System	SRP $\boldsymbol{x}$ sol-vdW2	SRP $\boldsymbol{x}$ -vdW1-ext	SRP $\boldsymbol{x}$ -vdW2-ext
N <sub>2</sub> + Ru(1010)	0.70	0.77	0.27
N <sub>2</sub> + Ru(0001)	0.66	0.34	0.01
H <sub>2</sub> + Ag(111)	-0.07	-0.90	-1.21
H <sub>2</sub> + Cu(110)	0.12	-0.46	-0.76
H <sub>2</sub> + Cu(100)	0.78	-0.42	-0.74
H <sub>2</sub> + Cu(111)	0.21	-0.42	-0.72
H <sub>2</sub> + Ni(111)	0.25	0.21	-0.31
H <sub>2</sub> + Ru(0001)	0.34	0.57	0.02
H <sub>2</sub> + Pt(111)	0.15	-0.06	-0.42
CH <sub>4</sub> + Ni(211)	0.42	0.32	-0.22
CH <sub>4</sub> + Ni(100)	0.19	-0.23	-0.60
CH <sub>4</sub> + Ni(111)	0.45	0.27	-0.21
CH <sub>4</sub> + Ru(0001)	0.67	0.13	-0.38
CH <sub>4</sub> + Pt(211)	0.50	0.32	-0.15
CH <sub>4</sub> + Ir(111)	0.53	0.39	-0.19
CH <sub>4</sub> + Pt(111)	0.55	0.24	-0.21

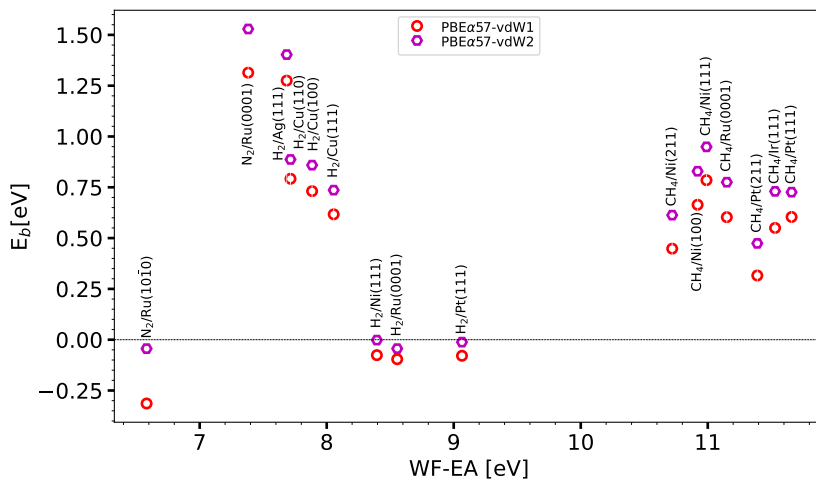


FIGURE 5.A.1: The barrier heights  $E_b$  computed with the  $\text{PBE}\alpha\text{-vdW1}$  and  $\text{PBE}\alpha\text{-vdW2}$  DFs with  $\alpha=0.57$  are shown as a function of the charge transfer parameter for the 16 systems present in the SBH16 database. These DFs may be viewed as the lower-limit expressions given by Eqs. 5.6b and 5.7b, respectively.

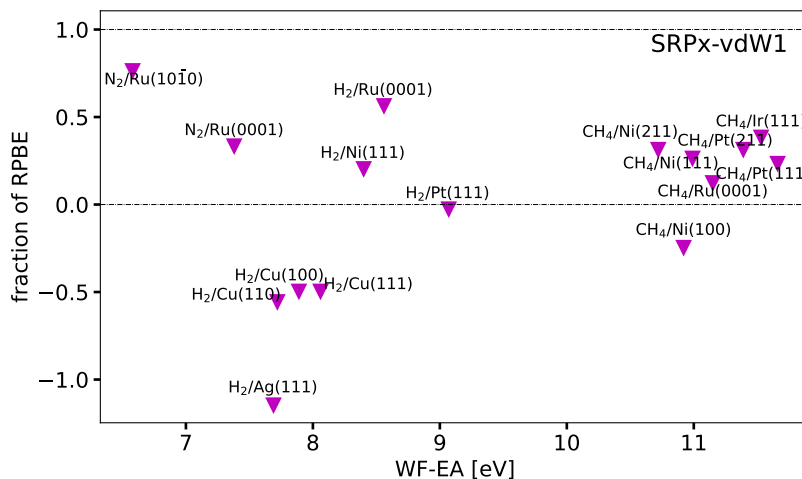


FIGURE 5.A.2: The optimum fraction of RPBE exchange  $x$  is shown as a function of  $\Delta E_{CT}$  for the  $\text{SRP}x\text{-vdW1}$  DF (Eq.5.3). Values falling between the two horizontal dot-dashed black lines could be obtained by the interpolation procedure illustrated in Figure 5.5.

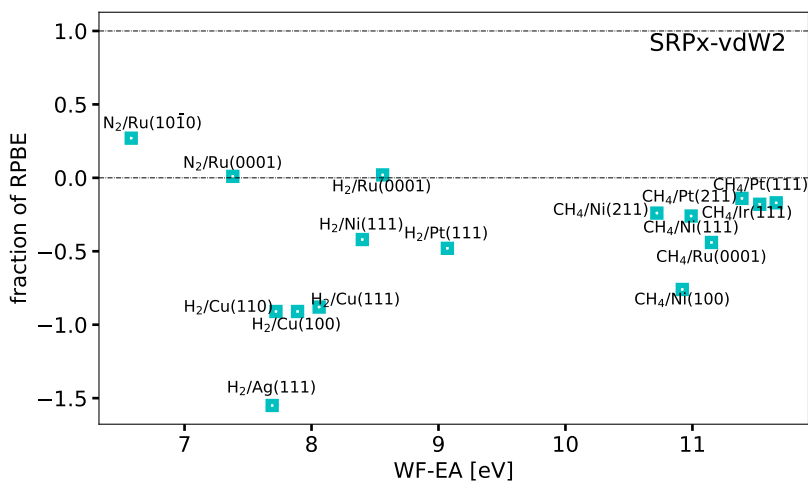


FIGURE 5.A.3: The optimum fraction of RPBE exchange  $\alpha$  is shown as a function of  $\Delta E_{CT}$  for the SRP $\alpha$ -vdW2 DF (Eq.5.4). Values falling between the two horizontal dot-dashed black lines could be obtained by the interpolation procedure illustrated in Figure 5.5.

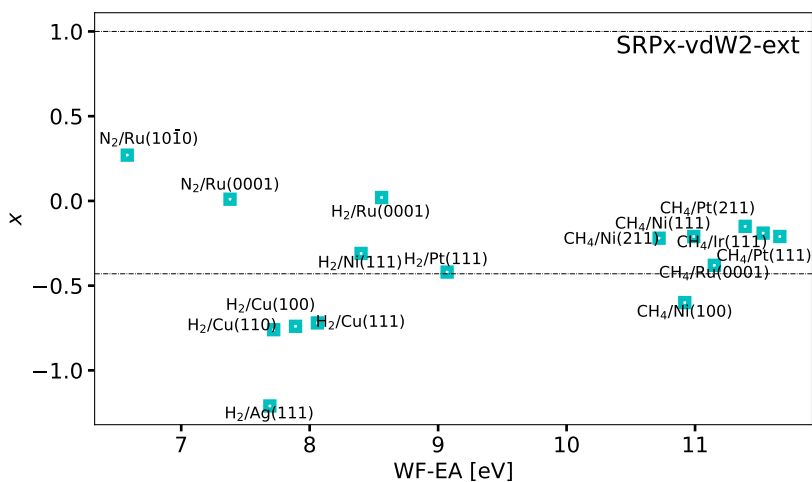


FIGURE 5.A.4: The optimum mixing parameter  $\alpha$  is shown as a function of  $\Delta E_{CT}$  for the SRP $\alpha$ -vdW2-ext DF (Eq.5.7). Values falling between the two horizontal dot-dashed black lines could be obtained by the interpolation procedure illustrated in Figure 5.5.



## References

- (1) Wolcott, C. A.; Medford, A. J.; Studt, F.; Campbell, C. T. Degree of rate control approach to computational catalyst screening. *J. Catal.* **2015**, *330*, 197–207.
- (2) Sabbe, M. K.; Reyniers, M.-F.; Reuter, K. First-principles kinetic modeling in heterogeneous catalysis: an industrial perspective on best-practice, gaps and needs. *Catal. Sci. Technol.* **2012**, *2*, 2010–2024.
- (3) Ertl, G. Primary steps in catalytic synthesis of ammonia. *J. Vac. Sci. Technol., A: Vacuum, Surfaces, and Films* **1983**, *1*, 1247–1253.
- (4) Honkala, K.; Hellman, A.; Remediakis, I.; Logadottir, A.; Carlsson, A.; Dahl, S.; Christensen, C. H.; Nørskov, J. K. Ammonia synthesis from first-principles calculations. *science* **2005**, *307*, 555–558.
- (5) Chorkendorff, I.; Niemantsverdriet, J. W., *Concepts of modern catalysis and kinetics*; Wiley Online Library: 2003; Vol. 138.
- (6) Kroes, G. J. Computational approaches to dissociative chemisorption on metals: towards chemical accuracy. *Phys. Chem. Chem. Phys.* **2021**, *23*, 8962–9048.
- (7) **Tchakoua, T.**; Gerrits, N.; Smeets, E. W. F.; Kroes, G. J. SBH17: Benchmark Database of Barrier Heights for Dissociative Chemisorption on Transition Metal Surfaces. *J. Chem. Theory Comput.* **2023**, *19*, 245–270.
- (8) Doblhoff-Dier, K.; Meyer, J.; Hoggan, P. E.; Kroes, G. J. Quantum Monte Carlo calculations on a benchmark molecule–metal surface reaction: H<sub>2</sub>+ Cu (111). *J. Chem. Theory Comput.* **2017**, *13*, 3208–3219.
- (9) Díaz, C.; Pijper, E.; Olsen, R. A.; Busnengo, H. F.; Auerbach, D. J.; Kroes, G. J. Chemically accurate simulation of a prototypical surface reaction: H<sub>2</sub> dissociation on Cu(111). *Science* **2009**, *326*, 832–834.
- (10) Sementa, L.; Wijzenbroek, M.; Van Kolck, B. J.; Somers, M. F.; Al-Halabi, A.; Busnengo, H. F.; Olsen, R. A.; Kroes, G. J.; Rutkowski, M.; Thewes, C., et al. Reactive scattering of H<sub>2</sub> from Cu(100): comparison of dynamics calculations based on the specific reaction parameter approach to density functional theory with experiment. *J. Chem. Phys.* **2013**, *138*, 044708.
- (11) Ghassemi, E. N.; Wijzenbroek, M.; Somers, M. F.; Kroes, G. J. Chemically accurate simulation of dissociative chemisorption of D<sub>2</sub> on Pt(111). *Chem. Phys. Lett.* **2017**, *683*, 329–335.

- (12) Ghassemi, E. N.; Smeets, E. W. F.; Somers, M. F.; Kroes, G. J.; Groot, I. M.; Juurlink, L. B.; Füchsel, G. Transferability of the specific reaction parameter density functional for  $\text{H}_2 + \text{Pt}(111)$  to  $\text{H}_2 + \text{Pt}(211)$ . *J. Phys. Chem. C* **2019**, *123*, 2973–2986.
- (13) Wijzenbroek, M.; Kroes, G. J. The effect of the exchange-correlation functional on  $\text{H}_2$  dissociation on  $\text{Ru}(0001)$ . *J. Chem. Phys.* **2014**, *140*, 084702.
- (14) **Tchakoua, T**; Smeets, E. W.; Somers, M.; Kroes, G. J. Toward a Specific Reaction Parameter Density Functional for  $\text{H}_2 + \text{Ni}(111)$ : Comparison of Theory with Molecular Beam Sticking Experiments. *J. Phys. Chem. C* **2019**, *123*, 20420–20433.
- (15) Smeets, E. W. F.; Kroes, G. J. Performance of Made Simple Meta-GGA Functionals with rVV10 Nonlocal Correlation for  $\text{H}_2 + \text{Cu}(111)$ ,  $\text{D}_2 + \text{Ag}(111)$ ,  $\text{H}_2 + \text{Au}(111)$ , and  $\text{D}_2 + \text{Pt}(111)$ . *J. Phys. Chem. C* **2021**, *125*, 8993–9010.
- (16) Shakouri, K.; Behler, J.; Meyer, J.; Kroes, G. J. Accurate neural network description of surface phonons in reactive gas-surface dynamics:  $\text{N}_2 + \text{Ru}(0001)$ . *J. Phys. Chem. Lett.* **2017**, *8*, 2131–2136.
- (17) Spiering, P.; Shakouri, K.; Behler, J.; Kroes, G. J.; Meyer, J. Orbital-dependent electronic friction significantly affects the description of reactive scattering of  $\text{N}_2$  from  $\text{Ru}(0001)$ . *J. Phys. Chem. Lett.* **2019**, *10*, 2957–2962.
- (18) Nattino, F.; Migliorini, D.; Kroes, G. J.; Dombrowski, E.; High, E. A.; Killelea, D. R.; Utz, A. L. Chemically accurate simulation of a polyatomic molecule-metal surface reaction. *J. Phys. Chem. Lett.* **2016**, *7*, 2402–2406.
- (19) Migliorini, D.; Chadwick, H.; Nattino, F.; Gutiérrez-González, A.; Dombrowski, E.; High, E. A.; Guo, H.; Utz, A. L.; Jackson, B.; Beck, R. D.; Kroes, G. J. Surface reaction barriometry: methane dissociation on flat and stepped transition-metal surfaces. *J. Phys. Chem. Lett.* **2017**, *8*, 4177–4182.
- (20) Nattino, F.; Díaz, C.; Jackson, B.; Kroes, G. J. Effect of surface motion on the rotational quadrupole alignment parameter of  $\text{D}_2$  reacting on  $\text{Cu}(111)$ . *Phys. Rev. Lett.* **2012**, *108*, 236104.
- (21) Dion, M.; Rydberg, H.; Schröder, E.; Langreth, D. C.; Lundqvist, B. I. Van der Waals Density Functional for General Geometries. *Phys. Rev. Lett.* **2004**, *92*, 246401.

- (22) Lee, K.; Murray, É. D.; Kong, L.; Lundqvist, B. I.; Langreth, D. C. Higher-accuracy van der Waals density functional. *Phys. Rev. B* **2010**, *82*, 081101.
- (23) Madsen, G. K. H. Functional form of the generalized gradient approximation for exchange: The PBE $\alpha$  functional. *Phys. Rev. B* **2007**, *75*, 195108.
- (24) Smeets, E. W. F.; Voss, J.; Kroes, G. J. Specific Reaction Parameter Density Functional Based on the Meta-Generalized Gradient Approximation: Application to H<sub>2</sub>+Cu(111) and H<sub>2</sub>+Ag(111). *J. Phys. Chem. A* **2019**, *123*, 5395–5406.
- (25) Gerrits, N.; Smeets, E. W.; Vuckovic, S.; Powell, A. D.; Doblhoff-Dier, K.; Kroes, G. J. Density functional theory for molecule–metal surface reactions: When does the generalized gradient approximation get it right, and what to do if it does not. *J. Phys. Chem. Lett.* **2020**, *11*, 10552–10560.
- (26) Hammer, B.; Hansen, L. B.; Nørskov, J. K. Improved adsorption energetics within density-functional theory using revised Perdew-Burke-Ernzerhof functionals. *Phys. Rev. B* **1999**, *59*, 7413–7421.
- (27) Nattino, F.; Migliorini, D.; Bonfanti, M.; Kroes, G. J. Methane dissociation on Pt(111): Searching for a specific reaction parameter density functional. *J. Chem. Phys.* **2016**, *144*, 044702.
- (28) Perdew, J. P.; Chevary, J. A.; Vosko, S. H.; Jackson, K. A.; Pederson, M. R.; Singh, D. J.; Fiolhais, C. Atoms, molecules, solids, and surfaces: Applications of the generalized gradient approximation for exchange and correlation. *Phys. Rev. B: Condens. Matter Mater. Phys.* **1992**, *46*, 6671–6687.
- (29) Perdew, J. P.; Burke, K.; Ernzerhof, M. Generalized Gradient Approximation Made Simple. *Phys. Rev. Lett.* **1996**, *77*, 3865–3868.
- (30) Perdew, J. P.; Ruzsinszky, A.; Csonka, G. I.; Vydrov, O. A.; Scuseria, G. E.; Constantin, L. A.; Zhou, X.; Burke, K. Restoring the Density-Gradient Expansion for Exchange in Solids and Surfaces. *Phys. Rev. Lett.* **2008**, *100*, 136406.
- (31) Wu, Z.; Cohen, R. E. More accurate generalized gradient approximation for solids. *Phys. Rev. B* **2006**, *73*, 235116.
- (32) Kresse, G.; Hafner, J. Ab initio molecular dynamics for liquid metals. *Phys. Rev. B* **1993**, *47*, 558–561.

- (33) Kresse, G.; Furthmüller, J. Efficiency of ab-initio total energy calculations for metals and semiconductors using a plane-wave basis set. *Comput. Mater. Sci.* **1996**, *6*, 15–50.
- (34) Kresse, G.; Furthmüller, J. Efficient iterative schemes for ab initio total-energy calculations using a plane-wave basis set. *Phys. Rev. B* **1996**, *54*, 11169.
- (35) Kresse, G.; Joubert, D. From ultrasoft pseudopotentials to the projector augmented-wave method. *Phys. Rev. B* **1999**, *59*, 1758–1775.
- (36) Bahn, S. R.; Jacobsen, K. W. An object-oriented scripting interface to a legacy electronic structure code. *Comput. Sci. Eng.* **2002**, *4*, 56–66.
- (37) Larsen, A. H.; Mortensen, J. J.; Blomqvist, J.; Castelli, I. E.; Christensen, R.; Dułak, M.; Friis, J.; Groves, M. N.; Hammer, B.; Hargus, C., et al. The atomic simulation environment—a Python library for working with atoms. *J. Phys.: Condens. Matter* **2017**, *29*, 273002.
- (38) Román-Pérez, G.; Soler, J. M. Efficient implementation of a van der Waals density functional: application to double-wall carbon nanotubes. *Phys. Rev. Lett.* **2009**, *103*, 096102.
- (39) Wellendorff, J.; Lundgaard, K. T.; Møgelhøj, A.; Petzold, V.; Landis, D. D.; Nørskov, J. K.; Bligaard, T.; Jacobsen, K. W. Density functionals for surface science: Exchange-correlation model development with Bayesian error estimation. *Phys. Rev. B* **2012**, *85*, 235149.
- (40) Tran, F.; Stelzl, J.; Blaha, P. Rungs 1 to 4 of DFT Jacob’s ladder: Extensive test on the lattice constant, bulk modulus, and cohesive energy of solids. *J. Chem. Phys.* **2016**, *144*, 204120.
- (41) Schimka, L.; Harl, J.; Stroppa, A.; Grüneis, A.; Marsman, M.; Mitterdorfer, F.; Kresse, G. Accurate surface and adsorption energies from many-body perturbation theory. *Nat. Mater.* **2010**, *9*, 741–744.
- (42) Klimeš, J.; Bowler, D. R.; Michaelides, A. Van der Waals density functionals applied to solids. *Phys. Rev. B* **2011**, *83*, 195131.
- (43) Hays, W. L., *Statistics*. Holt–Saunders: Tokyo, 1981.
- (44) Shukla, V.; Jiao, Y.; Lee, J.-H.; Schröder, E.; Neaton, J. B.; Hyldgaard, P. Accurate Nonempirical Range-Separated Hybrid van der Waals Density Functional for Complex Molecular Problems, Solids, and Surfaces. *Phys. Rev. X* **2022**, *12*, 041003.
- (45) Cooper, V. R. Van der Waals density functional: An appropriate exchange functional. *Phys. Rev. B* **2010**, *81*, 161104.

- (46) Berland, K.; Hyldgaard, P. Exchange functional that tests the robustness of the plasmon description of the van der Waals density functional. *Phys. Rev. B* **2014**, *89*, 035412.
- (47) Sun, J.; Ruzsinszky, A.; Perdew, J. P. Strongly constrained and appropriately normed semilocal density functional. *Phys. Rev. Lett.* **2015**, *115*, 036402.
- (48) Krukau, A. V.; Vydrov, O. A.; Izmaylov, A. F.; Scuseria, G. E. Influence of the exchange screening parameter on the performance of screened hybrid functionals. *J. Chem. Phys.* **2006**, *125*, 224106.
- (49) Shukla, V.; Jiao, Y.; Frostenson, C. M.; Hyldgaard, P. vdW-DF-ahcx: a range-separated van der Waals density functional hybrid. *J. Phys.: Condens. Matter* **2021**, *34*, 025902.
- (50) Gerrits, N.; Geweke, J.; Smeets, E. W. F.; Voss, J.; Wodtke, A. M.; Kroes, G. J. Closing the Gap Between Experiment and Theory: Reactive Scattering of HCl from Au(111). *J. Phys. Chem. C* **2020**, *124*, 15944–15960.
- (51) Behler, J.; Delley, B.; Lorenz, S.; Reuter, K.; Scheffler, M. Dissociation of O<sub>2</sub> at Al(111): The role of spin selection rules. *Phys. Rev. Lett.* **2005**, *94*, 036104.
- (52) Haas, P.; Tran, F.; Blaha, P. Calculation of the lattice constant of solids with semilocal functionals. *Phys. Rev. B* **2009**, *79*, 085104.
- (53) Arblaster, J. W. Crystallographic properties of ruthenium. *Platinum Met. Rev.* **2013**, *57*, 127–136.

## Samenvatting

Heterogeen gekatalyseerde processen zijn van groot belang voor de chemische industrie, en bekende voorbeelden van dergelijke processen zijn ammoniaksynthese en stoomreforming. Bij heterogeen gekatalyseerde processen op metalen oppervlakken is de snelheidsbepalende stap vaak de dissociatieve chemisorptie (DC, het proces waarbij de interactie van een molecuul met een oppervlak leidt tot het verbreken van een binding in het molecuul en de vorming van twee nieuwe bindingen van de moleculaire fragmenten met het oppervlak) van een molecuul op het oppervlak. Het begrijpen van hoe heterogene katalyse werkt is van groot belang. Ons begrip van de verschillende mechanismen die ten grondslag liggen aan de DC op metalen oppervlakken, zou aanzienlijk kunnen profiteren van de beschikbaarheid van een nauwkeurige database voor barrièrehoogtes van elementaire molecuul-metaaloppervlakreacties. Net als chemisorptie-energieën van (intermediaire) reactanten en producten, zijn nauwkeurige barrière's voor het beheersen van de snelheid van elementaire reacties de sleutel tot het begrijpen, beheersen en voorspellen van de snelheid van algehele heterogeen gekatalyseerde processen.

Idealiter zouden nauwkeurige barrièrehoogtes rechtstreeks uit gedetailleerde systematische experimenten worden gehaald. Het is echter niet mogelijk om barrièrehoogtes voor de DC direct te meten. Een waarneembare waarde die experimenteel kan worden gemeten en die sterk gerelateerd is aan de barrièrehoogte voor DC is de plakwaarschijnlijkheid ( $S_0$ ). De beste manier om toegang te krijgen tot barrièrehoogten met behulp van theorie is via een theoretische aanpak waarin potentiële energieoppervlakken (PEO's) worden berekend en gebruikt in dynamische berekeningen om  $S_0$  te evalueren als een functie van de gemiddelde invalsenergie. Vergelijking met experimentele  $S_0$  maakt het mogelijk om de nauwkeurigheid te evalueren van de elektronenstructuurmethode die wordt gebruikt om de PEO en de barrièrehoogte te berekenen. Alleen wanneer experimentele gegevens binnen zekere mate worden gereproduceerd ofwel binnen chemische nauwkeurigheid (d.w.z. met fouten kleiner dan 1 kcal/mol), kan worden beweerd dat de berekende barrièrehoogte van hoge nauwkeurigheid is. Deze

validatieprocedure vereist daarom dat dynamicaberekeningen worden uitgevoerd met een geschikt dynamisch model en dynamische methode. In deze procedure wordt de elektronenstructuurmethode gebruikt om de krachten te genereren die op de atomen werken (hetzij direct in *ab initio* moleculaire dynamica of dichtheidsfunctionaal moleculaire dynamica berekeningen of indirect vanuit een PEO dat was aangepast aan *ab initio* gegevens).

Op dit moment zijn er helaas nog geen *ab initio* of niet-empirische elektronenstructuurmethoden beschikbaar die de interactie-energieën tussen molecuul en metaaloppervlak tot op chemische nauwkeurigheid kunnen berekenen. Momenteel is de meest efficiënte elektronische structuurmethode die kan worden gebruikt om de PEO van de interactie van het molecuul met het metaaloppervlak in kaart te brengen, de dichtheidsfunctionaaltheorie (DFT) met behulp van een geschatte uitwisselingscorrelatiefunctieel (UCF), die meestal wordt genomen op het niveau van de gegeneraliseerde gradiëntbenadering (GGB). Aan het begin van dit onderzoek was nog niet goed bekend hoeveel fouten we hebben gemaakt bij het gebruik van een dergelijke benadering.

Om het probleem met de nauwkeurigheid van DFT te verhelpen, werd een implementatie van een specifieke reactieparameter (SRP) aanpak van DFT (SRP-DFT) voorgesteld. In deze benadering wordt de uitwisselingscorrelatiefunctieel uitgerust met één instelbare parameter. Deze parameter wordt gefit aan een reeks experimentele gegevens voor een molecuul dat reageert op het oppervlak. Vervolgens wordt de kwaliteit van de SRP functionaal getest door te controleren of deze ook kan worden gebruikt om andere experimenten op hetzelfde systeem te reproduceren. Met deze SRP benadering hebben we nu een kleine database verkregen met chemisch nauwkeurige barrières voor moleculen die reageren op metalen oppervlakken. Deze databank bestaat uit resultaten voor onder meer  $\text{H}_2+\text{Cu}(111)$ ,  $\text{H}_2+\text{Cu}(100)$ ,  $\text{H}_2+\text{Pt}(111)$ ,  $\text{H}_2+\text{Pt}(111)$ ,  $\text{CH}_4+\text{Ni}(111)$ ,  $\text{CH}_4+\text{Pt}(111)$  en  $\text{CH}_4+\text{Pt}(211)$ .

Het belangrijkste doel van dit proefschrift is om een nauwkeurige beschrijving te geven van waterstof ( $\text{H}_2$ ) gedissocieerd op metaaloppervlakken, een database te ontwikkelen van chemisch nauwkeurige barrières van moleculen ( $\text{H}_2$ ,  $\text{N}_2$ , and  $\text{CH}_4$ ) gedissocieerd op metaaloppervlakken en ook een SRP-database voor verschillende soorten combinaties van UCF's.

In **Hoofdstuk 2**, is het doel om de ontwikkeling van SRP-DF's uit te breiden. We onderzoeken eerst of de eerder afgeleide SRP-DF (PBE $\alpha$ 0.57-vdW-DF2) voor  $\text{H}_2+\text{Pt}(111)$  overdraagbaar is naar het  $\text{H}_2+\text{Ni}(111)$  en als niet, proberen we ook een SRP-DF af te leiden voor de DC van  $\text{H}_2$  op  $\text{Ni}(111)$ . Om deze vragen te beantwoorden, zijn 6D PEO's geconstrueerd voor de dissociatie van  $\text{H}_2+\text{Ni}(111)$  met behulp van negen verschillende UCF's. De berekende PEO's werden vervolgens geïnterpoleerd met behulp van de corrugatie reducerende procedure

(CRP) methode. Om te vergelijken met experimenteel reactiewaarschijnlijkheden, zijn quasi-klassieke baan- (QKB) en quantumdynamica (QD) berekeningen uitgevoerd met behulp van het Born-Oppenheimer statisch oppervlak (BOSS) model.

De onderzochte functionalen leveren een breed scala aan barrièrehogtes en barrièreposities op. De functionalen die van der Waals-correlatie bevatten, leveren barrières op die dichter bij het oppervlak liggen en een grotere energetische corrugatie vertonen dan functionalen die PBE-correlatie bevatten, zoals eerder ook al bij het gerelateerde  $\text{H}_2+\text{Ru}(0001)$  systeem is bevonden.

De functionalen PBE-vdW-DF2 en RPBE:PBE(50:50)-vdW-DF1 beschrijven de experimentele reactiewaarschijnlijkheden die door de Rendulic-groep zijn gemeten redelijk goed, waarbij PBE-vdW-DF2 de beste resultaten geeft. Uit de vergelijking met de meest recente moleculaire bundelexperimenten van de Rendulic-groep, concluderen we dat PBE-vdW-DF2 kan worden beschouwd als een kandidaat SRP-DF voor  $\text{H}_2+\text{Ni}(111)$ . De  $\text{PBE}\alpha 0.57\text{-vdW-DF2}$ , die een SRP-DF is voor  $\text{H}_2$  op  $\text{Pt}(111)$ , is echter geen SRP-DF voor  $\text{H}_2+\text{Ni}(111)$ , ook al behoren Ni en Pt tot dezelfde groep in het periodiek systeem.

De PBE-vdW-DF2  $S_0$  komen nog niet goed overeen met de meest recente experimenten van de Rendulic-groep voor invalsenergieën groter dan 0.3 eV. Voor invalsenergieën  $> 0.25$  eV, vonden we dat  $S_0$  een aanzienlijke afhankelijkheid begint te vertonen van de bundelcondities, zodat sommige van de geconstateerde verschillen te wijten kunnen zijn aan verschillende bundelparameters die kenmerkend zijn voor de experimentele bundels en de bundels gesimuleerd in de berekeningen. Andere mogelijke oorzaken van fouten in de experimenten zijn ook besproken. We achten het onwaarschijnlijk dat de verschillen tussen theorie en experiment te wijten zijn aan het gebruik van een onjuist dynamisch model (BOSS) of dynamische methode (QKB). In het bijzonder, behalve misschien voor  $\nu=0, j=0$ , waren de initiële toestands opgeloste reactiekansen berekend met QKB in de begintoestand in goede overeenstemming met de QD resultaten, zodat QKB nauwkeurige resultaten zou moeten geven voor de reactiewaarschijnlijkheden. Het is echter mogelijk dat de PBE-vdW-DF2 barrières voor dissociatie over de brug en holle locaties oplevert die te laag zijn. Om deze en andere vragen op te lossen, pleiten wij ervoor dat nieuwe experimenten met goed gedefinieerde condities worden uitgevoerd aan de reactiewaarschijnlijkheden van  $\text{H}_2$  op  $\text{Ni}(111)$  voor invalsenergieën  $> 0.2$  eV.

In **Hoofdstuk 3**, richten we ons op de ontwikkeling van een nieuwe database met barrièrehogtes voor de DC op metalen oppervlakken die kunnen worden gebruikt voor het benchmarken van elektronenstructuurmethoden. De nieuwe database heet SBH17 en bevat barrières voor 17 systemen, waaronder 8  $\text{H}_2$ -metaal systemen, 2  $\text{N}_2$ -metaal systemen en 7  $\text{CH}_4$ -metaal systemen. Voor 16



systemen overschrijdt de werkfunctie van het metaal - de elektronenaffiniteit van het molecuul (W-EA) de 7 eV. De barrièrehogtes komen uit SRP-DFT (14 systemen) en uit meer ad-hoc semi-empirisch (SE) procedures (3 systemen). De nieuwe database is bedoeld als vervanging van een oudere database (SBH10) die barrières bevatte voor 10 van de 17 nu behandelde systemen.

We hebben 14 DF's getest op de nieuwe database, waarvan drie GGB DF's, 4 meta-GGB DF's en 7 DF's met GGB uitwisseling en niet-lokale vdW-DF1 of vdW-DF2 correlatie. We hebben eerst getest hoe de prestaties van deze DF's afhangen van het gebruikte algoritme of de gebruikte procedure. Er werden drie verschillende algoritmen getest, die werden gelabeld als "hoog", "gemiddeld" en "licht", afhankelijk van de investering van computertijd die nodig was voor de berekening. Het gemiddelde algoritme is het beste compromis tussen nauwkeurigheid en computertijd. Hierin berekent men voor elke geteste DF de roosterconstante van de metalen in de database. Vervolgens wordt voor elke geteste DF, voor elk metalen oppervlak in de database een relaxatie uitgevoerd van de afstanden tussen de bovenste lagen. Vervolgens wordt voor elk systeem in de database en voor elke DF de barrièrehoogte berekend op basis van twee berekeningen. Een van deze berekeningen is voor een geometrie waarbij het molecuul zich in de gasfase bevindt, en de andere voor een geometrie waarbij het molecuul zich in de zadelpuntgeometrie bevindt. Deze geometrie van het zadelpunt is ofwel degene die eerder is verkregen uit een SRP-DFT-berekening (als de barrièrehoogte afkomstig is van SRP-DFT) of uit een berekening met een functionaal die naar verwachting het beste zal presteren (als de barrièrehoogte een schatting is op basis van experimentele gegevens).

Van de geteste DF's presteren de meta-GGB DF's het best bij het beschrijven van het metaal, gevolgd door PBE en optPBE-DF1. Wanneer de MAE als nauwkeurigheidscriterium wordt genomen, presteert de werkpaard PBE GGB DF het beste op de SBH17-database, met een MAE van 2.4 kcal/mol. Andere toppers zijn de MS2 meta-GGB functionaal en twee functionalen bestaande uit GGB uitwisseling en niet-lokale correlatie (SRP32-vdW-DF1 en PBE $\alpha$ 57-vdW-DF2). Verrassend genoeg onderschat geen van de geteste DF's systematisch reactiebarrières voor de DC op metalen, in tegenstelling tot bevindingen voor gasfasereacties. Deze bevinding zou aanwijzingen moeten geven van de oorsprong van tekortkomingen van semi-lokale DF's voor gasfasereactiebarrières, wat duidt op verder onderzoek naar deze onderwerpen.

Onze resultaten voor de nauwkeurigheid van de DF's voor de DC barrières zijn robuust in de mate dat hun rangschikking volgens de gemiddelde absolute fout (MAE) nogal ongevoelig is voor het verwijderen van de drie systemen ( $\text{N}_2 + \text{Ru}(10\bar{1}0)$ ,  $\text{CH}_4 + \text{Ru}(0001)$  en  $\text{CH}_4 + \text{Ni}(100)$ ) die de grootste fouten in de database opleveren, en voor het verwijderen van de drie systemen waarvoor

referentiebarrièrehoogten werden verkregen met een ad-hoc semi-empirische analyse. Het verbeteren van SBH17 door ervoor te zorgen dat alle referentiebarrièrehoogtes afkomstig zijn van SRP-DFT, zal waarschijnlijk de MAE's van de best presterende functionalen aanzienlijk verminderen, b.v. tot een fout van minder dan 2 kcal/mol voor PBE. Als wij de SBH17 met de oude SBH10 database vergelijken krijgen we verschillende resultaten met betrekking tot de relatieve nauwkeurigheid van de MS2 en BEEF-vdW-DF2 functionalen. Dit wijzen we toe aan een onjuiste behandeling van de oppervlakte-atomen in de overgangstoestanden in de eerdere studie aan de SBH10 database.

De DF's die het beste presteren voor DC barrières (d.w.z. kinetiek) zijn niet degenen die het beste presteren voor databases (CE26, CE21b) van chemisorptie-energieën op metalen (d.w.z. thermochemie). Deze trend loopt parallel in de prestaties van DF's op databases voor kinetiek (BH76, BH206) en thermochemie (AE6, TCE) in de gasfase. De meta-GGB MS2 DF is de functie met de beste algehele prestaties voor DC barrières en chemisorptie-energieën op metalen. Van de vijf GGA en meta-GGB DFen die in aanmerking kwamen vanwege hun prestaties op 6 databases voor kinetiek en thermochemie op metalen oppervlakken en in de gasfase (PBE, RPBE, revTPSS, MS2 en SCAN), liet MS2 opnieuw de beste algemene prestatie zien.

In **Hoofdstuk 4**, is het belangrijkste doel om de nauwkeurigheid van de QKB methode te evalueren, of, als alternatief, het belang van kwantumeffecten voor het plakken van H<sub>2</sub> op Al(110), voor omstandigheden die dicht bij de omstandigheden zouden moeten liggen waaronder moleculaire bundelexperimenten zijn uitgevoerd aan dit systeem. Voor dit doel zijn QKB en QD berekeningen uitgevoerd met het BOSS model op een PEO verkregen met DFT, die een minimale barrièrehoogte vertoont die dicht in de buurt komt van een recentelijk verkregen barrièrehoogte met quantum Monte Carlo (QMC) berekeningen. Om het aantal uit te voeren QD berekeningen klein te houden, werd een procedure "gedeeltelijk Monte-Carlo" (GMC) gebruikt waarbij Monte-Carlo-middeling over een selectie van de initiële rovibrationele toestanden van H<sub>2</sub> werd gebruikt. Deze procedure maakte de quasi-klassieke berekening mogelijk van reactiewaarschijnlijkheden met een relatieve fout < 7.5% voor vijf van de zes onderzochte begincondities, en van 16% voor één van deze condities, bij ongeveer een orde van grootte minder rekentijd.

De reactiewaarschijnlijkheden berekend met QD met behulp van de GMC procedure overschrijden die berekend met de QKB methode met 80 en 30% voor de twee bundelcondities die overeenkomen met de laagste invalsenegieën (5.1 en 6.0 kcal/mol), afnemend tot slechts 5% voor de energie met hoogste invalsenegie van 9.4 kcal/mol. De met QD berekende plakkanscurve wordt verschoven naar lagere energieën ten opzichte van de QKB curve met 0.21 tot 0.05 kcal/mol, waarbij de hoogste verschuiving wordt verkregen voor de laagste energie van

inval. Deze "quantum effecten" kunnen als vrij klein worden beschouwd voor moleculaire bundel-plak experimenten waarin de gemiddelde invalsenergieën (5.1-8.5 kcal/mol) veel kleiner zijn dan de minimale barrièrehogte van het onderzochte systeem (24.8 kcal/mol). De minimale quantum effecten worden verklaard op basis van de grote vibrationele doeltreffendheid van het systeem ( $> 1$  voor  $\nu=1$ ) en de breedte van de translatie-energieverdelingen van de moleculaire bundels die worden gebruikt in de experimenten die we behandelen, wat betekent dat vastplakken kan plaatsvinden via vibrationele geëxciteerde moleculen met hoge invalsenergie. We concluderen dat "quantumeffecten" naar verwachting geen grote rol zullen spelen in berekeningen die de nauwkeurigheid van elektronenstructuurmethoden zouden evalueren voor het bepalen van de minimale barrièrehogte voor DC in  $H_2+Al(110)$  op basis van bestaande moleculaire bundel-experimenten, aangezien het oordeel zou afhangen van de energieverschuiving tussen de berekende en de gemeten reactiewaarschijnlijkheden curve. Voor maximale betrouwbaarheid van de conclusies over nauwkeurigheid zou het echter goed zijn om rekening te houden met de kwantumeffecten, aangezien de maximale verschuiving (0.21 kcal/mol) niet verwaarloosbaar is op de schaal van "chemische nauwkeurigheid" (1 kcal/mol).

In **Hoofdstuk 5** ligt de nadruk op het uitleggen van enkele basisprincipes en het afleiden van de beste gemengde dichtheidsfunctionalen voor het beschrijven van dissociatieve chemisorptie op metaaloppervlakken. We hebben de afstembaarheid van verschillende uitdrukkingen voor gemengde dichtheidsfunctionalen onderzocht, waarin een mengparameter  $\alpha$  kan worden afgestemd om de gemengde DF in staat te stellen de referentiewaarde van de barrièrehogte voor dissociatieve chemisorptie van een molecuul op een metalen oppervlak te reproduceren. De gemengde functies worden getest op de barrières die zijn verzameld in de database die we SBH16 noemen, die gelijk is aan de vorige SBH17-database in **hoofdstuk 3**, met het  $H_2 + Pt(211)$  systeem eruit verwijderd.

Het verhogen van de fractie van RPBE-uitwisseling die is opgenomen in de gemengde DF's leidt tot hogere barrières. Alle geteste gemengde DF's zijn goed af te stemmen op hogere barrières, aangezien hun beperkende vormen (RPBE, RPBE-vdW1 en RPBE-vdW2) allemaal systematisch de barrièrehogte voor de systemen in de SBH16-database overschatten. Het blijkt dat de grootste uitdaging voor het vinden van een perfect afstembare gemengde DF voor het beschrijven van de SBH16-database het verkrijgen van een gemengde DF-expressie is met een goede vorm met lagere energie, die consequent de barrièrehogten onderschat voor systemen zoals die aanwezig zijn in SBH16. Dit doel wordt volledig bereikt met de gemengde SRP $\alpha$ sol DF die gebruikmaakt van PBE-correlatie en een combinatie van PBEsol en RPBE-uitwisseling. De gemengde SRP $\alpha$ sol-vdW2 DF zou de minimale barrièrehogte van 15 van de 16 systemen kunnen beschrijven

met behulp van vdW-DF2-correlatie, terwijl de gemengde SRP $\boldsymbol{x}$ -vdW1 DF dit kon doen voor 14 van de 16 systemen die vdW-DF1-correlatie gebruiken. Het kunnen gebruiken van gemengde DF's met verschillende correlatiefunctionalen kan belangrijk zijn voor het verkrijgen van een SRP DF voor een bepaald systeem, omdat het reproduceren van de minimale barrièrehoogte een noodzakelijke voorwaarde is voor het reproduceren van gemeten reactiewaarschijnlijkheden, zoals nu gebruikt voor het valideren van SRP-functionalen en barrièrehoogtes.

We hebben ook getest of en hoe de mengcoëfficiënt van de gemengde DF's gecorreleerd is met de ladingoverdrachtsparameter die het systeem beschrijft, d.w.z. het verschil tussen de werkfunctie van het metaaloppervlak en de elektronenaffiniteit van het molecuul. Het antwoord hangt af van welke gemengde DF wordt gebruikt. Voor de SRP $\boldsymbol{x}$  en SRP $\boldsymbol{x}$ sol DF's, die beide PBE-correlatie gebruiken, vonden we dat de optimale fractie van RPBE-uitwisseling afneemt met de parameter voor ladingoverdracht, net als verwacht wordt op basis van eerdere resultaten. De tegenovergestelde relatie en zwakkere correlatie werd echter gevonden voor de gemengde DF's die vdW-DF1- of vdW-DF2-correlatie bevatten.

## Curriculum vitae

Théophile Tchakoua is geboren op 3 juni 1988 te Foumban (Kameroen). In 2007 heeft hij zijn baccalauréat behaald aan de Lycée de Foumban. In datzelfde jaar is hij begonnen aan de bachelorstudie "Natuurkunde en scheikunde" aan de Universiteit Douala. Drie jaar later is hij, in 2010, overgestapt naar de bachelorstudie "Natuurkunde en scheikunde" aan de Universiteit Douala (Kameroen). Na deze studie in 2011, is hij aan de masterstudie "Physics and engineering sciences option Physics of matter and radiation" aan de Universiteit Douala begonnen. In 2014 heeft hij zijn masterstudie afgerond, waarna hij in datzelfde jaar is begonnen met de docent Natuurkunde opleiding aan de Universiteit Bamenda (Kameroen). In 2016 heeft hij zijn docent masterstudie afgerond, en in het volgende jaar 2017 heeft hij nog een stralingsdeskundige masterstudie afgerond in het IAEA programma in het Algiers nucleair onderzoekscentrum. In 2018 begon hij zijn promotieonderzoek in de groep Theoretische Chemie van Prof. dr. Geert-Jan Kroes, in het Leids Instituut voor Chemisch onderzoek. Vanaf april 2023 doet hij onderzoek bij de Utrecht Universiteit, in de "Materials Chemistry and Catalysis" groep van Dr. Nongnuch Artrith. Daar zal hij zich richten op het combineren van de voorspellende kracht van kwantumchemische berekeningen met de efficiëntie van AI/machine learning-benaderingen voor snelle en nauwkeurige in silico-voorspellingen voor grote systemen.

## List of publications

- **Tchakoua, T.**; Smeets, E. W.; Somers, M.; Kroes, G. J. Toward a Specific Reaction Parameter Density Functional for  $\text{H}_2 + \text{Ni}(111)$ : Comparison of Theory with Molecular Beam Sticking Experiments. *J. Phys. Chem. C* **2019**, *123*, 20420–20433
- **Tchakoua, T.**; Gerrits, N.; Smeets, E. W. F.; Kroes, G. J. SBH17: Benchmark Database of Barrier Heights for Dissociative Chemisorption on Transition Metal Surfaces. *J. Chem. Theory Comput.* **2023**, *19*, 245–270
- **Tchakoua, T.**; Powell, A. D.; Gerrits, N.; Somers, M. F.; Doblhoff-Dier, K.; Busnengo, H. F.; Kroes, G. J. Simulating highly activated sticking of  $\text{H}_2$  on Al(110): Quantum versus quasi-classical dynamics. *J. Phys. Chem. C* **2023**, *127*, 1932–7447
- **Tchakoua, T.**; Jansen, T.; van Nies, Y.; van den Elshout, R.; van Boxmeer, B. A. B.; Poort, S. P.; Ackermans, M. G.; Beltrão, G. S.; Hildebrand, S. A.; Beekman, S. E. J.; van der Drift, T.; Kaart, S.; Šantić, A.; Somers, M. F.; Kroes, G. J. Constructing mixed density functionals for describing dissociative chemisorption on metal surfaces: some basic principles. *J. Phys. Chem. C* **Submitted**

## Afterword

Chaque thèse est une histoire. Voici mon histoire, je la raconte. La partie remerciements est généralement un ardu exercice d'un travail de thèse. Ardu car, durant toutes ces années de travail, nous nous sommes côtoyés, nous avons les uns et autres échangés nos humeurs avec comme résultante, une dynamique d'humeurs alternative. Des humeurs parfois positives et négatives, nous avons toutefois su en tirer une leçon positive pour notre travail. Ardu également, car la crainte d'oublier quelqu'un ou chacun de ces moments est toujours présente. Bien qu'incapable de lister tout le monde, qui aurait contribué à la manifestation de la présente conception d'orfèvre, permettez-moi tout naturellement de remercier ceux sans qui cette thèse n'aurait jamais vu le jour: mes encadreurs **Geert-Jan Kroes** et **Mark Frans Somers**. Ils ont eu la patience de m'encadrer pour ces quatre dernières années. Ils m'ont facilité la tâche et ont permis à ce que ce projet de thèse voit le jour aujourd'hui, et ce malgré les deux années difficiles de la crise covid-19. Je vous suis redevable pour des nombreuses discussions que nous avons eues tous ensemble, non seulement au sujet de ce travail, mais aussi sur des orientations adressant la vie en général.

Cette thèse a été réalisé au sein du laboratoire de chimie théorique de l'université de Leiden (LIC). C'est pourquoi je veux remercier collégialement mes collègues de laboratoire **Guido, Elham, Nick, Andrew, Tim, Paul, Sayan, Davide, Francesco, Helen, Soroush, Khosrow, Bauke, Justina, Robert, Marten, Brian, Seeni, Hossein, Jonathon, Lukas, Floris, Joan, Jörg, Katharina, Thanja, Marc** pour les discussions scientifiques et aussi pour les meilleurs moments de chaque jour à la pause café.

Durant cette thèse, j'ai rencontré bien des gens au *Gorlaeus Building* et aussi dans les locaux de l'université de Leiden. Je ne peux sûrement pas tous les citer, mais je tiens à les remercier pour tout. Je remercie la secrétaire du département **Michelle** pour son assistance et ainsi que le personnel du service international pour étudiant étranger (SCIS), particulièrement **Yvonne, Esther, Simone, Saskia** pour toutes assistances en ce qui concerne les procédures administratives de l'IND.

J'adresse également mes remerciements à **Marius de Hond** avec qui j'ai parcouru toutes les artères de Leiden et qui, a pendant deux années été mon coach linguistique en néerlandais. Tu l'as toujours fait avec patience et méthode. Merci également à **Barbera** à travers le programme *Gilde Samenspraak*.

Dans cette longue liste des remerciements, je tiens à exprimer ma communion et toute ma gratitude à la communauté protestante de Leiden (**Protestantse Marekerkgemeente**) où j'ai durant ces dernières années entretenu et cultivé ma foi chrétienne à travers les sermons dominicaux ainsi que les activités des divers groupes d'étude biblique auxquelles j'ai participé. Merci pour l'attention particulière que j'ai reçue de votre part, ceci surtout pendant les moments épineux.

Je tiens aussi à remercier **Yassine Bensenane**, **Omar** et **Boubakar** pour leur amitié. Vous avez su au travers de nos différentes discussions m'encourager.

Et puis, la famille est certainement un soutien indispensable. Je remercie ma maman **Anne** qui a toujours été là pour moi. Tu comprends très bien pourquoi maman et vouloir donner une explication ici pour tout ce que tu as fait dans ma vie serait insignifiant. Je remercie mon grand-frère **Mesmer**, qui a été là et n'a cessé de m'encourager dans cette aventure.

En fin, j'ai réservé les derniers mots de ma plume et les plus beaux à **Cladis** et **Esther**. Je sais que ça n'a pas été facile de vivre pendant cinq années mon absence en tant que époux et père. Notre famille a grandi en même temps que ce projet de thèse, le premier servant de socle solide à l'épanouissement du second. Votre soutien et encouragement constants m'ont été d'un grand réconfort et ont contribué à l'aboutissement de ce travail. Trouvez ici le fruit de votre patience.